



# Role of mitochondrial soluble adenylyl cyclase, phosphodiesterases and Epac in cardiac mitochondrial function and cell death

Zhenyu Wang

## ► To cite this version:

Zhenyu Wang. Role of mitochondrial soluble adenylyl cyclase, phosphodiesterases and Epac in cardiac mitochondrial function and cell death. Cellular Biology. Université Paris Saclay (COMUE), 2016. English. NNT : 2016SACLS186 . tel-02181158

**HAL Id: tel-02181158**

**<https://theses.hal.science/tel-02181158>**

Submitted on 12 Jul 2019

**HAL** is a multi-disciplinary open access archive for the deposit and dissemination of scientific research documents, whether they are published or not. The documents may come from teaching and research institutions in France or abroad, or from public or private research centers.

L'archive ouverte pluridisciplinaire **HAL**, est destinée au dépôt et à la diffusion de documents scientifiques de niveau recherche, publiés ou non, émanant des établissements d'enseignement et de recherche français ou étrangers, des laboratoires publics ou privés.

NNT : 2016SACLS186

THESE DE DOCTORAT  
DE  
L'UNIVERSITE PARIS-SACLAY  
PREPAREE A UNIVERSITE PARIS SUD

ECOLE DOCTORALE N° 569 ITFA  
Innovation thérapeutique: du fondamental à l'appliqué

Spécialité de doctorat: Physiopathologie Moléculaire et Cellulaire

Par

**M. Zhenyu WANG**

Rôle de l'adénylate cyclase soluble, de phosphodiesterases et d'Epac  
dans la fonction mitochondriale cardiaque et la mort cellulaire

**Thèse présentée et soutenue à Châtenay-Malabry, le 11 Juillet 2016:**

**Composition du Jury :**

M. Christian POUS	Professeur, Université Paris-Saclay	Président
Mme. Delphine HAOUZI	CR, Université Montpellier	Rapporteur
M. Michelangelo CAMPANELLA	Reader, Royal Veterinary College	Rapporteur
M. Roberto MOTTERLINI	DR, University Paris-Est	Examineur
Mme. Nazanine MODJTAHEDI	CR, Université Paris-Saclay	Examinatrice
M. Jérémy FAUCONNIER	CR, Université Montpellier	Examineur
Mme. Catherine Brenner	DR, Université Paris-Saclay	Directeur de thèse

## Acknowledgements

Firstly, I would like to express my sincere gratitude to my supervisor Dr. Catherine Brenner for the extreme help to me during the entire period of my studies, for the continuous support of my Ph.D study and related research, for her patience, motivation, and immense knowledge, brilliant ideas. Her guidance helped me in all the time of research and writing of this thesis.

Besides my advisor, I would also like to thank Dr. Rodolphe Fischmeister for giving me the opportunity to work in this lab, and giving me the insightful comments and encouragement. I would thank Dr. Grégoire Vandecasteele for his help on construction mitochondrial cAMP sensor, FRET experiment, stimulating discussions, and correcting the manuscripts. I also thank Dr. Ana-Maria Gomez for manuscripts submission and correction.

I extend my sincere thanks to members of my thesis committee. I would like to thank Pr. Christian Poüs for accepting to be the president of my thesis committee. I really thank to Dr. Delphine Haouzi and Dr. Michelangelo Campanella for reviewing this thesis and helping me ameliorate the quality of thesis. I am also thankful to the examiners, Dr. Roberto Motterlini, Dr. Nazanine Modjtahedi and Dr. Jérémy Fauconnier for accepting to examine and evaluate my work.

My sincere thanks also goes to my colleagues for teaching me techniques and giving me the help during the experiment. I would like to express gratitude to Audry Varin for her help on plasmid and adenovirus purification; to Valerie Nicolas for her help on

confocal microscope; to Delphine Courilleau for her help on Epac experiments; to Philippe Mateo for his help on echocardiography; to Marta Lindner and Delphine Mika for their help on PDE experiments; to Florence Lefebvre for her help on isolation of adult cardiomyocytes; to Jessica Sabourin for her help on neonatal cardiomyocyte experiment; to Carole Oudot and Claire Nicolas on mitochondrial experiments; to Boris Manoury, LEROY Jérôme, Félix Peyre, Véronique Leblais, Milia Belacel ouari, Ibrahim Bedioune, Sarah Idres, Sara Karam, Hind Mehel, Pierre Bobin. Without their precious support it would not be possible to conduct this research.

In particular, I am grateful to Dawei Liu, Liang Zhang, Yueyi Wang and Linwei Li for their help and encouragements.

Last but not the least, I would like to thank my parents, my sister and my girlfriend for supporting me spiritually throughout my thesis and my life in general.



## Table of contents

<b>List of figures.....</b>	<b>III</b>
<b>List of tables.....</b>	<b>III</b>
<b>List of abbreviations .....</b>	<b>V</b>
<b>1 Introduction.....</b>	<b>1</b>
1.1 Mitochondria.....	1
1.1.1 Structure of mitochondria .....	1
1.1.2 Mitochondrial physiology .....	2
1.1.3 Mitochondria and cell death.....	7
1.1.4 Mitochondria and heart failure (HF).....	10
1.2 cAMP signalling pathway .....	16
1.2.1 cAMP production.....	17
1.2.2 cAMP targets .....	17
1.2.3 cAMP signalling pathway in the heart.....	22
1.2.4 sAC .....	24
1.2.5 cAMP signalling in mitochondria .....	30
1.3 Phosphodiesterases (PDEs).....	32
1.3.1 Overview of PDEs .....	32
1.3.2 PDE family.....	35
1.3.3 PDEs in mitochondria .....	44
<b>2. Objectives.....</b>	<b>46</b>
<b>3. Materials and methods .....</b>	<b>47</b>
3.1 Materials .....	47
3.1.1 Drugs and reagents.....	47
3.1.2 Antibodies .....	47
3.2 Methods used in cardiomyocytes.....	48
3.2.1 Surgical procedure and echocardiography .....	48
3.2.2 Isolation of ventricular cardiomyocytes of adult rats .....	49
3.2.3 Isolation of neonatal cardiomyocytes .....	50

3.2.4 Construction of mitochondria-targeted FRET sensor for cAMP .....	52
3.2.5 FRET imaging.....	53
3.2.6 Cell death measurement.....	53
3.2.7 PDE activity .....	54
3.2.8 SDS-PAGE and western blot .....	56
3.2.9 siRNA transfection to knockdown sAC and Epac1 .....	57
3.2.10 Mitochondrial transmembrane potential measurement in neonatal cardiomyocytes .....	57
3.2.11 Mitochondrial transmembrane potential measurement in adult cardiomyocytes .....	58
3.2.12 Measurement of mitochondrial $\text{Ca}^{2+}$ in cardiomyocytes .....	58
3.3 Methods used in isolated mitochondria .....	59
3.3.1 Animals .....	59
3.3.2 Isolation of rat cardiac mitochondria .....	59
3.3.3 Isolation of mouse cardiac mitochondria.....	60
3.3.4 Mitochondrial transmembrane potential ( $\Delta\Psi_m$ ) and swelling .....	61
3.3.5 Oxygen consumption .....	61
3.3.6 $\text{Ca}^{2+}$ accumulation measurement .....	62
3.3.7 cAMP measurement in isolated mitochondria.....	62
3.3.8 ATP measurement.....	63
3.3.9 Bioenergetic analysis in isolated mitochondria .....	63
<b>4 Results .....</b>	<b>65</b>
4.1 Article 1: A cardiac mitochondrial cAMP signaling pathway regulates calcium accumulation, permeability transition and cell death.....	65
4.2 Article 2: Phosphodiesterases localized in cardiac mitochondria regulate mitochondrial cAMP and membrane potential .....	87
<b>5 Discussion and perspectives .....</b>	<b>119</b>
<b>6 References .....</b>	<b>125</b>
<b>7 Annexes .....</b>	<b>164</b>

## List of figures

Figure 1 Mitochondrial architecture.....	2
Figure 2 Overview of fuel production within the mitochondria.....	3
Figure 3 Membrane potential generation in mitochondria.....	4
Figure 4 Mitochondrial $\text{Ca}^{2+}$ influx and efflux mechanisms.....	5
Figure 5 Mitochondrial oxidative stress.....	7
Figure 6 Molecular Structure of the mPTP.....	10
Figure 7 The anatomy of the heart and associated vessels.....	11
Figure 8 Damage induced by reactive oxygen species in mitochondria.....	13
Figure 9 $\text{Ca}^{2+}$ overload, impaired metabolism, and cell death in heart failure.....	15
Figure 10 Physiological and pathophysiological roles of the mPTP in the heart.....	16
Figure 11 Scheme of PKA holoenzyme activation.....	19
Figure 12 Schematic representation of Epac 1 and 2.....	20
Figure 13 cAMP-PKA signalling pathways in the heart.....	23
Figure 14 Cyclase-specific reagents to study sources of cAMP in mammalian cells...	25
Figure 15 Isoforms of soluble adenylyl cyclise.....	26
Figure 16 Bicarbonate induces active site closure.....	26
Figure 17 Mechanisms for the sAC-dependent regulation of cell death and growth...	29
Figure 18 Diagram of mito-sAC regulatory pathway of OXPHOS.....	32
Figure 19 Cyclic nucleotide signaling and regulation.....	33
Figure 20 Structure and domain organization of 11 mammalian PDEs families.....	34
Figure 21 Model for the mitochondrial cyclic nucleotide signaling system.....	45
Figure 22 Physiological roles of cAMP signalosome in cardiac mitochondria.....	119
Figure 23 Scheme of the location of actors of the mitochondrial cAMP pathway and their anchorage at the IM.....	122

## List of tables

Table 1.1 Antagonists and agonists of EPAC activity.....	21
Table 3.1 The reagents used for cell culture.....	47
Table 3.2 Primary antibodies.....	47
Table 3.3 Secondary antibodies.....	48
Table 3.4 Medium for adult cardiomyocytes.....	49
Table 3.5 10 × ADS Buffer.....	50
Table 3.6 Plating medium.....	50
Table 3.7 Buffer H.....	59
Table 3.8 Buffer H +BSA.....	59
Table 3.9 Buffer S.....	61
Table 3.10 Oxygen consumption buffer.....	62

## List of abbreviations

$\Delta\Psi_m$	Mitochondrial membrane potential
2HE	2-hydroxyestradiol
AC	Adenylate cyclase
ANT	Adenine nucleotide translocator
$\beta$ -AR	Beta-adrenergic receptor
BAY	BAY-60-7550
cAMP	Cyclic 3',5'- adenosine monophosphate
CCCP	Carbonyl cyanide m-chlorophenyl hydrazone
CFP	Cyan fluorescent protein
cGMP	Cyclic 3',5'- guanosine monophosphate
CIL	Cilostamide
CNG	Cyclic nucleotide-gated channels
COX	Cytochrome oxidase
CsA	Cyclosporin a
DMEM	Dulbecco's Modified Eagle Medium
DMSO	Dimethyl sulfoxide
EPAC	Exchange proteins activated by cAMP
FADH <sub>2</sub>	Flavin– adenine dinucleotide
FRET	Fluorescence resonance energy transfer
GAPDH	Glyceraldehyde 3-phosphate dehydrogenase
GEF	Guanine-nucleotide-exchange factor
GPCR	G-protein-coupled receptors
HCN channel	Hyperpolarization-activated cyclic nucleotide-gated channels
HCX	H <sup>+</sup> /Ca <sup>2+</sup> exchangers
HF	Heart failure
IBMX	3-isobutyl-1-methylxanthine
IM	Inner membrane
LTCC	L-type calcium channel

MCU	Mitochondrial calcium uniporter
MPT	Mitochondrial permeability transition
NADH	Nicotinamide adenine dinucleotide
NCX	Na <sup>+</sup> /Ca <sup>2+</sup> exchangers
OM	Outer membrane
PDE	Phosphodiesterase
PKA	Protein kinase A
PLB	Phospholamban
PTP	Permeability transition pore
RO	Ro-20-1724
ROS	Reactive oxygen species
RYP	Ryanodine receptor
sAC	Soluble adenylyl cyclase
sAC <sub>fl</sub>	Full-length soluble adenylyl cyclase
sAC <sub>t</sub>	Truncated soluble adenylyl cyclase
TNF $\alpha$	Tumor necrosis factor $\alpha$
TnI	Troponin I
UCR	Upstream conserved regions
VDAC	Voltage-dependent anion channel
YFP	Yellow fluorescent protein

# **1 Introduction**

## **1.1 Mitochondria**

### **1.1.1 Structure of mitochondria**

Mitochondria are double membrane organelle in eukaryotic cells, responsible for ATP production. Mitochondria are about 0.5–1 $\mu$ m in diameter and up to 7 $\mu$ m long. Their shape and number depend on the particular tissue. They may appear as spheres, rods or filamentous bodies, but the general architecture is conserved (Figure 1)<sup>1</sup>. The number of mitochondria per cell varies depending on the energy requirement: tissues with a high capacity to perform aerobic metabolic functions such as skeletal muscle or kidney will have a large number/mass of mitochondria.

Mitochondria have two membranes, each composed of a phospholipid bilayer. The two membranes are quite distinct in appearance and in physico-chemical properties. The outer membrane (OM) is the gateway to the mitochondrion. It has porins to allow small molecules to enter into intermembrane space and protein complexes to allow the import of cytosolic proteins. In contrast, the inner membrane (IM) encloses and convolutes into the mitochondrial matrix, forming cristae. This serves to increase the surface of the IM, which carries the main enzymatic machinery of oxidative phosphorylation. The IM is much less permeable to ions and small molecules than the OM, therefore providing compartmentalization through separation of the matrix from the cytosolic environment.

The membranes create two compartments: the intermembrane space and the matrix. The intermembrane space is the region between the IM and the OM. It has an important role in the primary function of mitochondria, which is oxidative phosphorylation. The matrix contains the enzymes that are responsible for the citric acid cycle reactions and other metabolic functions (see below). The matrix also contains dissolved oxygen (O<sub>2</sub>), water, carbon dioxide, and the recyclable intermediates that serve as energy shuttles.

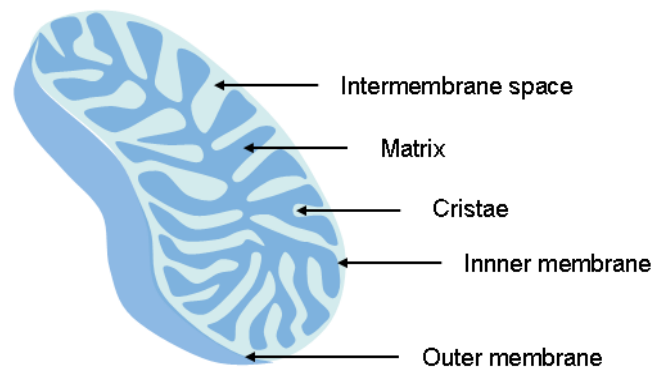


**Figure 1. Mitochondrial architecture.** Arrows indicate the 5 mitochondrial subcompartments.

## **1.1.2 Mitochondrial physiology**

### **1.1.2.1 Mechanism of energy production within mitochondria**

The citric acid cycle (also termed the tricarboxylic acid cycle or Krebs cycle) achieves the complete oxidation of acetyl–CoA, which is a central intermediate produced by various catabolic pathways such as glycolysis and fatty acid oxidation. The enzymes of this cycle are primarily located in the mitochondrial matrix, with the exception of succinate dehydrogenase, which is bound to the IM, forming part of complex II of the electron transport chain. The main function of the citric acid cycle is to oxidize the acetyl component of acetyl–CoA to two molecules of carbon dioxide and concomitantly to conserve the liberated free energy in the form of NADH (reduced form of nicotinamide–adenine dinucleotide) and FADH<sub>2</sub> (reduced form of flavin–adenine dinucleotide)<sup>2,3</sup>. The cellular energy carrier ATP is then produced by mitochondrial oxidative phosphorylation, for which NADH and FADH<sub>2</sub> are the substrates (Figure 2). Oxidative phosphorylation is an important cellular process in which O<sub>2</sub> and simple sugars are used to create ATP. Five protein complexes are involved in this process. The complexes are named complex I (NADH dehydrogenase), complex II (succinate dehydrogenase), complex III (cytochrome c reductase), complex IV (cytochrome-c oxidase) and complex V (ATPase). Within mitochondria, the five protein complexes are embedded in the IM. During oxidative phosphorylation, the protein complexes carry



out chemical reactions that drive the production of ATP<sup>4</sup>. Specifically, they create an unequal electrical charge on either side of the IM through a step-by-step transfer of negative electrons. This difference in electrical charge provides the energy for ATP production<sup>5</sup>.

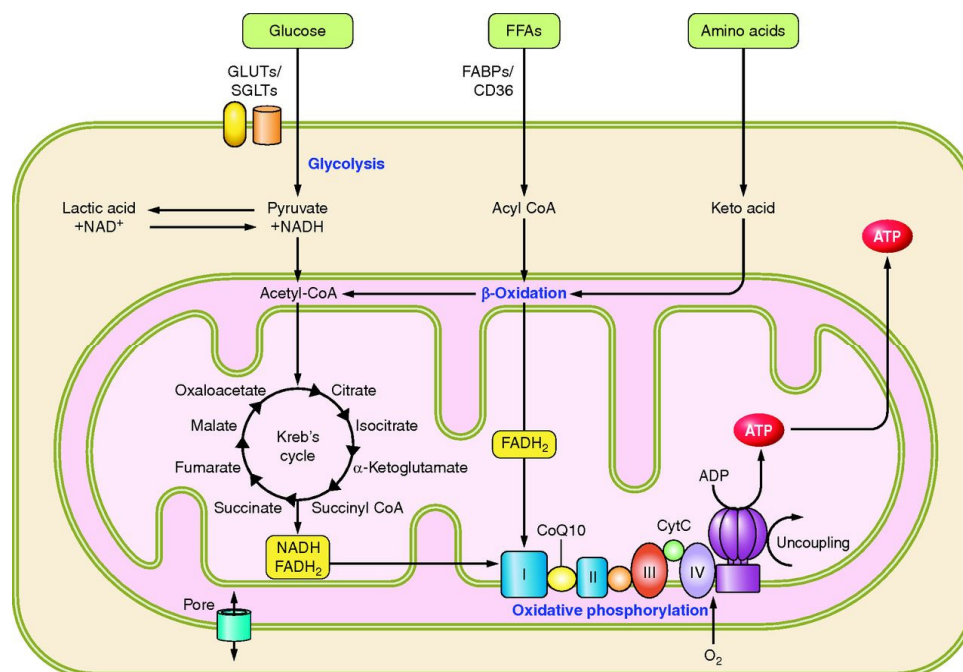


**Figure 2. Overview of fuel production within the mitochondria.** The major absorbed end products of food digestion are glucose (from carbohydrates), fatty acids (from lipids) and amino acids (from protein). All three classes of these nutrients can serve as fuel sources for the mitochondria to produce cellular energy in the form of ATP<sup>2</sup>.

### 1.1.2.2 Mitochondrial membrane potential

During normal mitochondrial respiration, electrons obtained from the oxidation of respiratory substrates are transferred along a chain of carriers that are situated in the inner mitochondrial membrane. Electrons from NADH and FADH<sub>2</sub> enter the electron-transport chain at complexes I and II, respectively. At complexes I, III and IV, the free energy released by the fall in redox potential of the passing electrons is used to translocate protons (H<sup>+</sup>) from the mitochondrial matrix into the intermembrane space<sup>6</sup>. This process generates a proton electrochemical potential gradient across the inner mitochondrial membrane, which is known as the proton-motive force. The proton-motive force is used to drive gradient-dissipating activities, including the generation of ATP by ATP synthase, which is the main pathway for the return of protons into the

matrix<sup>7</sup>. The proton-motive force has two components — the membrane potential, which arises from the net movement of positive charge across the inner mitochondrial membrane, and the pH gradient. Of these two components, the membrane potential contributes most of the energy that is stored in the gradient. At any given time, the membrane potential reflects the balance between processes that contribute to the generation of the proton gradient and those that consume it (Figure 3).

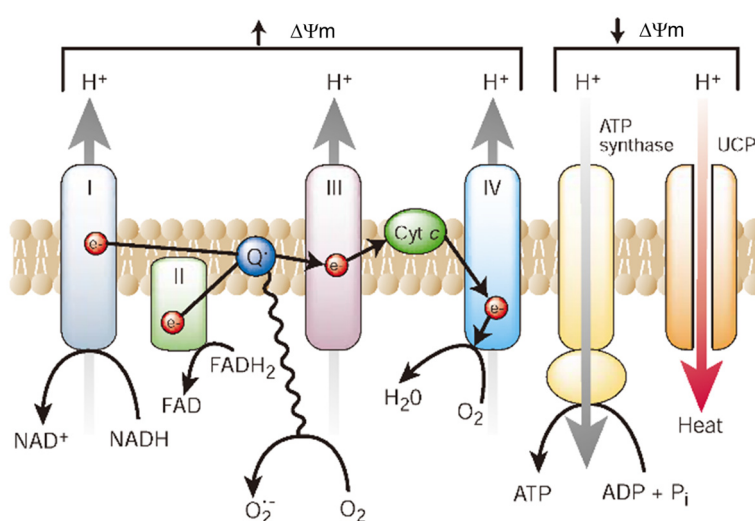


**Figure 3. Membrane potential generation in mitochondria.** Electron transport complexes I, II, III, IV and the mitochondrial ATP synthase (also known as complex V) work together in oxidative phosphorylation to harness energy for the cell. Complexes I, III and IV pump protons across the cristae membrane, creating the proton gradient that drives ATP synthesis<sup>8</sup>.

### 1.1.2.3 Mitochondrial calcium

In the heart, calcium (Ca<sup>2+</sup>)-based signalling is a universal mechanism through which extracellular as well as intracellular messengers modify the activity of target cells. Cells can decode Ca<sup>2+</sup> signals based on the characteristics of the intracellular changes in Ca<sup>2+</sup> concentration (amplitude, duration, frequency and localization) and generate outputs as diverse as proliferation or death<sup>9-11</sup>. Mitochondria are the first intracellular organelle to be associated with Ca<sup>2+</sup> handling<sup>12</sup>. Ca<sup>2+</sup> flowing through the plasma membrane via specialized channels or released from the endoplasmic reticulum/sarcoplasmic reticulum (ER/SR) predominantly enters into mitochondria. Indeed, Ca<sup>2+</sup> uptake into mitochondria is mainly mediated by a mitochondrial Ca<sup>2+</sup> uniporter (MCU) driven by

a highly negative membrane potential<sup>13-17</sup>. Another uptake system is a rapid uptake mode (RaM) which might contribute to mitochondrial  $\text{Ca}^{2+}$  uptake from fast cytosolic  $\text{Ca}^{2+}$  transients<sup>13,18</sup>. A mitochondrial ryanodine receptor is also reported to mediate  $\text{Ca}^{2+}$  uptake into rat heart mitochondria.  $\text{Ca}^{2+}$  accumulation by the MCU is counteracted by mitochondrial  $\text{Na}^+/\text{Ca}^{2+}$  exchangers (mNCX)<sup>19</sup> and mitochondrial  $\text{H}^+/\text{Ca}^{2+}$  exchangers (mHCX).  $\text{Ca}^{2+}$  efflux from mitochondria is mainly mediated by two pathways, an  $\text{Na}^+$ -dependent ( $\text{Na}^+-\text{Ca}^{2+}$  exchanger) pathway and an  $\text{Na}^+$ -independent ( $\text{H}^+-\text{Ca}^{2+}$  exchanger) pathway<sup>16</sup>. Under pathophysiological stress conditions, mitochondrial permeability transition pore (PTP) functions as a  $\text{Ca}^{2+}$  channel in mitochondria (Figure 4).

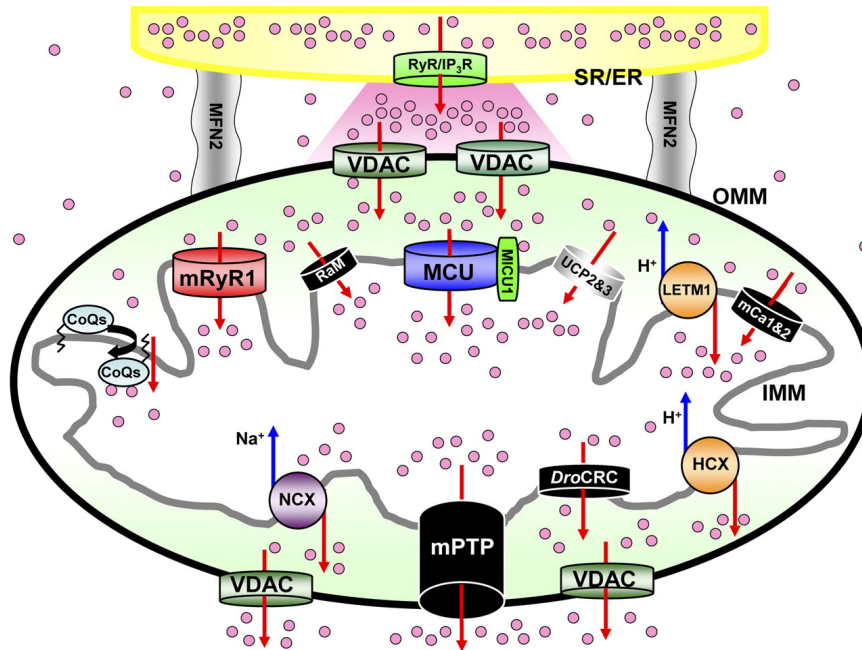


**Figure 4. Mitochondrial  $\text{Ca}^{2+}$  influx and efflux mechanisms.**  $\text{Ca}^{2+}$ -releasing sites of endoplasmic reticulum (ER)/Sarcoplasmic reticulum (SR),  $\text{IP}_3$  receptors ( $\text{IP}_3\text{R}$ ), or RyRs are facing microdomains between mitochondria and ER/SR.  $\text{Ca}^{2+}$  release from ER/SR dramatically changes  $[\text{Ca}^{2+}]$  at this microdomain. Then, mitochondria sense the high increases of  $[\text{Ca}^{2+}]$  at this microdomain, and  $[\text{Ca}^{2+}]$  propagates into the mitochondria matrix through a variety of  $\text{Ca}^{2+}$  channels/transporters. Mitochondrial  $\text{Ca}^{2+}$  influx is determined by the MCU, RaM, HCX, mRyR1. The mPTP, NCX, and HCX contribute to  $\text{Ca}^{2+}$  efflux in mammalian cells. Voltage-dependent anion-selective channels (VDAC) provide a pathway for  $\text{Ca}^{2+}$  and metabolite transport across the outer mitochondrial membrane (OM). The channels/transporters for which molecular identities are still unknown are shown as black. Red arrows show  $\text{Ca}^{2+}$  movements, and blue arrows show other ion movements<sup>13</sup>.

#### 1.1.2.4 Mitochondrial reactive oxygen species (ROS) production

Mitochondria are involved in maintaining a fine regulation of ROS level. The majority of cellular  $O_2$  that enters into mitochondria is reduced to water by the mitochondrial respiratory chain, whereas a fraction of consumed  $O_2$  can be converted to potentially cytotoxic ROS, such as superoxide anion radical ( $O_2^{\bullet-}$ ), due to the fact that the mitochondrion itself is the source of ROS. There are two major respiratory chain regions where ROS are produced, complex I (NADH coenzyme Q reductase) and complex III (ubiquinol cytochrome c reductase). Thus, any factor that affects the flow of electrons in the electron transport chain (ETC) can result in the leakage of electron to  $O_2$ , leading to the formation of  $O_2^{\bullet-}$ . The  $O_2^{\bullet-}$  is a primary radical that could produce other ROS, such as hydrogen peroxide ( $H_2O_2$ ) and hydroxyl radicals ( $^{\bullet}OH$ )<sup>20,21</sup>. An additional source, not linked to respiration, is located on the mitochondrial OM. The oxidative deamination of biogenic amines by monoamine oxidases is associated with a direct two-electron reduction of  $O_2$  to  $H_2O_2$  (Figure 5).

Of note, the compartmentalization of the sources of  $O_2^{\bullet-}$  and  $H_2O_2$  is functionally related and complementary to the cellular localization of antioxidant enzymes, such as superoxide dismutases, catalase, and glutathione peroxidases, leading to the establishment of regulated intracellular steady state levels of these two species in aerobic organisms<sup>22,23</sup>.

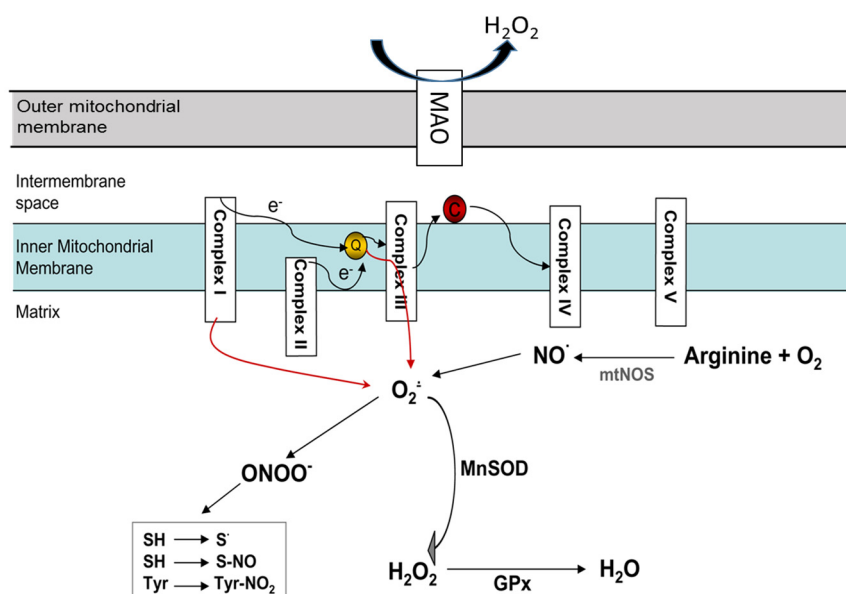


**Figure 5. Mitochondrial ROS stress.** In mitochondria, superoxide can be produced by respiratory complexes. Superoxide is detoxified by manganese superoxide dismutase (MnSOD) to hydrogen peroxide ( $H_2O_2$ ) in mitochondria. Glutathione peroxidases (GPxs) convert hydrogen peroxide to water. Nitric oxide (NO) generated from (mitochondrial) nitric oxide synthase (mt) NOS can compete with MnSOD and form peroxynitrite ( $ONOO^{\cdot}$ ). Monoamine Oxidases (MAO) catalyse the oxidative deamination of monoamines<sup>24</sup>.

### 1.1.3 Mitochondria and cell death

Mitochondria are deeply involved in cell fate via their numerous functions in energetic metabolism, cell growth and cell death<sup>25-27</sup>. In healthy cells, these functions are highly regulated to provide sufficient energy for cell function, maintain mitochondrial membrane integrity and avoid undesirable cell death. This is usually achieved by an orchestrated cooperation of molecular mechanisms controlling mitochondrial mass (mitophagy vs biogenesis), oxidative phosphorylation, redox and  $Ca^{2+}$  homeostasis, expression of pro- and anti-apoptotic proteins, and/or post-translational modification of mitochondrial proteins such as phosphorylation, acetylation, carbonylation and ubiquitination<sup>28-32</sup>. In the 90's, mitochondria have been demonstrated to control directly some forms of programmed/regulated cell death as well indirectly through energetic metabolism modulation. Since it is now admitted that several cell death modalities can be identified in mammals, it is important to re-evaluate the exact role of mitochondria in various processes such as apoptosis, necrosis, autophagic cell death, necroptosis and the so-called non-canonical cell deaths.

### **1.1.3.1 Mitochondrial oxidative stress and cell death**

Mitochondria consume most of the molecular oxygen available and represent the major site of ROS production in cells. ROS, if not detoxified, may cause cell dysfunction or death<sup>33</sup>. In fact, mitochondria are sensitive to the damaging effects of  $O_2^{\bullet-}$ <sup>34</sup>. Hence, ROS produced by the mitochondria can oxidize proteins and induce lipid peroxidation, thereby compromising the barrier properties of the mitochondrial membrane<sup>35</sup>. Another target of ROS is mitochondrial DNA (mtDNA), which is particularly susceptible to ROS-mediated damage due to its close proximity to the respiratory chain and the lack of protective histones<sup>22</sup>. Thus, the level of oxidatively modified bases in mtDNA is 10- to 20-fold higher than that in nuclear DNA<sup>36</sup>. mtDNA encodes several proteins essential for the function of the respiratory chain. Oxidative damage caused by ROS is probably a major cause of mitochondrial genomic instability and respiratory dysfunction<sup>37</sup>.

### **1.1.3.2 Mitochondrial $Ca^{2+}$ and cell death**

$Ca^{2+}$  plays a major role in cell death regulation. Mitochondrial  $Ca^{2+}$  accumulation can trigger the opening of a high-conductance pore in the IM. This phenomenon has been termed mitochondrial permeability transition (MPT) and is associated with drastic changes in mitochondrial morphology and functional activity. Pore opening is a  $Ca^{2+}$ -dependent process, but it can be facilitated by other factors, such as inorganic phosphate, ATP depletion, low pH and oxidative stress<sup>38</sup>. It is followed by osmotic swelling of the mitochondria matrix and rupture of the mitochondrial OM due to the difference in surface between OM and IM, leading to the release of mitochondrial intermembrane space proteins, including cytochrome *c*, into the cytosol. This event appears to play a key role in both apoptotic and necrotic cell death. The outcome seems correlated with the extent of the  $Ca^{2+}$  overload, which affects the duration of the PTP opening and thus the residual cellular ATP availability<sup>39</sup>. As ATP is required for apoptosis to progress, the PTP may ultimately control the switch between the two forms of cell death.

### 1.1.3.3 Mitochondrial permeability transition pore (mPTP) and cell death

The mPTP was initially characterized as a non-selective channel<sup>40-42</sup>. Pore opening is activated by  $\text{Ca}^{2+}$  together with phosphate and reactive oxygen species (ROS) and is inhibited by numerous factors including adenine nucleotides, low pH, divalent cations like  $\text{Mg}^{2+}$ , and CypD inhibitors<sup>43</sup>. While the biophysical properties of the mPTP are relatively well established, identification of the molecular constituents of the mPTP remains unresolved. Historically, biochemical studies suggested that the mPTP was constituted of the voltage-dependent anion channel (VDAC) in the OM, the adenine nucleotide translocator (ANT) in the IM, and CypD as its regulator in the matrix of the mitochondria (Figure 6)<sup>44</sup>. Recently, the mitochondrial F1F0ATP synthase has emerged as a strong candidate to be the core component of the mPTP in the IM<sup>45</sup>. The F1F0-ATP synthase is a multi-subunit enzymatic complex that couples proton translocation across the IM to ATP synthesis. The F0 proton-translocating domain of the ATP synthase is embedded in the inner membrane and is connected to the F1 catalytic domain through the central and peripheral stalks. Cyp D was initially found to modulate ATP synthase activity by binding to the OSCP subunit of the peripheral stalk and purified dimers of the F1F0-ATP synthase reconstituted into lipid bilayers recapitulated channel activity similar to that of the mPTP<sup>46</sup>. In addition to the potential mPTP constituents mentioned above, other proteins residing in the mitochondrial membrane have been suggested to be involved in the regulation of MPT. For example, the mitochondrial phosphate carrier (PiC) has been reported to be able to regulate MPT through interaction with Cyp D<sup>38,47</sup>. However, since the mPTP retained full function under phosphate free conditions, these findings collectively suggest that the PiC is not a direct pore component of the mPTP, but instead its ability to alter matrix Pi levels secondarily impacted pore opening<sup>46</sup>. In conclusion, future research is needed to fully identify the mPTP composition<sup>48</sup>.



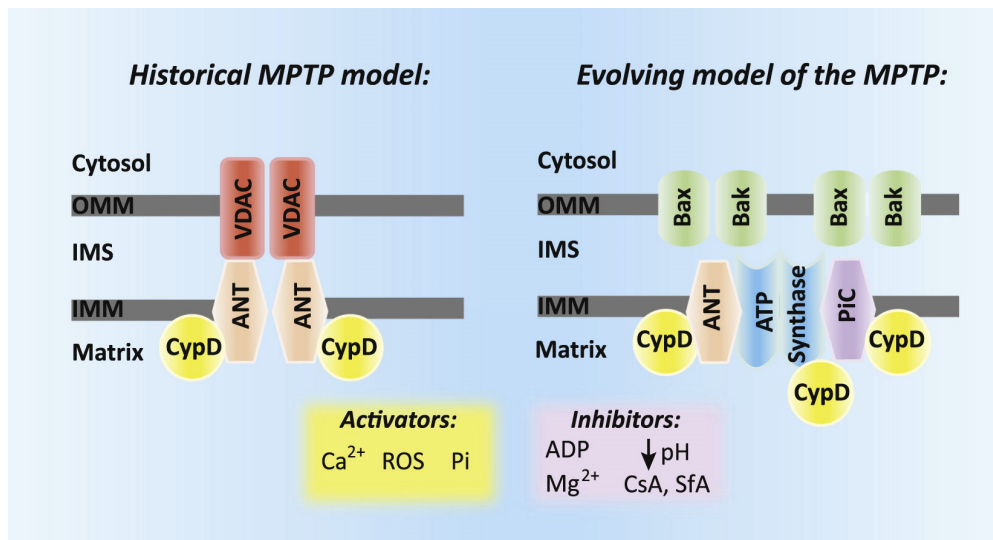


**Figure 6. Molecular Structure of the mPTP.** The original paradigm of the mPTP featured VDAC, ANT, and CypD as the core constituents of the complex (left). Genetic evaluation of putative mPTP components has shown that ANT, PiC, and CypD serve as pore regulators, while the BH3-domain pro-apoptotic proteins Bax/Bak function in the outer membrane to permit mitochondrial swelling and rupture once the inner membrane complex opens. The F1F0 ATP synthase has been suggested to be a candidate for the inner membrane pore-forming unit of the mPTP (right)<sup>46</sup>.

Mitochondrial membrane permeabilization is a critical step in the activation of cell death, either apoptotic or necrotic<sup>49</sup>. In the classical mitochondrial apoptotic pathway, OM permeabilization by the Bcl-2 family member proteins Bax and Bak allows for apoptogenic factors like cytochrome *c*, Smac/DIABLO and AIF to be released from the intermembrane space into the cytosol, leading to cell death<sup>50</sup>. In contrast, stimulation with Ca<sup>2+</sup> or ROS causes mPTP opening, leading to mitochondrial IM permeabilization,  $\Delta\Psi_m$  dissipation, respiratory chain dysfunction, cessation of mitochondrial ATP synthesis, organelle swelling, and outer membrane rupture<sup>38</sup>. This results in necrotic cell death, characterized by loss of plasma membrane integrity and membrane rupture<sup>51</sup>.

#### 1.1.4 Mitochondria and heart failure (HF)

##### 1.1.4.1 Heart anatomy

The heart consists of four compartments: the right and left atria and ventricles. The heart is oriented so that the anterior aspect is the right ventricle while the posterior aspect shows the left atrium (Figure 7). The atria form one unit and the ventricles another. The left ventricular free wall and the septum are much thicker than the right



ventricular wall. This is logical since the left ventricle pumps blood to the systemic circulation, where the pressure is considerably higher than for the pulmonary circulation, which arises from right ventricular outflow.

The heart has four valves. Between the right atrium and ventricle lies the tricuspid valve, and between the left atrium and ventricle is the mitral valve. The pulmonary valve lies between the right ventricle and the pulmonary artery, while the aortic valve lies in the outflow tract of the left ventricle.

The blood returns from the systemic circulation to the right atrium and from there goes through the tricuspid valve to the right ventricle. It is ejected from the right ventricle through the pulmonary valve to the lungs. Oxygenated blood returns from the lungs to the left atrium, and from there through the mitral valve to the left ventricle. Finally blood is pumped through the aortic valve to the aorta and the systemic circulation.

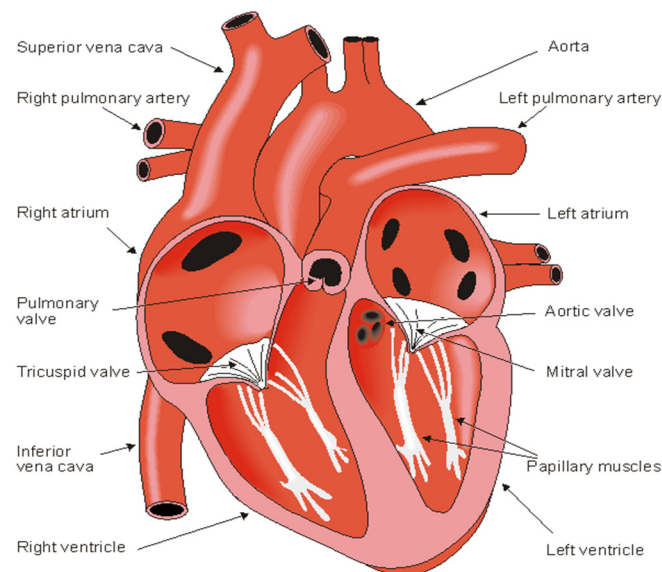


**Figure 7. The anatomy of the heart and associated vessels. (<http://www.bem.fi/book/06/06.htm>)**

#### **1.1.4.2 Heart failure**

HF is a complex multifactorial syndrome characterized by mechanical dysfunction of the myocardium and the inability of the heart to supply adequate amounts of blood to meet the perfusion and metabolic needs of the body<sup>52</sup>. Defects in bioenergetics, increased preload and afterload, altered signal transduction pathways, abnormalities of

Ca<sup>2+</sup> homeostasis, as well as neurohormonal dysregulation are major pathogenic factors for myocardial dysfunction in HF<sup>53</sup>. The mechanisms of HF are complex and multiple, but mitochondrial dysfunction appears to be a critical factor in the development of this disease. Thus, it is important to focus research efforts on targeting mitochondrial function in the failing heart in order to revive the myocardium and its contractile function.

#### **1.1.4.3 Mitochondrial energy synthesis and HF**

The high energy demands of the heart must be fulfilled in order to sustain continuous work. During HF, the dynamic metabolic network in the cardiomyocyte is perturbed, and these alterations cause energy depletion, directly affecting contractile function. Numerous studies have identified decreased high energy phosphate levels and flux as consistent features of HF. Importantly in human, HF changes all components of cardiac energetics: substrate utilization, ATP production and ATP transfer to the cardiac contractile apparatus<sup>54,55</sup>. Based on *in vivo* measurements by phosphorus magnetic resonance spectroscopy, ATP levels of patients with dilated cardiomyopathy (DCM) were reduced by 35%<sup>56</sup>. Diminished ATP levels are also found in a rat coronary ligation model of HF<sup>57</sup>. Similarly, a progressive decrease in ATP occurs during the development of HF in a canine model<sup>58</sup>. Mitochondrial structural abnormalities and decreased citrate synthase activity, provided further evidence of impaired mitochondrial function<sup>59</sup>. ATP synthase activity was decreased 50% in Doberman pinschers with inherited dilated cardiomyopathy<sup>60</sup>. Recently, Rosca et al. found that the ATP synthase activity in skeletal muscle mitochondria was also reduced in canine pacing-induced model of HF, suggesting systemic changes<sup>61</sup>. Thus, in multiple models, there is a clear decrease in ATP synthesis capacity and a decrease in overall ATP levels in HF.

#### **1.1.4.4 ROS and HF**

Mitochondria are considered a key source for pathological increases in ROS, mainly as a result of electron transport chain uncoupling at the level of complexes I and III<sup>62,63</sup>. The generated ROS under oxidative stress may contribute to potential mitochondrial

dysfunction, impairing myocardial energetics in HF<sup>64</sup>. Among the damage induced by generated ROS at the cellular level, mtDNA remains the major target (Figure 8)<sup>65</sup>. mtDNA contains about 16.5 kb of circular double-stranded DNA to encode 13 protein components of the ETC. Mitochondrial function is controlled by the mtDNA, as well as factors that regulate mtDNA transcription and/or replication. A large part of the  $O^{\cdot 2-}$ , which is formed inside the mitochondria cannot pass through the membrane and hence affect the DNA. However, in HF, impaired mitochondrial bioenergetic function with decreased electron transport systems could cause increased oxidative stress<sup>66-68</sup>. Thus, mitochondrial dysfunction and ROS are tightly linked elements of an interdependent feed-forward circuit that promotes the pathogenesis of HF.

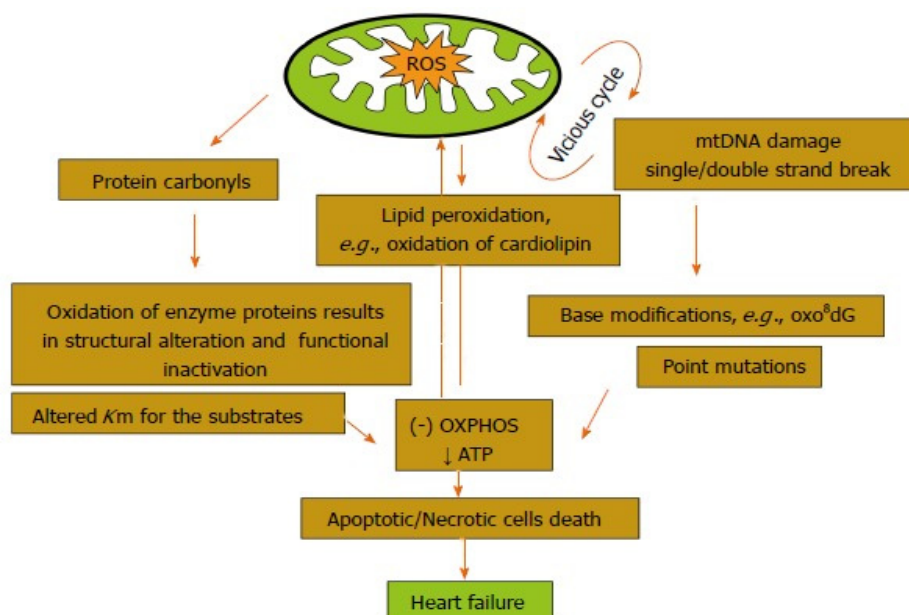


**Figure 8. Damage induced by reactive oxygen species in mitochondria.** OXPHOS: Oxidative phosphorylations; ROS: Reactive oxygen species<sup>65</sup>.

In addition to the mtDNA mutations, damage to protein and lipid molecules in the mitochondrial membrane can contribute to the declined OXPHOS. Cardiolipin, an essential phospholipid present in the IM of mitochondria that serves as a cofactor for a number of critical mitochondrial transport proteins and retains cytochrome *c* at the IM through the electrostatic interaction, declines during the oxidative damage<sup>69</sup>. Peroxidation of cardiolipin and its release into the cytosol can execute apoptotic cell death.

#### 1.1.4.5 Mitochondrial $\text{Ca}^{2+}$ and HF

HF is also characterized by dysregulation of  $\text{Ca}^{2+}$  homeostasis within the myocyte<sup>70-72</sup>. Mitochondrial  $\text{Ca}^{2+}$  uptake from the cytosol controls the rate of energy production, which is diminished in HF<sup>73</sup>. The MCU and the mNCX are the major pathways for  $\text{Ca}^{2+}$  transport across the cardiac mitochondrial IM<sup>74</sup>(Figure 9). In failing human cardiomyocytes, the kinetics of mitochondrial  $\text{Ca}^{2+}$  uptake are altered, and increased resting  $\text{Na}^+$  in HF contributes to impaired mitochondrial  $\text{Ca}^{2+}$  uptake<sup>75</sup>. Simulated ischemia studies in which the oxygen and glucose were excluded, show a rise in mitochondrial  $\text{Ca}^{2+}$ <sup>76-79</sup>. It is also observed that the rise in mitochondrial  $\text{Ca}^{2+}$  during ischemia was inhibited by clonazepam, an inhibitor of mNCX, suggesting a role for mitochondrial NCX operating in the reverse mode to increase mitochondrial  $\text{Ca}^{2+}$ <sup>76</sup>. Ru360, a specific MCU inhibitor, improves cardiac post-ischemic functional recovery in rats in vivo<sup>80</sup>. Interestingly, by directly patch clamping the IM of mitochondria from non-failing and failing human hearts, Michels et al. identified that the  $\text{Ca}^{2+}$  uptake is mediated by 2 mitochondrial  $\text{Ca}^{2+}$ -selective channels, which are functionally impaired in HF<sup>81</sup>. By using transgenic mice with enhanced sarcolemmal L-type  $\text{Ca}^{2+}$  channel activity, Nakayama et al. show that loss of Cyp D, a regulator of mPTP, blocked  $\text{Ca}^{2+}$  influx-induced necrosis of myocytes, HF, and isoproterenol-induced premature death<sup>70</sup>. Mitochondrial  $\Delta\Psi_m$ , cytochrome *c* oxidase levels, oxidase-dependent respiration and the rate of ATP synthesis were decreased in HF compared to normal controls, and these changes were reversed by treating for 24 hours with CsA<sup>82</sup>. These observations suggest that mPTP opening contributes to the loss of mitochondrial function observed in the failing hearts and inhibition of mPTP opening represents a potential therapeutic target for the treatment of HF.

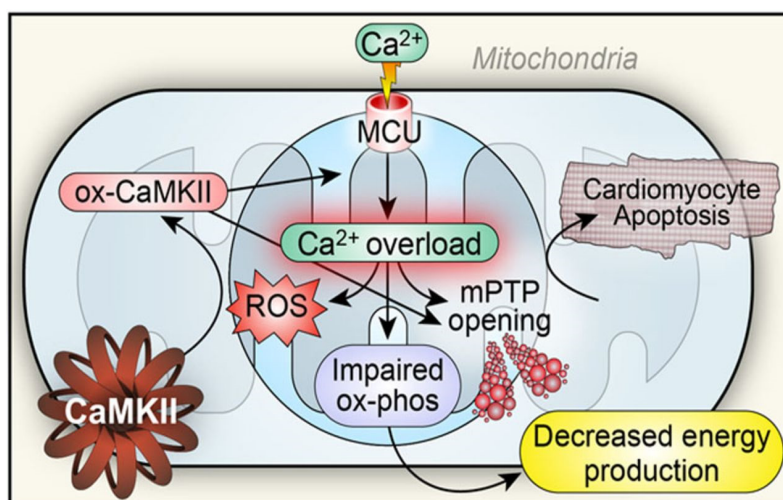


**Figure 9. Ca<sup>2+</sup> overload, impaired metabolism, and cell death in heart failure.** Excessive mitochondrial Ca<sup>2+</sup> triggers mPTP opening, leading to cell death. Mitochondria Ca<sup>2+</sup> overload also promotes ROS generation, which could oxidize CaMKII (ox-CaMKII) and cause sustained activation of CaMKII. The ox-CaMKII could enhance MCU activity and further increase mitochondrial Ca<sup>2+</sup> overload, promoting mPTP opening and impairing energy metabolism in heart failure<sup>68</sup>.

#### 1.1.4.6 mPTP and HF

Progression of HF is associated with diminished energy metabolism, Ca<sup>2+</sup> mishandling, and ROS generation that together can favor mPTP opening (Figure 10). Indeed, mPTP opening has been demonstrated in HF induced by myocardial infarction in rats<sup>83</sup> and intracoronary microembolizations in dogs<sup>84</sup>, as well as in Ca<sup>2+</sup>-induced cardiomyopathy<sup>85</sup> and diabetic cardiomyopathy<sup>86</sup>. Notably, some studies have demonstrated that the extent of mPTP opening in failing hearts 12 and 18 weeks after coronary artery ligation<sup>83</sup> is lower than that found following acute IR<sup>87-89</sup>. Mitochondrial Ca<sup>2+</sup> overload following ischemic injury, can promote opening of mPTP, contributing to the process of necrosis and/or apoptosis that lead to HF<sup>90-92</sup>. In animal models, inhibition of mPTP opening by either CsA or genetic ablation of Cyp D provides strong protection from both reperfusion injury and congestive HF and even, in a small group of patients<sup>93</sup>. It has been reported that CsA protects cells subjected to simulated ischemia and reperfusion. Protection was defined as the ability to recover rod shape and respond to electrical stimulation<sup>94</sup>. So, mPTP can be a target of pharmacological agents that interact directly with main pore components and block

pore opening or indirectly through reduction of the level of mPTP inducers to regulate HF. However, when used in a large clinical trial (CIRCUS), cyclosporin A failed to exhibit a cardioprotection against myocardial infarction damages<sup>95</sup>.

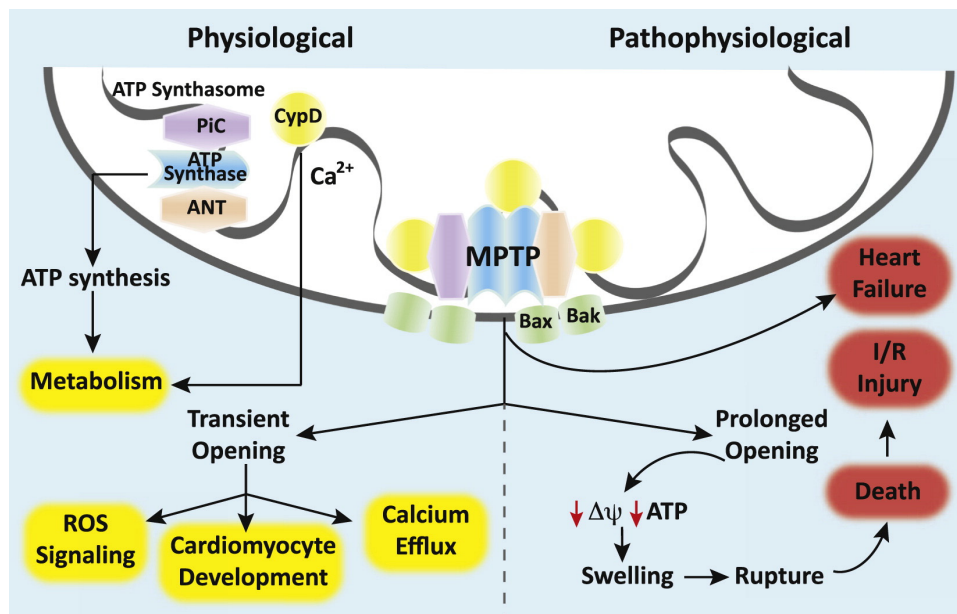


**Figure 10. Physiological and pathophysiological roles of the mPTP in the heart.** Transient opening of the mPTP is implicated in ROS signaling, cardiomyocyte development, and mitochondrial  $\text{Ca}^{2+}$  efflux. Key components of the mPTP (PiC, ANT, and the  $\text{F}_1\text{F}_0$ -ATP synthase) comprise the ATP synthasome, thereby providing a direct link to mitochondrial energy metabolism. Prolonged mPTP opening leads to loss of mitochondrial membrane potential, cessation of ATP synthesis, mitochondrial swelling, rupture, and death. Unregulated mPTP opening has been found to contribute to cardiac ischemia-reperfusion injury and the development of heart failure<sup>46</sup>.

## 1.2 cAMP signalling pathway

Cyclic adenosine 3', 5'-monophosphate (cAMP) is the first second messenger to be identified which has a fundamental role in the cellular response to many extracellular stimuli. cAMP activates intracellular targets including protein kinase A (PKA), the exchange proteins activated by cAMP (Epac), and cyclic nucleotide-gated channels. By activating these effectors, it controls numerous cellular functions, including cell growth, cell differentiation, cell movement, migration, learning and memory formation, control of hormone secretion, metabolism and gene transcription<sup>96</sup>. The intracellular cAMP levels are regulated by the balance of two enzymes: adenylyl cyclases (AC) and cyclic nucleotide phosphodiesterases (PDE).



### 1.2.1 cAMP production

The adenylate cyclase (AC) play a fundamental role in signal transduction membrane to the cytoplasm by ensuring the synthesis of cAMP from ATP. Indeed, in the presence of  $Mg^{2+}$ , they catalyze the conversion of ATP to cAMP and release pyrophosphate. Currently, in mammals, nine genes encode membrane nine isoforms (AC1-AC9) and a gene encodes a soluble isoform (sAC). This sAC is not regulated by G proteins but by  $HCO_3^-$  and  $Ca^{2+}$ <sup>97,98</sup>. Most AC (soluble AC are the exception) are activated downstream from G-protein-coupled receptors (GPCRs) such as the  $\beta$ -adrenoreceptor by interactions with a subunit of the Gs protein.

The AC 1 to 9 are transmembrane enzymes and are all activated subunit  $\alpha_s$  of G protein. Structurally, they consist of two transmembrane domains (M1 and M2) and two cytoplasmic domains (C1 and C2 subdivided into C1 $\alpha$ , C1 $\beta$  and C2 $\alpha$ , C2 $\beta$ ). Both M1 and M2 are 6 transmembrane helical segments. Despite their strong resemblance topology with transporters and ion channels, their function remains partially unknown<sup>99</sup>. C1 $\alpha$  areas (at the intracellular loop which links M1 and M2) and C2 $\alpha$  (at the C-terminus) are highly conserved and heterodimerize to form the catalytic site of the enzyme with the binding sites of the ATP and forskolin. The domain C1 $\beta$  is regulated by the complex  $Ca^{2+}$ /calmodulin (AC1, 3, 8) and has a phosphorylation site for PKA (AC5, 6); C2 $\beta$  and the field is only present in the isoforms AC1, 2, 3 and 8<sup>100</sup>. C1 $\alpha$  contains the site binding to the subunit I of the G protein (AC1, 3, 5, 6, 8) while the region has C2 $\alpha$  a binding site for  $\alpha_s$  and  $\beta\gamma$  subunits and a phosphorylation site for PKC.

### 1.2.2 cAMP targets

Three groups of direct cAMP effectors molecules have been described, which play a key role in the complexity and specificity of cAMP signaling: PKA, the guanine-nucleotide-exchange factor (GEF) Epac and cyclic nucleotide-gated ion channels.

#### 1.2.2.1 PKA

Protein kinase A (PKA) is a serine/threonine kinase that phosphorylates serine or threonine residue of substrate after the increase of cytoplasmic cAMP concentration.

Physiological regulation of PKA is versatile: for example in cardiac myocyte, phosphorylation of plasma membrane and SR proteins by PKA increases intracellular  $\text{Ca}^{2+}$  recruitment and enforces contraction. In the absence of cAMP, PKA is an enzymatically inactive tetrameric holoenzyme consisting of two catalytic subunits (C) bound to a regulatory subunit (R) dimer (Figure 11). cAMP binds co-operatively to two sites on each R promoter. Upon binding of four molecules of cAMP, the enzyme dissociates into an R subunit dimer with four molecules of cAMP bound and two free, active C subunits that phosphorylate serine and threonine residues on specific substrate proteins.

Initially, two different isozymes of PKA, termed type I and II (PKAI and PKAII, respectively), were identified based on their pattern of elution from DEAE-cellulose columns<sup>101,102</sup>. The PKAI and PKAII, eluting at salt concentrations between 25 to 50 mM and 150 to 200 mM NaCl, respectively, were shown to contain C subunits associated with two different R subunits, termed RI and RII. However, over the last 10 years molecular cloning techniques have revealed a great heterogeneity in both R and C subunits which reveal the potential of multiple isozymes of PKA.

Cloning of cDNAs for regulatory subunits have identified two RI subunits termed  $\text{RI}\alpha$ <sup>103,104</sup> and  $\text{RI}\beta$ <sup>105,106</sup> and two RII subunits termed  $\text{RII}\alpha$ <sup>107,108</sup> and  $\text{RII}\beta$ <sup>109,110</sup> as separate gene products. Furthermore, two distinct C subunits were initially identified by molecular cloning, and were designated  $\text{C}\alpha$ <sup>111</sup> and  $\text{C}\beta$ <sup>112,113</sup>. The cloning of the  $\text{C}\alpha$  and  $\text{C}\beta$  subunits from human testis by low homology screening also revealed an additional C subunit, designated  $\text{C}\gamma$ <sup>114</sup>. Recent work has also revealed the existence of splice variants of the human form of  $\text{C}\alpha$  ( $\text{C}\alpha 2$ ), and a splice variant of the bovine form of  $\text{C}\beta$  ( $\text{C}\beta 2$ ). Recently, three brain specific splice variants of the mouse  $\text{C}\beta$  form ( $\text{C}\beta$ -1,  $\text{C}\beta$ -2 and  $\text{C}\beta$ -3) have also been cloned.  $\text{C}\beta$  -1 correspond to the previously described  $\text{C}\beta$ <sup>112</sup>, whereas  $\text{C}\beta$  -2 and  $\text{C}\beta$  -3 represent N-terminal truncated splice variants, expected to be catalytically fully active.



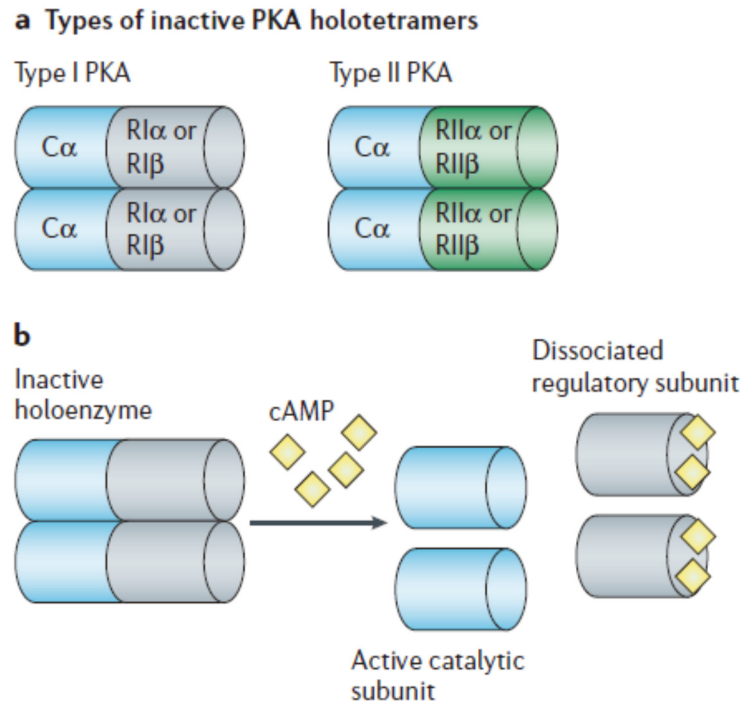


**Figure 11. Schematic diagram of PKA structure and activation.** a. Schematic of the inactive PKA holoenzyme depicts the type I and the type II holotetramer. b. Schematic illustration of cAMP-dependent activation of the PKA holotetramer. Two cAMP molecules bind to each regulatory subunit within an inactive holotetramer. The binding produces a conformation change, and the regulatory subunits dissociate from the catalytic units. The liberated catalytic units are enzymatically active and can phosphorylate downstream targets<sup>115</sup>.

### 1.2.2.2 Epac

Recently, a family of novel cAMP sensor proteins, named Epac (exchange protein directly activated by cAMP) or cAMP-GEF (cAMP-regulated guanine exchange factor), has been identified<sup>116,117</sup>. Epac proteins bind to cAMP with high affinity and activate the Ras superfamily small GTPases Rap1 and Rap2. Rap1 was initially identified as an antagonist for the transforming function of Ras<sup>118,119</sup>. Rap1 can be activated in response to a variety of second messengers including cAMP<sup>119</sup>. Although PKA can phosphorylate Rap1 at its C-terminus, PKA phosphorylation is not required for cAMP-dependent activation of Rap1.

Epacs are guanine nucleotide exchange factors (GEFs) for the Ras-like GTPases Rap1 and Rap2<sup>119</sup>. There are two mammalian Epac isoforms, Epac1 and Epac2<sup>116,117</sup> (Figure 12). Epac1 displays a wide tissue distribution, the expression of Epac2 is more restricted and appears to be limited to the brain, pancreas, testes, and other secretory cells<sup>117</sup>.

Epac1 and Epac2 share structural motifs throughout their regulatory and catalytic domains, with the dishevelled–EGL–pleckstrin homology domain (DEP), principal CNBD, Ras exchange motif (REM), Ras association domain (RA), and catalytic CDC25 homology domain (CDC25-HD) being heavily conserved between the two isoforms. The difference between Epac1 and Epac2 is the presence of an additional CNBD within the N terminus of Epac2 (CNBD1)<sup>120</sup>. CNBD1 exhibits a reduced affinity for cAMP and is unable to induce GEF activity following cAMP binding. Regulation of Epac activity is governed by intermolecular interactions between the regulatory CNBD and catalytic CDC25-HD domains. The ‘closed’ form of the enzyme is stabilised by a hinge helix and an ionic latch, which lock the CNBD over the CDC25-HD domain. These interactions inhibit GEF activity by limiting substrate access to the CDC25-HD<sup>121,122</sup>. Binding of cAMP releases salt bridges formed with the ionic latch and unwinds the hinge helix, thereby allowing the CNBD to rotate away, creating an ‘open’ form where the CDC25-HD is exposed for interaction with GDP-bound Rap1 and Rap2<sup>123-128</sup>. This triggers GDP release and subsequent GTP binding and activation, leading to downstream signalling<sup>129</sup>.

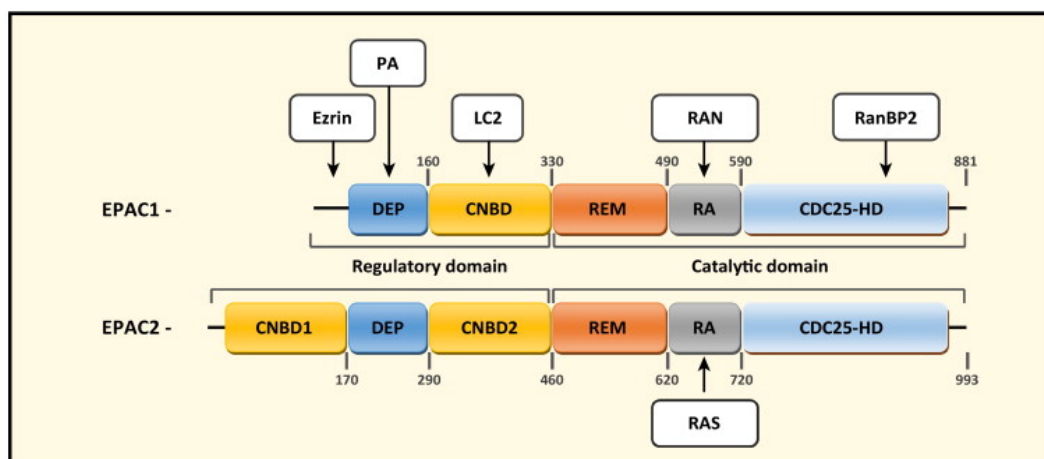


**Figure 12. Schematic representation of Epac 1 and 2.** Individual domains indicated: DEP, dishevelled–EGL–pleckstrin homology domain; CNBD, cyclic nucleotide-binding domain; REM, Ras exchange motif; RA, Ras association domain; CDC25-HD, CDC25 homology domain. Interacting partners are shown with their binding sites in the EPAC proteins indicated<sup>129</sup>.

The discovery of Epac proteins as a new family of intracellular cAMP effector suggests that the cAMP-mediated signaling mechanism is much more complex than what was believed earlier. Many cAMP-mediated effects, which were previously thought to act through PKA alone, may also be transduced by Epac. So far, extensive studies have shown that Epac proteins are involved in numerous of cAMP-related cellular functions such as cell adhesion<sup>130,131</sup>, cell-cell junction<sup>132,133</sup>, exocytosis/secretion<sup>134-137</sup>, cell differentiation<sup>138</sup> and proliferation<sup>139</sup>, gene expression<sup>140</sup>, apoptosis<sup>141,142</sup> and cardiac hypertrophy<sup>143,144</sup>.

**Table 1.1 Antagonists and agonists of EPAC activity**

<b>Antagonist</b>	<b>Chemical name</b>	<b>Isoform targeted</b>	<b>refs</b>
CE3F4	5,7-Dibromo-6-fluoro-2-methyl-1,2,3,4-tetrahydroquinoline-1-carbaldehyde	Epac1	145
ESI-05	4-Methyl-2,4,6-trimethylphenylsulfone	Epac2	146,147
ESI-07	Undisclosed	Epac2	146
ESI08 HJC0197/ HJC0198	5-Cyano-6-oxo-1,6-dihydro-pyrimidine	Epac1 and Epac2	147,148
ESI-09	3-(5-Tert-butyl-isoxazol-3-yl)-2-[(3-chloro-phenyl)-hydrazno]-3-oxo-propionitrile	Epac1 and Epac2	149,150
5225554 and 5376753	Undisclosed (barbituric/thiobarbituric acid)	Epac1	151,152
<b>Agonist</b>	<b>Chemical name</b>	<b>Isoform targeted</b>	<b>refs</b>
8-cpt-20-o-mecamp(007)	8-(4-Chlorophenylthio)-20-Omethyladenosine-30,50-cyclic monophosphate	Epac1 and Epac2	153,154
SUs	Tolbutamide Glibenclamide Gliclazide	Epac2	149,155-157
Scottish Biomedical (SB) compounds	Undisclosed	Epac1 and Epac2	158

### **1.2.2.3 HCN and CNG channels**

The HCN channels (activated cyclic nucleotide gated hyperpolarization channels) are voltage-gated channels, activated by hyperpolarization and regulated by cAMP and cGMP. These channels are thought to contribute to automation in cardiac cells sinoatrial node and atrioventricular<sup>159,160</sup>. Four isoforms (HCN 1-4) have been described in vertebrates. The HCN3 isoform is specifically expressed at the neurons while HCN 1, 2 and 4 are detected in the brain and heart. The isoform HCN2 is mainly expressed in the atrial and ventricular myocytes and the HCN4 is expressed in sino-atrial cells<sup>161,162</sup>.

CNG channels (cyclic nucleotide-gated channels) are cationic channels that are directly activated by cAMP or cGMP. CNG channels are non-selective cation channels that are found in the membranes of various tissue and cell types, and are significant in sensory transduction as well as cellular development. Unlike ligand-gated neurotransmitter receptors, CNG channels do not desensitize in the continuous presence of the ligand. Both the cooperative and sustained activation predestines CNG channels to serve as a molecular switch that faithfully tracks the cAMP or cGMP concentration in a cell. Although the channels do not desensitize, their activity is nonetheless modulated, notably by the  $\text{Ca}^{2+}$ -binding protein calmodulin and by phosphorylation.

### **1.2.3 cAMP signalling pathway in the heart**

In cardiac myocytes, cAMP generated in response to catecholamine and  $\beta$ -adrenoreceptors modulates many important processes such as contractility and relaxation. These effects are attributed to act mainly through the intracellular cAMP receptor, PKA. PKA has been shown to phosphorylate key  $\text{Ca}^{2+}$  handling proteins such as voltage gated L-type  $\text{Ca}^{2+}$  channel<sup>163</sup>, ryanodine receptor (RyR)<sup>164</sup>, and phospholamban<sup>165,166</sup>. These result in an increase in the sarcoplasmic reticulum  $\text{Ca}^{2+}$  release via RyR2 and enhanced uptake by SR  $\text{Ca}^{2+}$  pump, causing larger intracellular  $\text{Ca}^{2+}$  transients. Increased  $\text{Ca}^{2+}$  transients significantly enhance contractility. In addition,  $\beta$ -adrenoreceptors stimulation leads to PKA-mediated phosphorylation of troponin I (TnI), accelerating troponin C- $\text{Ca}^{2+}$  off rate and allowing faster force development and

shortening during systole and faster force relaxation and re-lengthening<sup>167</sup>. Catecholamines also induce PKA-mediated phosphorylation of phospholamban, a negative regulator of the sarcoplasmic reticulum  $\text{Ca}^{2+}$  ATPase, resulting in increased  $\text{Ca}^{2+}$  re-uptake in the sarcoplasmic reticulum and myofilament relaxation<sup>167</sup>. In addition to the machinery involved in the control of excitation-contraction coupling, other proteins expressed in cardiac myocytes are affected by cAMP and PKA-mediated phosphorylation, including metabolic enzymes and transcription factors<sup>168</sup> (Figure 13).

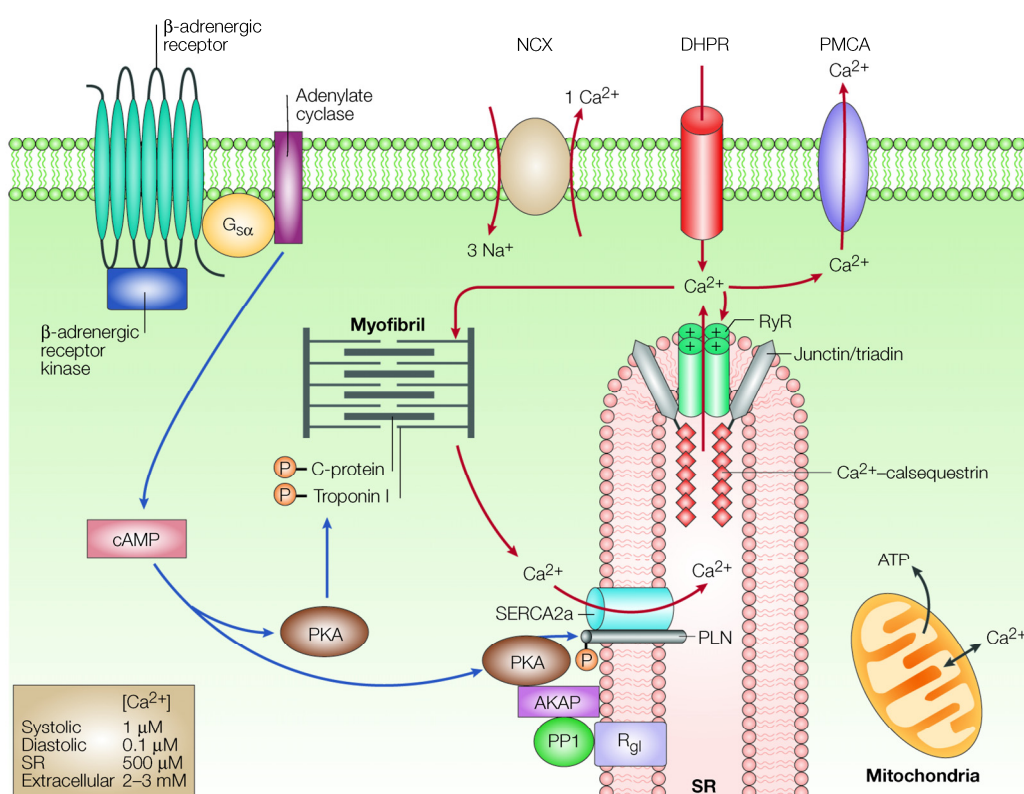


**Figure 13. cAMP-PKA signalling pathways in the heart.** Gs-protein activation via  $\beta$ -adrenoceptors increases cAMP by activating adenylyl cyclase. cAMP then activates PKA and causes increased cellular influx of  $\text{Ca}^{2+}$  by phosphorylation and activation of L-type  $\text{Ca}^{2+}$  channels, and enhanced release of  $\text{Ca}^{2+}$  by the sarcoplasmic reticulum in the heart. These and other intracellular events increase heart rate, dromotropy and relaxation rate<sup>169</sup>.

cAMP can also regulate cardiac functions through Epac. Epac activation induces an increase in spontaneous  $\text{Ca}^{2+}$ -oscillations in neonatal rat cardiac myocytes<sup>170</sup>. Epac activation also enhances cell-cell coupling between myocytes through gap junction formation<sup>171</sup>. Epac1 activation causes an increase in cell surface area, protein synthesis, and atrial natriuretic factor expression in adult rat ventricular cardiac myocytes<sup>172</sup>.

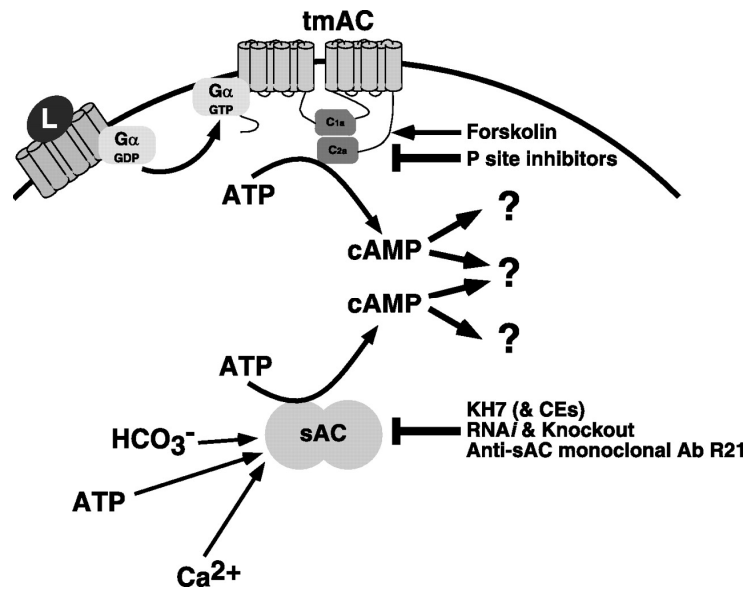
Hypertrophy-inducing Epac1 signaling involves small GTPases, phospholipase C, calcineurin and CaMKII, which activate nuclear factor of activated T-cells and myocyte enhancer factor 2<sup>173</sup>.

Although acute stimulation of the cAMP pathway is physiological and has beneficial effects on cardiac function, long-term sustained activation produces detrimental effects on the myocardium by inducing hypertrophy, dysfunction and ultimately HF<sup>174</sup>. This has been shown using different TG animal models including cardiac overexpression of the catalytic subunit of PKA,  $\beta$ 1- and  $\beta$ 2-ARs, Gs $\alpha$  protein, which all show dilated cardiomyopathy and HF as they age. Significant desensitization of  $\beta$ -ARs are observed in the development of cardiac hypertrophy and the progression of heart failure<sup>175</sup>. Transgenic mice that lack a hypertrophic response mechanism suffer less cardiac dysfunction than normal mice when facing long-term mechanical stress<sup>176</sup>.

#### **1.2.4 sAC**

##### **1.2.4.1 Overview of sAC**

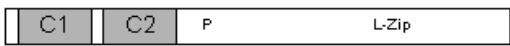

There are 10 known isoforms of adenylyl cyclase, 9 of which are membrane bound and are activated via stimulation of the Gs subunit of G-protein coupled receptors. The 10<sup>th</sup> member of this family is a soluble adenylyl cyclase, which has no transmembrane domains. Soluble adenylyl cyclase (sAC) can be differentiated from transmembrane ACs by its insensitivity to forskolin and G-protein stimulation. It is activated by bicarbonate, Ca<sup>2+</sup> and unique sensitivity to pharmacological and genetic modulators<sup>177-180</sup>. In contrast to membrane localization, sAC localizes to discrete compartments in the cell such as microtubules, mitochondria, the microtubule-organizing center, and the nucleus<sup>181-184</sup>. sAC was originally isolated from the testis<sup>185,186</sup> and has also been found in other tissues<sup>187,188</sup> (Figure 14).



**Figure 14. Cyclase-specific reagents to study sources of cAMP in mammalian cells.** L refers to ligand of G protein-coupled receptor; Gα-GDP and Gα-GTP refer to the inactive and active forms of the α-subunit of heterotrimeric G protein; C1α and C2α refer the two catalytic domains of tmACs; CE refers to catechol derivatives of estrogen, such as 2 or 4-hydroxyestradiol, which inhibit sAC by chelating the magnesium ion in the enzyme's active site. KH7 is a specific sAC inhibitor, which works via an unknown mechanism, identified in a small molecule screen<sup>189</sup>.

It was described as having two variants; an 187kDa full-length form (sACfl) and a 48kDa truncated version (sACt)<sup>186</sup>. The latter is a product of alternative splicing<sup>190</sup>. The full length protein consists of 2 catalytic subunits: a consensus P-loop (ATP/GTP binding site), and a leucine zipper sequence (dimerization/DNA binding domain) (Figure 13). In contrast, sACt consists only of the 2 catalytic subunits and is approximately 20 fold more active than the full-length form<sup>191</sup>. The catalytic domains of sAC are more closely related to those of cyanobacteria and myxobacteria than they are to transmembrane ACs<sup>186,191</sup>. Neither sACfl nor sACt contain a membrane-spanning domain. A third variant of sAC has recently been described which arises from an alternate start site preceding exon 5 and is found in somatic tissues<sup>192</sup>. The structure of the various isoforms is detailed below in Figure 15.



ISOFORM		SIZE	ACTIVITY
sAC <sub>fl</sub>		187 Kd	1X
sAC <sub>t</sub>		~50 Kd	20X

**Figure 15. Isoforms of soluble adenylyl cyclise.** In addition to its two catalytic domains (C1 and C2), sAC<sub>fl</sub> contains consensus P-loop (P) and Leucine Zipper (L-Zip) sequences. sAC<sub>t</sub>, which consists of just the catalytic domains, is 20 times more active than sAC<sub>fl</sub><sup>191</sup>.

#### 1.2.4.2 Stimulation of sAC

sAC is direct stimulation by  $\text{HCO}_3^-$  to produce cAMP, turning sAC into a putative physiological acid/base sensor<sup>177</sup>. The molecular mechanism of  $\text{HCO}_3^-$  stimulation has been elucidated for CyaC, a cyanobacterial adenylyl cyclase related to sAC<sup>193</sup>. This mechanism is believed to also apply to mammalian sAC<sup>194</sup>. Briefly,  $\text{HCO}_3^-$  induces an allosteric change that results in an increase in the  $V_{\text{max}}$  of sAC without changing its  $K_m$  for substrate ATP. The stimulatory effect of  $\text{HCO}_3^-$  on sAC and sAC-like enzymes is strictly dependent on a specific amino acid residue that is a threonine in mammals and a serine in bacteria and mollusks. The bicarbonate effect on sAC crystals is specific and pH-independent and cannot be induced with other anions, such as nitrate or acetate. Most markedly, bicarbonate induced closure of the active site and facilitated binding of the second metal ion (ion A), which serves as the catalytic metal (Figure 16).

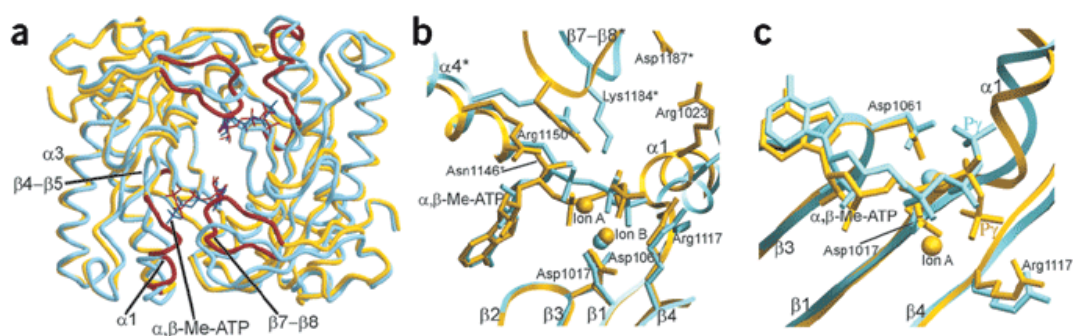


**Figure 16. Bicarbonate induces active site closure.** (a) Overlay of sAC structures in the open state (blue) and after bicarbonate addition (yellow and red). (b) Active site before (blue) and after (yellow) the bicarbonate-induced active site closure, showing the recruited second metal ion and the structural rearrangements described in the text. (c) Close-up view for the remodeling of Pβ and Py of the ATP analog upon bicarbonate induced active site closure<sup>193</sup>.



sAC is also activated by  $\text{Ca}^{2+}$ . In the presence of magnesium, high concentrations of  $\text{Ca}^{2+}$  stimulate the activity of sAC by increasing the enzyme's affinity for the substrate ATP from a  $K_m$  of about 10 mM to 1 mM<sup>179</sup>. X-ray crystallography revealed that  $\text{Ca}^{2+}$  replaces magnesium at the ion B pocket of the active site, coordinating the  $\beta$  and  $\gamma$ -phosphates of the bound substrate analog<sup>193</sup>. Therefore, while sAC is active with either magnesium or  $\text{Ca}^{2+}$  occupying both ion sites, its activity is highest with magnesium in the ion A site and  $\text{Ca}^{2+}$  in the ion B site<sup>195</sup>.

$\text{Ca}^{2+}$  may play a second modulatory role on sAC. Sub-micromolar concentrations of  $\text{Ca}^{2+}$  were observed to stimulate native sAC protein immunoprecipitated from testis<sup>196</sup>. Stimulation was independent of calmodulin and appeared to be due to an increase of  $V_{max}$ , not substrate affinity. These results suggest that post-translational modifications or interaction with an unknown regulatory protein may alter the  $\text{Ca}^{2+}$  affinity of the enzyme or confer some additional modulatory mechanism<sup>195</sup>.

#### **1.2.4.3 sAC and cell growth**

The role of sAC in cell growth has been reported<sup>197-199</sup>. First, the existence of a bicarbonate-sensitive nuclear cAMP signaling microdomain that mediates the PKA-dependent activation of the transcription factor CREB is revealed. This nuclear cAMP signaling pathway has been found to function independently from canonical tmAC signaling<sup>198</sup>. sAC migrates into the nucleus when differentiated cells are induced to re-enter the cell cycle. These reports support that sAC may be involved in cell proliferation. Suppressing the sAC activity of LNCaP and PC3 cells through sAC inhibitor treatment or sAC knockdown significantly reduced the rate of proliferation, leading to lactate dehydrogenase release, and induced apoptosis<sup>200</sup>. Subsequent analysis of the underlying cellular mechanisms revealed that the inhibition of sAC leads to cell cycle arrest in G2 phase. This effect results from the sAC inhibition-induced down-regulation of cyclin B<sub>1</sub> and CDK1, which are the key proteins involved in the G2/M transition.

sAC also seems to play a role in non-proliferative cell growth. An initial study demonstrated that sAC is expressed in embryonic neurons and generates cAMP in

response to netrin-1<sup>201</sup>. Moreover, the overexpression of sAC promotes axonal outgrowth, whereas sAC inhibition interferes with the effects of netrin-1. In agreement with this study, a recent report demonstrated that stimulating sAC with bicarbonate increases axon growth in cultured retinal ganglion cells, whereas suppressing sAC attenuates axon growth<sup>202</sup>. In particular, high levels of sAC expression were observed in rat embryonic neurons from the dorsal root ganglia and dorsal spinal cord as well as in rat postnatal retinal ganglion cells<sup>201,202</sup>, but only low levels of sAC expression could be found in embryonic dorsal root ganglia and spinal commissural neurons in the model used in the Moore et al. study<sup>203</sup> (Figure 15).

#### **1.2.4.4 sAC and cell death**

Initial studies on the intracellular distribution of sAC revealed co-localization of this cyclase within mitochondria<sup>184</sup>. Since mitochondria play an important role in apoptosis<sup>204</sup>, sAC may modulate the mitochondrial apoptosis pathway. It has been found that sAC is a key enzyme that controls the stress-induced activation of the mitochondrial apoptosis pathway. Further analyses of the downstream signaling revealed a key role for PKA in sAC signaling. In a recent study, the sAC/PKA axis is involved in the activation of the mitochondrial apoptosis pathway in oxysterol-treated smooth muscle cells<sup>205</sup>. An increase in intracellular cAMP concentrations under acidic stress in endothelial cells is detected<sup>206</sup>, while it is not possible to detect a rise in total cAMP or in the sAC-specific cAMP pool in ischemic cardiomyocytes or in oxysterol-treated smooth muscle cells<sup>205,207</sup>. Incubating endothelial cells or cardiomyocytes under simulated ischemia leads to  $\text{Ca}^{2+}$  overload<sup>208-210</sup>, which may contribute to the activation of sAC.

Furthermore, in another study, the translocation of sAC is accompanied by mitochondrial translocation of the pro-apoptotic protein Bax. Bax translocation seems to be a key downstream event in sAC-dependent apoptosis. Treatment with a Bax-inhibiting peptide prevented apoptosis<sup>207</sup>, inhibiting sAC or PKA abrogated the mitochondrial Bax translocation<sup>205,207</sup>. In addition, phosphorylation of Bax by PKA promotes mitochondrial Bax binding<sup>211</sup>. Therefore, mitochondrial sAC-translocation,

rather than activation, seemed to be the key mechanism responsible for triggering sAC-dependent apoptosis. In particular, the compartmentalization of PKA within mitochondrial microdomains<sup>212,213</sup> and the contribution of PKA to mitochondrial apoptosis<sup>214,215</sup> have both been demonstrated. Therefore, the stress-induced translocation of sAC from the cytosol to the mitochondria may lead to the selective activation of PKA localized within mitochondrial microdomains followed by the phosphorylation and activation of a sub-mitochondrial Bax pool and the release of cytochrome *c*. The precise mechanisms promoting mitochondrial translocation of sAC in response to different stress stimuli remains under investigation.

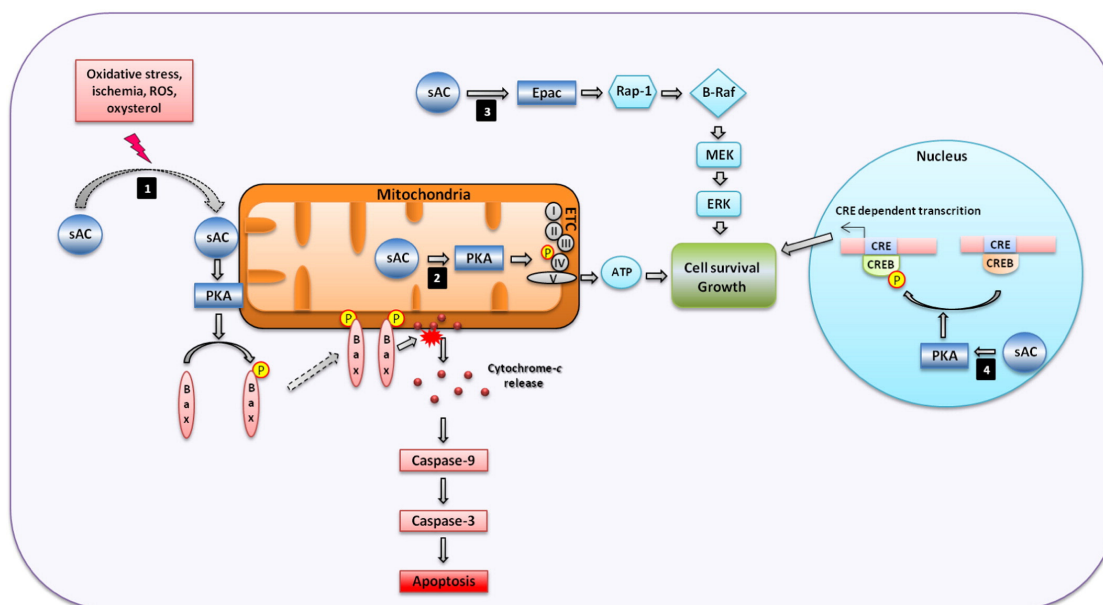


**Figure 17. Mechanisms for the sAC-dependent regulation of cell death and growth.** (1) Various stress factors lead to the translocation of the cytosolic pool of sAC to the mitochondria. The subsequent activation of PKA localized proximal to the outer mitochondrial membrane leads to the phosphorylation of the pro-apoptotic protein Bax followed by the binding of Bax to mitochondria, which activates the mitochondrial pathway of apoptosis. (2) Conversely, the intra-mitochondrial sAC/PKA pathway promotes cell survival via the phosphorylation/activation of several proteins in the mitochondrial electron transport chain (ETC), which leads to increased mitochondrial ATP synthesis. (3) Outside the mitochondria, sAC promotes cells proliferation and survival through the activation of the EPAC/B-Raf pathway. (4) The presence of a nuclear sAC/PKA/CREB pathway may contribute further to cell survival and growth<sup>200</sup>.

An important feature of sAC-dependent apoptosis is the generation of ROS. It has been demonstrated that the involvement of PKA in ROS production induced by various

stresses<sup>216,217</sup>. ROS has also been found to contribute to oxysterol or ischemia/reperfusion-induced apoptosis and cell death<sup>205,207,218-220</sup>. In contrast, Acin-Perez et al. suggest that intra-mitochondrial sAC/PKA signaling limits mitochondrial ROS production and that inhibiting sAC or PKA leads to a significant increase in ROS production<sup>221,222</sup>(Figure 17).

### **1.2.5 cAMP signalling in mitochondria**

#### **1.2.5.1 sAC localization in mitochondria**

sAC was first shown to be localized in mitochondria in COS7 cells stained with both  $\alpha$ N-term and  $\alpha$ C-term sAC antisera and the MitoTracker green<sup>223</sup>. In that work, sAC was detected in the mitochondria of cardiac and skeletal muscle. Functionally, DiPilato et al proposed for the first time that cAMP within mitochondrial matrix is not generated in the cytosol and transported across the inner membrane<sup>224</sup>, because the IM is impermeant to cAMP. Instead, Acin-Perez et al showed that matrix cAMP originated inside the mitochondria by the action of sAC, in response to metabolically generated carbon dioxide<sup>225</sup>. Several studies have confirmed the presence of this signaling pathway in the mitochondrial matrix, using different approaches, such as cAMP specific FRET sensors<sup>226,227</sup>. It was also shown that sAC activation increases ATP production in cells and isolated mitochondria<sup>226,228</sup>. sAC inhibition could decrease the ATP production, O<sub>2</sub> consumption, and cytochrome oxidase (COX) activity, whereas sAC activation by HCO<sub>3</sub><sup>-</sup> and Ca<sup>2+</sup> stimulates oxidative phosphorylation<sup>226,228</sup>.

#### **1.2.5.2 sAC activation in mitochondria**

HEK293 cell line expressing the full-length sAC cDNA accumulated cAMP upon sAC stimulation with HCO<sub>3</sub><sup>-</sup>. HCO<sub>3</sub><sup>-</sup> could significantly increase the COX activity and ATP synthesis in isolated mouse liver mitochondria. OXPHOS activity is increased by both HCO<sub>3</sub><sup>-</sup> and by exogenously generated CO<sub>2</sub>. These effects are not due to pH changes<sup>225</sup>. Di Benedetto et al. recently showed that CHO cells treated with 50 mM NaHCO<sub>3</sub> displayed a biphasic kinetic of cAMP generation, with an initial rise followed by a

plateau by using the cAMP sensor 4mt-H30<sup>226</sup>. Conversely, cells treated with the sAC inhibitor hydroxyl-estradiol (2HE) showed a significant decrease in cAMP generation.

In order to assess whether  $\text{Ca}^{2+}$  could stimulate cAMP inside mitochondria, CHO cells were transfected with 4mtH30<sup>229</sup>. Cytosolic  $\text{Ca}^{2+}$  increase from intracellular stores release, induced by the IP3-generating agonist ATP in combination with the SERCA pump inhibitor TBHQ, resulted in a significant increase in mitochondrial cAMP signal, indicating that  $\text{Ca}^{2+}$  stimulates sAC inside mitochondria<sup>226</sup>. It is also shown that overexpression of MCU resulted in an increase in mitochondrial cAMP, while MCU silencing decreased mitochondrial cAMP<sup>226</sup>. Moreover, increased frequency and amplitude of mitochondrial  $\text{Ca}^{2+}$  oscillations triggered an increase of cAMP in neonatal rat cardiomyocytes transfected with mtH30 sensor.

### **1.2.5.3 cAMP effectors in mitochondria**

PKA is reported to localize in the mitochondrial matrix<sup>230-232</sup>. Schwoch et al. found a two fold increase in PKA-specific activity in the mitochondrial matrix fraction relative to the whole mitochondrion, and they also demonstrated that both forms of regulatory subunits (RI and RII) reside on the matrix side of the mitochondrial IM in a variety of rat tissues, including liver, skeletal muscle, pancreas, and kidney<sup>231,233</sup>. PKA was independently found in the mitochondrial IM fraction from bovine heart<sup>230,232,234</sup>. And both RI and RII subunits were found in the IM and matrix of mitochondrial preparations, and the C subunit was found to be enriched in the matrix<sup>230-232</sup>. Matrix-confined PKA was proposed to phosphorylate cytochrome c oxidase (COXIV-I) to enhance oxidative phosphorylation<sup>225</sup>(Figure 18). However, prior data suggested that PKA activation inhibits OXPHOS<sup>235-237</sup>. In another study, hypoxia and ischemia increased mitochondrial PKA activity in heart. The PKA-dependent phosphorylation of COX subunits was postulated to reduce COX activity, leading to mitochondrial dysfunction in myocardial injury<sup>238</sup>. Recently, Lefkimmiatis et al found that the mitochondrial matrix of HEK and HeLa cells contains low or null PKA activity by using mitochondrial targeting FRET sensor<sup>227</sup>. And they also found that the OMM is rich in PKA activity<sup>227</sup>. Together with the observation that the intermembrane space contains

a functional AKAP<sup>239</sup>, they assumed that PKA targets might be phosphorylated during their transition into the matrix<sup>227</sup>.

Epac, another cAMP downstream effector, has been identified in mitochondria during interphase in COS-7 cells by co-localization of Epac-GFP with MitoTracker<sup>240</sup>. Moreover, the GTP-binding protein Rap1 has also found in mitochondria<sup>241,242</sup>. To date, the function of Epac in mitochondria is still unknown, and its association with this organelle requires further investigation.

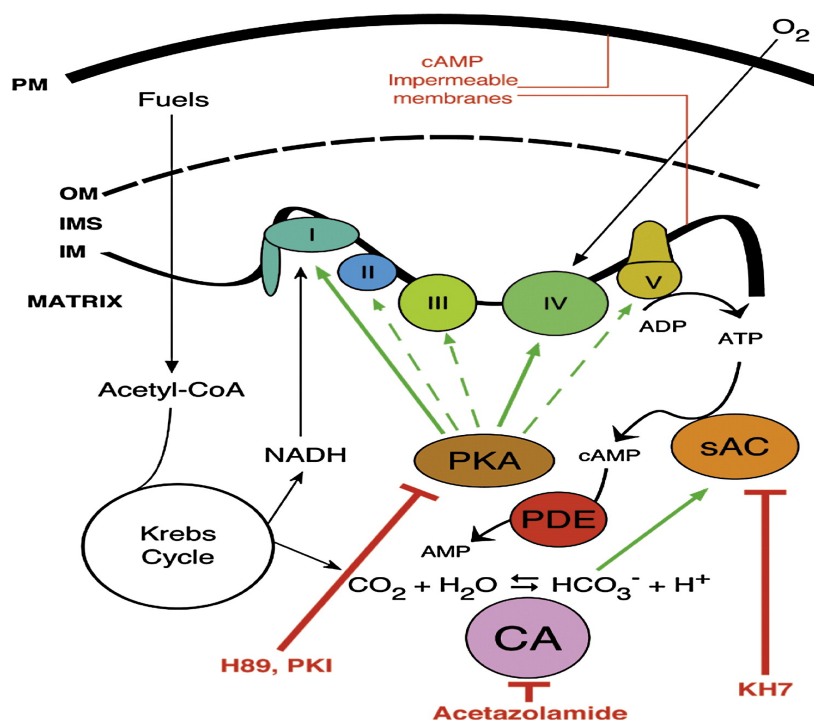


**Figure 18. Diagram of mito-sAC regulatory pathway of OXPHOS.** Activators and inhibitors of the various steps of the mito-sAC pathway are indicated<sup>225</sup>.

## 1.3 Phosphodiesterases (PDEs)

### 1.3.1 Overview of PDEs

Phosphodiesterases (PDEs) are a class of key enzymes which degrade cyclic Adenosine Monophosphate (cAMP) and/or cyclic Guanosine Monophosphate (cGMP) by hydrolysis of phosphodiester bonds. Thereby, they regulate intracellular levels of these ubiquitous second messengers. Cyclic nucleotides have been reported to play important

role in the regulation of a host of cellular functions involved in signal transduction and synaptic transmission.

PDEs constitute a large superfamily which contains 11 PDE families (PDE1 to PDE11), comprising 21 genes. PDE families are structurally related and highly regulated but differ in primary structures, catalytic properties, responses to specific inhibitors and modulators, and in their subcellular localization and targeting to specific, multimolecular regulatory complexes. These 11 PDE families can be grouped into three categories based on their substrate specificity. PDE4, PDE7 and PDE8 selectively hydrolyze cAMP, whereas PDE5, PDE6, and PDE9 hydrolyze cGMP. PDE1, PDE2, PDE3, PDE10 and PDE11 degrade both cAMP and cGMP with varying affinities, depending on the isoform<sup>230</sup>(Figure 19).

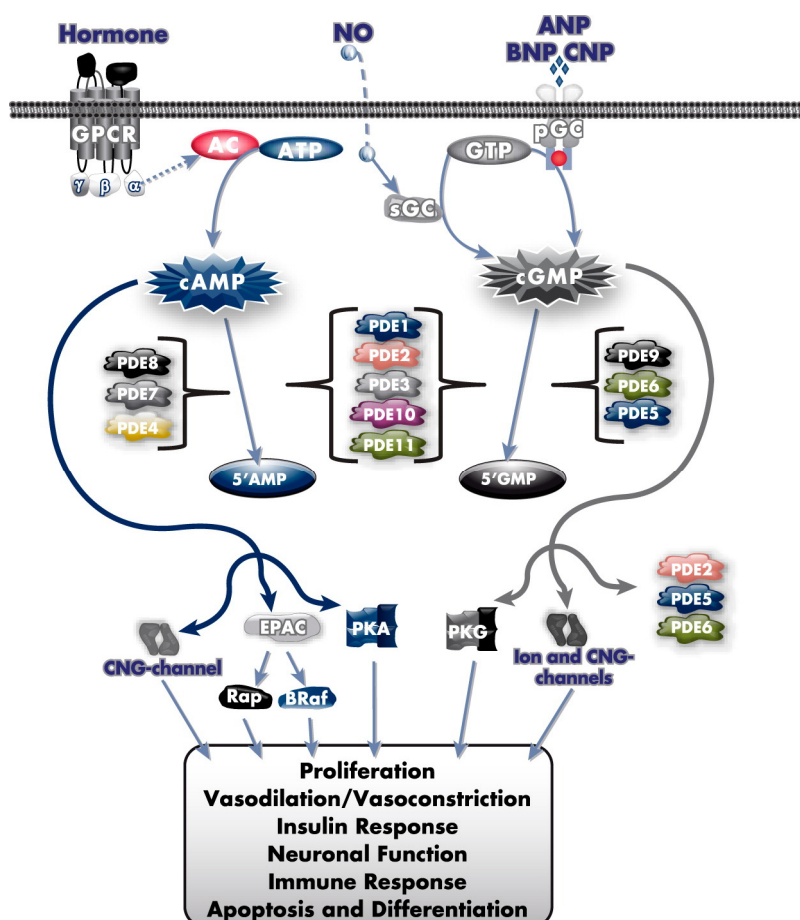


**Figure 19. Cyclic nucleotide signaling and regulation.** AC, adenylyl cyclase; ANP, atrial natriuretic peptide; BNP, B-type natriuretic peptide; B-Raf, B-Raf protein kinase; CNG-channel, cyclic nucleotide-gated channel; CNP, C-type natriuretic peptide; pGC, particulate guanylyl cyclase; PKG, cGMP-dependent protein kinase; Rap, Ras-related protein; sAC soluble AC; sGC, soluble guanylyl cyclase<sup>243</sup>.



PDE isoforms share a common structural organization, with a conserved catalytic domain in the C-terminal portion, followed by a short hydrophilic C-terminal tail and preceded by an N-terminal regulatory region (Figure 18). Catalytic domains contain family-specific sequences that determine differences in substrate affinities, catalytic properties, and sensitivities to specific effectors and inhibitors, as well as common structural determinants involving in cleavage of cyclic phosphate bonds. N-terminal contains structural determinants involving in selective responses of individual PDEs to specific signals that regulate catalytic activity, protein–protein interactions, or targeting to specific subcellular locations. These regulatory domains contain auto inhibitory modules, dimerization domains, GAF domains, sites for phosphorylation by PKA, PKG, Ca<sup>2+</sup>/calmodulin-dependent sensitive protein kinases, Protein kinase B (PKB/Akt), Protein kinase C etc (Figure 20).

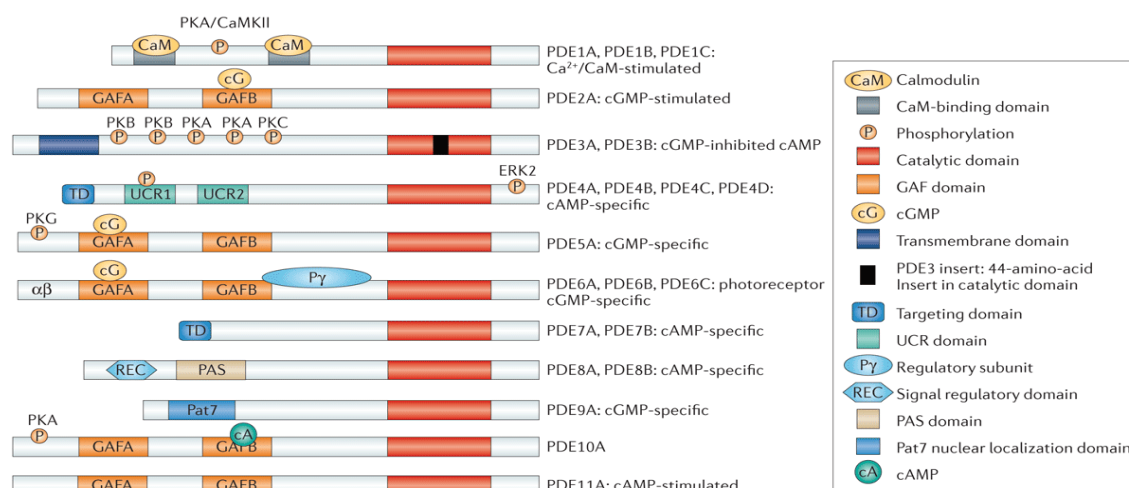


**Figure 20. Structure and domain organization of 11 mammalian PDE families.**

The conserved catalytic domain (shown in red) is located in the carboxy-terminal portion of the PDEs. The catalytic domain of PDE3 contains a unique 44-amino-acid insert (shown in black). Many of the PDE families contain amino-terminal subdomains (such as GAF domains, transmembrane domains, targeting domains, upstream conserved regions (UCRs), PAS domains and REC domains) and N-terminal hydrophobic regions that are important in subcellular localization, in the incorporation of PDEs into compartmentalized signalosomes, in interactions with signalling molecules and molecular scaffolds, and in the regulation of PDE activity. GAF domains regulate the allosteric binding of cGMP (to PDE2, PDE5, PDE6 and PDE11), the allosteric binding of cAMP (to PDE10) and the regulation of catalytic activity (in PDE2, PDE5 and PDE6). Phosphorylation sites are labelled on the figure<sup>244</sup>.



### 1.3.2 PDE family

#### 1.3.2.1 PDE1

PDE1 is known as  $\text{Ca}^{2+}$ - and calmodulin-dependent phosphodiesterase. PDE1 has three subtypes, PDE1A, PDE1B and PDE1C, which divide further into various isoforms. All PDE1 enzymes hydrolyze both cAMP and cGMP. PDE1A and PDE1B preferentially hydrolyse cGMP, whereas PDE1C hydrolyses cAMP and cGMP with similar  $K_m$  values. PDE1A is highly expressed in the brain, liver, spermatozoa<sup>245</sup> kidney, pancreas, and thyroid gland<sup>246</sup>. PDE1B is expressed in the brain, heart, and skeletal muscle<sup>247</sup>. PDE1C is mainly expressed in brain, heart<sup>248,249</sup>, olfactory epithelium<sup>250</sup> and testis<sup>251</sup>.

PDE1 activity is shown to be up-regulated in left ventricular tissue, in a rat model of pressure overload by banding aorta, suggesting that the increase in cGMP-PDE activity in response to pressure overload plays an important role in neutralizing cGMP action in cardiac tissue<sup>252</sup>. PDE1A plays a critical role in cardiac fibroblast activation and cardiac fibrosis<sup>253</sup>. PDE1B-deficient mice show increased locomotor activity and deficits in spatial learning<sup>254</sup>. PDE1C plays a critical role in regulating collagen homeostasis during pathological vascular remodeling<sup>255</sup>. PDE1C and PDE1A are up regulated in idiopathic pulmonary arterial hypertension lungs and in lungs from animal models of pulmonary hypertension. And inhibition of PDE1 reverses structural lung vascular remodelling and right heart hypertrophy<sup>256</sup>.

PDE1 can be inhibited by IC224 with an  $\text{IC}_{50}$  of 0.08  $\mu\text{M}$  and selectivity over other PDEs 100 fold<sup>257</sup>. PDE1 is also inhibited by IC96340 with the  $\text{IC}_{50}$  of 440nM for PDE1A, 210nM for PDE1B and 60nM for PDE1C respectively<sup>244</sup>.

#### 1.3.2.2 PDE2

PDE2 is encoded by a single gene PDE2A which gives rise to three PDE2 variants, the soluble PDE2A1<sup>258</sup>, and the membrane-associated PDE2A2 and PDE2A3 isoforms<sup>259,260</sup>. These isozymes share the same C-terminal but differ in their N-terminal sequences. Two distinct GAF domains, GAF-A and GAF-B, are present in the N-terminal portion of PDE2A and have distinct functions in dimerization and in cGMP

binding, respectively<sup>261</sup>. The binding of cGMP (1–5 mM) to GAF-B domain allosterically and positively stimulates up to a 30-fold increase in cAMP hydrolysis<sup>262</sup>. This specific regulation gives a major feedback role for PDE2 to control the cross talk between cGMP and cAMP pathways<sup>263</sup>. PDE2 is expressed in a wide variety of tissues, including brain, heart, liver, adrenal gland, platelets, endothelial cells, neurons, and macrophages<sup>264-268</sup>.

PDE2 tightly controls the activity of LTCCs in various species including humans<sup>269-272</sup>. A stimulation of the soluble guanylyl cyclase leads to a dramatic local decrease in cAMP in the vicinity of LTCCs due to the activation of PDE2<sup>271</sup>. In frog cardiac myocytes, it has been shown that the PDE2 activity is physiological coupled to the decrease in Ca channel activity. More recently, a study on neonatal rat cardiomyocytes has demonstrated that PDE2 restricts cAMP signals, and hence inotropism, generated after a  $\beta$ -AR stimulation by Iso using the FRET-based imaging technique<sup>273</sup>. Some research demonstrated that cGMP alters the local activation of PKA isoforms localized to different subcellular compartments, modifying the phosphorylation of downstream targets and cell contraction. In their study, PDE2 activity is preferentially coupled to PKA-RII compartment and cGMP mediated activation of PDE2 is responsible for the opposing effects of cGMP on local cAMP signals<sup>274</sup>.

PDE2 is selectively inhibited by EHNA in comparison with other PDEs when activated by cGMP<sup>275</sup>, with an IC<sub>50</sub> value of 2  $\mu$ M for activated PDE2 and 38  $\mu$ M for basal PDE2<sup>276</sup>. However, EHNA is also a potent adenosine deaminase inhibitor<sup>277</sup> (K<sub>i</sub> = 10 nM. Bay 60–7550<sup>278</sup>, IC933<sup>257</sup>, PDP<sup>279</sup> and oxindole<sup>280</sup> are new specific PDE2 inhibitors.

### **1.3.2.3 PDE3**

PDE3 is encoded by PDE3A and PDE3B genes. PDE3A has three variants PDE3A1 (136 kDa), PDE3A2 (118 kDa) and PDE3A3 (94 kDa)<sup>281</sup>, whereas only a single PDE3B1 variant has been identified<sup>262</sup>. PDE3A and PDE3B display highly structural homology and similar kinetic properties. They both contain 44 amino acids insert in the

catalytic domain and N-terminal hydrophobic membrane association regions<sup>262,276</sup>. PDE3 family members contain multiple phosphorylation sites in their N-terminal region, which can be phosphorylated by PKA, PKB and PKC in response to hormonal stimulation<sup>282</sup>.

PDE3 hydrolyzes both cAMP and cGMP, the rate for cAMP hydrolysis is 10-fold greater than for cGMP, and the substrate affinity for cGMP is higher than cAMP. cGMP behaves as a competitive inhibitor for cAMP hydrolysis and therefore participates in cAMP/cGMP crosstalk. PDE3A is expressed in heart, vascular and placental smooth muscle, platelets, and corpus cavernosum smooth muscle, whereas PDE3B is mainly associated with adipocytes, hepatocytes and spermatocytes. PDE3B is also expressed in the cardiovascular system but at much lower levels than PDE3A<sup>283</sup>.

PDE3A is responsible for effects of PDE3 inhibitors on platelet activation/aggregation, basal myocardial contractility, and vascular smooth muscle proliferation/remodeling<sup>284-286</sup>. PDE3A plays an important role in SMC phenotype switch and growth. It has been observed a decrease in PDE3A expression in synthetic VSMC or in response to in vivo vascular damage<sup>287</sup>. Recently, Begum et al showed that PDE3A regulates VSMC growth via inhibition of mitogen activated protein kinase signalling and alteration in critical cell cycle regulatory protein<sup>288</sup>. PDE3B plays a crucial role in the regulation of energy homeostasis<sup>289</sup>. In adipocytes, insulin-mediated phosphorylation/activation of membrane associated PDE3B leads to a reduction in PKA activity and inhibition of lipolysis. Inhibition of adipocyte PDE3B blocks the antilipolytic action of insulin and reduces insulin-stimulated lipogenesis and glucose uptake<sup>290</sup>.

The first potent and selective inhibitor for PDE3 was cilostamide, which inhibits platelet aggregation<sup>291</sup>. Medicinal chemistry has been focusing on PDE3 inhibitors, giving rise to amrinone, milrinone and enoximone. Recently, the PDE3 inhibitor cilostazol and OPC33540 were developed by Otsuka<sup>244</sup>.

#### 1.3.2.4 PDE4

PDE4 is the largest PDE family, specifically hydrolyzing cAMP. The PDE4 enzymes are universally selective for cAMP with  $K_m$  values typically between 1 and 10  $\mu$ M.  $V_{max}$  values of the PDE4 enzymes for cAMP, although lower than those for PDE1s and PDE2s, are comparable with those for most other PDEs. It is encoded by 4 genes: PDE4A (seven variants), PDE4B (four variants), PDE4C (seven variants) and PDE4D (nine variants)<sup>244,292,293</sup>. These proteins contain a unique amino acid signature region called upstream conserved regions 1 and 2 (UCR1 and UCR2)<sup>294</sup>. Long PDE4 isoforms contain both UCR1 and UCR2, short PDE4 forms lack UCR1, and super-short isoforms contain only half of UCR2. UCR1 contains a PKA phosphorylation site which attenuates the ability of UCR1 to interact with UCR2 and thereby activates PDE4 activity<sup>295</sup>.

PDE4A is expressed in brain heart and small intestine<sup>296,297</sup>. Immune cells highly express PDE4, especially PDE4B and PDE4D isoforms<sup>298,299</sup>. PDE4C expression is ubiquitous but has been reported to be low in the lung and absent in blood<sup>300</sup>.

The PDE4 family modulates  $\beta$ 2-adrenergic responses in pulmonary smooth muscle and cardiac tissue. PDE4 interaction with the protein mAKAP is involved in the control of local cAMP and normal myocardial functioning, as well as in the development of myocyte hypertrophy<sup>292,301</sup>. It has been demonstrated that this PDE4B plays an important role in immune cells by using PDE4B knock-out mice. PDE4B was found to be essential for mounting an inflammatory response to lipopolysaccharide in monocytes<sup>302</sup> and macrophages<sup>303</sup>. PDE4B is required for tumor necrosis factor  $\alpha$  production. PDE4D deficiency promotes heart failure progression as demonstrated in PDE4D knock out mice<sup>304</sup>. PDE4D interacts with the sarcolemmal RyR. PDE4D knockout mice develop progressive cardiomyopathy and accelerated heart failure after myocardial infarction<sup>304</sup>.

Rolipram, the first PDE4 inhibitor, was developed as a potential drug to treat depression as it was demonstrated that elevation of cAMP could enhance noradrenergic

eurotransmission in the central nervous system. Cilomilast (GSK), Roflumilast (Altana), GSK256066 (GSK), AWD 12–281 (Elbion/GSK), Apremilast (Celgene), Quinolyl oxazole (Merck) are also PDE4 inhibitors.

### 1.3.2.5 PDE5

PDE5 specifically hydrolyses cGMP<sup>305-307</sup> and is encoded by one gene PDE5A with three variants: PDE5A1 (100 kDa), PDE5A2 (95 kDa) and PDE5A3 (95 kDa). PDE5A contains two GAF domains: GAF-A and GAF-B. GAF-A is responsible for allosteric binding of cGMP, which promotes PDE5 phosphorylation, increasing both catalytic activity and cGMP-binding affinity<sup>308,309</sup>.

PDE5 is expressed in vascular smooth muscle including the vascular tissues of the penis, and also in platelets<sup>310-312</sup>. Expression in cardiomyocytes in animals and humans has also been reported. PDE5A1 and PDE5A2 are widely expressed, whereas specific expression of PDE5A3 in smooth and/or cardiac muscle has been reported<sup>311</sup>.

PDE5A is as a regulator of vascular smooth muscle contraction through regulation of cGMP, especially in the lung and penis. In the corpus cavernosum of the penis, PDE5 inhibition enhances relaxation of smooth muscle induced by NO and cGMP, and thereby stimulates penile erection<sup>313-315</sup>. Similarly in the lung, PDE5 inhibition opposes smooth muscle vasoconstriction<sup>262</sup>. PDE5 is also thought to be important in the regulation of platelet aggregation<sup>316,317</sup> and has been implicated in enhancing learning and memory<sup>318</sup>. In the heart, PDE5 inhibition may offer protection against ischemia/reperfusion injury<sup>319-321</sup> and in certain heart failure models<sup>322</sup>.

Zaprinast (M&B 22948) was the first selective PDE5 inhibitor<sup>323</sup>, and it was used to investigate various functional implications of PDE5. Sildenafil was the first potent and selective PDE5 inhibitor (Viagra<sup>TM</sup>, Pfizer Inc.) for erectile dysfunction<sup>314</sup>. Thereafter, compounds more potent were developed. Tadalafil (Cialis<sup>TM</sup>, Lilly-ICOS) was synthesized with greater selectivity for PDE5 versus PDE1-4 than sildenafil and with the highest long-lasting effect (>7h)<sup>324</sup>. Vardenafil (Levitra <sup>TM</sup>, Bayer-GSK) was

synthesized with the lowest IC<sub>50</sub>. Avanafil (Vivus), Udenafil (Dong-A) and Mirodenafil (SK Life Science) are also PDE5 inhibitors<sup>244</sup>.

#### **1.3.2.6 PDE6**

PDE6 family members, also known as photoreceptor PDEs, specifically hydrolyze cGMP. There are three genes in the family, PDE6A, PDE6B, and PDE6C. PDE6 is composed of two large catalytic subunits associated with two copies of small inhibitory subunits. The catalytic subunits are encoded by PDE6A for rod  $\alpha$  subunit, PDE6B for rod  $\beta$  subunit and PDE6C for cone  $\alpha'$  subunit.

PDE6A and PDE6B are expressed in rods, and PDE6C is expressed in cones. PDE6 isoforms are highly expressed in the photoreceptor outer segments of the mammalian retina<sup>325,326</sup> and in the pineal gland<sup>327</sup>.

PDE6 was shown to play an important role in phototransduction. The main function of the rod PDE is to reduce the steady-state concentration of cGMP in response to light stimulus. This decrease in cGMP concentration leads to the closure of CNG cationic channels and generation of cell membrane hyperpolarization. This initial signal was transmitted via second order retinal neurons to the optic nerve and to the brain<sup>328</sup>. Mutation in genes generating defective PDE6 causes cGMP accumulation in photoreceptor cell leading to cell death.

Sildenafil, vardenafil, and udenafil inhibit PDE6, with lower affinities than those for PDE5A, but this inhibition has been suggested to be the source of some of the visual side effects reported with sildenafil usage.

#### **1.3.2.7 PDE7**

The PDE7 family is highly selective for cAMP<sup>329-331</sup> (214–216). This family includes two genes PDE7A and PDE7B, with alternative splicing for PDE7A giving rise to PDE7A1 (57 kDa), PDE7A2 (50 kDa) and PDE7A3 (50 kDa). The K<sub>m</sub> for cAMP hydrolysis is about 0.1  $\mu$ M for PDE7A and is slightly lower for PDE7B. The V<sub>max</sub>

values for PDE7A and PDE7B have been reported to be very low (<1 nmol/min/ mg) in comparison with those for most other PDEs<sup>329,331</sup>.

PDE7A1 protein has been found in a wide variety of immune cells and has thus engendered a great deal of interest as a target for treating inflammation<sup>332</sup>. PDE7A1 protein is primarily cytosolic, whereas PDE7A2 is mostly associated with a particulate fraction and its expression is not widespread but is high in heart<sup>330</sup>.

Initial studies suggested that PDE7A could be induced in T lymphocytes in response to activation of the T-cell receptor. PDE7 antisense oligonucleotides inhibited proliferation and IL-2 production in a PKA-dependent manner<sup>333</sup>. Zhang et al found that CLL patients with PDE7B mRNA levels in the top quartile have a several-year shorter median time-to-treatment compared to that of patients whose CLL cells express lower levels of PDE7B mRNA<sup>334</sup>. PDE7 is also involved in Alzheimer's disease and Parkinson's disease. Studies have shown that some recently described PDE7 inhibitors may play a role in the treatment of neurological diseases in mouse models<sup>335</sup>.

A great deal of effort from the pharmaceutical industry has been invested in developing PDE7 selective inhibitors. ASB16165 (Asubio) inhibits T lymphocyte activation and suppresses skin inflammation<sup>335,336</sup>. Selective PDE7 inhibitors (such as BRL-50481 and IR-202) and the dual PDE4–PDE7 inhibitor (IR-284) increased cAMP–PKA signalling and apoptosis in CLL cells<sup>334,337</sup>.

### **1.3.2.8 PDE8**

PDE8 specifically hydrolyzes cAMP with the highest affinity among all PDEs<sup>338,339</sup>. The PDE8 family consists of two highly homologous genes, PDE8A and PDE8B. Five splice variants have been identified for PDE8A<sup>340</sup> (PDE8A1 to PDE8A5) and PDE8B<sup>282</sup> (PDE8B1 to PDE8B5). The primary structure of both PDE8A and PDE8B enzymes includes N-terminal REC and PAS domains<sup>341,342</sup>. Three putative PKA and PKG phosphorylation sites are located between the PAS domain and the catalytic domain.

PDE8A mRNA expression is widespread and has been detected in a variety of tissues but is highest in testis, spleen, small intestine, ovary, colon and kidney<sup>339,340,343</sup>. PDE8B1 is the most abundant variant in the thyroid gland<sup>344</sup>, whereas PDE8B1 and PDE8B3 are equally expressed in the placenta. PDE8B was found to be expressed in the normal and hyperplastic human adrenal cortex and in the adrenal gland of newborn mice

A possible role for PDE8A in T-cell activation has been suggested<sup>262</sup>, and PDE8 has also been reported to regulate lymphocyte chemotaxis and adhesion<sup>345,346</sup>. PDE8 regulates excitation–contraction coupling in ventricular myocytes, revealing its participation in cardiac function<sup>347</sup>.

PDE8-selective inhibitor, PF-04957325 potentiates adrenocorticotropin stimulation of steroidogenesis by increasing cAMP-dependent protein kinase activity in both primary isolated adrenocortical cells and Y-1 cells<sup>348</sup>.

### **1.3.2.9 PDE9**

The PDE9 family specifically hydrolyses cGMP with the highest affinity amongst all PDE families. PDE9A is the only isoform identified to date. Twenty-one splice variants arise from the single PDE9A gene<sup>349</sup>. The primary structure of PDE9A is relatively simple as it does not appear to contain any GAF domains or other N-terminal regulatory sequences found in other PDEs.

Several studies have reported PDE9A mRNA tissue localization. It is widely expressed and has been found in nearly every tissue tested, with especially high levels detected in kidney, brain, spleen, various gastrointestinal tissues, and prostate<sup>339,343,349</sup>. Despite this high number of mRNA transcripts, only PDE9A1 and PDE9A6 (originally named PDE9A5) proteins have been shown to be expressed and were characterized<sup>350</sup>.

In PDE9A knock out mice, cGMP levels were increased in brain cortex, hippocampus striatum, cerebellum, and cerebrospinal fluid; in wild-type mice, inhibition of PDE9A with PF-4181366 increased cGMP in the same brain regions as well as in the cerebrospinal fluid<sup>351</sup>. Furthermore, PDE9A genomic location maps to a region



containing genes involved in several neurological diseases, including bipolar disorder<sup>352</sup>.

BAY 73-6691 inhibits PDE9A with a 25-fold greater selectivity compared with all other PDEs. An orally bioavailable PDE9 inhibitor was synthesized for use as a potential hypoglycemic agent. Recently, PF-04447943, a brain penetrant PDE9A inhibitor that enhances synaptic plasticity and cognitive function in rodents has been published<sup>353</sup>.

#### **1.3.2.10 PDE10**

The PDE10 family is a dual-substrate gene family encoded by the unique gene PDE10A. At present, four variants, PDE10A1-4, have been described. PDE10 isoforms contain two GAF domains and hydrolyze both cAMP and cGMP, with a higher affinity for cAMP than cGMP.

PDE10A is mainly expressed in the brain, with the highest expression in the striatal area, and it is also present in the cerebellum, thalamus, hippocampus, and spinal cord<sup>354-357</sup>, as well as in the testis, especially in the developing spermatocytes. PDE10 is also expressed in the thyroid and pituitary gland, but the physiological functions of the enzyme in these tissues are still unknown.

Dysregulation of PDE10A is thought to be associated with the progressive neurodegenerative Huntington's disease because PDE10A2 mRNA decreases before the onset of motor symptoms in the striatal region of brains from transgenic Huntington's disease mice<sup>358,359</sup>. Chronic inhibition of altered expression of overlapping striatal genes involved in Huntington's disease, suggesting that inhibition of PDE10 might provide protective effects in Huntington's disease<sup>360</sup>. PDE10A knockout mice also show decreased exploratory activity and delayed acquisition of conditioned avoidance behavior<sup>361</sup>. Inhibition of PDE10A produced beneficial effects in murine and rat antipsychotic models and increased social behavior. In these studies, inhibition of PDE10A improved dopaminergic and glutamatergic dysfunction.

The first known potent and specific PDE10A inhibitor is papaverine, with an EC<sub>50</sub> value of 36 nM<sup>362</sup>. TP-10, a new potent and very specific PDE10 inhibitor, synthesized by Pfizer, was under investigation in preclinical study as a new therapeutic approach for the treatment of schizophrenia<sup>363</sup>.

#### **1.3.2.11 PDE11**

PDE11 is the most recently discovered PDE enzyme family<sup>364,365</sup>. It is encoded by only one PDE11A gene. Four different variants (PDE11A1–4) have been identified<sup>366–368</sup>. The longest variant, PDE11A4, has two N-terminal GAF domains, whereas the other variants are truncations of this variant of varying lengths. PDE11 exhibits dual substrate specificity and hydrolyzes cAMP and cGMP with similar affinities.

In humans, PDE11A is highly expressed in skeletal muscle and prostate. Its expression is seen in testis, pituitary gland, heart, kidney, and liver<sup>365,369</sup>. Among all PDE11A variant proteins, only PDE11A4 protein has been detected in human tissues by immunohistochemical analysis<sup>370</sup>, with expression demonstrated in prostate, leydig and spermatogenic cells of the testis, kidney, adrenal, colon, and skin epidermis<sup>371</sup>.

Little is known about the function of PDE11A. Recent studies with a PDE11 knockout mouse model suggest that PDE11 may be important for sperm development and function. Ejaculated sperm from knockout mice displayed slightly lower sperm concentration and decreased viability compared with controls, and the sperm had a lower rate of forward progression<sup>372</sup>.

There are no specific inhibitors for PDE11A. PDE11A is inhibited by dipyridamole (IC<sub>50</sub> = 0.9–1.8 μM), zaprinast (IC<sub>50</sub> = 5–33 μM), IBMX (IC<sub>50</sub> = 25–81 μM) and is insensitive to EHNA, rolipram and milrinone<sup>373</sup>.

#### **1.3.3 PDEs in mitochondria**

PDE activity has been observed in mitochondria. Acin-Perez et al. isolated mitoplasts from mouse liver. After the content of the matrix was made accessible by sonication, they found that some factors present in the matrix degraded exogenous cAMP. This

cAMP catabolic activity was fully inhibited by IBMX, indicating the presence of intramitochondrial PDE activity<sup>225</sup>. PDE4 co-localization with mitochondria, apparently through an interaction with the protein “disrupted in schizophrenia 1” (DISC1), was previously reported<sup>374</sup>. More recently, mitochondrial PDE2A is shown to be located in the matrix and that the unique N terminus of PDE2A isoform 2 specifically leads to mitochondrial localization of this isoform in liver and brain. Authors also showed that mitochondrial PDE2A forms a local signaling system with sAC in the matrix, which regulates the activity of the respiratory chain (Figure 21)<sup>375</sup>. Zhang et al reported that *Drosophila* protein Prune is a cyclic nucleotide PDE that localizes to the mitochondrial matrix. Knocking down prune in cultured cells reduces mitochondrial transcription factor A (TFAM) and mitochondrial DNA (mtDNA) levels. Their data suggest that Prune stabilizes TFAM and promotes mitochondrial DNA (mtDNA) replication through downregulation of mitochondrial cAMP signaling<sup>376</sup>.

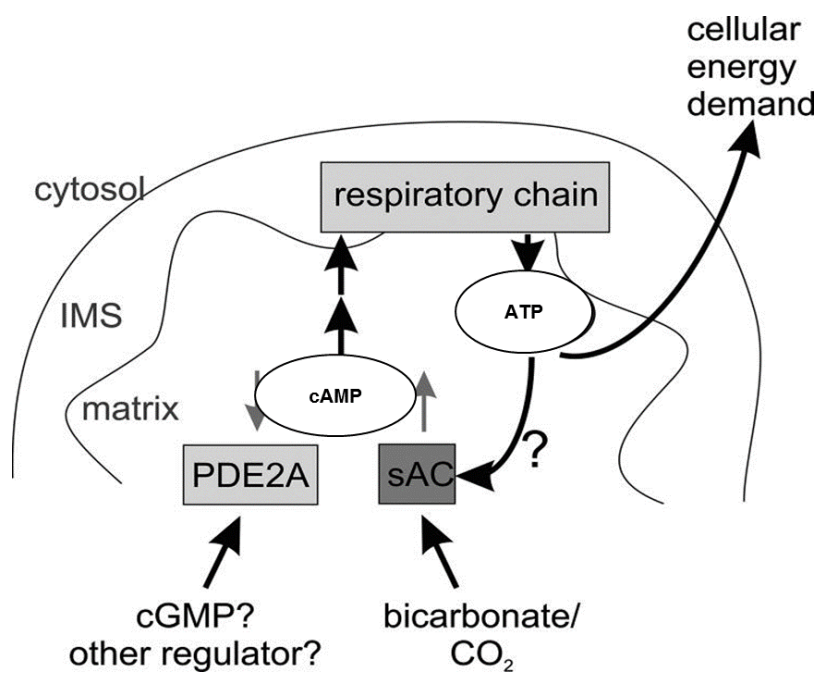


**Figure 21. Model for the mitochondrial cyclic nucleotide signaling system.** cAMP is formed inside the mitochondrial matrix by a sAC isoform and stimulates the respiratory chain. The cAMP signals are terminated through degradation by PDE2A isoform 2. Thus, formation of cAMP is stimulated by bicarbonate, which activates sAC, and degradation is stimulated by cGMP or a yet to be identified regulatory ligand for the PDE2A2 GAF domains. IMS, intermembrane space<sup>375</sup>.

## 2. Objectives

cAMP is a major second messenger in many organs, particularly in the heart, where it regulates diverse physiological processes such as  $\text{Ca}^{2+}$  homeostasis, beating frequency and myocardial contractility, as well as cell death. In addition to tmACs, cAMP can also be generated by sAC, which is not regulated by heterotrimeric G proteins or forskolin, but can be activated by  $\text{HCO}_3^-$  and  $\text{Ca}^{2+}$ . sAC was found inside mitochondria to regulate respiration in brain and liver in response to  $\text{HCO}_3^-$  and/or  $\text{Ca}^{2+}$ . As a result, this pathway serves as a mechanism for metabolic adaptation to mitochondrial dysfunction and could be a potential novel target to treat genetic mitochondrial diseases. The existence and role of a functional cyclic nucleotide signaling pathway in the heart mitochondria has not been demonstrated.

The aim of this thesis was to investigate the existence of cAMP signalling pathway in cardiac mitochondria. Using cellular and subcellular approaches, we investigated the role of cAMP on mitochondrial function and cell death, apoptosis as well as necrosis in primary cardiomyocytes. Based on the use of mitochondria isolated from rat heart, we characterized cAMP signalling pathway relative proteins; sAC, PKA, Epac1 and Epac2 and study their functions by pharmacological modulation and/or siRNA silencing. Moreover, we investigate the cAMP pathway in a rat model of HF induced by aortic stenosis.

Another approach was to study the various isoforms of PDEs and their effect on cardiac mitochondrial functions. We investigated the existence of PDE isoforms in isolated mitochondria from rat, mice and transgenic mice for PDE2 and study their ability to degrade cAMP in isolated mitochondria/living cells. After, the effects of different PDE isoforms on mitochondrial function by pharmacological or genetic modulation are investigated. In determining the role of mitochondrial cAMP signalling pathway, this thesis should provide a better general knowledge of cyclic nucleotide signalling in hearts.

### 3. Materials and methods

#### 3.1 Materials

##### 3.1.1 Drugs and reagents

Most of drugs and reagents were purchased from Sigma-Aldrich (St Quentin, Fallavier, France). The reagents used for cell culture and their origin were summarized in Table 3.1.

**Table 3.1 The reagents used for cell culture**

Reagents	Company	City/State
DMEM	Gibco	USA
Opti-MEM	Gibco	USA
Antibiotic-antimycotic	Gibco	USA
EDTA	Gibco	USA
PBS	Gibco	USA
FBS	PAA	France
Lipofectamine 2000	Invitrogen	USA

##### 3.1.2 Antibodies

The primary and secondary antibodies used in this study were shown in Tables 3.2 and 3.3, respectively.

**Table 3.2 Primary antibodies**

Primary antibodies	Company/ Provider	City/State
sAC	Abcam; CEP Biotech	UK; USA
Epac1, 2	Cell signaling	USA
ANT	Abcam	UK
GAPDH	Cell signaling	USA
TnI	Cell signaling	USA
PLB	Cell signaling	USA
MCU	Biorbyt	USA
PDE2A	Santa Cruz	USA
PDE3A	Chen Yan(University of Rochester)	USA
PDE4A	Marco Conti (University of California, San Francisco)	USA
PDE4B	Marco Conti	USA
PDE4D	Marco Conti	USA

**Table 3.3 Secondary antibodies**

Second antibodies	Company	City/State
Donkey anti-Mouse IgG	Jackson immunoresearch	USA
Donkey anti-Rabbit IgG	Jackson immunoresearch	USA
Donkey anti-Goat IgG	Jackson immunoresearch	USA

## **3.2 Methods used in cardiomyocytes**

All animal care and experimental procedures conformed to the European Community guiding principles in the care and use of animals (Directive 2010/63/EU of the European Parliament) and authorizations to perform animal experiments according to this directive were obtained from the French Ministry of Agriculture, Fisheries and Food (No. D-92-283, 13 December 2012). All studies involving rats and mice are reported in accordance with the ARRIVE guidelines for reporting experiments involving animals. A total of 60 healthy, 4 Sham and 4 HF rats and 30 PDE2 WT and TG were used in the experiments described here.

### **3.2.1 Surgical procedure and echocardiography**

Male Wistar rats at three weeks of age (60–70 g; Janvier, Le Genest St Isle, France) were anesthetized with pentobarbital (60 mg/kg). The thoracic cage was opened and a stainless steel hemoclip was placed on the ascending aorta, to promote HF after 22 weeks, as previously described<sup>377</sup>. Sham-operated animals were used as controls. Cardiac structure and function was evaluated by echocardiography. Cardiac and pulmonary hypertrophy was determined as a ratio of organ weight to tibia length and to body weight as described<sup>378</sup>. Sham-operated animals were used as controls. Cardiac structure and function was evaluated by echocardiography. Cardiac and pulmonary hypertrophy was determined as a ratio of organ weight to tibia length and to body weight. Transthoracic two-dimensional-guided M-mode echocardiography of rats was performed using an echocardiograph with a 15 MHz Linear transducer (Vivid 9, General Electric Healthcare, Vélizy Villacoublay, France) under 3% isoflurane gas anesthesia and fractional release was calculated as described<sup>378,379</sup>.

### 3.2.2 Isolation of ventricular cardiomyocytes of adult rats

Male Wistar rats (250–300 g) were subjected to an aesthesia by intraperitoneal injection of pentothal (0.1 mg/g) and hearts were excised rapidly. Individual ARVMs were obtained by retrograde perfusion of the heart as previously described. The hearts were perfused retrogradely at a constant flow of 6 mL/min at 37°C with a  $\text{Ca}^{2+}$ -free Ringer solution containing (in mM): NaCl 117, KCl 5,  $\text{NaHCO}_3$  4.4,  $\text{KH}_2\text{PO}_4$  1.5,  $\text{MgCl}_2$  1.7, D-glucose 11.7, Na-phosphocreatine 10, taurine 20, and 4-(2-hydroxyethyl)piperazine-1-ethanesulfonic acid (HEPES) 21, pH 7.1 during 5 min, followed by a perfusion at 4 mL/min for 1 h with the same solution containing 1 mg/mL of collagenase A and 300 mM ethylene glycol tetraacetic acid (EGTA) and  $\text{CaCl}_2$  to adjust free  $\text{Ca}^{2+}$  concentration to 20  $\mu\text{M}$ . The ventricles were then separated from atria, finely chopped, and gently agitated to dissociate individual cells. The resulting cell suspension was filtered on gauze, and the cells were allowed to settle down. The supernatant was discarded and cells were resuspended four more times with Ringer solution at increasing  $\text{Ca}^{2+}$  concentration from 20 to 300  $\mu\text{M}$ . Freshly isolated cells were suspended in minimal essential medium (MEM: M 4780) containing 1.2 mM  $\text{Ca}^{2+}$  supplemented with 2.5% foetal bovine serum, 1% penicillin–streptomycin, 20 mM HEPES (pH 7.6), and plated on 35 mm, laminin-coated culture dishes (10  $\mu\text{g/mL}$ ) at a density of  $2 \times 10^4$  cells per dish. After 1 h, the medium was replaced by 300  $\mu\text{L}$  of FBS-free MEM.

**Table 3.4 Medium for adult cardiomyocytes**

	M1	M2
MEM	yes	yes
$\text{CaCl}_2$	1.2mM	1.2mM
FBS	2.5%	0
HEPES	2%	2%
penicillin streptomycin	1%	1%
pH	7.6	7.6

### 3.2.3 Isolation of neonatal cardiomyocytes

#### A. Preparation of media

All media should be prepared from sterile ingredients or sterilized by 0.22  $\mu$ m filtration. Stated volumes are sufficient for 20-50 hearts (20 – 100 $\times 10^6$  myocytes). 1 $\times$  ADS buffer was diluted by sterile water.

**Table 3.5 10  $\times$  ADS Buffer**

Reagents	Weight (g)
NaCl	17
HEPES	11.9
NaH <sub>2</sub> PO <sub>4</sub>	0.3
Glucose	2.5
KCl	1
MgSO <sub>4</sub> (anhydrous)	0.25
pH	7.35

**Table 3.6 Plating medium**

Reagents	Volume (mL)
DMEM	75.5
Medium 199	17
Horse serum	5
Newborn calf serum	0.5
Penicillin/Streptomycin	1
Glutamine	1
pH	7.4

#### B. Enzyme solution

Pancreatin (30mg) and Collagenase type II (26mg) were weighted, and dissolved in 20mL of 1 $\times$  ADS buffer. The enzymes were diluted into 60mL, filtered and kept on ice or at 4°C.

#### C. Dissection of rats

Four Petri dishes were put on ice, and filled partly with 1 $\times$  ADS buffer. The rats were quickly decapitated. Then the heart was performed a 1-1.5 cm long midline cut



through sternum, the heart was forced out by pressing down on either side of the cut with gloved fingers. Hearts were removed with forceps and placed in the Petri dish with chilled  $1\times$  ADS buffer. Needed numbers of rats were repeated. (Cell yield is  $\sim 10^6$  cells per heart.) Hearts were transferred to a second dish, using forceps to remove atria and large vessels. Hearts were transferred to a third dish, if necessary. Hearts were chopped with scissors to very small pieces (0.3 mm, able to pass through 10 ml pipette). The chopped hearts were transferred to the conical flask with stirrer.

#### D. Digestion of tissue

The buffer was removed as much as possible, and replaced with 7-8 mL of enzyme solution. After, the heart was placed in incubator at  $37^{\circ}\text{C}$  on a magnetic stirrer, stirring at 200 rpm for 20 min. The supernatant was transferred to one of the Falcon tubes with 1 mL of NCS, repeated 7 times. The supernatant was centrifuged at 1500 rpm for 5 min (without brake), then supernatant was removed and discarded. The pellet was gently resuspended in 2 mL of NCS and placed in the incubator.

#### E. Separation of cells

Preparation of the percoll gradient:

- Percoll stock – in 50 mL Falcon, prepare 18 mL of percoll, add 2 mL of  $10\times$ ADS buffer, shake well to mix.
- Bottom percoll – in 50 mL Falcon tube, prepare 8.45 mL of percoll stock, and add 4.55 mL of  $1\times$  ADS buffer.
- Top percoll – in 50 mL Falcon tube, prepare 7.75 mL of percoll stock, add 9.25 mL of  $1\times$  ADS buffer and  $\sim 20\ \mu\text{L}$  of phenol red.

Bottom percoll (3mL) was prepared in 15mL of falcon tubes. And after 4 mL of top percoll was added into each tube, very slowly. Cells from all Falcon tubes were pooled together (in the first one), and centrifuged at 1500 rpm for 5 min. The supernatant was removed and replaced with ADS  $1\times$  to final volume of 8 mL, resuspended gently. The cell suspension (2mL) was slowly added to the top of percoll gradient in all Falcon

tubes. Cell suspension was centrifuged at 3,000 rpm for 30 min without brake. For cultivation of fibroblasts, the fibroblast fraction (disk on top of top percoll) was aspirated and transferred to 50 mL Falcon tube, adding ADS 1× to the final volume of 40 mL. The myocytes fraction (disk between top and bottom percoll) was aspirated and transferred to 50 mL Falcon tube, adding ADS 1× to the final volume of 50 mL.

#### F. Plating of cells

The cells were centrifuged at 1500 rpm for 5 min without brake. The supernatant was removed and replaced with 10 mL of plating medium. Cells were counted and diluted to desired concentration. Then cells were plated in the dishes. If several different concentrations were needed, faster plating method was to calculate amount of medium and cell suspension for every dish, filling the dish with medium and adding cells. The dishes were gently shaken to promote better cell distribution.

#### G. Coating plating dishes

The dishes were rinsed 2 times in PBS and coated with 0.2% laminin in PBS. They were incubated at least 1 hour at 37°C. Then liquid was aspirated and allowed to dry out.

### 3.2.4 Construction of mitochondria-targeted FRET sensor for cAMP

The mitochondrial targeting sequence 4mt, encoding four copies of the signal sequence from subunit VIII of human cytochrome C oxidase, was amplified using the Advantage Polymerase (Clontech) and primers F (ACTATAGGGAGACCCAAGCTTATG) and R (TGGTGGCGGCAAGCTTCTTGCTCACCATGGTGGC). The pcDNA-4mt-D3-cpv vector used as a matrix for amplification of 4mt was a kind gift from Dr. Roger Tsien (HHMI investigator at the University of California San Diego, USA). The PCR fragment was cloned into the HindIII restriction site of pcDNA3-Epac-S<sup>H187</sup> using the Infusion HD Cloning system (Clontech). Epac-S<sup>H187</sup> encodes for a fourth generation Epac1-based cAMP sensor and was a kind gift from Dr. Kees Jalink (The Netherlands Cancer Institute, Amsterdam, Netherlands)<sup>380</sup>. Once the pcDNA-4mt-Epac-S<sup>H187</sup> vector was amplified in Stellar E. coli (Clontech) bacteria, its identity with parental sequences

was verified by PCR using primers F (ACTCACTATAGGGAGACC) and R (TGCGGCCGCCATGGTGGC), and DNA double strand sequencing (INSERM U1056 – UMR 5165 CNRS UPS – UDEAR, Toulouse, France). Adenoviruses encoding Epac-S<sup>H187</sup> and 4mt-Epac-S<sup>H187</sup> were generated by Welgen, Inc.

### **3.2.5 FRET imaging**

Fluorescence resonance energy transfer (FRET) imaging experiments were performed 48h after infection of neonatal cardiomyocytes. Cells were bathed in Hepes-buffered Ringer's solution containing: 125 mM NaCl, 25 mM Hepes, 10 mM glucose, 5 mM K<sub>2</sub>HPO<sub>4</sub>, 1 mM MgSO<sub>4</sub>, and 1 mM CaCl<sub>2</sub>, pH 7.4. For sAC activation by HCO<sub>3</sub><sup>-</sup>, the medium was the Krebs-Henseleit solution containing: 120 mM NaCl, 2.09 mM K<sub>2</sub>HPO<sub>4</sub>, 0.34 mM KH<sub>2</sub>PO<sub>4</sub>, 24 mM NaHCO<sub>3</sub>, 1 mM MgSO<sub>4</sub>, 1 mM CaCl<sub>2</sub>, and 10 mM D-glucose. Krebs-Henseleit solution was gassed continuously with 95% O<sub>2</sub>/5% CO<sub>2</sub> to maintain a pH of 7.4<sup>227</sup>. Real-time FRET experiments were performed at room temperature.

Images were captured every 5 s using the 40× oil immersion objective of an inverted microscope (Nikon TE 300) connected to a software-controlled (Metafluor, Molecular Devices) cooled charge-coupled device camera (Sensicam PE; PCO, Kelheim, Germany). CFP was excited during 150-300 ms by a Xenon lamp (100 W, Nikon, Champigny-sur-Marne, France) using a440/20BP filter and a 455LP dichroic mirror. Dual emission imaging of CFP and YFP was performed using an Optosplit II emission splitter (Cairn Research, Faversham, UK) equipped with a 495LP dichroic mirror and BP filters 470/30 and 530/30, respectively. Average fluorescence intensity was measured in a region of interest comprising the entire cell. Data were expressed as a percentage increase of the CFP/YFP ratio measured before application of the drug. Ratio images were obtained with ImageJ software (National Institutes of Health).

### **3.2.6 Cell death measurement**

Neonatal cardiomyocytes were isolated as above described. Cells were plated on 35 mm, laminin-coated culture dishes (10 µg/mL) at a density of  $4 \times 10^5$  cells per dish.

The day after, cells were infected with sACt and sACfl adenoviruses (generous gift M. Conti, University of California, CA) in Opti-MEM<sup>®</sup> (Life technologies, St Aubin, France) for 24h. After, cells were treated with 10  $\mu$ M CPT for 48 h or 300  $\mu$ M H<sub>2</sub>O<sub>2</sub> for 24 h or 10 ng/ml TNF $\alpha$ /0.1  $\mu$ g/ml actinomycin D for 24 h. For apoptosis and necrosis measurement, cell were labelled with Apoptosis/ Necrosis Detection Kit (blue, green, red) (Abcam) for 1h at room temperature<sup>381</sup>. Then cells were washed with washing buffer. The cell viability, apoptosis and necrosis were measured with Tecan Infinite 200 at Ex/Em = 405/450 nm, Ex/Em = 490/525 nm and Ex/Em = 546/647 nm respectively. For nuclei apoptosis measurement, replaced the medium with 2.5 $\mu$ g/mL Hoechst (Invitrogen) staining solution (diluted in Opti-MEM medium) and incubated at 37°C for 15min. Rinsed cells with PBS twice. Aspirated PBS and added fresh Opti-MEM medium to cells. Neonatal cells were stained with Hoechst dye for 15min at 37°C as described by the manufacturer. Cells were imaged with Zeiss microscope.

### 3.2.7 PDE activity

cAMP-PDE activity was measured in the supernatant according to a modification of the two-step assay procedure method described by Thompson and Appleman. In the presence of PDEs, [3H]-cAMP was hydrolyzed into [3H]-5'AMP. Addition of snake venom from *Crotalus atrox* (containing 5'-nucleotidase) will promote the degradation of [3H]-5'AMP into [3H]-adenosine. [3H]-cAMP and [3H]-adenosine will be separated by using an anion-exchange resin column which retains [3H]-cAMP but releases [3H]-adenosine. Thus, quantification of the radioactivity present in the eluate represents the quantity of [3H]-adenosine, reflecting the cAMP-PDE activity of the cell lysate. If the reaction was performed in the presence of a PDE inhibitor, the concentration of [3H]-adenosine and the related radioactivity will decrease. Thus, the difference of radioactivity in the absence and presence of PDE inhibitor directly reflects the activity of the inhibited PDE.

### 3.2.7.1 Composition of the solutions

#### Lysis buffer

Reagents	final concentration
Hepes	20mM
NaCl	150mM
EDTA	2mM
Glycerol	10%
NP-40	0.50%
microcystin	1 $\mu$ M
pH	8.0

#### Incubation Mix, 2 mL

Reagents	final concentration
Tris-HCl	40mM
$\beta$ -ME	20mM
MgCl <sub>2</sub>	40mM
cAMP	4 $\mu$ M
<sup>3</sup> H-cAMP	1.75 $\mu$ Ci/mL
pH	8.0

#### Stop Solution, 100mL

Reagents	final concentration
Tris-HCl	40mM
EDTA	10mM

#### Tris-BSA

Reagents	final concentration
Tris-HCl	40mM
BSA	0.1%

### 3.2.7.2 Protein extraction from heart

Tissues (20-50 mg) were weighted and placed in a tube containing ceramic balls (1.4 mm) with 200  $\mu$ L of lysis buffer in the tube. The tube was placed into the Tissue Homogenizer (Precellys<sup>®</sup> 24, Bertin). The two following protocols were carried out: 6500 sec 2 $\times$ 10 on - 5sec off. After, samples were transferred on ice about 10 min and centrifuged for 10min (12,000g at 4° C). The supernatant was transferred into a tube

and putted in ice. The protein concentration was measured on the supernatant by BCA protein assay according to the manufacturer's instructions.

### 3.2.7.3 cAMP-PDE activity assay on heart lysate

All reagents and samples were kept on ice. Tubes were labelled and put in ice water.

Preparation of the two following series of tubes (final volume in each tube was 200 $\mu$ L), each condition in triplicate.

Blank tubes	Sample tubes
20 $\mu$ L lysis buffer	20 $\mu$ L samples
50 $\mu$ L 0.08% DMSO (in H <sub>2</sub> O)	50 $\mu$ L 0.08% DMSO or PDE inhibitors
80 $\mu$ L Tris-BSA	80 $\mu$ L Tris-BSA
50 $\mu$ L incubation mix	50 $\mu$ L incubation mix

Samples (20 $\mu$ L) were prepared as follows, depending on the wanted protein concentration. After the preparation, the tubes were vortexed immediately and incubated for 25 min at 34°C in a water bath. Then the tubes were put on the ice immediately. 200 $\mu$ L of the stop solution was rapidly added to stop the enzymatic reaction. The tubes were vortexed and boiled in the water for 1 min. After, the tubes were transferred on ice. 50 $\mu$ L snake venom solution was added into each tube. After vortex, the tubes were allowed to react for 20 min at 34°C in a water bath. After incubation, the tubes were put on ice. 1 mL of methanol was added and the tubes were vortexed again. Chromatographic separation was performed using the anion-exchange resin. The radioactivity present in the eluate was counted using aliquid scintillation counter. The blank value was subtracted from each value. The residual hydrolytic activity observed in the presence of PDE inhibitors was expressed as a percentage of the total cAMP-PDE activity, corresponding to the cAMP-PDE activity in the absence of inhibitor.

### 3.2.8 SDS-PAGE and western blot

The cells were detached in the lysis buffer containing: 50 mM Hepes, 400 mM NaCl, 1 mM EGTA, 10% glycerol, 1.5 mM MgCl<sub>2</sub> and 1% Triton X 100 (pH 8.0) by using the dispenser. The cells were collected and put on ice for 30min. then cell were centrifuged at 12,000g for 20min at 4°C. The supernatant was transferred to a new tube and kept

on ice. The protein concentration was determined by BCA assay. The protein samples were diluted with Sample Buffer (Laemmli 2×, Sigma), mixed and heated for 5min at 95°C. Then the samples were loaded in the precast gel and migrated for 15min at 300V. After the migration, the membrane and bottom stack were placed on the cassette base of Trans Blot Turbo (Bio Rad), then the gel was place on top of membrane. The assembled sandwich was rolled to expel trapped air bubbles. The cassette lid was closed and locked. Proteins are transferred for 3min at 2.5V. After the transfer, the membrane was blocked with 5% of milk in PBS-Tween and incubated with diluted primary antibody in 5% w/v milk PBS-Tween at 4°C with gentle shaking, overnight. The day after, the membrane was washed with PBS-Tween for 6×5min and incubated with Horseradish Peroxidase-Conjugated secondary antibody for 1h at room temperature. The membrane was washed again with PBS-Tween for 6×5min after the secondary antibody. Then the membrane was incubated with an ultra-sensitive enhanced chemiluminescent substrate for 5min. Images were taken with a gel imaging system (Bio Rad)<sup>382</sup>.

### **3.2.9 siRNA transfection to knockdown sAC and Epac1**

On-Target plus SMART pool siRNA, a mixture of four siRNA provided as a single reagent were purchased from Dharmacon. At day 0, neonatal cardiomyocytes were plated overnight on 35 mm, laminin-coated culture dishes (10 µg/mL) at  $4 \times 10^5$ . At day 1, the cells were transfected with 50 nM sAC/Epac1 or non-targeting control siRNA using Lipofectamine® RNAiMAX Transfection Reagent for 48 h. Extinction of protein expression was evaluated by western blot.

### **3.2.10 Mitochondrial transmembrane potential measurement in neonatal cardiomyocytes**

Isolated rat cardiomyocytes were loaded with 100 nM TMRM at 37°C for 15 min. After, the sarcolemmal membrane was permeabilized by perfusion of digitonin (5 µg/mL) in a Ca<sup>2+</sup> free internal solution that contained 50 mM KCl, 80 mM potassium aspartate, 4 mM sodium pyruvate, 20 mM HEPES, 3 mM MgCl<sub>2</sub>, 3 mM Na<sub>2</sub>ATP, 5.8 mM glucose,

and 0.5 mM EGTA (pH 7.3 with KOH). Then the free  $\text{Ca}^{2+}$  concentration in the internal solution was increased to 200 nM. The  $\text{Ca}^{2+}$  was calculated using the maxchelator program from Stanford. Images were acquired with a Leica (SP5) confocal microscope (Mannheim, Germany). Excitation was achieved by a white light laser fitted at 549 nm and emission collected at 570 nm. Analyses were made with Image J program (Wayne Rasband, National Institutes of Health, USA).

### **3.2.11 Mitochondrial transmembrane potential measurement in adult cardiomyocytes**

Mitochondrial transmembrane potential ( $\Delta\Psi_m$ ) was measured according to the manufacturer's instructions using Mito-ID<sup>®</sup> (Enzo Life Sciences, Villeurbanne, France). The orange fluorescence emission (Excitation = 540 nm, Emission = 570 nm) associated with energized mitochondria with high transmembrane potential and the green fluorescence emission (Excitation = 485 nm, Emission = 530 nm) associated with depolarized mitochondria with low transmembrane potential were recorded. The images were acquired under a 63 $\times$  Plan-Apochromat (NA 1.40) oil immersion objective lens using a confocal microscope (Leica).

### **3.2.12 Measurement of mitochondrial $\text{Ca}^{2+}$ in cardiomyocytes**

Isolated neonatal or adult rat cardiomyocytes were loaded with 5  $\mu\text{M}$  Rhod-2 at 37°C for 30 min. To remove cytosolic Rhod-2, the sarcolemmal membrane was permeabilized by perfusion of digitonin (5  $\mu\text{g/mL}$ ) in a  $\text{Ca}^{2+}$  free internal solution that contained 50 mM KCl, 80 mM potassium aspartate, 4 mM sodium pyruvate, 20 mM HEPES, 3 mM  $\text{MgCl}_2$ , 3 mM  $\text{Na}_2\text{ATP}$ , 5.8 mM glucose, and 0.5 mM EGTA (pH 7.3 with KOH). After the sarcolemmal membrane was permeabilized, the free  $\text{Ca}^{2+}$  concentration in the internal solution was increased to 600 nM. The  $\text{Ca}^{2+}$  was calculated using the maxchelator program from Stanford. Images were acquired with a Leica (SP5) confocal microscope. Excitation was achieved by a white light laser fitted at 552 nm and emission collected at 575 nm. Analyses were made with Image J program.



### 3.3 Methods used in isolated mitochondria

#### 3.3.1 Animals

Adult male Wistar rats (180-200 g in body weight) were purchased from Elevage Janvier (Le Genest St Isle, France). All experiments performed conform to the European Community guiding principles in the care and use of animals (86/609/CEE, CE Off J no. L358, December 18, 1986), the local ethics committee (CREEA Ile-de-France Sud) guidelines, and the French decree no. 97-848 of October 19, 1987 (J Off République Française, October 20, 1987, pp 12245-12248). Authorizations to perform animal experiments according to this decree were obtained from the French Ministry of Agriculture, Fisheries and Food (no. 92-283, June 27, 2007).

#### 3.3.2 Isolation of rat cardiac mitochondria

Mitochondria were isolated from the heart of adult male Wistar rats at 8-10 weeks of age 275-375g; Janvier, Le Genest St Isle, France) as described <sup>382</sup>. The following solutions were prepared in advance as shown in Table 3.7.

**Table 3.7 Buffer H**

Reagents	Cocentration(mM)
Sucrose 0.3 M	300
TES 5 mM	5
EGTA 0.2 mM	0.2
pH	7.2 with KOH

**Table 3.8 Buffer H +BSA**

Reagents	Cocentration(mM)
Sucrose 0.3 M	300
TES 5 mM	5
EGTA 0.2 mM	0.2
BSQ	1mg/mL
pH	7.2 with KOH

The heart was taken out of the rat after injection of pentobarbital and placed in cold buffer H. It was rinsed free of blood by using ice-cold buffer H. The heart was cut into

pieces in 10mL of Buffer H with a scalpel blade and transferred into a 50mL falcon tube. The heart was grinded with the Polytron 2-3 times rapidly. Then it was homogenized using the Potter. The homogenate was transferred to a 15mL Falcon tube and 5mL of Buffer H with BSA was added to fill the tube to 15mL and centrifuged at 500 g for 10 min at 4°C. The supernatant was collected by eliminating the maximum of lipids and the pellet was discarded. The supernatant was centrifuged at 3,000 g for 10 min at 4°C, 2 times. After the centrifugation, the supernatant was removed and the pellet was gently resuspended in 200µL Buffer H without BSA. Mitochondrial protein concentration was determined by the BCA method following manufacturer's instruction using bovine serum albumin as standard. The mitochondria were kept on ice until use or frozen at -80°C in the presence of protease inhibitors.

### **3.3.3 Isolation of mouse cardiac mitochondria**

Mitochondria were isolated from the female mice heart at 15-20 weeks of age (Janvier, Le Genest St Isle, France) as described. The heart was taken out of the mouse after injection of pentobarbital and placed in cold buffer H on cooling plate. And blood was carefully eliminated. Heart was transferred into 4 ml of ice cold buffer and cut into small pieces with cooled scissors. Then the tissue was transferred into 7 ml KONTES® Dounce Tissue Grinder, and dounced 20 times with pestle A and B. Homogenate tissue was transferred to 15 mL Falcon tube. Homogenate was centrifuged at 1,000 g for 10 minutes at 4°C .supernatant was transferred to new 15 ml Falcon tube and centrifuged 12,000 g for 10 minutes at 4°C. The supernatant was removed and the mitochondrial pellet was carefully resuspended in 4ml isolation buffer centrifuged at 12,000 g for 10 minutes at 4°C. The final mitochondrial pellet was resuspended in 100 µL buffer H. Mitochondria were used freshly for functional experiments or frozen at -80°C in the presence of protease inhibitors.

### 3.3.4 Mitochondrial transmembrane potential ( $\Delta\Psi_m$ ) and swelling

The following solutions were prepared in advance as shown in Table 3.5

**Table 3.9 Buffer S**

Reagents	Cocentration(mM)
Sucrose	200
Succinate	5
MOPS	10
EGTA	10
H <sub>3</sub> PO <sub>4</sub>	1
pH	7.4 with KOH

Buffer S was prepared with final concentration of 2 $\mu$ M rotenone. The compounds to be tested were prepared in 10 $\times$  concentrations with buffer S. 20 $\mu$ L of compounds or buffer S (control) was added into 96 wells black microtiter plate with transparent and flat bottom. 80 $\mu$ L of buffer S was added to per well. Freshly isolated cardiac mitochondria were diluted at 0.25  $\mu$ g/ $\mu$ L with buffer S and rhodamine 123 was added to obtain a final concentration of 1 $\mu$ M. 100 $\mu$ L of mitochondria were added in each well. The plate was shaken for 5s and then measure was started for 60min with 2 parameters at room temperature using Tecan Infinite 200 spectrofluorimeter (Männedorf, Switzerland). For membrane potential, the fluorescence at  $\lambda_{ex}$  = 485nm and  $\lambda_{em}$  = 535nm was measured. For swelling, absorbance at 540nm was measured<sup>382</sup>.

### 3.3.5 Oxygen consumption

Isolated mitochondria (50  $\mu$ g proteins) from rat heart were incubated with drugs in a buffer containing 250 mM sucrose, 30 mM K<sub>2</sub>HPO<sub>4</sub>, 1 mM EGTA, 5 mM MgCl<sub>2</sub>, 15 mM KCl, and 1 mg/mL bovine serum albumin (BSA) (pH 7.4) supplemented with respiratory substrates and MitoXpress, an oxygen-sensitive phosphorescent dye (LUXCEL, Cork, Ireland). Oxygen consumption was measured in real time for 60 min at 30°C in 96-well plates using Tecan Infinite 200 (Excitation = 380 nm; Emission = 650 nm) in the presence of 1.65 mM ADP and with 5 mM malate and 12.5 mM glutamate<sup>382</sup>.

**Table 3.10 Oxygen consumption buffer**

Reagents	Cocentration(mM)
Sucrose	250
KCl	15
MgCl <sub>2</sub>	5
EGTA	1
K <sub>2</sub> HPO <sub>4</sub>	30

### 3.3.6 Ca<sup>2+</sup> accumulation measurement

Isolated mitochondria (25 µg proteins) were incubated with 5 µM Rhod-2 (Enzo Life Sciences, Villeurbanne, France) in the buffer containing 200 mM sucrose, 10 mM MOPS, 10 µM EGTA, 1 mM H<sub>3</sub>PO<sub>4</sub>, 5 mM succinate and 2 µM rotenone for 30 min in dark at room temperature. After, the mitochondria were washed 2 times. Then, the mitochondria were treated with various drugs for 10 min before applying Ca<sup>2+</sup>. Fluorescence was measured in real time for 60 min at room temperature in 96-well plates using Tecan Infinite 200 (Excitation =552 nm; Emission =581 nm).

### 3.3.7 cAMP measurement in isolated mitochondria

cAMP measurements were performed according to the manufacturer's instructions using monoclonal anti-cAMP antibodybased direct cAMP ELISA Kit (New East Biosciences, King of Prussia, PA, USA) on freshly isolated mitochondria from rat hearts (500 µg proteins per sample). The mitochondria were incubated with different drugs for 30 min at RT. Then they are centrifuged at 3,000 g for 10min at 4°C. The pellet was lysate in 0.1M HCl+1% Triton X 100 for 10 min and centrifuged for at 12,000g for 10min at 4°C. The supernatant were kept on ice. Neutralizing Reagent (50 µL) was added into each well, except the TA (Total Activity) and Blank wells. 100 µL of 0.1M HCl was added into the NSB (None Specific Binding) and the Bo (0 pmol/mL Standard) wells. 100 µL of Standards and sample were added into the appropriate wells. 50 µL of 0.1 M HCl, 50 µL of Conjugate and 50 µL of Antibody were added into the NSB wells, the TA and Blank wells and all the wells, except the Blank, TA and NSB wells respectively. The plate was incubated at room temperature for 2 hours on a plate shaker at 250~500 rpm. After the incubation, the contents were removed from the wells

and washed by adding 400  $\mu$ L of wash solution to every well, repeated 2 more times for a total of 3 washes. After the final wash, the wells were aspirated, and firmly taped the plate on a lint free paper towel to remove any remaining wash buffer. 5  $\mu$ L of the Conjugate was added to the TA wells. 200  $\mu$ L of the Substrate solution was added to every well. Then the plate was incubated at room temperature for 15 minutes without shaking. (Substrate A and B were mixed together in equal volumes within 15 minutes of use, protected from light.) After, 50  $\mu$ L of Stop Solution was added to every well to stop the reaction and the plate was read immediately. The reading is performed at 450 nm, preferably with correction between 570 and 590 nm<sup>225,379,383</sup>.

### 3.3.8 ATP measurement

ATP measurements in isolated mitochondria were performed according to manufacturer's instructions using ATP Bioluminescence Assay Kit CLSII (Roche, Basel, Switzerland). The mitochondria were incubated with different drugs for 30 min at RT. Then they are centrifuged at 10,000 g for 10min at 4°C. The pellet was lysate in 200 $\mu$ L lysis reagent for 30min on ice and then boil 2 min and centrifuged at 10, 000g for 10min at 4°C. After the centrifugation, the supernatant was collected and diluted 5 times with dilution buffer. ATP standard was diluted with dilution buffer by serial dilution in the range of  $10^{-6}$  to  $10^{-12}$  M. 50  $\mu$ L of sample and ATP standard were added into the 96 well plate with 20  $\mu$ L of the luciferase and read immediately.

### 3.3.9 Bioenergetic analysis in isolated mitochondria

The XFe96 Extracellular Flux Analyzer (Seahorse Biosciences, North Billerica, MA, USA) was used to measure mitochondrial bioenergetic function<sup>384</sup>. Respiration by the mitochondria (0.5  $\mu$ g/well) was sequentially measured in a coupled state with substrate present (basal respiration, State 2) in Mitochondrial Assay Solution (70 mM sucrose, 220 mM mannitol, 10 mM  $\text{KH}_2\text{PO}_4$ , 5 mM  $\text{MgCl}_2$ , 2 mM HEPES, 1 mM EGTA and 0.2% (w/v) fatty acid-free BSA, pH 7.2). State 3 initiated with ADP, state 4 induced with the addition of oligomycin (State 4o), and FCCP-induced maximal uncoupler-stimulated respiration (State 3u) were sequentially measured. At the end of the

experiment the Complex III inhibitor, antimycin A was applied to completely shut down the mitochondrial respiration. Injections were as follows: port A, 20  $\mu\text{L}$  of 40 mM ADP (4 mM, final); port B, 22  $\mu\text{L}$  of 25  $\mu\text{g/mL}$  oligomycin (2.5  $\mu\text{g/mL}$ , final); port C, 24  $\mu\text{L}$  of 40  $\mu\text{M}$  FCCP (4  $\mu\text{M}$ , final); and port D, 26  $\mu\text{L}$  of 40  $\mu\text{M}$  antimycin A (4  $\mu\text{M}$ , final).

## **4 Results**

### **4.1 Article 1: A cardiac mitochondrial cAMP signaling pathway regulates calcium accumulation, permeability transition and cell death**

# A cardiac mitochondrial cAMP signaling pathway regulates calcium accumulation, permeability transition and cell death

Z Wang<sup>1</sup>, D Liu<sup>1</sup>, A Varin<sup>1</sup>, V Nicolas<sup>2</sup>, D Courilleau<sup>2</sup>, P Mateo<sup>1</sup>, C Caubere<sup>3</sup>, P Rouet<sup>3</sup>, A-M Gomez<sup>1</sup>, G Vandecasteele<sup>1</sup>, R Fischmeister<sup>1,2</sup> and C Brenner<sup>\*,1,2</sup>

Although cardiac cytosolic cyclic 3',5'-adenosine monophosphate (cAMP) regulates multiple processes, such as beating, contractility, metabolism and apoptosis, little is known yet on the role of this second messenger within cardiac mitochondria. Using cellular and subcellular approaches, we demonstrate here the local expression of several actors of cAMP signaling within cardiac mitochondria, namely a truncated form of soluble AC (sAC<sub>t</sub>) and the exchange protein directly activated by cAMP 1 (Epac1), and show a protective role for sAC<sub>t</sub> against cell death, apoptosis as well as necrosis in primary cardiomyocytes. Upon stimulation with bicarbonate (HCO<sub>3</sub><sup>-</sup>) and Ca<sup>2+</sup>, sAC<sub>t</sub> produces cAMP, which in turn stimulates oxygen consumption, increases the mitochondrial membrane potential ( $\Delta\Psi$ m) and ATP production. cAMP is rate limiting for matrix Ca<sup>2+</sup> entry via Epac1 and the mitochondrial calcium uniporter and, as a consequence, prevents mitochondrial permeability transition (MPT). The mitochondrial cAMP effects involve neither protein kinase A, Epac2 nor the mitochondrial Na<sup>+</sup>/Ca<sup>2+</sup> exchanger. In addition, in mitochondria isolated from failing rat hearts, stimulation of the mitochondrial cAMP pathway by HCO<sub>3</sub><sup>-</sup> rescued the sensitization of mitochondria to Ca<sup>2+</sup>-induced MPT. Thus, our study identifies a link between mitochondrial cAMP, mitochondrial metabolism and cell death in the heart, which is independent of cytosolic cAMP signaling. Our results might have implications for therapeutic prevention of cell death in cardiac pathologies.

*Cell Death and Disease* (2016) 7, e2198; doi:10.1038/cddis.2016.106; published online 21 April 2016

Mitochondria are involved in cell life and fate decision through their multiple biological functions in energetic metabolism, reactive oxygen species (ROS) detoxification and cell death.<sup>1–3</sup> These functions are crucially regulated to provide sufficient energy for cell functions, maintain mitochondrial membrane integrity and avoid excessive cell death.<sup>4,5</sup> Moreover, mitochondria may participate in Ca<sup>2+</sup> homeostasis via matrix Ca<sup>2+</sup> accumulation through the mitochondrial Ca<sup>2+</sup> uniporter (MCU), Ca<sup>2+</sup> release into the cytosol and propagation to other mitochondria, notably in excitable cells.<sup>6–8</sup> In cardiomyocytes, intracellular Ca<sup>2+</sup> movements are crucial for proper myofibril contraction and relaxation and energetic metabolism. Moreover, recent studies in cardiomyocyte-specific mutant mouse lacking the MCU showed a link between mitochondrial Ca<sup>2+</sup> uptake and energetic supply in relation with cardiac workload during acute stress.<sup>9,10</sup> In contrast, excessive mitochondrial Ca<sup>2+</sup> accumulation, ROS production and adenine nucleotide depletion result in the sudden opening of a megachannel, namely the permeability transition pore complex. The prolonged opening of this unspecific pore leads to the mitochondrial permeability transition (MPT), cell death, inflammation and irreversible

tissue damage.<sup>11,12</sup> MPT can be a critical event in severe cardiac diseases such as ischemia–reperfusion injury and heart failure (HF) as well as a radiation-induced cardiotoxicity.<sup>11,13,14</sup> Hence, MPT inhibition by cyclosporin A (CsA) has been shown to limit cardiac damages and improve cell survival. Inhibition of MPT has thus become an attractive therapeutic strategy in cardioprotection.<sup>15</sup>

Cyclic 3',5'-adenosine monophosphate (cAMP) is a major second messenger in many organs, particularly in the heart, where it regulates diverse physiological processes such as Ca<sup>2+</sup> homeostasis, beating frequency and myocardial contractility as well as cell death.<sup>16</sup> In the working myocardium, cAMP can activate protein kinase A (PKA) and/or the exchange protein directly activated by cAMP (Epac) to mediate diverse biological effects, including cardiac remodeling and hypertrophy.<sup>17–22</sup> In addition to tmACs, cAMP can also be generated by soluble adenylyl cyclase (sAC), which is not regulated by heterotrimeric G proteins or forskolin (FSK), but can be activated by bicarbonate (HCO<sub>3</sub><sup>-</sup>) and Ca<sup>2+</sup>.<sup>16,23,24</sup> sAC was found inside mitochondria in the brain and liver and in certain mammalian cell types.<sup>25–29</sup> In the liver and brain, in response to HCO<sub>3</sub><sup>-</sup> and/or Ca<sup>2+</sup>, mitochondrial cAMP

<sup>1</sup>INSERM UMR-S 1180, Faculté de Pharmacie, Université Paris-Sud, Université Paris-Saclay, Châtenay-Malabry, France; <sup>2</sup>UMS-IPSIT, Université Paris-Sud, Université Paris-Saclay, Châtenay-Malabry, France and <sup>3</sup>INSERM I2MC, UMR 1048, Université Paul Sabatier, Toulouse, France

\*Corresponding author: C Brenner, INSERM UMR-S 1180, Faculté de Pharmacie, Université Paris-Sud, Université Paris-Saclay, 5 Rue J-B Clément, Châtenay-Malabry Cedex 92296, France. Tel: (+33) 6 60 99 32 77; Fax: (+33) 1 46 83 54 75; E-mail: catherine.brenner-jan@u-psud.fr

**Abbreviations:** 2HE, 2-hydroxyestradiol; AC, adenylyl cyclase; ANT, adenine nucleotide translocase; CCCP, carbonyl cyanide m-chlorophenyl hydrazone; CsA, cyclosporine A;  $\Delta\Psi$ m, mitochondrial membrane potential; Epac, exchange protein directly activated by cAMP; HCO<sub>3</sub><sup>-</sup>, bicarbonate; HF, heart failure; IM, inner membrane; MCU, mitochondrial calcium uniporter; mNCX, mitochondrial Na<sup>+</sup>/Ca<sup>2+</sup> exchanger; MPT, mitochondrial permeability transition; OM, outer membrane; PKA, protein kinase A; ROS, reactive oxygen species; sAC, soluble adenylyl cyclase; sAC<sub>fl</sub>, full-length soluble adenylyl cyclase; sAC<sub>t</sub>, truncated soluble adenylyl cyclase

Received 13.1.16; revised 17.3.16; accepted 21.3.16; Edited by G Raschella



stimulates oxidative phosphorylation and ATP production.<sup>30</sup> In coronary endothelial cells,  $\text{HCO}_3^-$  indirectly modulates the cell fate through apoptosis.<sup>31,32</sup> As a result, this pathway serves as a mechanism for metabolic adaptation to mitochondrial dysfunction and could be a potential novel target to treat genetic mitochondrial diseases.<sup>33</sup> Altogether, these findings suggest that mitochondrial sAC functions as a metabolic sensor to stimulate mitochondrial biological functions. If proven in primary cardiomyocytes, this intramitochondrial cAMP pathway might have clinical implication in HF as patients diagnosed with HF have markedly impaired mitochondrial metabolism and cAMP signaling, both contributing to cardiomyocyte dysfunction.<sup>16,34</sup>

Intrigued by these previous findings, we tested the existence of a cAMP mitochondrial pathway in differentiated adult and neonatal cardiomyocytes and observed that activation of this pathway prevents various cell deaths. Our results also show that cardiac mitochondria isolated from adult rat hearts contain a truncated form of sAC ( $\text{sAC}_t$ ) as a source of cAMP as well as Epac1. A role of this local pathway is to control mitochondrial  $\text{Ca}^{2+}$  entry through the MCU and to prevent the deleterious consequences of mitochondrial  $\text{Ca}^{2+}$  overload such as dissipation of mitochondrial membrane potential ( $\Delta\Psi_m$ ) and induction of MPT. Interestingly, this mitochondrial  $\text{sAC}_t$ -Epac1-MCU pathway remains functional in a rat model of HF induced by aortic stenosis and its activation prevents MPT.

## Results

**Mitochondrial cAMP prevents cardiac cell death, apoptosis as well as necrosis.** To evaluate the capacity of sAC and cAMP to regulate the cardiomyocyte cell fate, we infected primary neonatal cardiomyocytes with two adenoviruses to overexpress the full-length sAC ( $\text{sAC}_f$ ) and the  $\text{sAC}_t$ , respectively, 24 h before cell death induction by three different cell death inducers, that is, camptothecin,  $\text{H}_2\text{O}_2$  and  $\text{TNF-}\alpha$ +actinomycin D. We showed that the stimulation of endogenous sAC with  $\text{HCO}_3^-$  as well as overexpression of  $\text{sAC}_t$  prevented the various cell death modalities, apoptosis as well as necrosis measured by annexin/7-AAD labeling (Figures 1a and b). In contrast, inhibition of sAC with 2-hydroxyestradiol (2HE), a sAC inhibitor,<sup>29</sup> aggravated significantly cell deaths (Figure 1a). We observed also that cAMP protects from nuclei alterations measured by counting Hoechst-stained nuclei exhibiting morphologic and biochemical alterations, that is, pycnosis and karyorrhexis (Figures 1c–f).

**Mitochondrial sAC produces locally cAMP and regulates  $\Delta\Psi_m$  upon calcium overload.** As mitochondria may be impermeant to cytosolic cAMP,<sup>35</sup> we constructed an adenovirus encoding a cAMP-sensitive fluorescence resonance energy transfer (FRET) sensor (Epac- $\text{S}^{\text{H187}}$ )<sup>36</sup> fused with a 4mt sequence and infected rat neonatal cardiomyocytes with this sensor, 4mt-Epac- $\text{S}^{\text{H187}}$ . The localization of 4mt-Epac- $\text{S}^{\text{H187}}$  in mitochondria was shown by colocalization of its green fluorescence with mitotracker red fluorescence (Pearson's coefficient:  $0.92 \pm 0.02$ ,  $n=6$ ) (Figure 2a). Following

infection with 4mt-Epac- $\text{S}^{\text{H187}}$ , we sequentially treated the cells with  $\text{HCO}_3^-$  to activate sAC, FSK to activate tmAC and 8-CPT-2'-OMe-cAMP-AM (8CPT-cAMP AM), a permeant cAMP analog, to directly activate the sensor (Figure 2b). Addition of  $\text{HCO}_3^-$  induced an increase in cAMP measured by 4mt-Epac- $\text{S}^{\text{H187}}$  (Figure 2b), which was virtually absent when the cells were infected with the cytoplasmic cAMP sensor Epac- $\text{S}^{\text{H187}}$  (Figure 2c). On the contrary, FSK induced a large response of cAMP measured with the cytoplasmic sensor (Figure 2c) and a smaller response of cAMP measured with the mitochondrial sensor (Figure 2b). These results are compatible with  $\text{HCO}_3^-$ -activating sAC in mitochondria and FSK increasing cAMP in the cytoplasm by activating tmAC. The small response to FSK observed with 4mt-Epac- $\text{S}^{\text{H187}}$  might be due to incomplete targeting of the probe to mitochondria. Of note, 4mt-Epac- $\text{S}^{\text{H187}}$  has a much higher dynamic range than previously published sensors such as mito-EpacH90,<sup>35</sup> so that even a small expression of the probe in the cytosol would lead to a detectable signal. Alternatively, the small response to FSK measured with 4mt-Epac- $\text{S}^{\text{H187}}$  might be due to  $\text{Ca}^{2+}$  stimulation of sAC in the matrix upon FSK stimulation as suggested previously,<sup>29</sup> or to a small permeability of the mitochondrial inner membrane (IM) to cAMP. Interestingly, 2HE totally prevented the mitochondrial cAMP increase elicited by  $\text{HCO}_3^-$  (Figure 2d). This confirms the involvement of a mitochondrial sAC as a source of cAMP in cardiomyocytes.

To address the role of sAC in the regulation of mitochondrial function, cardiomyocytes were transfected with siRNA control and siRNA against sAC for 48 h. Next, they were loaded with the fluorescent  $\Delta\Psi_m$  indicator, TMRM, permeabilized and treated with  $\text{Ca}^{2+}$ . The decrease in the level of sAC did not induce any changes of the mitochondrial network (Figures 2e and f). However, the measure of the TMRM fluorescence ratio showed that silencing of sAC markedly aggravated the loss of  $\Delta\Psi_m$  induced by  $\text{Ca}^{2+}$ , suggesting a role of cAMP in  $\Delta\Psi_m$  control in stress conditions.

**cAMP is produced by  $\text{sAC}_t$  in isolated mitochondria.** Mitochondria were isolated from rat heart ventricles by differential centrifugation and extensive washes.<sup>37</sup> First, we analyzed their morphology by transmission electron microscopy (Figure 3a) and their purity by western blotting (Figure 3b). As expected, mitochondria appeared round-shaped (mean diameter,  $0.8 \mu\text{m}$ ) and presented numerous cristae, compatible with a high respiratory capacity. In comparison with rat ventricles homogenate (H), isolated mitochondria (M) were enriched in the adenine nucleotide translocase (ANT), an IM protein and almost not contaminated by cytosolic proteins such as GAPDH, myofibrillar proteins such as troponin I (TnI) and sarcoplasmic reticulum-associated proteins such as phospholamban (PLB) (Figure 3b). Using specific monoclonal antibodies, we detected the  $\text{sAC}_t$  (48 kDa) and the  $\text{sAC}_f$  (187 kDa) in H fraction, whereas only the short form, which is the active form,<sup>38</sup> was found in the mitochondria preparation (Figure 3b). Next, we measured cAMP production in freshly isolated mitochondria. We observed that  $\text{HCO}_3^-$  and also, to a lesser extent,  $\text{Ca}^{2+}$ -stimulated cAMP production in a dose-dependent manner and potentiated the response to ADP

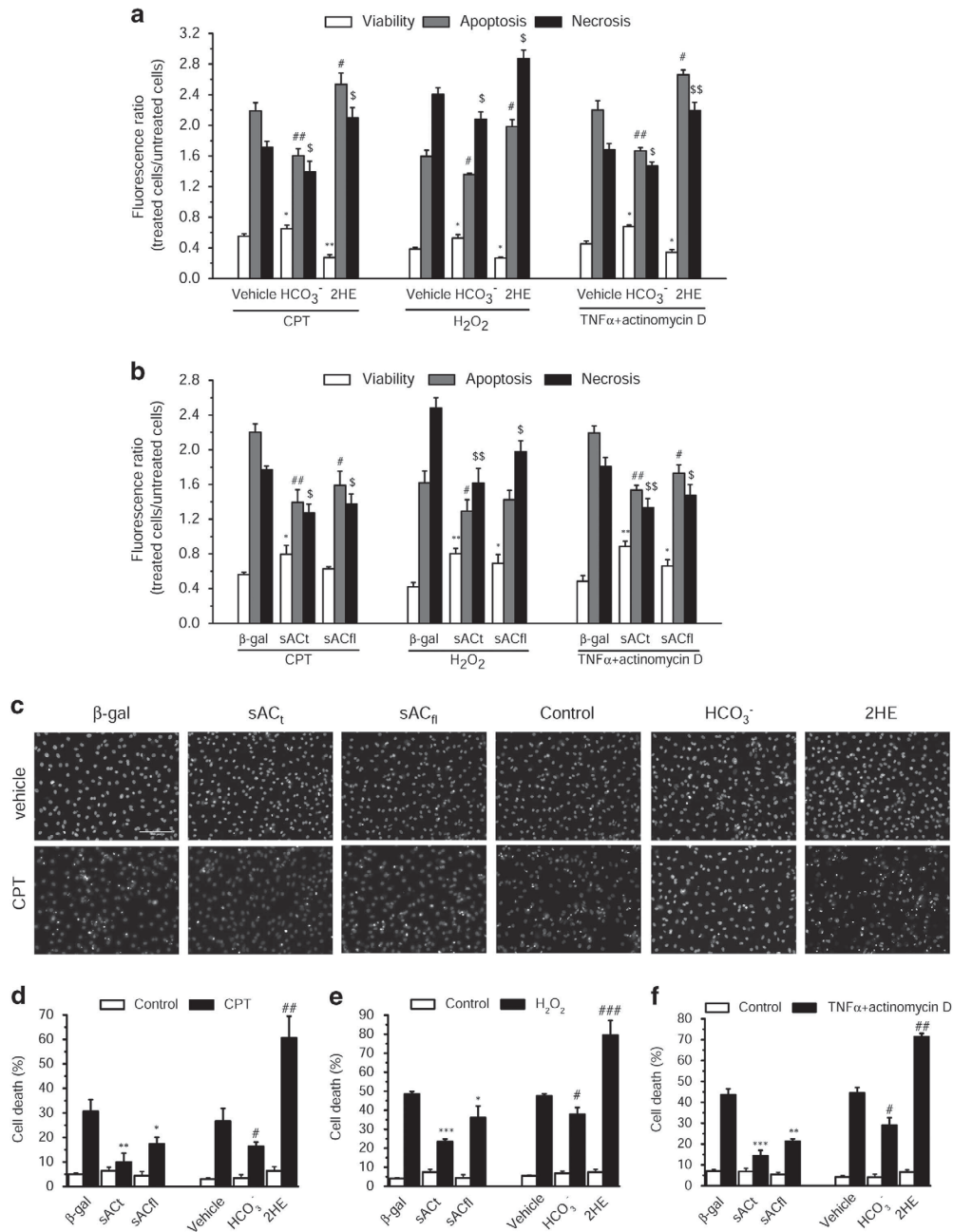


**Figure 1** Mitochondrial cAMP protects cell death induced by camptothecin (CPT), hydrogen peroxide ( $\text{H}_2\text{O}_2$ ) and tumor necrosis factor- $\alpha$  (TNF $\alpha$ ) in neonatal cardiomyocytes. (a) Cells were treated with vehicle, 15 mM  $\text{HCO}_3^-$  and 25  $\mu\text{M}$  2HE in the presence of 10  $\mu\text{M}$  CPT for 48 h or 300  $\mu\text{M}$   $\text{H}_2\text{O}_2$  for 24 h or 10 ng/ml TNF $\alpha$ /0.1  $\mu\text{g}/\text{ml}$  actinomycin D for 24 h. (b) Cells were infected by adenoviruses encoding  $\beta$ -galactosidase ( $\beta$ -gal), sAC $_t$  and sAC $_f$  for 24 h and then treated with 10  $\mu\text{M}$  CPT for 48 h or 300  $\mu\text{M}$   $\text{H}_2\text{O}_2$  for 24 h or 10 ng/ml TNF $\alpha$ /0.1  $\mu\text{g}/\text{ml}$  actinomycin D for 24 h. \* $P$  < 0.05, \*\* $P$  < 0.01 versus vehicle or  $\beta$ -gal viability; # $P$  < 0.05, ## $P$  < 0.01 versus vehicle or  $\beta$ -gal apoptosis; \$\$\$ $P$  < 0.001 versus vehicle or  $\beta$ -gal necrosis ( $n$  = 3). (c) Representative fluorescence images of nuclear staining with Hoechst 33342. (d–f) Quantitative analysis of cell death rate. Cells were infected with adenoviruses encoding  $\beta$ -gal, sAC $_t$  and sAC $_f$  for 24 h and then treated with CPT (10  $\mu\text{M}$ ) for 48 h,  $\text{H}_2\text{O}_2$  (300  $\mu\text{M}$ ) or TNF $\alpha$ /actinomycin D (10 ng/ml, 0.1  $\mu\text{g}/\text{ml}$ ) for 24 h, or cells were treated with vehicle, 15 mM  $\text{HCO}_3^-$  and 25  $\mu\text{M}$  2HE in the presence of CPT (10  $\mu\text{M}$ ) for 48 h,  $\text{H}_2\text{O}_2$  (300  $\mu\text{M}$ ) or TNF $\alpha$ /actinomycin D (10 ng/ml, 0.1  $\mu\text{g}/\text{ml}$ ) for 24 h. \* $P$  < 0.05, \*\* $P$  < 0.01, \*\*\* $P$  < 0.001 versus  $\beta$ -gal; # $P$  < 0.05, ## $P$  < 0.01, ### $P$  < 0.001 versus vehicle ( $n$  = 3)

(Figure 3c). Although a small stimulatory effect of  $\text{Ca}^{2+}$  on cAMP production was observed at 0.1  $\mu\text{M}$ , when increasing the concentration to 10  $\mu\text{M}$ , mitochondria lost their membrane potential (not shown), lowering markedly cAMP production (Figure 3c).  $\text{Ca}^{2+}$  effects were abolished in the presence of RU360, confirming that the effect on cAMP levels is due to a

specific uptake of  $\text{Ca}^{2+}$  within the matrix. Similarly, when mitochondria were depolarized by the protonophore carbonyl cyanide *m*-chlorophenyl hydrazone (CCCP), no cAMP production was detected even in the presence of  $\text{HCO}_3^-$  (Figure 3d). Moreover, 2HE reduced basal and fully blocked  $\text{HCO}_3^-$ -stimulated cAMP production (Figure 3d). As a control,

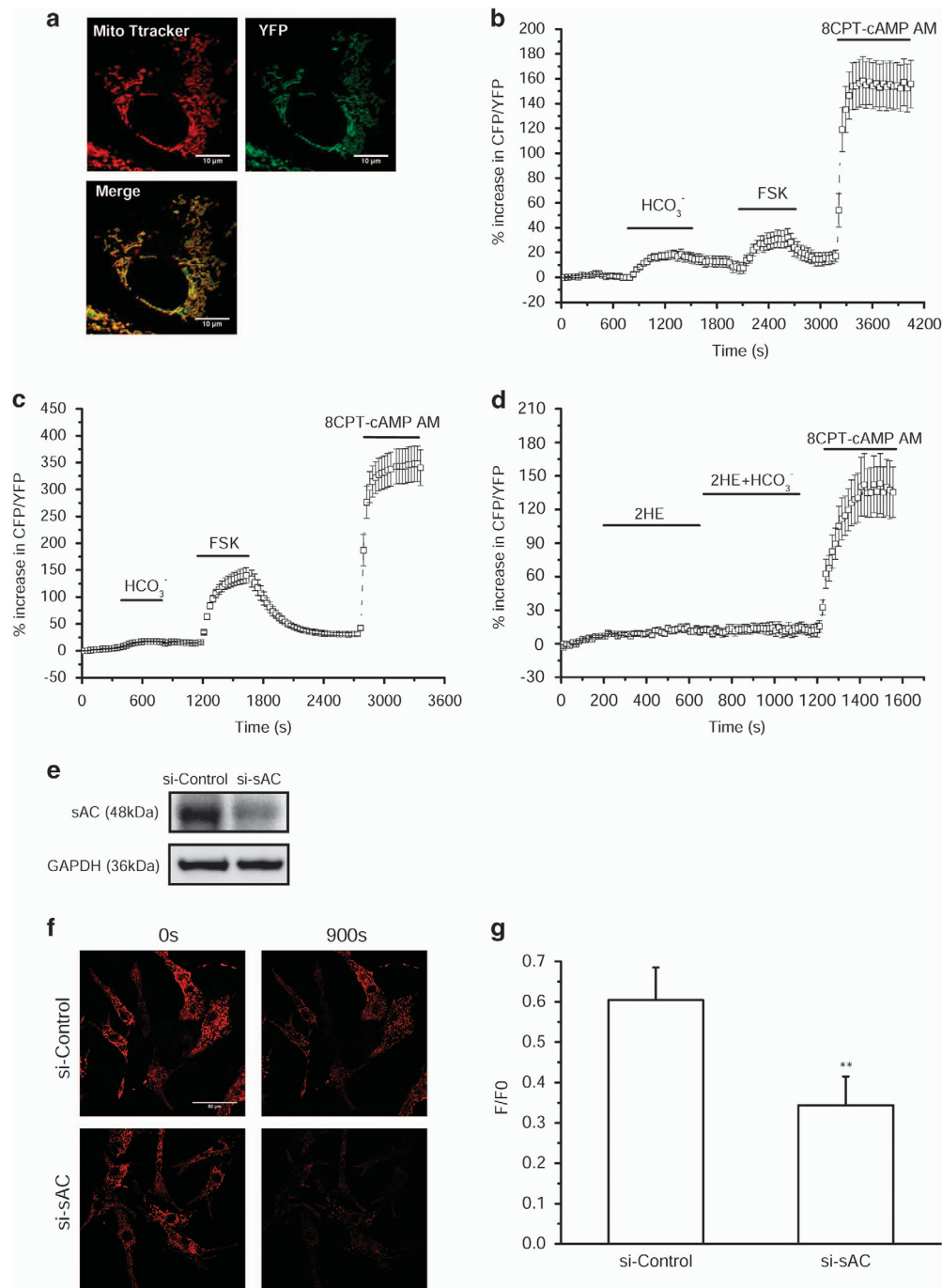


**Figure 2** Mitochondrial sACt produces locally cAMP and regulates  $\Delta\Psi_m$  upon calcium overload. **(a)** Mitochondrial localization of the 4mt-Epac-S<sup>H187</sup> cAMP sensor in rat isolated neonatal cardiomyocytes. Confocal images of cardiomyocytes infected with 4mt-Epac-S<sup>H187</sup> (green) and stained with MitoTracker Red. The colocalization of 4mt-Epac-S<sup>H187</sup> with MitoTracker is shown in yellow. Bar scale, 10  $\mu$ M. **(b and c)** Representative kinetics of percentage increase in CFP/YFP recorded in rat neonatal cardiomyocytes infected with either 4mt-Epac-S<sup>H187</sup> **(b)** or Epac-S<sup>H187</sup> sensor **(c)** and sequentially stimulated with 24 mM HCO<sub>3</sub><sup>-</sup>, 25  $\mu$ M FSK and 20  $\mu$ M 8CPT-cAMP AM. **(d)** Representative kinetics of percentage increase in CFP/YFP recorded in rat neonatal cardiomyocytes infected with 4mt-Epac-S<sup>H187</sup> exposed to 25  $\mu$ M 2HE in the absence or presence of 24 mM HCO<sub>3</sub><sup>-</sup>, and finally to 20  $\mu$ M 8CPT-cAMP AM **(b, n = 19; c, n = 6; d, n = 7)**. **(e)** sAC expression in neonatal rat cardiomyocytes transfected with non-targeting small interfering RNA (siRNA) (si-Control) or sAC siRNA (si-sAC). **(f)** Representative confocal images of tetramethylrhodamine, methyl ester (TMRM)-labeled permeabilized neonatal rat cardiomyocytes transfected with si-Control or si-sAC at time 0 s (left) and 900 s (right) after Ca<sup>2+</sup> (600 nM) addition. Bar scale, 50  $\mu$ M. **(g)** Averaged values of mitochondrial membrane potential (measured as F/F<sub>0</sub>, where F is the TMRM fluorescence signal at 900 s and F<sub>0</sub> is the signal at time 0 s of Ca<sup>2+</sup> addition) ( $n = 50$ ). \*\* $P < 0.01$  versus si-Control

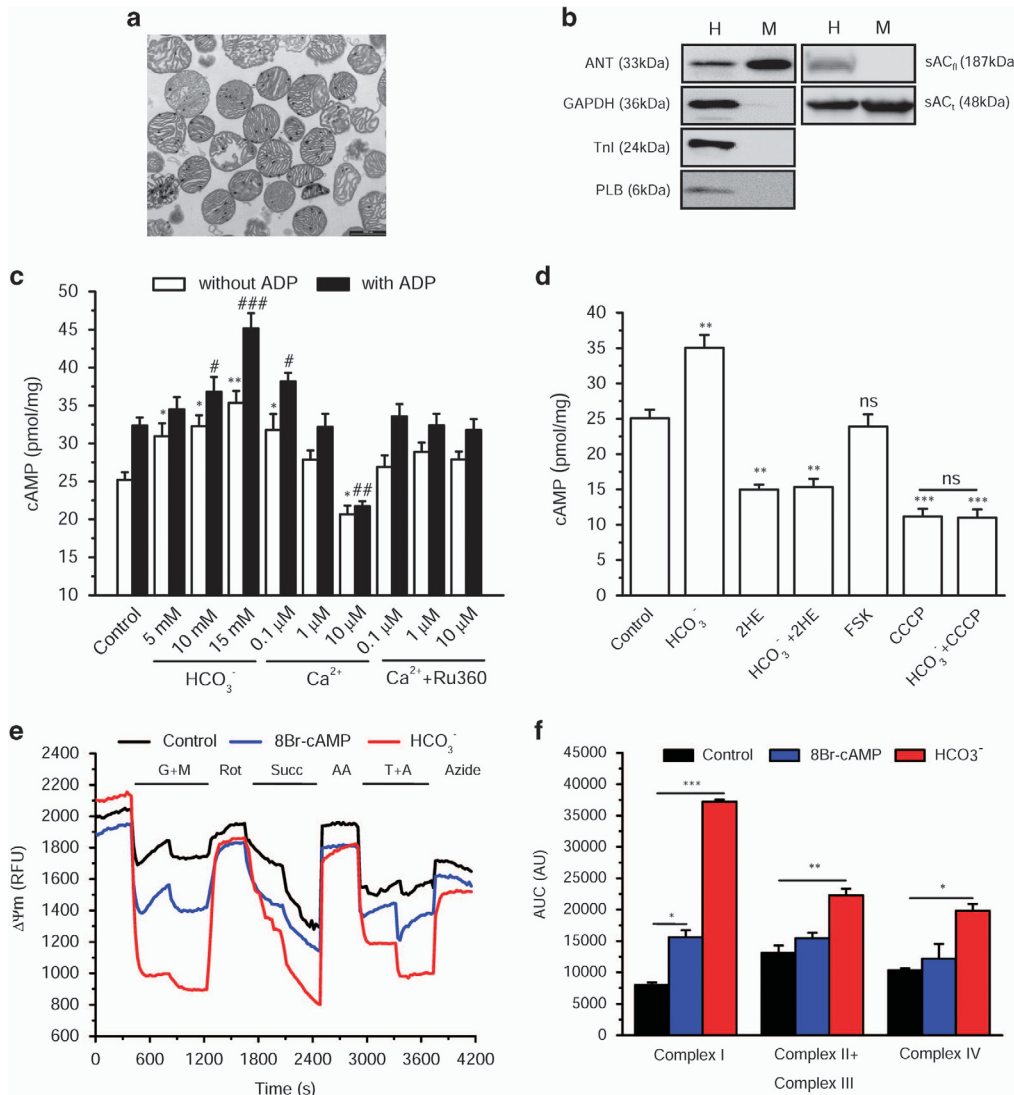


**Figure 3** cAMP produced by sAC regulates mitochondrial transmembrane inner potential ( $\Delta\Psi_m$ ). (a) Transmission electron microscopy image of isolated subsarcolemmal mitochondria from rat heart ventricles. Bar scale, 1  $\mu\text{M}$ . (b) Purity analysis of mitochondrial fraction by western blot. Protein ANT, inner membrane; glyceraldehyde 3-phosphate dehydrogenase (GAPDH), cytosol; PLB, sarcoplasmic reticulum; Tnl, myofibrils; sAC<sub>II</sub> and sAC<sub>I</sub> were probed in heart homogenate (H) and mitochondria (M). Results are representative of three independent experiments. (c) cAMP levels produced in isolated mitochondria in the presence of  $\text{HCO}_3^-$ ,  $\text{Ca}^{2+}$  and  $\text{Ca}^{2+}$ +Ru360 (a MCU inhibitor, 1 nM), under basal condition or upon stimulation with 1.65 mM ADP, determined by enzyme-linked immunosorbent assay (ELISA) ( $n=4-5$ ). (d) cAMP levels in isolated mitochondria under basal condition or in the presence of 15 mM  $\text{HCO}_3^-$ , 25  $\mu\text{M}$  2HE,  $\text{HCO}_3^-$ +2HE, 25  $\mu\text{M}$  FSK, 5  $\mu\text{M}$  CCCP or CCCP+ $\text{HCO}_3^-$ , determined by ELISA. Control, untreated mitochondria; NS, not significant ( $n=3-7$ ). (e)  $\Delta\Psi_m$  was evaluated with Rhod123 fluorescence in the absence or presence of 1 mM 8Br-cAMP or 15 mM  $\text{HCO}_3^-$  in isolated cardiac mitochondria with different respiratory substrates: 0.25 mM malate (M) and 0.5 mM glutamate (G) for complex I (inhibited by 2  $\mu\text{M}$  rotenone (Rot)); 0.5 mM succinate (Succ) for complexes II and III (blocked by the complex III inhibitor antimycin A (AA), 0.25  $\mu\text{g}/\text{ml}$ ) and 0.05 mM TMPD (T) with 0.2 mM ascorbate (A) for complex IV (inhibited by 5 mM sodium azide). RFU, relative fluorescence unit. (f) Comparison of 8Br-cAMP and  $\text{HCO}_3^-$  effects on  $\Delta\Psi_m$  stimulated with various respiratory substrates. Areas under the curve (AUC) were calculated from experiments such as that shown in (e) ( $n=3$ ). AU, arbitrary units. \* $P<0.05$ , \*\* $P<0.01$ , \*\*\* $P<0.001$  versus Control; # $P<0.05$ , ## $P<0.01$  versus Control with ADP

FSK had no stimulatory effect on cAMP in isolated mitochondria, confirming clearly the absence of tmAC within mitochondria (Figure 3d).

**cAMP increases  $\Delta\Psi_m$ , respiration and ATP levels.** Next, the  $\Delta\Psi_m$  was monitored with the probe, rhodamine 123 (Rhod123), in the presence of various respiratory substrates (Figures 3e and f). We used 8Br-cAMP, a membrane-permeant cAMP analog, as a control, and  $\text{HCO}_3^-$  to stimulate

endogenous production of cAMP. Figure 3e shows that 8Br-cAMP slightly hyperpolarized mitochondria in condition of complex I-driven respiration, but failed to have any effect in the presence of respiratory substrates for complexes II–IV. In contrast,  $\text{HCO}_3^-$  triggered a hyperpolarization in all conditions of substrates (Figure 3f). This hyperpolarization was accompanied by an increase in oxygen consumption in response to  $\text{HCO}_3^-$  (Figure 4a). Finally, when mitochondria were stimulated by  $\text{HCO}_3^-$  or  $\text{Ca}^{2+}$ , this led to an increase in



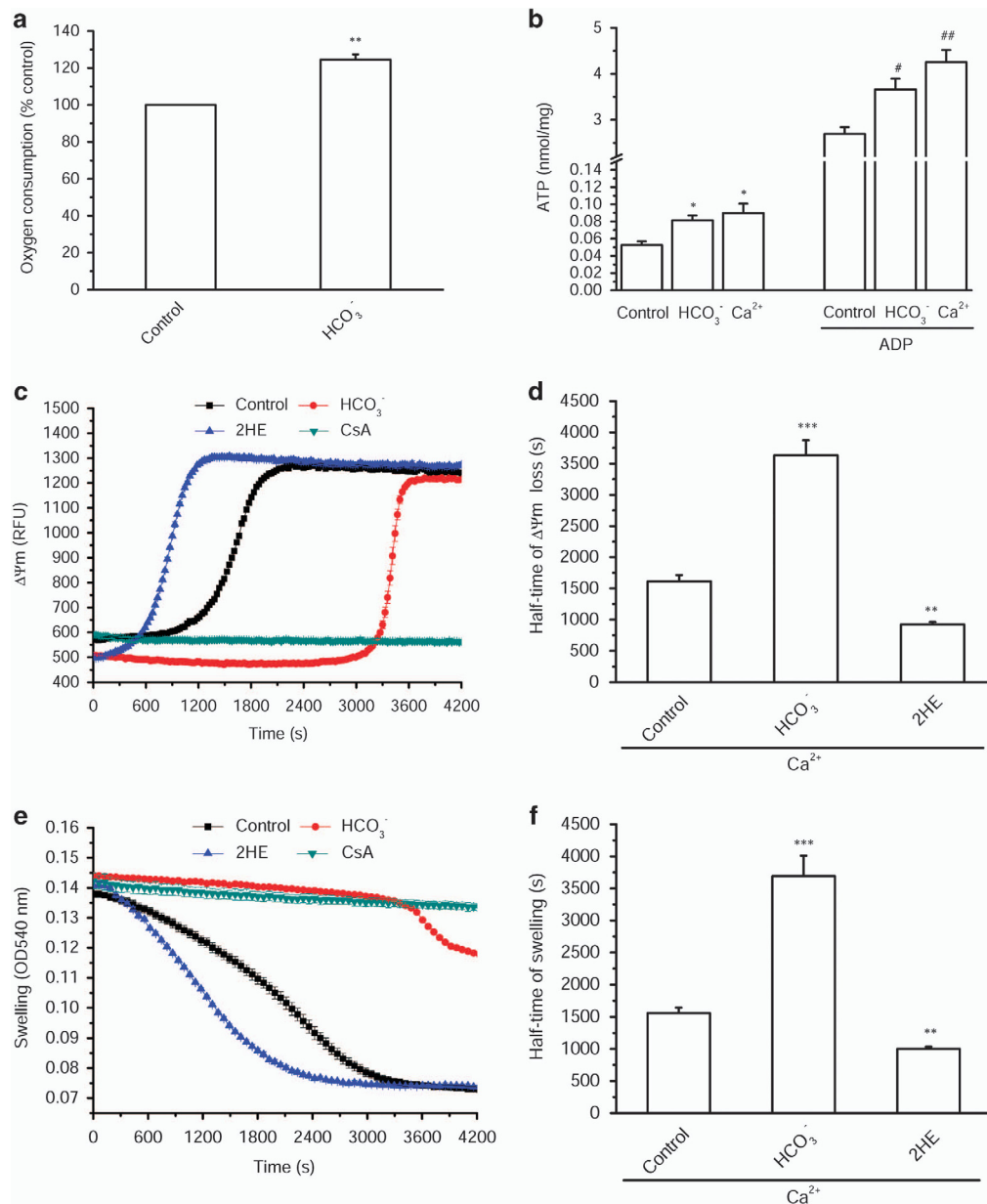


**Figure 4** cAMP regulates mitochondrial respiration, ATP levels and Ca<sup>2+</sup> induced mitochondrial depolarization and swelling. (a) Oxygen consumption of mitochondria measured with the probe MitoXpress in the presence or absence of 15 mM HCO<sub>3</sub><sup>-</sup> driven by 2.5 mM malate and 5 mM glutamate with 1.65 mM ADP. Control was normalized at 100% (*n* = 5). (b) ATP production in the presence of 15 mM HCO<sub>3</sub><sup>-</sup> and 0.1 μM Ca<sup>2+</sup> with or without 1.65 mM ADP stimulation driven by 5 mM succinate (*n* = 4). \**P* < 0.05 versus Control; #*P* < 0.05, ##*P* < 0.01 versus Control with ADP. (c) Effect of 15 mM HCO<sub>3</sub><sup>-</sup>, 25 μM 2HE and 5 μM CsA on ΔΨm loss induced by 10 μM Ca<sup>2+</sup>. (d) Average half-time values of ΔΨm loss induced by 10 μM Ca<sup>2+</sup> calculated from panels (c) (*n* = 7–20). (e) Effect of 15 mM HCO<sub>3</sub><sup>-</sup>, 25 μM 2HE and 5 μM CsA on mitochondrial swelling induced by 10 μM Ca<sup>2+</sup>. (f) Average half-time values of mitochondrial swelling induced by 10 μM Ca<sup>2+</sup> calculated from panel e (*n* = 7–20). \*\**P* < 0.01, \*\*\**P* < 0.001 versus Control

ATP production both in the absence and presence of ADP (Figure 4b). These data indicate that cAMP produced by a mitochondrial sAC stimulates the oxidative phosphorylation increasing ΔΨm and mitochondrial ATP synthesis.

**cAMP delays Ca<sup>2+</sup>-induced MPT.** We hypothesized that the cyclic nucleotide could have a role in the regulation of MPT.<sup>39</sup> In isolated cardiac mitochondria, MPT can be elicited by 10 μM Ca<sup>2+</sup> and prevented by 5 μM CsA and detected as a loss of ΔΨm and a matrix swelling.<sup>37</sup> We used two robust

miniaturized assays<sup>37,40</sup> to concomitantly measure the effect of sAC inhibition by 25 μM 2HE on mitochondrial depolarization (Figures 4c and d) and matrix swelling (Figures 4e and f) induced by 10 μM Ca<sup>2+</sup>. sAC inhibition by 2HE accelerated the depolarization (Figures 4c and d) and swelling (Figures 4e and f) induced by Ca<sup>2+</sup>, as shown by the decreased half-time of ΔΨm loss and swelling (Figures 4d and f). Conversely, 15 mM HCO<sub>3</sub><sup>-</sup> slowed both processes (Figures 4d and f), suggesting that cAMP elevation confers a protection of mitochondria from Ca<sup>2+</sup>-induced MPT.

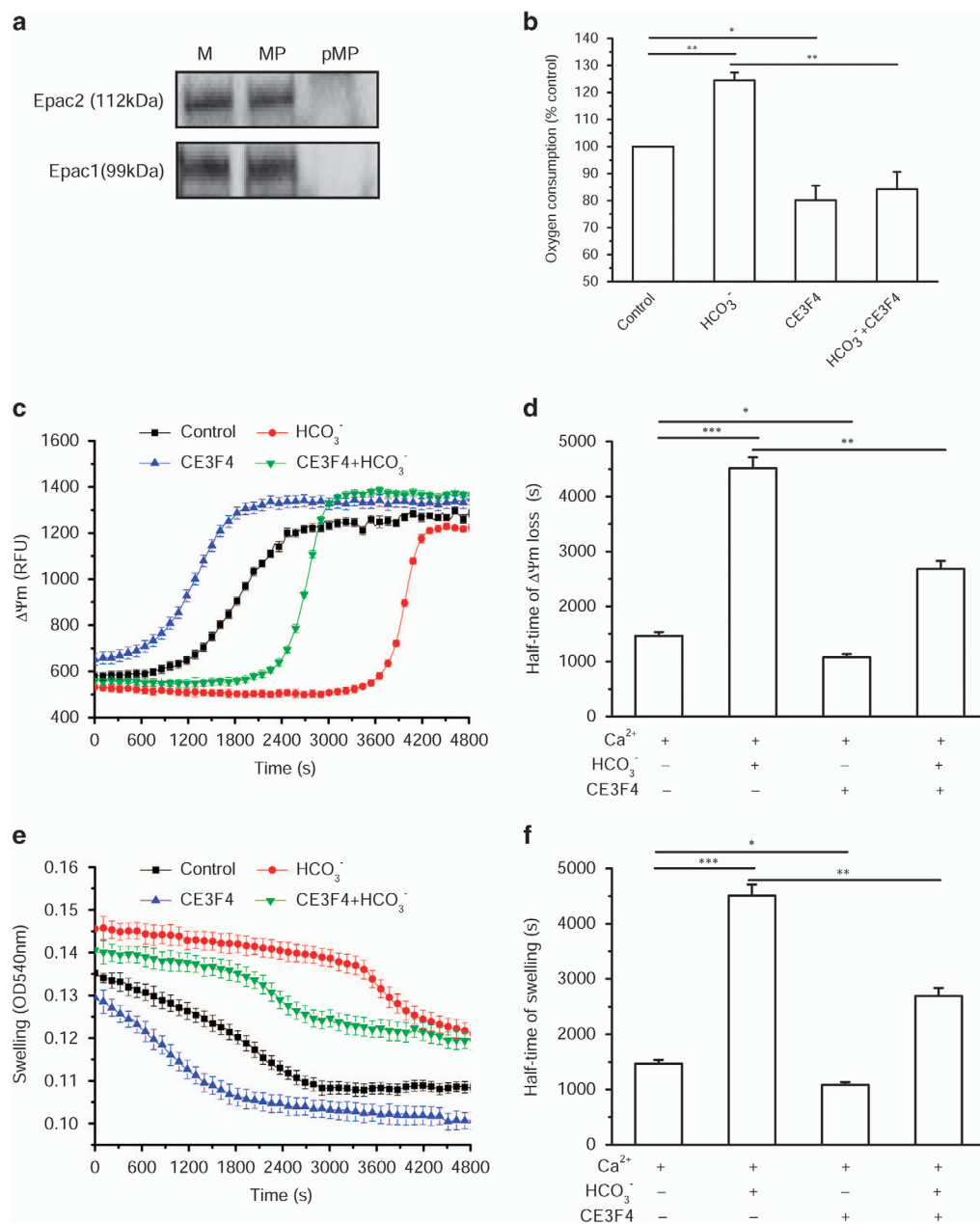


**Figure 5** Epac1 mediates cAMP effect on respiration and permeability transition. (a) Western blot analysis of Epac1 and Epac2 isoforms in mitochondria (M), mitoplast (MP) and postmitoplast fraction (pMP). (b) Oxygen consumption measurement with the MitoXpress probe in the absence or presence of 15 mM HCO<sub>3</sub><sup>-</sup>, 50 μM CE3F4 and HCO<sub>3</sub><sup>-</sup>+CE3F4. Control, untreated mitochondria, has been normalized to 100% (n = 5). (c) Effects of CE3F4 on ΔΨm induced by 10 μM Ca<sup>2+</sup>. (d) Average half-time values of ΔΨm loss induced by 10 μM Ca<sup>2+</sup> calculated from experiments such as that shown in (c) (n = 15). (e) Effects of CE3F4 on mitochondrial swelling induced by 10 μM Ca<sup>2+</sup>. (f) Average half-time values of mitochondrial swelling induced by 10 μM Ca<sup>2+</sup> calculated from experiments such as that shown in (e) (n = 15). \*P < 0.05, \*\*P < 0.01, \*\*\*P < 0.001 versus Control

**Mitochondrial cAMP effects are independent of PKA.** cAMP effects are classically mediated by activation of two main effectors, PKA and Epac to regulate a plethora of biological functions in the heart.<sup>19</sup> In mitochondria, PKA has been reported to be associated with outer membrane (OM) or to be in the matrix for controlling mitochondrial dynamics and oxidative metabolism.<sup>35,41,42</sup> We thus examined whether PKA was involved in the mitochondrial cAMP effects by testing the effects of two different pharmacological PKA inhibitors, H89 and KT5720, on the induction of MPT by Ca<sup>2+</sup>. As shown in

Supplementary Figure 1, these inhibitors had no significant effect on ΔΨm and swelling, indicating that PKA may not be involved in MPT regulation.

**Epac1 mediates cAMP effect on respiration and MPT.** Then, we checked the expression of Epac isoforms. As shown in Figure 5a, both Epac1 and Epac2 isoforms were found in isolated cardiac mitochondria as well as in mitoplasts generated by osmotic shock, but were absent in the postmitoplast supernatant. This suggests that Epac can be

anchored to the IM facing the mitochondrial matrix or the intermembrane space or localized in the matrix.

To evaluate the functional role of Epac, we used three pharmacological Epac inhibitors exhibiting different specificities and tested their effects on  $\text{Ca}^{2+}$ -induced depolarization and swelling as well as oxygen consumption. We used ESI09, a pan-Epac inhibitor, ESI05, an Epac2-selective inhibitor,<sup>21,43</sup> and CE3F4, an Epac1-selective inhibitor.<sup>44</sup> As shown in Figure 5b, Epac1 inhibition with 50  $\mu\text{M}$  CE3F4 decreased basal oxygen consumption and also prevented the stimulatory effect of  $\text{HCO}_3^-$ . Moreover, CE3F4 accelerated  $\text{Ca}^{2+}$ -induced depolarization (Figures 5c and d) and swelling (Figures 5e and f). Similar findings were obtained with ESI09 but not with ESI05 (Supplementary Figure 2). These data thus point to Epac1 as a key effector in mitochondrial cAMP effects.

Next, we tested the effect of Epac1 on the level of matrix  $\text{Ca}^{2+}$  using the Rhod-2 probe, and CGP37157, a mitochondrial  $\text{Na}^+/\text{Ca}^{2+}$  exchanger (mNCX) inhibitor, appeared to accelerate  $\text{Ca}^{2+}$  entry in isolated mitochondria (Figures 6c and d). This effect was similar to that of CE3F4. However, the combination of both inhibitors produced an additive effect, suggesting that they act via two distinct mechanisms. Thus, it is unlikely that Epac1 regulates mNCX. To examine the role of MCU, we used RU360, a highly specific MCU inhibitor. As anticipated, RU360 (from 0.2 to 1 nM) induced a dose-dependent inhibition of  $\text{Ca}^{2+}$  entry (Supplementary Figure 3). Interestingly, inhibition of Epac in the presence of non-maximal concentrations of RU360 partially restored  $\text{Ca}^{2+}$  entry within mitochondria (Figures 6e and f and Supplementary Figure 3), but this effect was abrogated when the MCU was fully inhibited with 1 nM RU360 (Supplementary Figure 3a). These results suggest that MCU is the major effector of Epac1 for the regulation of mitochondrial  $\text{Ca}^{2+}$  movements.

**Epac1 mediates mitochondrial  $\text{Ca}^{2+}$  accumulation and  $\Delta\Psi\text{m}$  loss in cardiomyocytes.** The Epac1 silencing by siRNA indicated that a decreased level of Epac1 in neonatal rats decreased  $\Delta\Psi\text{m}$  (Figures 7a and c) and in parallel accelerated the mitochondrial calcium entry (Figures 7d and e), as does the inhibitor CE3F4 in adult permeabilized cardiomyocytes upon addition of  $\text{Ca}^{2+}$  (Figures 7f and g). At this concentration,  $\text{Ca}^{2+}$  did not affect  $\Delta\Psi\text{m}$ , avoiding any artifact since most ions and metabolites transports are dependent of the  $\Delta\Psi\text{m}$  (Supplementary Figures 4a and b). We also checked that our conditions of fluorescence excitation did not trigger MPT (Supplementary Figures 4c and d). Altogether, these results suggest that Epac1 has a role in reducing the entry of  $\text{Ca}^{2+}$  in mitochondria, and then indirectly stabilizes the  $\Delta\Psi\text{m}$  in primary cardiomyocytes.

**The mitochondrial cAMP pathway can prevent MPT in HF rat model.** To evaluate the ability of the mitochondrial cAMP pathway to regulate MPT in a pathological model, we induced HF in rats by transverse aortic constriction (TAC) during 22 weeks.<sup>45</sup> As shown in Supplementary Figure 5a, TAC rats showed a strong cardiac and lung hypertrophy. Accordingly, cardiac function and the fractional shortening of the left ventricle were diminished (Supplementary Figures 5b and c). Expression level of various proteins was analyzed in heart ventricle homogenates and mitochondrial fraction. As shown

in Figures 8a and b, sAC<sub>t</sub> protein expression was reduced and Epac1 expression was increased in homogenate and mitochondria from HF as compared with sham hearts. MCU expression was similar in mitochondrial fraction from HF and sham rats. To explore how HF affects mitochondrial  $\text{Ca}^{2+}$ -induced MPT,  $\text{Ca}^{2+}$ -induced mitochondrial depolarization and  $\text{Ca}^{2+}$  accumulation was measured in isolated mitochondria from HF and sham rats. As shown in Figures 8c and d and Supplementary Figures 6a–d,  $\text{Ca}^{2+}$  induced a faster depolarization and  $\text{Ca}^{2+}$  uptake in HF than in sham mitochondria. In line with this,  $\text{Ca}^{2+}$  induced a faster mitochondrial swelling in HF than in sham mitochondria (Figure 8e and Supplementary Figures 6e and f). This confirms that MPT is altered in HF, which could make mitochondria more vulnerable to  $\text{Ca}^{2+}$  overload.<sup>46</sup> Interestingly, mitochondria from HF rats still responded to  $\text{HCO}_3^-$  stimulation of mitochondrial cAMP production by sAC, by delaying  $\Delta\Psi\text{m}$  loss,  $\text{Ca}^{2+}$  entry and MPT (i.e. matrix swelling). These effects were blunted by sAC or Epac1 inhibition with CE3F4 (Figures 8c–e and Supplementary Figures 6a–f).

## Discussion

In this study, we characterized a functional cAMP pathway within the mitochondria of neonatal and adult cardiomyocytes, which can regulate mitochondrial function and cell death. cAMP is locally produced within the mitochondria by a  $\text{Ca}^{2+}/\text{HCO}_3^-$ -sensitive sAC<sub>t</sub> and activates Epac1 to stimulate oxidative metabolism while preventing MPT by limiting mitochondrial  $\text{Ca}^{2+}$  accumulation via MCU. As  $\text{HCO}_3^-$  production can be catalyzed by carbonic anhydrase from  $\text{CO}_2$  and  $\text{H}_2\text{O}$ ,  $\text{CO}_2$  being produced by the Krebs cycle and the pyruvate dehydrogenase inside mitochondrial matrix, our data thus link, for the first time, mitochondrial metabolism, cAMP and cell death in the heart, independently of cytosolic cAMP signaling.

Our data are in good agreement with pioneer studies revealing the existence of a mitochondrial cAMP signaling in various cell types.<sup>27–29</sup> Prompted by the observation that a G-protein- and FSK-insensitive sAC is present in various organelles,<sup>38,47–49</sup> Acin-Perez *et al.*<sup>27</sup> discovered a  $\text{CO}_2$ - $\text{HCO}_3^-$ -sAC-cAMP-PKA (mito-sAC) signaling cascade entirely contained within the mitochondria. This mito-sAC cascade serves as a metabolic sensor modulating ATP generation and ROS production in response to nutrient availability.<sup>29</sup> By targeting the recently developed Epac-S<sup>H187</sup> cAMP FRET sensor<sup>36</sup> to the mitochondria, we showed that sAC activation by  $\text{HCO}_3^-$  increases mitochondrial cAMP in neonatal cardiomyocytes, as shown earlier in HeLa and CHO cells.<sup>35</sup> We showed that the constitutive mitochondrial cAMP signaling pathway regulates  $\Delta\Psi\text{m}$  and MPT not only in healthy but also in failing heart mitochondria and that these functions are mediated by Epac1.

**A functional mito-sAC pathway in mitochondria from adult heart.** Although it was already known that sAC can be localized into mitochondria,<sup>47–49</sup> little was known about their biological function in the organelle. Here, we identified endogenous sAC<sub>t</sub> in cardiac mitochondria and mitoplasts. We showed for the first time that increasing intramitochondrial cAMP level delays the onset of MPT, while stimulating oxygen consumption. Although  $\text{HCO}_3^-$  and  $\text{Ca}^{2+}$  enhanced

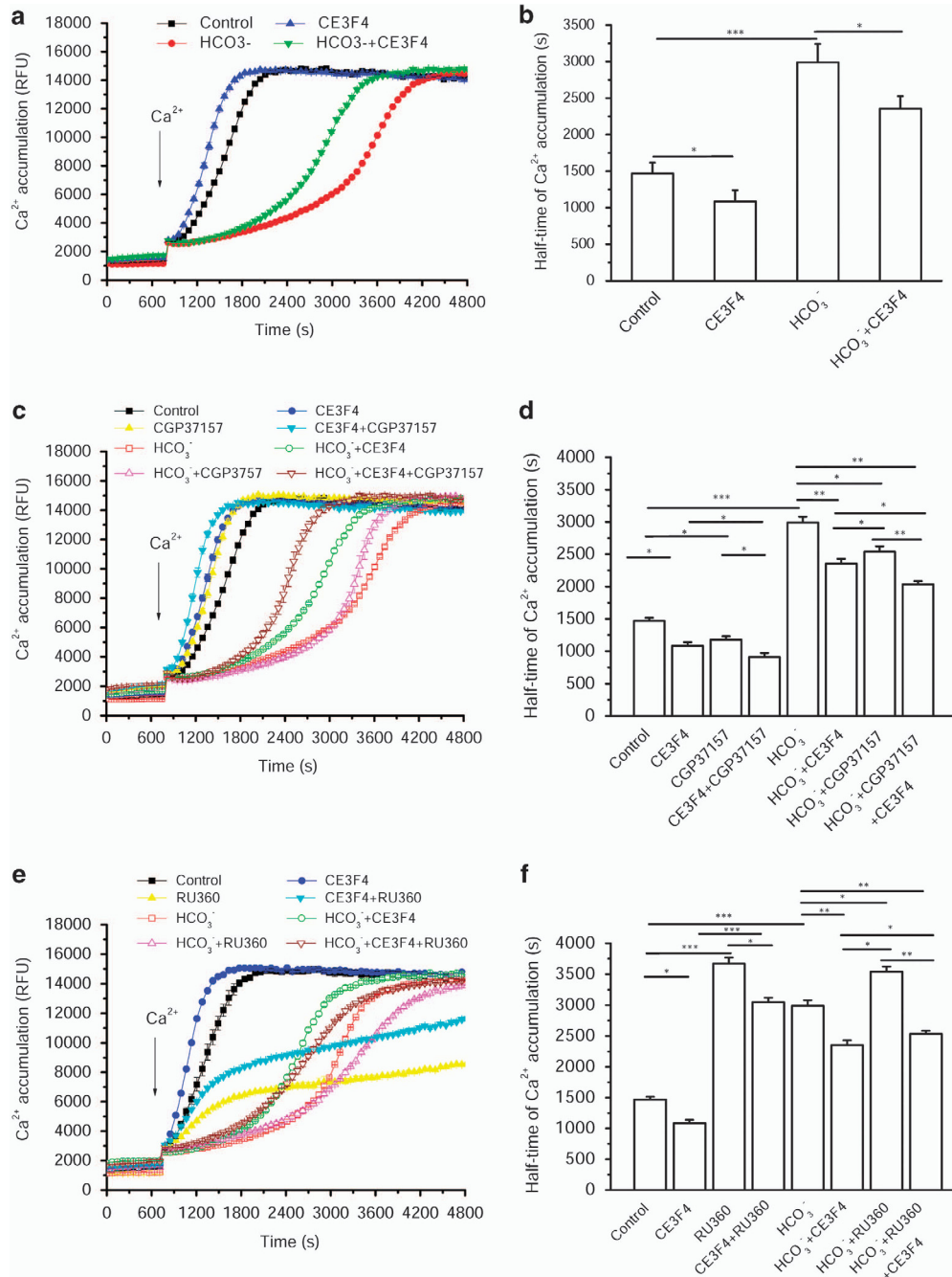


**Figure 6** Epac1 prevents  $\text{Ca}^{2+}$  entry into mitochondria via the  $\text{Ca}^{2+}$  uniporter and not the  $\text{Na}^+/\text{Ca}^{2+}$  exchanger. (a) Measurement of  $\text{Ca}^{2+}$  accumulation in isolated mitochondria using Rhod-2.  $\text{HCO}_3^-$  was used at 15 mM, and CE3F4 was used at 50  $\mu\text{M}$ . (b) Half-time of  $\text{Ca}^{2+}$  entry into mitochondria calculated from experiments such as that shown in (a) ( $n=5$ ). (c) Time course of  $\text{Ca}^{2+}$  accumulation in isolated mitochondria in the presence of 15 mM  $\text{HCO}_3^-$ , 50  $\mu\text{M}$  CE3F4 and 10  $\mu\text{M}$  CGP37157 (a mNCX inhibitor). (d) Half-time of  $\text{Ca}^{2+}$  accumulation into mitochondria calculated from experiments such as that shown in (c) ( $n=5$ ). (e) Time course of  $\text{Ca}^{2+}$  accumulation in isolated mitochondria in the presence of 15 mM  $\text{HCO}_3^-$ , 50  $\mu\text{M}$  CE3F4 and 0.4 nM Ru360 (a MCU inhibitor). (f) Half-time of  $\text{Ca}^{2+}$  accumulation into mitochondria calculated from experiments such as that shown in (e) ( $n=5$ ). \* $P<0.05$ , \*\* $P<0.01$  and \*\*\* $P<0.001$

cAMP production,  $\text{HCO}_3^-$  was more potent than  $\text{Ca}^{2+}$ , which is in line with the fact that  $\text{HCO}_3^-$  and  $\text{Ca}^{2+}$  stimulatory effects are not redundant:  $\text{HCO}_3^-$  modulates the active site of sAC, whereas  $\text{Ca}^{2+}$  increases ATP affinity.<sup>27</sup> Interestingly, a specific inhibitor of sAC, 2HE, totally prevented the effects of  $\text{HCO}_3^-$  and  $\text{Ca}^{2+}$ , indicating that sAC may be the unique source of mitochondrial cAMP.

**Effectors of mitochondrial cAMP.** While PKA is the canonical mediator of cAMP in a number of cell functions and cell subcompartments, and was shown earlier to regulate mitochondrial ATP and ROS production,<sup>27,29,50,51</sup> PKA was clearly not involved in the induction of MPT by  $\text{Ca}^{2+}$  as H89 and KT5720 failed to modulate it. We thus focused our interest on Epac, because it emerged in the past decade as



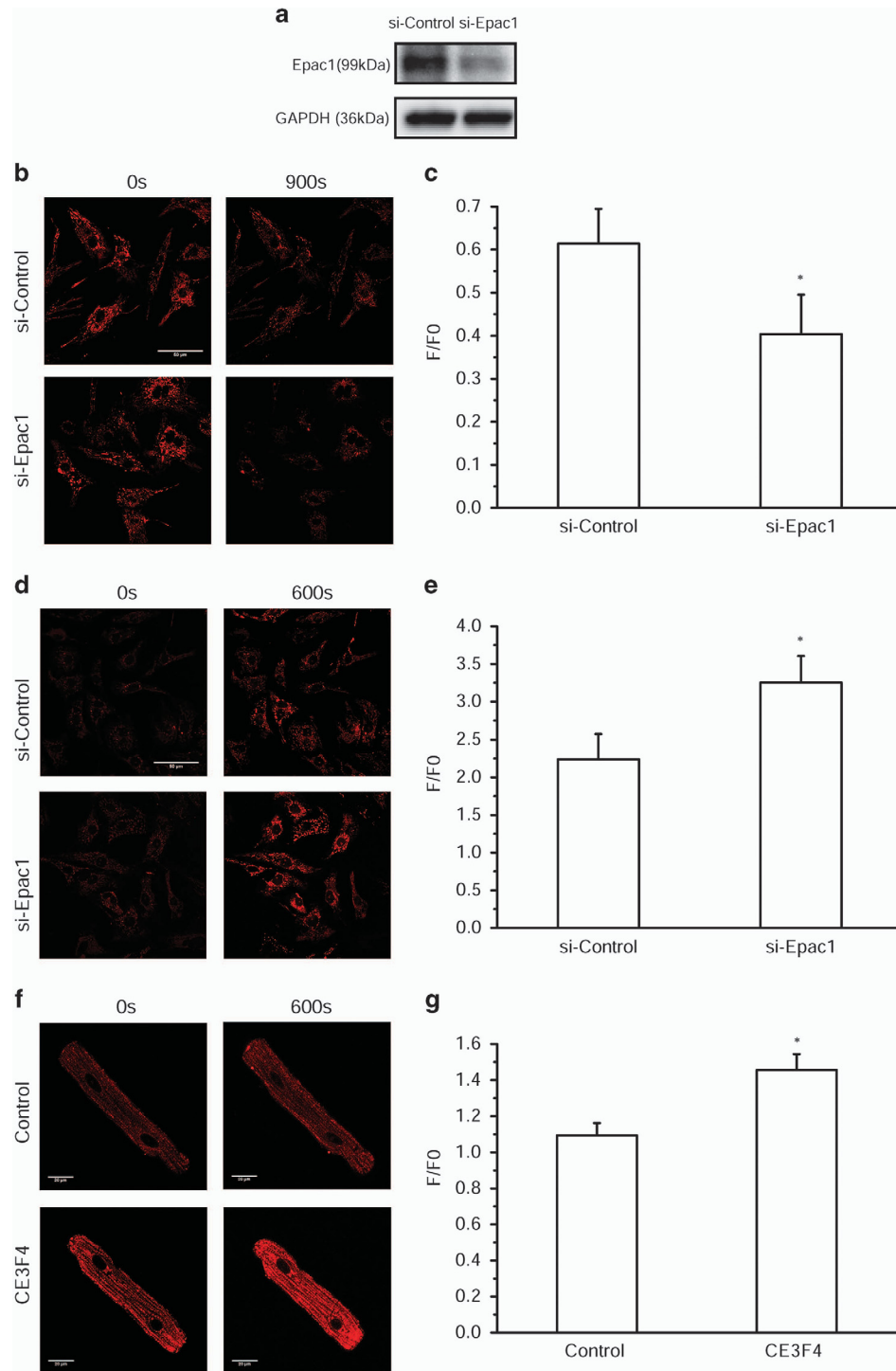


**Figure 7** Epac1 mediates mitochondrial calcium accumulation and  $\Delta\Psi_m$  loss *in cellulo*. **(a)** Epac1 expression in neonatal rat cardiomyocytes transfected with non-targeting small interfering RNA (siRNA) (si-Control) or Epac1 siRNA (si-Epac1). **(b)** Representative confocal images of TMRM-labeled permeabilized neonatal rat cardiomyocytes transfected with si-Control or si-Epac1 at time 0 s (left) and 900 s (right) after  $\text{Ca}^{2+}$  (600 nM) addition. Bar scale, 50  $\mu\text{M}$ . **(c)** Averaged values of  $\Delta\Psi_m$  (measured as F/F0, where F is the TMRM fluorescence signal at 900 s and F0 is the signal at time 0 s of  $\text{Ca}^{2+}$  addition) ( $n = 36$ ). **(d)** Representative confocal images of Rhod-2 AM-labeled permeabilized neonatal rat cardiomyocytes transfected with si-Control or si-Epac1 at time 0 s (left) and 600 s (right) after  $\text{Ca}^{2+}$  (200 nM) addition. Bar scale, 50  $\mu\text{M}$ . **(e)** Averaged values of intramitochondrial  $\text{Ca}^{2+}$  accumulation (measured as F/F0, where F is the Rhod-2 fluorescence signal at 600 s and F0 is the signal at time 0 s of  $\text{Ca}^{2+}$  addition) ( $n = 30$ ). **(f)** Representative confocal images of Rhod-2 AM-labeled permeabilized adult rat ventricular myocytes at time 0 s (left) and 600 s (right) after  $\text{Ca}^{2+}$  (200 nM) addition in the absence (top) or presence (bottom) of CE3F4. Bar scale, 20  $\mu\text{M}$ . **(g)** Averaged values of intramitochondrial  $\text{Ca}^{2+}$  accumulation (measured as F/F0, where F is the Rhod-2 fluorescence signal at 600 s and F0 is the signal at time 0 s of  $\text{Ca}^{2+}$  addition) ( $n = 10$ ). \* $P < 0.05$  versus si-Control or Control

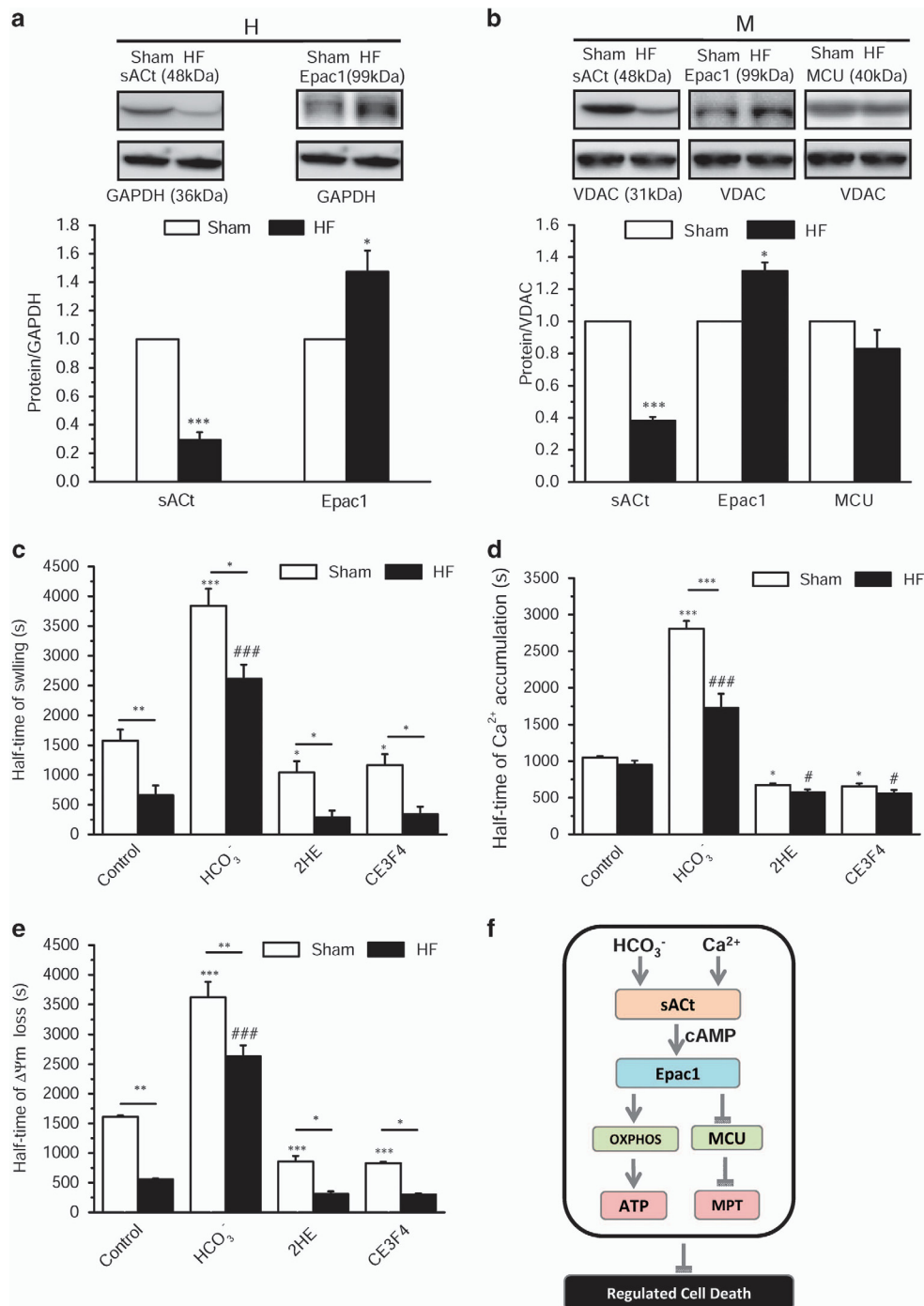


**Figure 8** Expression levels of sAct, Epac1 and MCU in hearts and mitochondria isolated from sham and HF rats and cAMP regulation of  $\Delta\Psi_m$  and  $\text{Ca}^{2+}$  uptake. (a) Expression level of sAct and Epac1 in sham (white bars) and HF (black bars) heart homogenates (H) normalized by glyceraldehyde 3-phosphate dehydrogenase (GAPDH). Representative western blot images are shown on top (sham on left and HF on right). (b) Expression level of sAct, Epac1 and MCU proteins relative to voltage-dependent anion channel (VDAC) in isolated mitochondria (M) in HF versus sham. Representative blots are shown on top (sham on left and HF on right). Data are mean  $\pm$  S.E.M. of four sham and four HF rats, detected in four independent immunoblots. (c) Half-time of  $\Delta\Psi_m$  loss induced by  $10 \mu\text{M}$   $\text{Ca}^{2+}$  calculated from experiments such as shown in Supplementary Figures 6a and b. (d) Half-time of  $\text{Ca}^{2+}$  accumulation calculated from experiments such as shown in Supplementary Figures 6c and d. (e) Half-time of swelling induced by  $10 \mu\text{M}$   $\text{Ca}^{2+}$  calculated from experiments such as that shown in Supplementary Figures 6e and f. \* $P < 0.05$ , \*\* $P < 0.01$ , \*\*\* $P < 0.001$  versus sham control; # $P < 0.05$ , ### $P < 0.001$  versus HF control ( $n = 4$ ). (f) Hypothetical scheme showing the local role of mitochondrial cAMP signaling pathway. Within the mitochondrion,  $\text{HCO}_3^-$  and calcium stimulate the production of cAMP by sAct, which activates mitochondrial cAMP production. In turn, cAMP stimulates oxidative phosphorylation and inhibits permeability transition via activation of mitochondrial Epac1

another important player in cAMP signaling.<sup>20</sup> Although Epac possesses a mitochondrial-targeting sequence at its N terminus and has been shown to be localized inside mitochondria by heterologous expression,<sup>52</sup> to our knowledge there has been no report on a role for this protein in mitochondrial function. Although the Epac2-selective inhibitor ESI05 had no effect, the non-selective inhibitor ESI09 or the Epac1-selective inhibitor CE3F4 antagonized the induction of MPT by  $\text{Ca}^{2+}$ . This indicates that Epac1 but not Epac2 is involved in the regulation of MPT. We found also that CE3F4 inhibits oxygen consumption. As the efficiency of CE3F4 to regulate oxygen consumption with a better efficiency than MPT, we speculate that Epac1 could have several targets, which remain to be identified, regulating differentially various mitochondrial functions.

In neonatal rat cardiomyocytes, silencing of Epac1 modulated the  $\text{Ca}^{2+}$  entry and the  $\Delta\Psi\text{m}$ . In the heart, Epac1 was recently shown to be localized and functionally involved also in nuclear signaling, whereas Epac2 is located at the T tubules and regulates arrhythmogenic sarcoplasmic reticulum  $\text{Ca}^{2+}$  leak.<sup>53</sup> While the intermediate downstream effector(s) of mitochondrial Epac1 still need to be identified, our results indicate that Epac1 activation may inhibit MCU activity. This hypothesis is supported by the fact that inhibition of MCU, but not of mNCX, mimics the effects of mitochondrial cAMP elevation in preventing MPT. Thus, we propose that activation of mitochondrial Epac1 protects the organelle from  $\text{Ca}^{2+}$  overload and from subsequent MPT via MCU modulation.

**Possible implications of the mitochondrial cAMP pathway for cell death and cardioprotection.**  $\text{Ca}^{2+}$  overload is considered as a conserved inducer of regulated cell death modalities.<sup>54</sup> Using modulation of sAC by genetic and pharmacological manipulations in primary cardiomyocytes, our study demonstrates for the first time that activation of the mitochondrial cAMP pathway exerts an inhibition on MPT *in vitro* and on various cell death modalities, that is, extrinsic and intrinsic apoptosis as well as necrosis. Conversely, pharmacological inhibition of sAC increased markedly nuclear damage and cell death. Thus, the targeted activation of this mitochondrial cAMP pathway may preserve cardiomyocytes from mitochondrial  $\text{Ca}^{2+}$  overload and cell death *in vivo*. In that respect, in a pathological rat model of HF induced by pressure overload, which goes along with strong cardiac hypertrophy, cardiac function alteration, tissue remodeling, bioenergetic alterations and cardiomyocyte cell death,<sup>45,46</sup> sACt is down-regulated and Epac1 is upregulated in mitochondria. However, the increase in Epac1 did not compensate the decrease of sACt in terms of function, suggesting that the level of cAMP is limiting for Epac1 in the control of MPT in cardiac mitochondria. Moreover, we found that the MPT alterations can be alleviated by stimulation of the mitochondrial cAMP pathway. Thus, this new mitochondrial cAMP/sAC/Epac1/MCU pathway might have therapeutic implications to regulate cell death in cardiac pathologies, such as HF and/or myocardial infarction.<sup>54,55</sup>

## Material and Methods

Unless specified, all reagents and chemicals are from Sigma-Aldrich (Saint-Quentin Fallavier, France) and of analytical grade.

**Animals.** All animal care and experimental procedures conformed to the European Community guiding principles in the care and use of animals (Directive 2010/63/EU of the European Parliament) and authorizations to perform animal experiments according to this decree were obtained from the French Ministry of Agriculture, Fisheries and Food (No. D-92-283, 13 December 2012). All studies involving rats are reported in accordance with the ARRIVE guidelines for reporting experiments involving animals.<sup>56</sup> A total of 60 healthy, 4 sham and 4 HF rats were used in the experiments described here.

**Surgical procedure and echocardiography.** Male Wistar rats at 3 weeks of age (60–70 g; Janvier, Le Genest St Isle, France) were anesthetized with pentobarbital (60 mg/kg). The thoracic cage was opened and a stainless-steel hemoclip was placed on the ascending aorta, to promote HF after 22 weeks, as described previously.<sup>57</sup> Sham-operated animals were used as controls. Cardiac structure and function was evaluated by echocardiograph. Cardiac and pulmonary hypertrophy was determined as a ratio of organ weight to tibia length and to body weight.<sup>57</sup> Transthoracic two-dimensional-guided M-mode echocardiography of rats was performed using an echocardiograph with a 15 MHz linear transducer (Vivid 9; General Electric Healthcare, Vélizy Villacoublay, France) under 3% isoflurane gas anesthesia and fractional release was calculated as described.<sup>57</sup>

**Isolation of cardiac mitochondria.** Mitochondria were isolated from the heart of adult male Wistar rats at 8–10 weeks of age (275–375 g; Janvier) as described.<sup>37</sup> Briefly, the heart was rapidly removed and placed into a cold buffer containing 0.3 M sucrose, 0.2 mM EGTA and 5 mM TES (pH 7.2). The heart was grinded with Polytron fastly and homogenized by using the Potter. The homogenate was centrifuged at  $500 \times g$  for 10 min at 4 °C. Then, the supernatant was carefully removed and centrifuged again at  $3000 \times g$  for 10 min at 4 °C. The pellets were washed in the isolation buffer and the mitochondria were kept on ice until use within 3 h.

**Mitochondrial transmembrane potential and swelling in isolated mitochondria.** Isolated mitochondria (25  $\mu\text{g}$  proteins) were incubated with  $\text{Ca}^{2+}$  and drugs in 96-well microtiter plates.<sup>37</sup>  $\Delta\Psi\text{m}$  was measured using the fluorescent probe, Rhod123 (excitation = 485 nm and emission = 535 nm; Enzo Life Sciences, Villeurbanne, France) in a buffer containing 200 mM sucrose, 10 mM MOPS, 10  $\mu\text{M}$  EGTA, 1 mM  $\text{H}_3\text{PO}_4$ , 5 mM succinate and 2  $\mu\text{M}$  rotenone (pH 7.4) using Tecan Infinite 200 spectrofluorimeter (Tecan, Männedorf, Switzerland). In parallel, matrix swelling was measured via light absorbance at 540 nm.<sup>37</sup>

**Oxygen consumption.** Isolated mitochondria (50  $\mu\text{g}$  proteins) were incubated with drugs in a buffer containing 250 mM sucrose, 30 mM  $\text{K}_2\text{HPO}_4$ , 1 mM EGTA, 5 mM  $\text{MgCl}_2$ , 15 mM KCl and 1 mg/ml bovine serum albumin (BSA) (pH 7.4) supplemented with respiratory substrates and MitoXpress, an oxygen-sensitive phosphorescent dye (LUXCEL, Cork, Ireland). Oxygen consumption was measured in real time for 60 min at 30 °C in 96-well plates using Tecan Infinite 200 (excitation = 380 nm and emission = 650 nm) in the presence of 1.65 mM ADP and with 5 mM malate and 12.5 mM glutamate.<sup>37</sup>

**Mitochondrial  $\text{Ca}^{2+}$  uptake in isolated mitochondria.** Isolated mitochondria (25  $\mu\text{g}$  proteins) were incubated with 5  $\mu\text{M}$  Rhod-2 (Enzo Life Sciences) in the buffer containing 200 mM sucrose, 10 mM MOPS, 10  $\mu\text{M}$  EGTA, 1 mM  $\text{H}_3\text{PO}_4$ , 5 mM succinate and 2  $\mu\text{M}$  rotenone for 30 min in dark at room temperature. Afterwards, the mitochondria were washed two times. Then, the mitochondria were treated with various drugs for 10 min before applying  $\text{Ca}^{2+}$ . Fluorescence was measured in real time for 60 min at room temperature in 96-well plates using Tecan Infinite 200 (excitation = 552 nm and emission = 581 nm).

**cAMP measurements by ELISA.** cAMP measurements were performed according to the manufacturer's instructions using monoclonal anti-cAMP antibody-based direct cAMP ELISA Kit (New East Biosciences, King of Prussia, PA, USA) on freshly isolated mitochondria from rat hearts (500  $\mu\text{g}$  proteins per sample) treated or not by  $\text{HCO}_3^-$ ,  $\text{Ca}^{2+}$  and  $\text{Ca}^{2+}$ +Ru360 for 20 min at room temperature before centrifugation and lysis. The sensitivity of cAMP detection is 29.6 fmol/ml.<sup>57,58</sup>

**ATP measurements.** ATP measurements in isolated mitochondria were performed according to manufacturer's instructions using ATP Bioluminescence Assay Kit CLSII (Roche, Basel, Switzerland).

**Western blotting.** Total mitochondrial proteins were resolved on 4–15% Tris-glycine SDS-PAGE gels and electroblotted onto polyvinylidene fluoride membranes (Bio-Rad, Marnes La Coquette, France). Following electrotransfer, membranes were blocked for 1 h at room temperature in 5% BSA-PBST (10 mM Tris-HCl, pH 8.0/150 mM NaCl/0.1% Tween-20). Next, membranes were incubated overnight at 4 °C with primary antibody. The day after, the membranes were washed six times with PBST and incubated with peroxidase-conjugated secondary antibody at room temperature for 1 h. Peroxidase activity was detected with enhanced chemiluminescence (ECL Advance Western Blotting Detection Kit; Thermo Scientific, Villebon sur Yvette, France). For protein detection, the following antibodies were used: sAC (Abcam Cambridge, UK; CEP Biotech, Tamarac, FL, USA), Epac1, 2 (Cell Signaling, Danvers, MA, USA), ANT (Abcam), GAPDH (Cell Signaling), VDAC (Genosphere, Paris, France), Trn1 (Cell Signaling), PLB (Cell Signaling) and MCU (Biorbyt, Berkeley, CA, USA).

#### Construction of mitochondria-targeted FRET sensor for cAMP.

The mitochondrial-targeting sequence 4mt, encoding four copies of the signal sequence from subunit VIII of human cytochrome C oxidase, was amplified using the Advantage Polymerase (Clontech, Mountain View, CA, USA) and primers F, 5'-ACTATAGGGAGACCCAGCTTATG-3' and R, 5'-TGGTGGCGGCAAGCTTCTTGCTCACCATGGTGGC-3'. The pcDNA-4mt-D3-cpv vector used as a matrix for amplification of 4mt was a kind gift from Dr. Roger Tsien (HHMI investigator at the University of California San Diego, San Diego, CA, USA). The PCR fragment was cloned into the *Hind*III restriction site of pcDNA3-Epac-S<sup>H187</sup> using the Infusion HD Cloning System (Clontech). Epac-S<sup>H187</sup> encodes for a fourth-generation Epac1-based cAMP sensor and was a kind gift from Dr. Kees Jalink (The Netherlands Cancer Institute, Amsterdam, Netherlands).<sup>36</sup> Once the pcDNA-4mt-Epac-S<sup>H187</sup> vector was amplified in *Stellar Escherichia coli* (Clontech) bacteria, its identity with parental sequences was verified by PCR using primers F, 5'-ACTACTA TAGGGAGACC-3' and R, 5'-TGCGGCCGCCATGGTGGC-3', and DNA double-strand sequencing (INSERM U1056 – UMR 5165 CNRS UPS – UDEAR, Toulouse, France). Adenoviruses encoding Epac-S<sup>H187</sup> and 4mt-Epac-S<sup>H187</sup> were generated by Welgen Inc (Worcester, MA, USA).

#### Cardiomyocyte isolation, adenoviral infection and cell death evaluation.

Adult and neonatal cardiomyocytes were isolated as described previously.<sup>59,60</sup> For FRET experiments, neonatal cardiomyocytes were plated on 35-mm, laminin-coated culture dishes (10 µg/ml) at a density of  $4 \times 10^5$  cells per dish. The day after, cells were infected with Epac-S<sup>H187</sup> and 4mt-Epac-S<sup>H187</sup> adenoviruses in Opti-MEM (Life Technologies, St Aubin, France) for 48 h. Similarly, adenoviruses expressing sACt and sACf were used (generous gift from Pr. M Conti, University of California, San Francisco, CA, USA). For confocal microscopy experiments, adult cardiomyocytes were plated on 35-mm, laminin-coated culture dishes (10 µg/ml) at a density of  $2 \times 10^4$  cells per dish. For cell death evaluation, neonatal cells were stained with Apoptosis/Necrosis Detection Kit (Abcam) for 1 h at room temperature as described by the manufacturer.

**siRNA transfection to knockdown sAC and Epac1.** On-Target plus SMART pool siRNA, a mixture of four siRNA provided as a single reagent were purchased from Dharmacon (Lafayette, CO, USA). At day 0, neonatal cardiomyocytes were plated overnight on 35-mm, laminin-coated culture dishes (10 µg/ml) at  $4 \times 10^5$ . At day 1, the cells were transfected with 50 nM sAC/Epac1 or non-targeting control siRNA using Lipofectamine RNAi MAX Transfection Reagent (ThermoScientific, Waltham, MA, USA) for 48 h.

#### Mitochondrial transmembrane potential measurement in neonatal cardiomyocytes.

Isolated rat cardiomyocytes were loaded with 100 nM TMRM at 37 °C for 15 min. Afterwards, the sarcolemmal membrane was permeabilized by perfusion of digitonin (5 µg/ml) in a Ca<sup>2+</sup>-free internal solution that contained 50 mM KCl, 80 mM potassium aspartate, 4 mM sodium pyruvate, 20 mM HEPES, 3 mM MgCl<sub>2</sub>, 3 mM Na<sub>2</sub>ATP, 5.8 mM glucose and 0.5 mM EGTA (pH 7.3 with KOH). Then, the free Ca<sup>2+</sup> concentration in the internal solution was increased to 200 nM. The Ca<sup>2+</sup> was calculated using the Maxchelator program from the Stanford University (Stanford, CA, USA). Images were acquired with a Leica (SP5) confocal microscope (Mannheim, Germany). Excitation was achieved by a white light laser fitted at 549 nm and emission collected at 570 nm. Analyses were made with Image J program (Wayne Rasband, National Institutes of Health, USA).

**Measurement of mitochondrial Ca<sup>2+</sup> in cardiomyocytes.** Isolated neonatal or adult rat cardiomyocytes were loaded with 5 µM Rhod-2 at 37 °C for 30 min. To remove cytosolic Rhod-2, the sarcolemmal membrane was permeabilized by perfusion of digitonin (5 µg/ml) in a Ca<sup>2+</sup>-free internal solution that contained 50 mM KCl, 80 mM potassium aspartate, 4 mM sodium pyruvate, 20 mM HEPES, 3 mM MgCl<sub>2</sub>, 3 mM Na<sub>2</sub>ATP, 5.8 mM glucose and 0.5 mM EGTA (pH 7.3 with KOH). After the sarcolemmal membrane was permeabilized, the free Ca<sup>2+</sup> concentration in the internal solution was increased to 200 nM. The Ca<sup>2+</sup> was calculated using the Maxchelator program from Stanford University. Images were acquired with a Leica (SP5) confocal microscope. Excitation was achieved by a white light laser fitted at 552 nm and emission collected at 575 nm. Analyses were made with Image J program.

**FRET measurements of cAMP levels.** FRET imaging experiments were performed 48 h after infection of neonatal cardiomyocytes. Cells were bathed in Hepes-buffered Ringer's solution containing: 125 mM NaCl, 25 mM HEPES, 10 mM glucose, 5 mM K<sub>2</sub>HPO<sub>4</sub>, 1 mM MgSO<sub>4</sub> and 1 mM CaCl<sub>2</sub>, pH 7.4. For sAC activation by HCO<sub>3</sub><sup>-</sup>, the medium was the Krebs–Henseleit solution containing: 120 mM NaCl, 2.09 mM K<sub>2</sub>HPO<sub>4</sub>, 0.34 mM KH<sub>2</sub>PO<sub>4</sub>, 24 mM NaHCO<sub>3</sub>, 1 mM MgSO<sub>4</sub>, 1 mM CaCl<sub>2</sub> and 10 mM D-glucose. Krebs–Henseleit solution was gassed continuously with 95% O<sub>2</sub>/5% CO<sub>2</sub> to maintain a pH of 7.4.<sup>35</sup> Real-time FRET experiments were performed at room temperature. Images were captured every 5 s using the x40 oil-immersion objective of an inverted microscope (Nikon, Champigny sur Marne, France) connected to a Cool SNAP HQ2 camera (Photometrics, Tucson, AZ, USA) controlled by the Metafluor software (Molecular Devices, Sunnyvale, CA, USA). The donor (mTurquoise2)<sup>36</sup> was excited during 300 ms by a xenon lamp (Nikon) using a 440/20BP filter and a 455LP dichroic mirror. Dual-emission imaging of donor and acceptor was performed using a dual-view emission splitter equipped with a 510 LP dichroic mirror and BP filters 480/30 and 535/25 nm, respectively.

**Data analysis.** Results are expressed as mean ± S.E.M. The Origin software (Northampton, MA, USA) was used for statistical analysis. Differences between groups have been analyzed by one-way ANOVA and Student's *t*-test. A value of *P* < 0.05 were considered as statistically significant. The number of animals, cells and independent experiments performed is indicated in the figure legends.

#### Conflict of Interest

The authors declare no conflict of interest.

**Acknowledgements.** This work has been funded by INSERM (AMG, CB, GV, RF), the Investment for the Future program ANR-11-IDEX-0003-01 within the LABEX ANR-10-LABX-0033 (CB, GV, RF) and ANR (ANR-13-ISOV-0001-01, CB). ZW and DL are supported by a fellowship from the China Scholarship Council. The Leica microscope was funded by CORDDIM (Investissement 2010, COD100296). We thank Florence Lefebvre for her assistance in adult cardiomyocyte isolation and Valérie Domergue for animal housing and care at the Animex facility, IPSIT, Châtenay-Malabry, France. We also thank Christine Longin for Transmission Electron Microscopy at INRA, Jouy-en-Josas, France. We are also thankful to Jessica Sabourin, Cécile Martel, Delphine Mika and Jérôme Leroy for helpful discussions.

- Green DR, Reed JC. Mitochondria and apoptosis. *Science* 1998; **281**: 1309–1312.
- Brenner C, Kroemer G. Apoptosis. Mitochondria – the death signal integrators. *Science* 2000; **289**: 1150–1151.
- Desagher S, Martinou JC. Mitochondria as the central control point of apoptosis. *Trends Cell Biol* 2000; **10**: 369–377.
- Kroemer G, Galluzzi L, Brenner C. Mitochondrial membrane permeabilization in cell death. *Physiol Rev* 2007; **87**: 99–163.
- Duchen MR, Szabadkai G. Roles of mitochondria in human disease. *Essays Biochem* 2010; **47**: 115–137.
- Ichas F, Jouaville L, Mazat J. Mitochondria are excitable organelles capable of generating and conveying electrical and calcium signals. *Cell* 1997; **89**: 1145–1153.
- Rizzuto R, Pozzan T. Microdomains of intracellular Ca<sup>2+</sup>: molecular determinants and functional consequences. *Physiol Rev* 2006; **86**: 369–408.
- Viola HM, Hool LC. Cross-talk between L-type Ca<sup>2+</sup> channels and mitochondria. *Clin Exp Pharmacol Physiol* 2010; **37**: 229–235.
- Luongo TS, Lambert JP, Yuan A, Zhang X, Gross P, Song J et al. The mitochondrial calcium uniporter matches energetic supply with cardiac workload during stress and modulates permeability transition. *Cell Rep* 2015; **12**: 23–34.



10. Kwong JQ, Lu X, Correll RN, Schwaneckamp JA, Vagnozzi RJ, Sargent MA *et al.* The mitochondrial calcium uniporter selectively matches metabolic output to acute contractile stress in the heart. *Cell Rep* 2015; **12**: 15–22.
11. Griffiths EJ, Halestrap AP. Mitochondrial non-specific pores remain closed during cardiac ischaemia, but open upon reperfusion. *Biochem J* 1995; **307**(Part 1): 93–98.
12. Halestrap AP, Richardson AP. The mitochondrial permeability transition: a current perspective on its identity and role in ischaemia/reperfusion injury. *J Mol Cell Cardiol* 2015; **78C**: 129–141.
13. Boerma M. Experimental radiation-induced heart disease: past, present, and future. *Radiat Res* 2012; **178**: 1–6.
14. Kwong JQ, Molkentin JD. Physiological and pathological roles of the mitochondrial permeability transition pore in the heart. *Cell Metab* 2015; **21**: 206–214.
15. Piot C, Croisille P, Staat P, Thibault H, Rioufol G, Mewton N *et al.* Effect of cyclosporine on reperfusion injury in acute myocardial infarction. *N Engl J Med* 2008; **359**: 473–481.
16. Guellich A, Mehl H, Fischmeister R. Cyclic AMP synthesis and hydrolysis in the normal and failing heart. *Pflügers Archiv* 2014; **466**: 1163–1175.
17. de Rooij J, Zwartkruis FJ, Verheijen MH, Cool RH, Nijman SM, Wittinghofer A *et al.* Epac is a Rap1 guanine-nucleotide-exchange factor directly activated by cyclic AMP. *Nature* 1998; **396**: 474–477.
18. Kawasaki H, Springett GM, Toki S, Canales JJ, Harlan P, Blumenstiel JP *et al.* A Rap guanine nucleotide exchange factor enriched highly in the basal ganglia. *Proc Natl Acad Sci USA* 1998; **95**: 13278–13283.
19. Schmidt M, Dekker FJ, Maarsingh H. Exchange protein directly activated by cAMP (epac): a multidomain cAMP mediator in the regulation of diverse biological functions. *Pharmacol Rev* 2013; **65**: 670–709.
20. Metrich M, Berthouze M, Morel E, Crozatier B, Gomez AM, Lezoualc'h F. Role of the cAMP-binding protein Epac in cardiovascular physiology and pathophysiology. *Pflügers Archiv* 2010; **459**: 535–546.
21. Chen H, Wild C, Zhou X, Ye N, Cheng X, Zhou J. Recent advances in the discovery of small molecules targeting exchange proteins directly activated by cAMP (EPAC). *J Med Chem* 2014; **57**: 3651–3665.
22. Parnell E, Palmer TM, Yarwood SJ. The future of EPAC-targeted therapies: agonism versus antagonism. *Trends Pharmacol Sci* 2015; **36**: 203–214.
23. Litvin TN, Kamenetsky M, Zarifian A, Buck J, Levin LR. Kinetic properties of 'soluble' adenylyl cyclase. Synergism between calcium and bicarbonate. *J Biol Chem* 2003; **278**: 15922–15926.
24. Jaiswal BS, Conti M. Calcium regulation of the soluble adenylyl cyclase expressed in mammalian spermatozoa. *Proc Natl Acad Sci USA* 2003; **100**: 10676–10681.
25. Spät A, Katona D, Rajki A, Di Benedetto G, Pozzan T. Calcium-dependent mitochondrial cAMP production enhances aldosterone secretion. *Mol Cell Endocrinol* 2015; **412**: 196–204.
26. Kamenetsky M, Middelhaufe S, Bank EM, Levin LR, Buck J, Steegborn C. Molecular details of cAMP generation in mammalian cells: a tale of two systems. *J Mol Biol* 2006; **362**: 623–639.
27. Acin-Perez R, Salazar E, Kamenetsky M, Buck J, Levin LR, Manfredi G. Cyclic AMP produced inside mitochondria regulates oxidative phosphorylation. *Cell Metab* 2009; **9**: 265–276.
28. Zippin JH, Levin LR, Buck J. CO<sub>2</sub>/HCO<sub>3</sub><sup>-</sup>-responsive soluble adenylyl cyclase as a putative metabolic sensor. *Trends Endocrinol Metab* 2001; **12**: 366–370.
29. Di Benedetto G, Scalzotto E, Mongillo M, Pozzan T. Mitochondrial Ca<sup>2+</sup> uptake induces cyclic AMP generation in the matrix and modulates organelle ATP levels. *Cell Metab* 2013; **17**: 965–975.
30. Acin-Perez R, Russwurm M, Gunnewig K, Gertz M, Zoidl G, Ramos L *et al.* A phosphodiesterase 2A isoform localized to mitochondria regulates respiration. *J Biol Chem* 2011; **286**: 30423–30432.
31. Kumar S, Flacke JP, Kostin S, Appukuttan A, Reusch HP, Ladilov Y. SLC4A7 sodium bicarbonate co-transporter controls mitochondrial apoptosis in ischaemic coronary endothelial cells. *Cardiovasc Res* 2011; **89**: 392–400.
32. Kumar S, Kostin S, Flacke JP, Reusch HP, Ladilov Y. Soluble adenylyl cyclase controls mitochondria-dependent apoptosis in coronary endothelial cells. *J Biol Chem* 2009; **284**: 14760–14768.
33. Acin-Perez R, Salazar E, Brosel S, Yang H, Schon EA, Manfredi G. Modulation of mitochondrial protein phosphorylation by soluble adenylyl cyclase ameliorates cytochrome oxidase defects. *EMBO Mol Med* 2009; **1**: 392–406.
34. Neubauer S. The failing heart – an engine out of fuel. *N Engl J Med* 2007; **356**: 1140–1151.
35. Lefkimmiatis K, Leroni D, Hofer AM. The inner and outer compartments of mitochondria are sites of distinct cAMP/PKA signaling dynamics. *J Cell Biol* 2013; **202**: 453–462.
36. Klarenbeek J, Goedhart J, van Batenburg A, Groenewald D, Jalink K. Fourth-generation epac-based FRET sensors for cAMP feature exceptional brightness, photostability and dynamic range: characterization of dedicated sensors for FLIM, for ratiometry and with high affinity. *PLoS One* 2015; **10**: e0122513.
37. Wang Z, Nicolas C, Fischmeister R, Brenner C. Enzymatic assays for probing mitochondrial apoptosis. *Methods Mol Biol* 2015; **1265**: 407–414.
38. Buck J, Sinclair ML, Schapal L, Cann MJ, Levin LR. Cytosolic adenylyl cyclase defines a unique signaling molecule in mammals. *Proc Natl Acad Sci USA* 1999; **96**: 79–84.
39. Brenner C, Moulin M. Physiological roles of the permeability transition pore. *Circ Res* 2012; **111**: 1237–1247.
40. Belzacq-Casagrande AS, Martel C, Pertuiset C, Borgne-Sanchez A, Jacotot E, Brenner C. Pharmacological screening and enzymatic assays for apoptosis. *Front Biosci* 2009; **14**: 3550–3562.
41. Sardaneli AM, Technikova-Dobrova Z, Scacco SC, Speranza F, Papa S. Characterization of proteins phosphorylated by the cAMP-dependent protein kinase of bovine heart mitochondria. *FEBS Lett* 1995; **377**: 470–474.
42. Carlucci A, Lignitto L, Feliciello A. Control of mitochondria dynamics and oxidative metabolism by cAMP, AKAPs and the proteasome. *Trends Cell Biol* 2008; **18**: 604–613.
43. Chen H, Ding C, Wild C, Liu H, Wang T, White MA *et al.* Efficient synthesis of ESI-09, a novel non-cyclic nucleotide EPAC antagonist. *Tetrahedron Lett* 2013; **54**: 1546–1549.
44. Courilleau D, Bouysson P, Fischmeister R, Lezoualc'h F, Blondeau JP. The (R)-enantiomer of CE3F4 is a preferential inhibitor of human exchange protein directly activated by cyclic AMP isoform 1 (Epac1). *Biochem Biophys Res Commun* 2013; **440**: 443–448.
45. Joubert F, Wilding JR, Fortin D, Domergue-Dupont V, Novotova M, Ventura-Clapier R *et al.* Local energetic regulation of sarcolemmal and myosin ATPase is differently impaired in rats with heart failure. *J Physiol* 2008; **586**(Part 21): 5181–5192.
46. Marcil M, Ascah A, Matas J, Bélanger S, Descheppe C, Burelle Y. Compensated volume overload increases the vulnerability of heart mitochondria without affecting their functions in the absence of stress. *J Mol Cell Cardiol* 2006; **41**: 998–1009.
47. Zippin JH, Chen Y, Nahirney P, Kamenetsky M, Wuttke MS, Fischman DA *et al.* Compartmentalization of bicarbonate-sensitive adenylyl cyclase in distinct signaling microdomains. *FASEB J* 2003; **17**: 82–84.
48. Sulimovici S, Lunenfeld B. Effect of gonadotrophins on adenylate cyclase of the outer and inner membrane subfractions of rat testis mitochondria. *FEBS Lett* 1974; **41**: 345–347.
49. Fine AS, Egnor RW, Forrester E, Stahl SS. Adenylate cyclase localization in unfixed specimens of rat oral mucosa and isolated mitochondria. *J Histochem Cytochem* 1982; **30**: 1171–1178.
50. Papa S, De Rasmio D, Scacco S, Signorile A, Technikova-Dobrova Z, Palmisano G *et al.* Mammalian complex I: a regulable and vulnerable pacemaker in mitochondrial respiratory function. *Biochim Biophys Acta* 2008; **1777**: 719–728.
51. Acin-Perez R, Gatti DL, Bai Y, Manfredi G. Protein phosphorylation and prevention of cytochrome oxidase inhibition by ATP: coupled mechanisms of energy metabolism regulation. *Cell Metab* 2011; **13**: 712–719.
52. Qiao J, Mei FC, Popov VL, Vergara LA, Cheng X. Cell cycle-dependent subcellular localization of exchange factor directly activated by cAMP. *J Biol Chem* 2002; **277**: 26581–26586.
53. Pereira L, Rehmann H, Lao DH, Erickson JR, Bossuyt J, Chen J *et al.* Novel Epac fluorescent ligand reveals distinct Epac1 vs. Epac2 distribution and function in cardiomyocytes. *Proc Natl Acad Sci USA* 2015; **112**: 3991–3996.
54. Galluzzi L, Bravo-San Pedro JM, Vitale I, Aaronson SA, Abrams JM, Adam D *et al.* Essential versus accessory aspects of cell death: recommendations of the NCCD 2015. *Cell Death Differ* 2015; **22**: 58–73.
55. Kung G, Konstantinidis K, Kitsis RN. Programmed necrosis, not apoptosis, in the heart. *Circ Res* 2011; **108**: 1017–1036.
56. Kilkeny C, Browne W, Cuthill IC, Emerson M, Altman DG. Animal research: reporting *in vivo* experiments: the ARRIVE guidelines. *Br J Pharmacol* 2010; **160**: 1577–1579.
57. Hubert F, Belacel-Ouari M, Manoury B, Zhai K, Domergue-Dupont V, Mateo P *et al.* Alteration of vascular reactivity in heart failure: role of phosphodiesterases 3 and 4. *Br J Pharmacol* 2014; **171**: 5361–5375.
58. Chen Y, Cann MJ, Litvin TN, Iourgenko V, Sinclair ML, Levin LR *et al.* Soluble adenylyl cyclase as an evolutionarily conserved bicarbonate sensor. *Science* 2000; **289**: 625–628.
59. Morel E, Marcantoni A, Gastineau M, Birkedal R, Rochais F, Garnier A *et al.* cAMP-binding protein Epac induces cardiomyocyte hypertrophy. *Circ Res* 2005; **97**: 1296–1304.
60. Rochais F, Vandecasteele G, Lefebvre F, Lugnier C, Lum H, Mazet J *et al.* Negative feedback exerted by cAMP-dependent protein kinase and cAMP phosphodiesterase on subsarcolemmal cAMP signals in intact cardiac myocytes: an *in vivo* study using adenovirus-mediated expression of CNG channels. *J Biol Chem* 2004; **279**: 52095–52105.



**Cell Death and Disease** is an open-access journal published by Nature Publishing Group. This work is licensed under a Creative Commons Attribution 4.0 International License. The images or other third party material in this article are included in the article's Creative Commons license, unless indicated otherwise in the credit line; if the material is not included under the Creative Commons license, users will need to obtain permission from the license holder to reproduce the material. To view a copy of this license, visit <http://creativecommons.org/licenses/by/4.0/>

Supplementary Information accompanies this paper on Cell Death and Disease website (<http://www.nature.com/cddis>)

## Supplemental Material

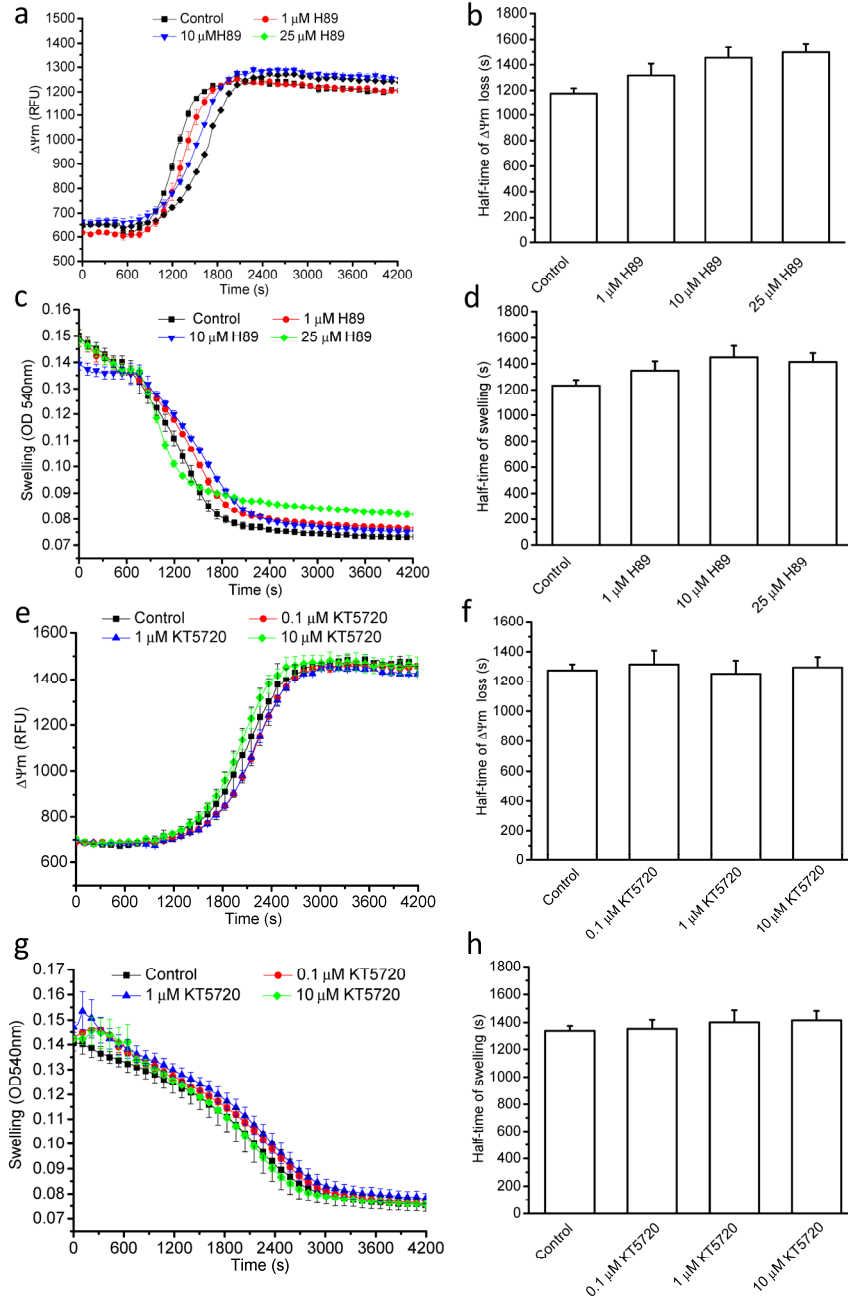
# **A cardiac mitochondrial cAMP signaling pathway regulates calcium accumulation, permeability transition and cell death**

Wang et al.

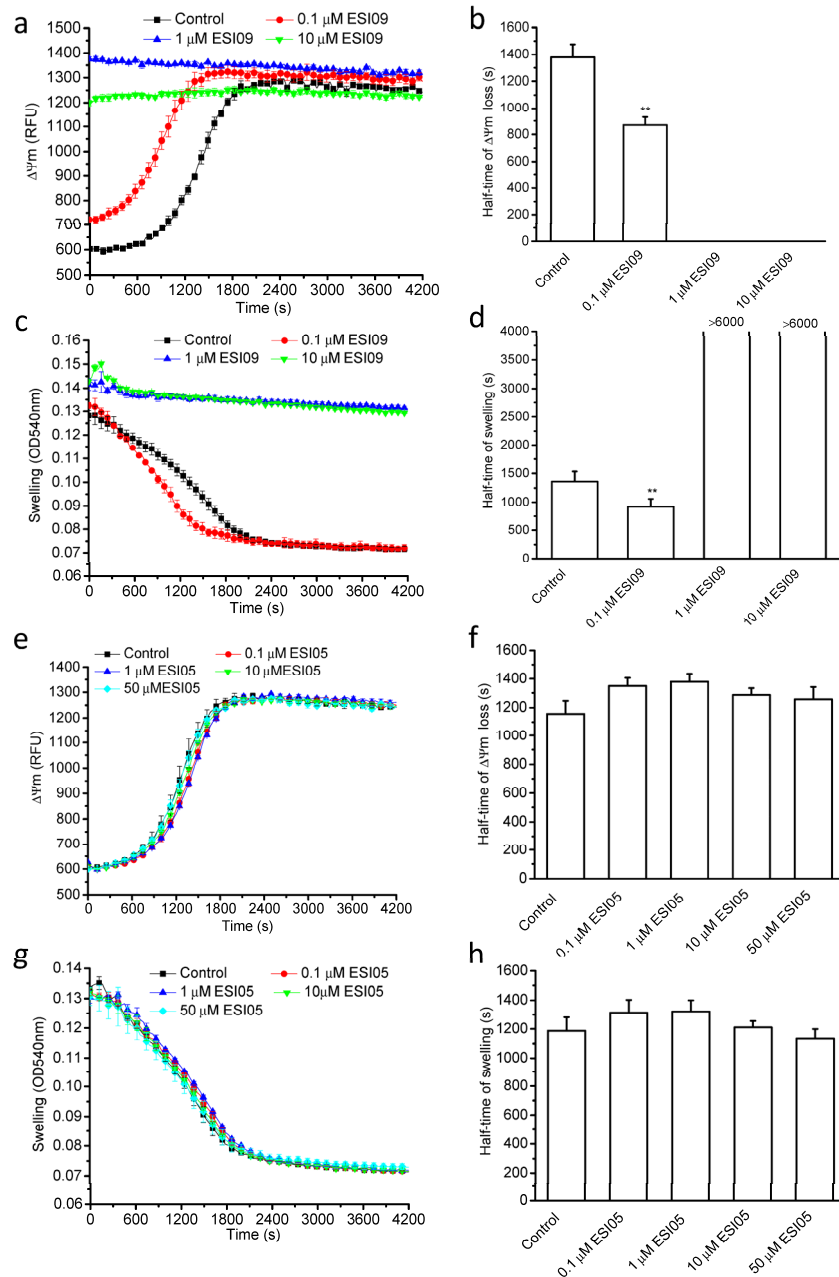
## **Supplemental methods**

### **Mitochondrial transmembrane potential measurement in adult cardiomyocytes**

Mitochondrial transmembrane potential ( $\Delta\Psi_m$ ) was measured according to the manufacturer's instructions using Mito-ID<sup>®</sup> (Enzo Life Sciences, Villeurbanne, France). The orange fluorescence emission (Excitation = 540 nm, Emission = 570 nm) associated with energized mitochondria with high transmembrane potential and the green fluorescence emission (Excitation = 485 nm, Emission = 530 nm) associated with depolarized mitochondria with low transmembrane potential were recorded. The images were acquired under a 63×Plan-Apochromat (NA 1.40) oil immersion objective lens using a confocal microscope (Leica SP8).

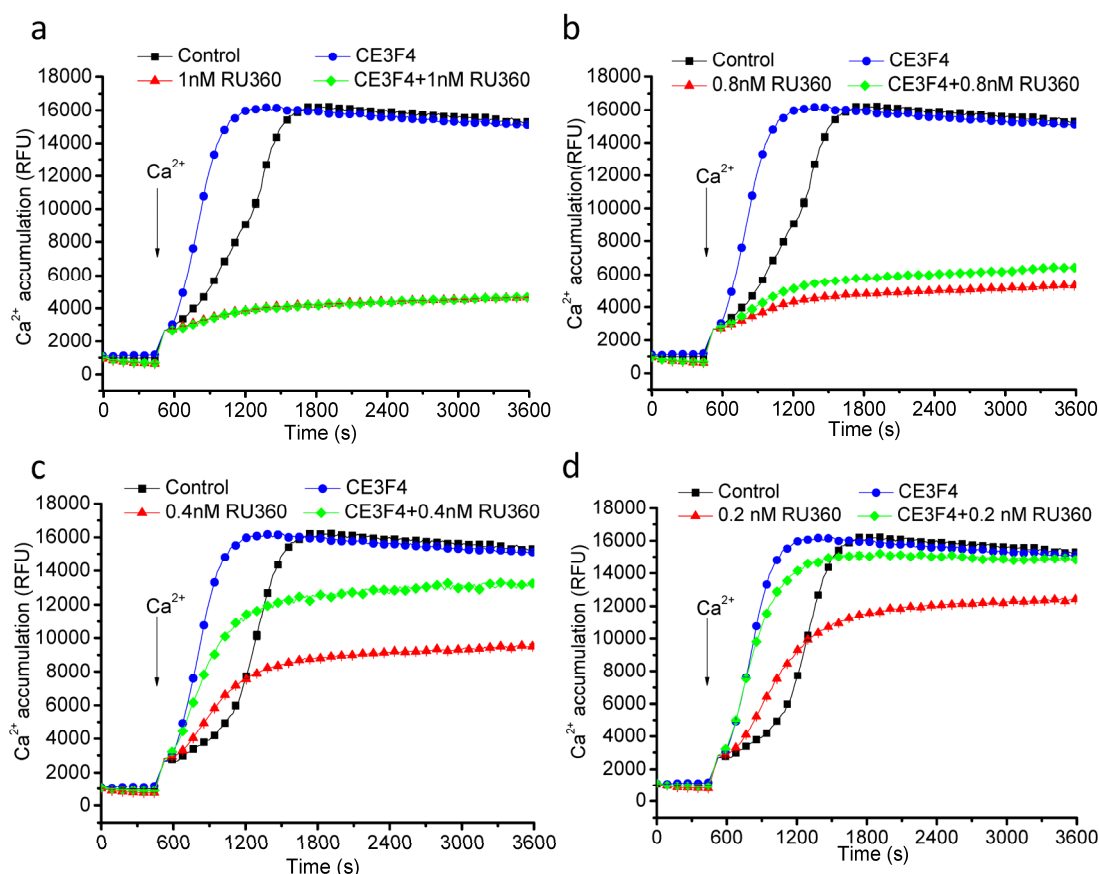


**Supplemental Figure1. PKA is not involved in the  $\text{Ca}^{2+}$  effects on mitochondrial membrane potential and swelling.** (a) Effect of H89 (1  $\mu\text{M}$ , 10  $\mu\text{M}$  and 25  $\mu\text{M}$ ) on  $\Delta\Psi_m$  loss induced by 10  $\mu\text{M}$   $\text{Ca}^{2+}$ . (b) Half-time of  $\Delta\Psi_m$  loss induced by 10  $\mu\text{M}$   $\text{Ca}^{2+}$  calculated from experiments such as shown in (a). (c) Effects of H89 (1  $\mu\text{M}$ , 10  $\mu\text{M}$  and 25  $\mu\text{M}$ ) on mitochondrial matrix swelling induced by 10  $\mu\text{M}$   $\text{Ca}^{2+}$ . (d) Half-time of mitochondrial swelling induced by 10  $\mu\text{M}$   $\text{Ca}^{2+}$  calculated from experiments such as shown in (c). (e) Effect of KT5720 (0.1  $\mu\text{M}$ , 1  $\mu\text{M}$  and 10  $\mu\text{M}$ ) on  $\Delta\Psi_m$  loss induced by 10  $\mu\text{M}$   $\text{Ca}^{2+}$ . (f) Half-time of  $\Delta\Psi_m$  loss induced by 10  $\mu\text{M}$   $\text{Ca}^{2+}$  calculated from experiments such as shown in (e). (g) Effect of KT5720 (0.1  $\mu\text{M}$ , 1  $\mu\text{M}$  and 10  $\mu\text{M}$ ) on mitochondrial matrix swelling induced by 10  $\mu\text{M}$   $\text{Ca}^{2+}$ . (h) Half-time of mitochondrial swelling induced by 10  $\mu\text{M}$   $\text{Ca}^{2+}$  calculated from experiments such as shown in (g) (n=3-4).

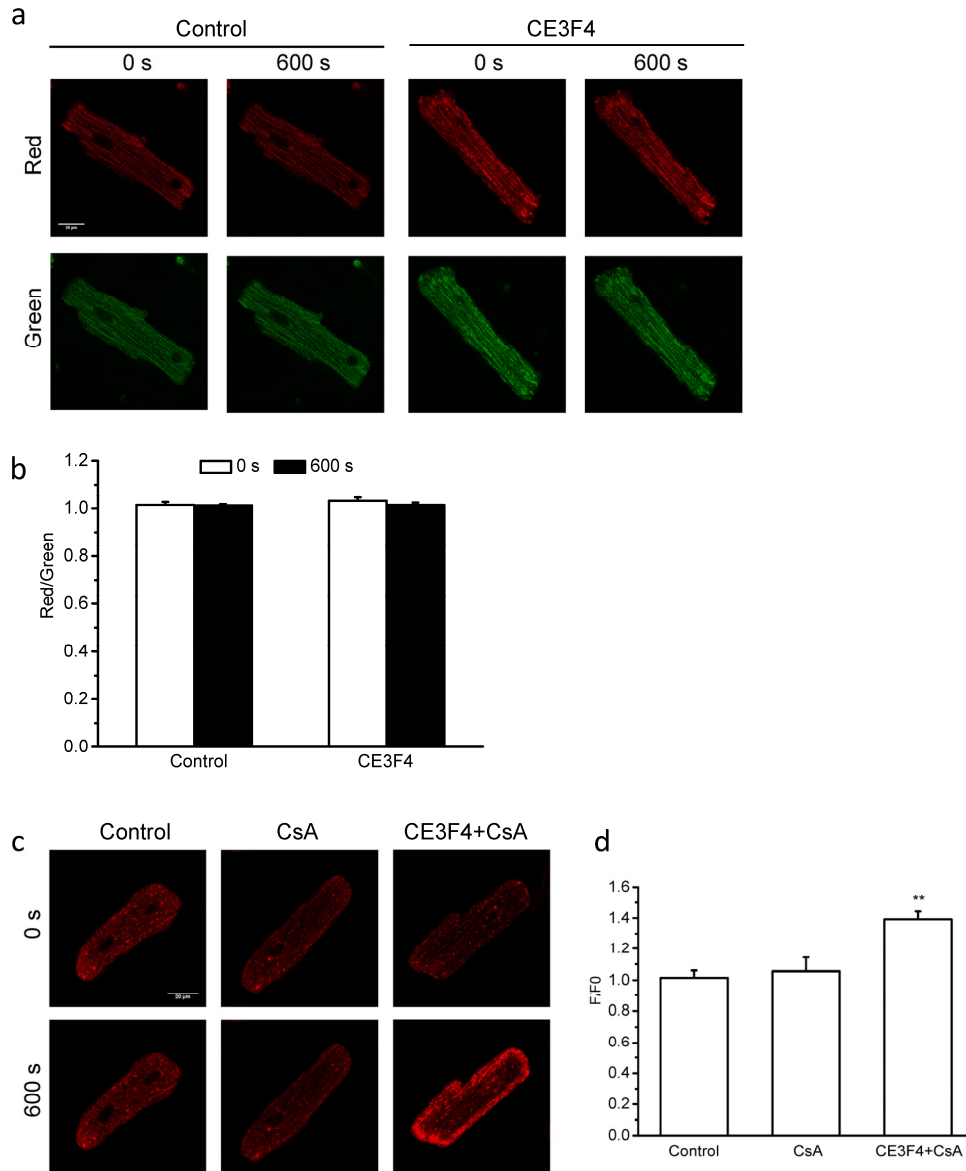


**Supplemental Figure 2. Epac2 is not involved in the  $\text{Ca}^{2+}$  effects on mitochondrial function.** (a) Effect of ESI09 (0.1  $\mu$ M, 1  $\mu$ M and 10  $\mu$ M) on  $\Delta\Psi_m$  loss induced by 10  $\mu$ M  $\text{Ca}^{2+}$ . (b) Half-time of  $\Delta\Psi_m$  loss induced by 10  $\mu$ M  $\text{Ca}^{2+}$  calculated from experiments such as shown in (a). (c) Effects of ESI09 (0.1  $\mu$ M, 1  $\mu$ M and 10  $\mu$ M) on mitochondrial matrix swelling induced by 10  $\mu$ M  $\text{Ca}^{2+}$ . (d) Half-time of mitochondrial swelling induced by 10  $\mu$ M  $\text{Ca}^{2+}$  calculated from experiments such as shown in (c). (e) Effect of ESI05 (0.1  $\mu$ M, 1  $\mu$ M, 10  $\mu$ M and 25  $\mu$ M) on  $\Delta\Psi_m$  loss induced by 10  $\mu$ M  $\text{Ca}^{2+}$ . (f) Half-time of mitochondrial swelling induced by 10  $\mu$ M  $\text{Ca}^{2+}$  calculated from experiments such as shown in (e). (g) Effect of ESI05 (0.1  $\mu$ M, 1  $\mu$ M, 10  $\mu$ M and 25  $\mu$ M) on mitochondrial matrix swelling induced by 10  $\mu$ M  $\text{Ca}^{2+}$ . (h) Half-time of mitochondrial swelling induced by 10  $\mu$ M  $\text{Ca}^{2+}$  calculated from experiments such as shown in (g). \*\* $P < 0.01$  (n=3-9).

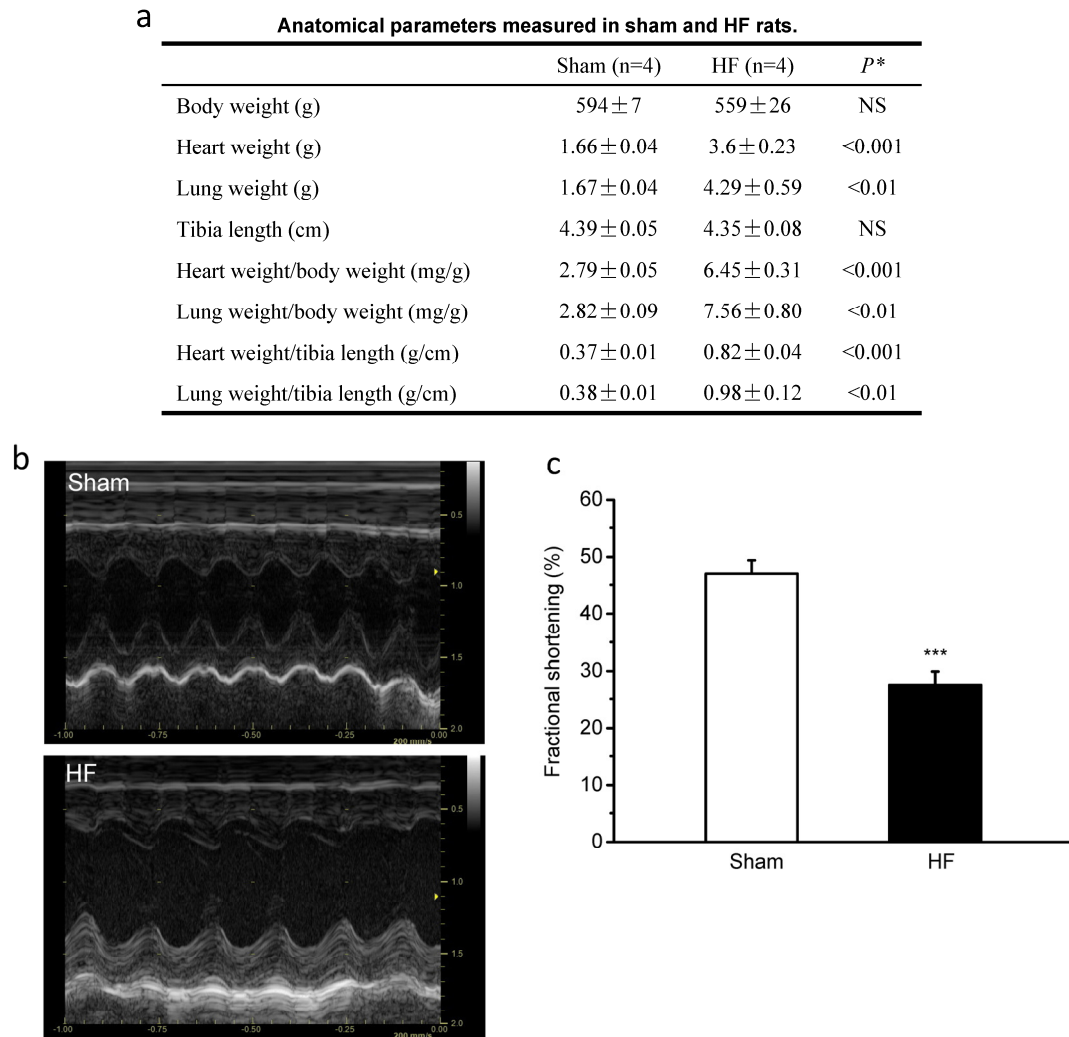




**Supplemental Figure 3. Effect of RU360 and CE3F4 on mitochondrial Ca<sup>2+</sup> levels measured with Rhod-2 in isolated mitochondria.** (a) Measurement of Ca<sup>2+</sup> accumulation in isolated mitochondria using 2  $\mu$ M Rhod-2 in the absence or presence of 50  $\mu$ M CE3F4, 1 nM RU360 or both. (b) Measurement of Ca<sup>2+</sup> accumulation in isolated mitochondria using 2  $\mu$ M Rhod-2 in the absence or presence of CE3F4, 0.8 nM RU360 or both. (c) Measurement of Ca<sup>2+</sup> accumulation in isolated mitochondria using 2  $\mu$ M Rhod-2 in the absence or presence of CE3F4, 0.4 nM RU360 or both. (d) Measurement of Ca<sup>2+</sup> accumulation in isolated mitochondria using 2  $\mu$ M Rhod-2 in the absence or presence of CE3F4, 0.2 nM RU360 or both (n=3).

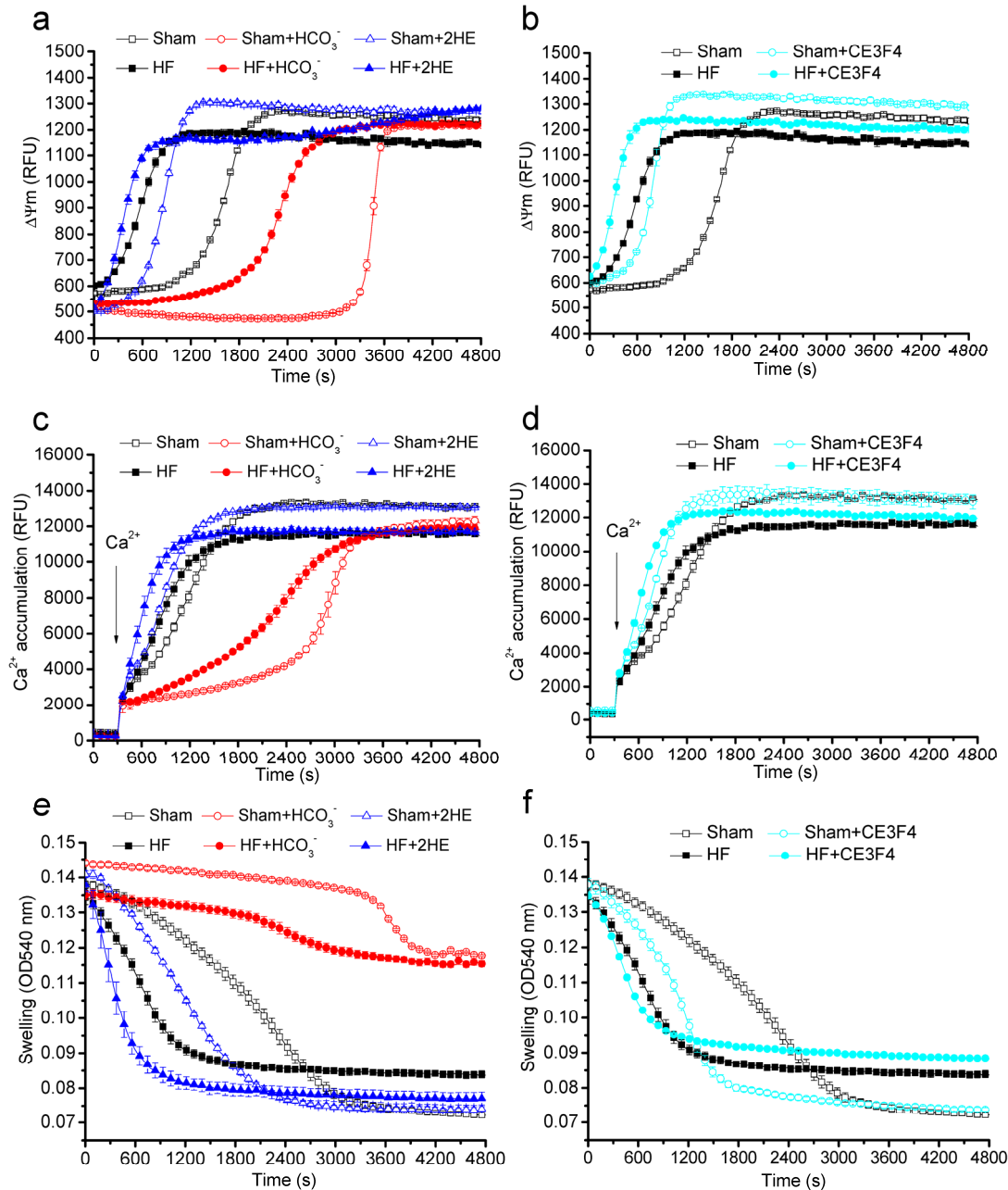


**Supplemental Figure 4.  $\text{Ca}^{2+}$  concentrations did not affect the mitochondrial potential and did not involve the PTPC. (a)** Confocal images of adult rat cardiomyocytes showing JC10 fluorescence in two emissions channels 525 nm (green images) and 590 nm (red images). The green fluorescence shows depolarized mitochondria (monomeric probe), whereas red fluorescence shows energized mitochondria (aggregated probe). Cardiomyocytes were labeled with JC10 for 15 min then permeabilized with 5  $\mu\text{g}/\text{mL}$  digitonin. Then the cells were exposed to 50  $\mu\text{M}$  CE3F4 or vehicle for 10 min and 200 nM free  $\text{Ca}^{2+}$  was applied at time 0 s. Bar size, 20  $\mu\text{m}$ . **(b)** Red to green ratio of JC10 measured from confocal images such as shown in **(a)** ( $n=6$ ). **(c)** Representative recording of confocal images of Rhod-2-labeled cardiomyocytes at time 0 s and 600 s. Cells were sequentially permeabilized with digitonin in  $\text{Ca}^{2+}$  free internal solution, treated with 50  $\mu\text{M}$  CE3F4, CE3F4 + 1  $\mu\text{M}$  CsA or vehicle for 10 min, then 200 nM  $\text{Ca}^{2+}$  was applied. Bar = 20  $\mu\text{m}$ . **(d)** Mean changes in Rhod-2 signal ( $n=9$ ). \*\* $P<0.01$ .



**Supplemental Figure 5. Anatomical parameters and echocardiographic analysis of Sham and HF rat.**

**(a)** Anatomical parameters measured in sham and HF rats. Values are mean ± SEM; n= number of animals. \* Statistical differences between heart failure (HF) rats and sham values; NS: not significant. HF was induced by transverse aortic constriction (TAC) as described in material and methods. **(b)** Representative echocardiographic images from Sham and HF rat hearts. **(c)** Fractional release in Sham and HF rat hearts. \*\*\*  $P < 0.001$  (n=4).



**Supplemental Figure 6. cAMP regulation of mitochondrial membrane potential and Ca<sup>2+</sup> uptake are preserved in HF rats.** Evaluation of  $\Delta\Psi_m$  in Sham and HF cardiac isolated mitochondria induced by 10  $\mu\text{M}$  Ca<sup>2+</sup> in response to sAC stimulation by 15 mM HCO<sub>3</sub><sup>-</sup> and sAC inhibition by 25  $\mu\text{M}$  2HE (**a**) and Epac1 inhibition by 50  $\mu\text{M}$  CE3F4 (**b**). Mitochondrial Ca<sup>2+</sup> accumulation following addition of 10  $\mu\text{M}$  Ca<sup>2+</sup> in response to sAC stimulation by 15 mM HCO<sub>3</sub><sup>-</sup> and sAC inhibition by 25  $\mu\text{M}$  2HE (**c**) and Epac1 inhibition by 50  $\mu\text{M}$  CE3F4 (**d**). Evaluation of mitochondrial swelling in Sham and HF cardiac isolated mitochondria induced by 10  $\mu\text{M}$  Ca<sup>2+</sup> in response to sAC stimulation by 15 mM HCO<sub>3</sub><sup>-</sup> and sAC inhibition by 25  $\mu\text{M}$  2HE (**e**) and Epac1 inhibition by 50  $\mu\text{M}$  CE3F4 (**f**). Panels (a-f) display one experiment representative of 4 experiments done in triplicate.

## **4.2 Article 2: Phosphodiesterases localized in cardiac mitochondria regulate mitochondrial cAMP and membrane potential**

# Phosphodiesterases localized in cardiac mitochondria regulate mitochondrial cAMP and membrane potential

WANG Z<sup>1</sup>, LIU D<sup>1</sup>, LINDNER M<sup>1</sup>, MIKA D<sup>1</sup>, VANDECASTEELE G<sup>1</sup>, FISCHMEISTER R<sup>1,2</sup>, and BRENNER C<sup>1,2</sup>

<sup>1</sup>INSERM UMR-S 1180, Faculty of Pharmacy, Univ Paris-Sud, University Paris-Saclay, Chatenay-Malabry, France

<sup>2</sup>IPSIT-US31-UMS3679, Faculty of Pharmacy, Univ Paris-Sud, University Paris-Saclay, Chatenay-Malabry, France

Short title: cardiac mitochondrial PDEs

Correspondance to    Dr Catherine Brenner  
INSERM UMR-S 1180  
Faculté de Pharmacie  
Université Paris-Sud  
5 Rue J.-B. Clément  
92296 Châtenay-Malabry Cedex  
France.  
E-mail: catherine.brenner-jan@u-psud.fr

**Abbreviations:**  $\Delta\Psi_m$ , mitochondrial membrane potential; Bay, Bay-60-7550; Cil, Cilostamide; CsA, cyclosporine A; FCCP, Carbonyl cyanide-p-trifluoromethoxyphenylhydrazone;  $\text{HCO}_3^-$ , bicarbonate; HF, heart failure; IM, inner membrane; sAC, soluble adenylyl cyclase; PDE, phosphodiesterase; Ro, Ro-20-1724.

## **Abstract**

Mitochondria plays a role in energy production as well as a role in many other essential cellular processes including ATP and metabolite synthesis, redox balance, calcium homeostasis and cell death. Recently, a cardiac mitochondrial cAMP production was shown to stimulate respiration, and inhibit calcium accumulation, permeability transition and cell death. Here, we identified PDE2A, PDE3A, PDE4A, PDE4B and PDE4D proteins in rat cardiac mitochondria. We found these PDE isoforms could regulate mitochondrial cAMP level by radioenzymatic assay in cardiac mitochondrial lysates and by FRET in live neonatal cardiomyocytes. PDE2 represented 35% of total mitochondrial cAMP-PDE activity and its activity was enhanced ~3-fold by 5  $\mu$ M cGMP. PDE3 and PDE4 activities represented, respectively, 30% and 25% of total in mitochondria isolated from adult rat heart. Functional assay showed that upon  $\text{HCO}_3^-$  stimulation, inhibition of PDEs delays the mitochondrial membrane potential loss and matrix swelling induced by calcium. In addition, we found that PDE2A and PDE4D expression are altered in heart failing mitochondria. Interestingly, in mitochondria isolated from transgenic PDE2A mice, the OXPHOS activity was significantly lower than wild-type mice. Thus, our study identify a new regulation of cAMP levels and signaling cascade in mitochondria by PDE, which may have implications for the metabolic control of cardiac function.

**Keywords:** PDE, cAMP, mitochondrial membrane potential,

## Introduction

The heart is highly energy-dependent with most of its energy provided by mitochondria. Mitochondria also play a role in many other essential cellular processes including metabolite synthesis, redox balance, calcium ( $\text{Ca}^{2+}$ ) homeostasis and cell death<sup>1,2,3</sup>. Therefore, maintaining a functional population of mitochondria is critical for cardiac function and identification of novel regulatory mechanisms of mitochondrial function is a crucial challenge. Recently, a soluble adenylyl cyclase (sAC) has been revealed to serve as a local source of the second messenger cAMP in the mitochondrial matrix in response to bicarbonate ( $\text{HCO}_3^-$ ) and  $\text{Ca}^{2+}$ . In liver and brain, mitochondrial cAMP stimulates oxidative phosphorylation and ATP production in response to  $\text{HCO}_3^-$  and/or  $\text{Ca}^{2+}$ . In coronary endothelial cells,  $\text{HCO}_3^-$  is transported into mitochondria and this leads to cAMP production by sAC, which indirectly modulates the cell fate through apoptosis<sup>5, 6</sup>. As a result, this pathway serves as a mechanism for metabolic adaptation to mitochondrial dysfunction and could be a potential novel target to treat genetic mitochondrial diseases<sup>7</sup>. In line with these studies, we recently showed a protective role for cAMP against cell death, apoptosis as well as necrosis in primary cardiomyocytes. Moreover, upon stimulation with  $\text{HCO}_3^-$  and  $\text{Ca}^{2+}$ , sAC produces cAMP, which in turn stimulates oxygen consumption, increases the mitochondrial membrane potential ( $\Delta\Psi_m$ ) and ATP production. In addition, cAMP is rate limiting for matrix  $\text{Ca}^{2+}$  entry via Epac1 and the mitochondrial  $\text{Ca}^{2+}$  uniporter and, as a consequence, prevents mitochondrial permeability transition<sup>8</sup>.

Phosphodiesterases (PDEs) are a class of key cellular enzymes, which degrade cyclic adenosine monophosphate (cAMP) and/or cyclic guanosine monophosphate (cGMP) by hydrolysis of phosphodiester bonds<sup>9</sup>. Thereby, they regulate intracellular levels of these ubiquitous second messengers. Cyclic nucleotides have been reported to play important role in the regulation of a host of cellular functions involved in signal transduction, synaptic transmission and to be involved in the pathogenesis of heart failure<sup>10</sup>. In mammalian cells, PDEs constitute a large



superfamily which contains 11 PDE families<sup>11, 12</sup> (PDE1 to PDE11), and non-generic PDEs such as the protein human Prune<sup>13, 14</sup>.

In isolated mitoplasts from mouse liver, cAMP catabolic activity was fully inhibited by IBMX, confirming the presence of intra-mitochondrial PDE activity<sup>15</sup>. It has been reported that PDE4 co-localized with mitochondria, apparently through an interaction with the protein disrupted in schizophrenia<sup>16</sup>. More recently, mitochondrial PDE2A is shown to be located in the matrix and that the unique N terminus of PDE2A isoform 2 specifically leads to mitochondrial localization of this isoform in liver and brain<sup>4, 17</sup>. Thus, mitochondrial PDE2A forms a local signalling system with sAC in the matrix, which regulates the activity of the respiratory chain<sup>4</sup>. Moreover, it has been reported that *Drosophila* Prune is a cyclic nucleotide phosphodiesterase that localizes to the mitochondrial matrix. Knocking down prune in cultured cells reduces mitochondrial transcription factor A (TFAM) and mitochondrial DNA (mtDNA) levels. These data suggest that Prune stabilizes TFAM and promotes mitochondrial DNA (mtDNA) replication through down regulation of mitochondrial cAMP signaling<sup>18</sup>.

To gain new insights into the control of the cardiac mitochondrial pool of cAMP, we investigated various isoforms of phosphodiesterases (PDEs) in isolated rat or mouse heart mitochondria. Our results showed that, at least, PDE2A, 3A, 4A, 4B and 4D can be detected within mitochondria. These PDEs controlled cAMP level with sAC to regulate mitochondrial functions. Our findings unravel an upstream regulation of cAMP in cardiac mitochondria, which may have implications for the metabolic control of cardiac function.

## **Results**

### **PDEs are expressed in cardiac mitochondria**

To identify the existence of PDEs in cardiac mitochondria, we isolated subsarcolemmal mitochondria from rat heart ventricles by differential centrifugation and extensive washes<sup>19</sup>. Western blot analysis of PDE protein expression revealed positive bands for PDE2A, 3A, 4A, 4B and 4D subtypes in cardiac mitochondria as well as in heart homogenate (Fig.1A). We next determined which mitochondrial subcompartment contains PDE2A, we isolated mitoplasts from rat heart, which contain inner membrane and matrix, but almost no intermembrane space or outer membrane protein. Western blots of mitoplasts isolated from rat heart showed positive bands of the expected molecular mass, whereas they are absent in the post-mitoplast fraction (Fig.1B). To confirm this, we analyzed our mitochondrial population by transmission electron microscopy and immunolabelling, which showed PDE2A is undoubtedly localized in the mitochondrial matrix. Due to insufficient specificity of their antibodies or unavailability, other PDEs were not investigated by this approach.

### **cAMP-PDE activity in cardiac mitochondria.**

To evaluate the activity of different PDE isoforms to hydrolyse cAMP, a radioenzymatic assay was conducted in the presence of different PDE inhibitors<sup>20</sup>. As shown in Fig. 2A and 2B, the major PDE in heart is PDE4. Whereas PDE2 represented the largest mitochondrial cAMP PDE activity (35% of total) and its activity was enhanced ~3-fold by 5  $\mu$ M cGMP and was inhibited by the PDE2 inhibitor, Bay 60-7550 (Bay, 100 nM). PDE3 and PDE4 activities represented, respectively, 30% and 25% of total, and they were inhibited by their respective inhibitors, cilostamide (Cil, 1  $\mu$ M) and Ro 20-1724 (Ro, 10  $\mu$ M). Accordingly, measurements mitochondrial cAMP levels by ELISA of under basal condition or following stimulation of isolated mitochondria with bicarbonate confirmed that inhibition of PDE2, 3 and 4 families leads to an increase in cAMP level (Fig. 2C).

### **FRET measurements of cAMP signals in mitochondria**

We then evaluated the functional contribution of the different PDE isoforms in controlling intracellular cAMP concentration in neonatal cardiac mitochondria. To do this, we constructed an adenovirus encoding a cAMP sensitive FRET sensor (Epac-S<sup>H187 21</sup>) fused with a 4mt sequence and infected rat neonatal cardiomyocytes with this new targeted sensor, 4mt-Epac-S<sup>H187</sup>. The localization of 4mt-Epac-S<sup>H187</sup> in mitochondria was shown by co-localization of its green fluorescence with mitotracker red fluorescence<sup>8</sup>. cAMP changes were monitored in real-time by fluorescence imaging using the FRET-based cAMP sensor 4mt-Epac-S<sup>H187</sup>. In basal condition, inhibition of PDE2, PDE3 with Bay (100nM) and Cil (1μM) caused a slight increase in mitochondrial cAMP level (Fig. 3A and Fig. 3C). And inhibition of PDE4 with Ro (10μM) resulted in 25% of increase in mitochondrial cAMP (Fig. 3E). To evaluate the effect of PDE family on cAMP response to sAC stimulation, HCO<sub>3</sub><sup>-</sup> was applied before PDE inhibitors. HCO<sub>3</sub><sup>-</sup> alone caused 15% of increases in cAMP level. HCO<sub>3</sub><sup>-</sup> plus Bay or Cil resulted in 40% of increase (Fig. 3B and Fig. 3D). In parallel, the cAMP level was increased 80% by PDE4 inhibition following sAC activation (Fig. F).

### **PDEs regulate Ca<sup>2+</sup>-induced mitochondrial permeability transition (MPT)**

We previously showed that in cardiac isolated mitochondria, MPT can be elicited by 10 μM Ca<sup>2+</sup> and prevented by 5 μM cyclosporin A (CsA) which is detected as a loss of ΔΨ<sub>m</sub> and a matrix swelling. Interestingly, cAMP elevation confers a protection of mitochondria from Ca<sup>2+</sup>-induced MPT<sup>8</sup>. As PDE may blunt the cAMP signal, we measured the ΔΨ<sub>m</sub> level and swelling induced by Ca<sup>2+</sup> in the presence of different PDE inhibitors as a function of time. We used two robust miniaturized assays<sup>19, 22</sup> to concomitantly measure the effect of PDEs. As a result, PDEs inhibition did not affect the ΔΨ<sub>m</sub> loss and swelling induced by Ca<sup>2+</sup> under basal condition. However, upon stimulation of HCO<sub>3</sub><sup>-</sup>, inhibition of PDE2, 3 and 4 slowed both processes compared to HCO<sub>3</sub><sup>-</sup> alone (Fig.4).

### **Functional bioenergetic analysis of mitochondria isolated from WT and TG mice**

In order to examine the bioenergetic function of mitochondria from WT and TG mice, we chose to assess mitochondrial function using the Seahorse XF<sup>e</sup>96 machine, which allows real-time assessment of oxygen consumption rates in isolated mitochondria. We took advantage of the generation and characterization of PDE2A WT and TG mice (Linder et al., in revision) and isolated mitochondria from PDE2A WT and TG mice. Firstly, we checked the expression of PDE2A in WT and TG mice. As shown in Fig. 5A and B, the PDE2A levels in heart and mitochondria were much higher in PDE2 TG mice than in WT mice (~20 fold). To measure mitochondrial coupling between mitochondrial ETC and oxidative phosphorylation (using succinate as the substrate), the rates of basal complex II respiration as well as states 3 (ADP-stimulated respiration), state 4o (oligomycin A, an ATP synthase inhibitor), and state 3u (FCCP, an H<sup>+</sup> ionophore and uncoupler of oxidative phosphorylation) were consecutively measured. Compared to mitochondria isolated from WT mice, those from TG mice exhibited a lower rate in complex II driven basal respiration, in ADP-driven state 3 respiration and in FCCP induced state 3u respiration (Fig.5C and D).

### **The effect of PDE2 on Ca<sup>2+</sup>-induced mitochondrial permeability transition (MPT)**

To evaluate the effect of PDE2 on MPT, we measured the  $\Delta\Psi_m$  loss and matrix swelling induced by Ca<sup>2+</sup> in mitochondria isolated from WT and TG mice. sAC inhibition by 2HE accelerated the depolarization and swelling induced by Ca<sup>2+</sup>, as shown by the decreased half time of  $\Delta\Psi_m$  loss and swelling (Fig. 6). Conversely, 15 mM HCO<sub>3</sub><sup>-</sup> slowed both processes (Fig. 6) suggesting that cAMP elevation confers a protection of mitochondria from Ca<sup>2+</sup>-induced MPT. Mitochondria isolated from PDE2 TG mice showed a faster  $\Delta\Psi_m$  loss and swelling compared to mitochondria isolated from WT mice (Fig. 6).

### **The effect of PDE2 on mitochondrial Ca<sup>2+</sup> accumulation**

We previously showed that stimulation of sAC with HCO<sub>3</sub><sup>-</sup> prevented Ca<sup>2+</sup> accumulation in

mitochondria isolated from rat heart. To determine whether  $\Delta\Psi_m$  loss and swelling are correlated with  $\text{Ca}^{2+}$  accumulation, we measured the  $\text{Ca}^{2+}$  accumulation with Rhod 2 in WT and TG mice. 2HE accelerated  $\text{Ca}^{2+}$  accumulation into mitochondria and  $\text{HCO}_3^-$  delay this process in both WT and TG mice. Similar to  $\Delta\Psi_m$  loss and swelling, mitochondrial  $\text{Ca}^{2+}$  accumulation is faster in TG mice than in WT mice (Fig.7).

## Discussion

Our results revealed the expression of various PDE in cardiac mitochondria and demonstrate in the control of cAMP levels inside mitochondria. Among the various PEs identified, PDE2 was the most abundant and we showed its role in the regulation of respiration and  $\text{Ca}^{2+}$ -dependent MPT.

The cyclic nucleotide signalling pathway regulates a vast number of physiological processes, including visual transduction, cell proliferation and differentiation, gene expression, apoptosis and metabolic pathways such as steroidogenesis, insulin secretion and glycogen synthesis, as well as glycogenolysis, lipogenesis and lipolysis<sup>11, 23, 24</sup>. Once synthesized by adenylyl cyclases or guanylyl cyclases, respectively, cAMP and cGMP transduce signal-encoded information by acting through a number of cellular effectors. cAMP and cGMP signals could be blunted by PDEs. Recently the existence cAMP signalling pathway in mitochondria has been evidenced in various organs such as brain, liver and heart. It was also shown that cAMP increases ATP production in cells and isolated mitochondria<sup>7, 25</sup>. cAMP level decrease due to sAC inhibition could decrease the ATP production,  $\text{O}_2$  consumption, and cytochrome oxidase (COX) activity, whereas sAC activation by  $\text{HCO}_3^-$  and  $\text{Ca}^{2+}$  stimulates oxidative phosphorylation<sup>7, 25</sup>. Different PDE subtypes have been found in subcellular compartment including nuclear, endoplasmic reticulum, sarcoplasmic reticulum and Golgi<sup>26</sup>. However, little was known about mitochondrial PDEs. Thus, until now, only PDE4 and PDE2 have been found in mitochondria<sup>4, 16, 17</sup>. Acin-Perez et al find that mitochondrial PDE2A is located in the matrix and that the unique N

terminus of PDE2A isoform 2 specifically leads to mitochondrial localization of this isoform rodent liver and brain. PDE4B was reported to partially colocalize with DISC1 in the mitochondria of SH-SY5Y and LAN5 cells<sup>27</sup>. Asirvatham et al showed that mitochondrial AKAP149 bind to PKA and PDE4A comprising regulatory modules to maintain cAMP homeostasis in the T cell<sup>28</sup>. In this study, we identified that PDE2A, 3A, 4A, 4B and 4D were localized in mitochondria matrix from rat heart by detecting them in mitoplasts by western blot and in isolated mitochondria by immunolabelling and transmission electron microscopy.

Acin-Perez et al showed that PDE2A was present in brain and liver mitochondrial fractions and to be responsible for cAMP degrading PDE activity. In contrast, PDE4 had no significant effect on cAMP-degrading activity from liver mitochondria, but showed almost the same activity as PDE2 in brain mitochondria<sup>4</sup>. In isolated rat heart mitochondria, we showed that PDE2 represented the largest mitochondrial cAMP degrading PDE activity (35% of total), followed by PDE3 and PDE4, which represented 30% and 25% of total respectively. Our cardiac mitochondrial PDE2 activity correlated with Acin-Perez's data, who propose that PDE2 is the main PDE in heart, liver and brain. However, in neonatal cardiomyocytes infected with 4mt-Epac-S<sup>H187</sup>, inhibition of PDE2 and 3 caused about 2.5% increase in cAMP and inhibition of PDE4 resulted in 25% increase in basal condition. And upon HCO<sub>3</sub><sup>-</sup> stimulation, i.e. upon increased cAMP levels, inhibition of PDE2 and 3 caused 40% and inhibition of PDE4 reached to 80%. This revealed a difference in PDE2 activity in isolated mitochondria from adult rat heart and in neonatal cardiomyocytes, which is not observed for PDE3 and PDE4<sup>29</sup>.

In cardiac mitochondria, we have shown that mitochondrial cAMP stimulates oxygen consumption and ATP production<sup>8</sup>. Consistent with this, Acin-Perez reported that inhibition of PDE2 caused an increase in oxygen consumption and ATP production in mouse brain mitochondria. Here, using PDE2 TG mice, we showed that mitochondria isolated from PDE2 TG mice had a lower oxygen consumption rate than WT mice. In addition, we previously

reported that cAMP produced with mitochondria regulates  $\text{Ca}^{2+}$  accumulation and permeability transition<sup>8</sup>. Here, we found that upon  $\text{HCO}_3^-$  stimulation to increase cAMP, inhibition of PDE2, PDE3 and PDE4 delayed these processes, although inhibition of PDEs did not have effect in basal condition. 8Br-cGMP also delayed the  $\text{Ca}^{2+}$  accumulation and permeability transition in isolated mitochondria indicating that cGMP has the similar effect as cAMP on mitochondrial function (not shown). Moreover, mitochondria isolated from PDE2 TG mice showed a faster  $\Delta\Psi_m$  loss and swelling compared to mitochondria isolated from WT mice confirming the results obtained in isolated mitochondria treated with PDE2 inhibitor. These results indicate that cAMP degrading PDEs forms a local mitochondrial signalling pathway controlling cAMP produced locally by sAC, and regulate mitochondrial  $\text{Ca}^{2+}$  accumulation and permeability transition.

cAMP levels are up-regulated in HF, contributing to the HF progression. Here, we showed that as expected PDE4D was up-regulated in heart homogenate, but also in mitochondria isolated from HF rat, whereas PDE 4A and 4B were significantly decreased in HF heart, but did not change in mitochondria (Fig S1). This shows a regulatory control of PDE expression in mitochondria and suggests a putative role in cardiac pathology that deserves further investigation in the future.

Altogether, our present work demonstrates that PDE2, 3 and 4 are localized in cardiac mitochondria and they can degrade cAMP and subsequently regulate  $\text{Ca}^{2+}$  accumulation and permeability transition. Given the role of ATP and  $\text{Ca}^{2+}$  in the heart, our findings may have implications for the metabolic control of cardiac function.

## **Materials and methods**

Unless specified, all reagents and chemicals are from SIGMA Aldrich and of analytical grade.

### **Animals**

All animal care and experimental procedures conformed to the European Community guiding principles in the care and use of animals (Directive 2010/63/EU of the European Parliament) and authorizations to perform animal experiments according to this decree were obtained from the French Ministry of Agriculture, Fisheries and Food (No. D-92-283, 13 December 2012). All studies involving rats are reported in accordance with the ARRIVE guidelines for reporting experiments involving animals <sup>30</sup>.

### **Isolation of rat cardiac mitochondria**

Mitochondria were isolated from the heart of adult male Wistar rats at 8-10 weeks of age (275-375g; Janvier, Le Genest St Isle, France) as described <sup>19</sup>. Briefly, the heart was rapidly removed and placed into a cold buffer containing 0.3 M sucrose, 0.2 mM EGTA, 5 mM TES (pH 7.2). The heart was grinded with Polytron fastly and homogenized by using the Potter. The homogenate was centrifuged at 500 g for 10 min, 4°C. Then the supernatant was carefully removed and centrifuged again at 3,000 g for 10 min, 4°C. The pellets were washed in the isolation buffer and mitochondria kept on ice until use.

### **Isolation of mouse cardiac mitochondria**

Mitochondria were isolated from female mice heart at 15-20 weeks of age (Janvier, Le Genest St Isle, France) as described. Briefly, the heart was rapidly removed and placed into a cold buffer containing 0.3 M sucrose, 0.2 mM EGTA, 5 mM TES (pH 7.2). The heart was homogenized by using the Potter. The homogenate was centrifuged at 3,000 g for 10 min, 4°C. Then the supernatant was carefully removed and centrifuged again at 12,000 g for 10 min, 4°C. The pellets were washed in the isolation buffer and mitochondria kept on ice until use.



### **Mitoplast preparation**

Freshly isolated mitochondria were incubated in H<sub>2</sub>O containing 15 mM KCl to induce an osmotic shock for 30 min at 4°C and then, collected by centrifugation.

### **Measurement of mitochondrial transmembrane potential and swelling in isolated mitochondria**

Isolated mitochondria (25 µg proteins) were incubated with Ca<sup>2+</sup> and drugs in 96 well microtiter plates<sup>19</sup>. Mitochondrial transmembrane potential was measured using the fluorescent probe, rhodamine 123 (Rhod123, Excitation = 485 nm and Emission = 535 nm, Enzo Life Sciences, Villeurbanne, France) in a buffer containing 200 mM sucrose, 10 mM MOPS, 10 µM EGTA, 1 mM H<sub>3</sub>PO<sub>4</sub>, 5 mM succinate and 2 µM rotenone (pH 7.4) using Tecan Infinite 200 spectrofluorimeter. In parallel, matrix swelling was measured via absorbance at 540 nm<sup>8, 19</sup>.

### **Measurement of mitochondrial Ca<sup>2+</sup> in isolated mitochondria**

Isolated mitochondria (25 µg proteins) were incubated with 5 µM Rhod-2 (Enzo Life Sciences, Villeurbanne, France) in the buffer containing 200 mM sucrose, 10 mM MOPS, 10 µM EGTA, 1 mM H<sub>3</sub>PO<sub>4</sub>, 5 mM succinate and 2 µM rotenone for 30 min in dark at room temperature. After, the mitochondria were washed 2 times. Then the mitochondria were treated with various drugs for 10 min before applying Ca<sup>2+</sup>. Fluorescence was measured in real time for 60 min at room temperature in 96-well plates using Tecan Infinite 200 (Excitation =552 nm; Emission =581 nm).

### **cAMP measurements by ELISA**

cAMP measurements were performed according to the manufacturer's instructions using monoclonal anti-cAMP antibodybased direct cAMP ELISA Kit (New East Biosciences, King of Prussia, PA, USA) on freshly isolated mitochondria from rat hearts (500 µg proteins per sample) treated or not by HCO<sub>3</sub><sup>-</sup> and PDE inhibitors for 20 min at room temperature before centrifugation and lysis<sup>8</sup>.

### **Cyclic AMP-PDE activity assay**

The cAMP-PDE activity was measured in the supernatant according to a modification of the two-step assay procedure method described by Thompson and Appleman<sup>31</sup>, using 20 µg of heart homogenate proteins/ 200 µg of mitochondria proteins in a total volume of 200 µl including 10 mM Tris-HCl, pH 8.0, 10 mM MgCl<sub>2</sub>, 5 mM β-mercaptoethanol and 1 µM cAMP and supplemented with 10<sup>5</sup> cpm [<sup>3</sup>H]-cAMP, as detailed previously<sup>32</sup>. To evaluate PDE families-specific activities, the assay was performed in the absence or presence of either one or a combination of several selective PDE inhibitors: 100 nM Bay for PDE2, 1 µM Cil for PDE3, 10 µM Ro for PDE4 and 500 µM IBMX as a non-selective PDE inhibitor. The residual hydrolytic activity observed in the presence of PDE inhibitors was expressed as a percentage of the total cAMP-PDE activity, corresponding to the cAMP-PDE activity in the absence of inhibitor.

### **Bioenergetic analysis in isolated mitochondria**

The XF<sup>96</sup> Extracellular Flux Analyzer (Seahorse Biosciences, North Billerica, MA, USA) was used to measure mitochondrial bioenergetic function<sup>33</sup>. Respiration by the mitochondria (0.5 µg/well) was sequentially measured in a coupled state with substrate (basal respiration, State 2). State 3 initiated with 2 mM ADP, state 4 induced with the addition of 2.5 µg/ml oligomycin (State 4o), and 2 µM FCCP-induced maximal uncoupler-stimulated respiration (State 3u) were sequentially measured. At the end of the experiment the Complex III inhibitor, 4 µM antimycin A was applied to completely shut down the mitochondrial respiration. This ‘coupling assay’ examines the degree of coupling between the electron transport chain (ETC.), and the oxidative phosphorylation (OXPHOS), and can distinguish between ETC. and OXPHOS with respect to mitochondrial function/ dysfunction.

## **Western blotting**

Total mitochondrial proteins were resolved on 4–15% Tris-glycine SDS-PAGE gels and electroblotted onto polyvinylidene fluoride (PVDF) membranes (Bio-Rad, Marnes La Coquette). Following electrotransfer, membranes were blocked for 1 h at room temperature in 5% BSA-PBST (10 mM Tris HCl, pH 8.0/150 mM NaCl/0.1% Tween 20). Next, membranes were incubated overnight at 4°C with primary antibody. The day after, the membranes were washed six times with PBST and incubated with peroxidase-conjugated secondary antibody at room temperature for 1 h. Peroxidase activity was detected with enhanced chemiluminescence (ECL Advance Western blotting detection kit; Thermo Scientific, Villebon sur Yvette, France). For protein detection, the following antibodies were used: PDE2A (Santa Cruz, CA, USA), PDE3A (Chen Yan, University of Rochester), PDE4A (Marco Conti, University of California, San Francisco), PDE4B (Marco Conti), PDE4D (Marco Conti), GAPDH (Cell signalling, Danvers, MA, USA), VDAC (Genosphere, Paris, France).

## **Construction of mitochondria-targeted FRET sensor for cAMP**

The mitochondrial targeting sequence 4mt, encoding four copies of the signal sequence from subunit VIII of human cytochrome C oxidase, was amplified using the Advantage Polymerase (Clontech) and primers F (ACTATAGGGAGACCCAAGCTTATG) and R (TGGTGGCGGCAAGCTTCTTGCTCACCATGGTGGC). The pcDNA-4mt-D3-cpv vector used as a matrix for amplification of 4mt was a kind gift from Dr. Roger Tsien (HHMI investigator at the University of California San Diego, USA). The PCR fragment was cloned into the HindIII restriction site of pcDNA3-Epac-S<sup>H187</sup> using the Infusion HD Cloning system (Clontech). Epac-S<sup>H187</sup> encodes for a fourth generation Epac1-based cAMP sensor and was a kind gift from Dr. Kees Jalink (The Netherlands Cancer Institute, Amsterdam, Netherlands)<sup>21</sup>. Once the pcDNA-4mt-Epac-S<sup>H187</sup> vector was amplified in Stellar *E. coli* (Clontech) bacteria, its identity with parental sequences was verified by PCR using primers F

(ACTCACTATAGGGAGACC) and R (TGCGGCCGCCATGGTGGC), and DNA double strand sequencing (INSERM U1056 – UMR 5165 CNRS UPS – UDEAR, Toulouse, France). Adenoviruses encoding Epac-S<sup>H187</sup> and 4mt-Epac-S<sup>H187</sup> were generated by Welgen, Inc.

### **Cardiomyocyte isolation and adenoviral infection**

Neonatal cardiomyocytes were isolated as previously described<sup>34 35</sup>. For FRET experiments, neonatal cardiomyocytes were plated on 35 mm, laminin-coated culture dishes (10 µg/mL) at a density of  $4 \times 10^5$  cells per dish. The day after, cells were infected with Epac-S<sup>H187</sup> and 4mt-Epac-S<sup>H187</sup> adenoviruses in Opti-MEM<sup>®</sup> (Life technologies, St Aubin, France) for 48h. Similarly, adenoviruses expressing sAC<sub>i</sub> and sAC<sub>fl</sub> were used (generous gift of Pr. M. Conti, University of California, San Francisco, CA, USA).

### **Fluorescence resonance energy transfer measurements of cAMP levels**

Fluorescence resonance energy transfer (FRET) imaging experiments were performed 48h after infection of neonatal cardiomyocytes. Cells were bathed in Hepes-buffered Ringer's solution containing: 125 mM NaCl, 25 mM Hepes, 10 mM glucose, 5 mM K<sub>2</sub>HPO<sub>4</sub>, 1 mM MgSO<sub>4</sub>, and 1 mM CaCl<sub>2</sub>, pH 7.4. For sAC activation by HCO<sub>3</sub><sup>-</sup>, the medium was the Krebs-Henseleit solution containing: 120 mM NaCl, 2.09 mM K<sub>2</sub>HPO<sub>4</sub>, 0.34 mM KH<sub>2</sub>PO<sub>4</sub>, 24 mM NaHCO<sub>3</sub>, 1 mM MgSO<sub>4</sub>, 1 mM CaCl<sub>2</sub>, and 10 mM D-glucose. Krebs-Henseleit solution was gassed continuously with 95% O<sub>2</sub>/5% CO<sub>2</sub> to maintain a pH of 7.4. Real-time FRET experiments were performed at room temperature. Images were captured every 5 s using the 40× oil immersion objective of an inverted microscope (Nikon, Champigny sur Marne, France) connected to a Cool SNAP HQ2 camera (Photometrics, Tucson, AZ, USA) controlled by the Metafluor software (Molecular Devices, Sunnyvale, CA, USA). The donor (mTurquoise2)<sup>21</sup> was excited during 300 ms by a Xenon lamp (Nikon) using a 440/20BP filter and a 455LP dichroic mirror. Dual-emission imaging of donor and acceptor was performed using a Dual-View emission

splitter equipped with a 510 LP dichroic mirror and BP filters 480/30 and 535/ 25 nm, respectively.

### **Data Analysis**

Results are expressed as mean  $\pm$  SEM. The Origin software was used for statistical analysis. Differences between groups have been analyzed by one-way ANOVA and Student *t* test. A value of  $p < 0.05$  were considered as statistically significant. The number of animals, cells and independent experiments performed is indicated in the figure legends.

### **Conflict of Interest**

The authors declare no conflict of interest.

### **Acknowledgments**

This work has been funded by INSERM (CB, GV, RF), the Investment for the Future program ANR-11-IDEX-0003-01 within the LABEX ANR-10-LABX-0033 (CB, GV, RF) and ANR (ANR-13-ISV1-0001-01, CB). Zhenyu WANG and Dawei Liu are supported by a fellowship from the China Scholarship Council. The Seahorse apparatus was co-funded by CORDDIM (Investissement 2015) and IPSIT.

## Reference

1. Brenner C, Kroemer G. Apoptosis. Mitochondria--the death signal integrators. *Science* 2000, **289**(5482): 1150-1151.
2. Weinberg SE, Chandel NS. Targeting mitochondria metabolism for cancer therapy. *Nature chemical biology* 2015, **11**(1): 9-15.
3. Vandecasteele G, Szabadkai G, Rizzuto R. Mitochondrial calcium homeostasis: mechanisms and molecules. *IUBMB life* 2001, **52**(3-5): 213-219.
4. Acin-Perez R, Russwurm M, Gunnewig K, Gertz M, Zoidl G, Ramos L, *et al.* A phosphodiesterase 2A isoform localized to mitochondria regulates respiration. *The Journal of biological chemistry* 2011, **286**(35): 30423-30432.
5. Kumar S, Flacke JP, Kostin S, Appukuttan A, Reusch HP, Ladilov Y. SLC4A7 sodium bicarbonate co-transporter controls mitochondrial apoptosis in ischaemic coronary endothelial cells. *Cardiovascular research* 2011, **89**(2): 392-400.
6. Kumar S, Kostin S, Flacke JP, Reusch HP, Ladilov Y. Soluble adenylyl cyclase controls mitochondria-dependent apoptosis in coronary endothelial cells. *The Journal of biological chemistry* 2009, **284**(22): 14760-14768.
7. Acin-Perez R, Salazar E, Brosel S, Yang H, Schon EA, Manfredi G. Modulation of mitochondrial protein phosphorylation by soluble adenylyl cyclase ameliorates cytochrome oxidase defects. *EMBO molecular medicine* 2009, **1**(8-9): 392-406.
8. Wang Z, Liu D, Varin A, Nicolas V, Courilleau D, Mateo P, *et al.* A cardiac mitochondrial cAMP signaling pathway regulates calcium accumulation, permeability transition and cell death. *Cell death & disease* 2016, **7**: e2198.
9. Bender AT, Beavo JA. Cyclic nucleotide phosphodiesterases: molecular regulation to clinical use. *Pharmacological reviews* 2006, **58**(3): 488-520.
10. Sharma S, Kumar K, Deshmukh R, Sharma PL. Phosphodiesterases: Regulators of cyclic nucleotide signals and novel molecular target for movement disorders. *European journal of pharmacology* 2013, **714**(1-3): 486-497.
11. Conti M, Beavo J. Biochemistry and physiology of cyclic nucleotide phosphodiesterases: essential components in cyclic nucleotide signaling. *Annual review of biochemistry* 2007, **76**: 481-511.
12. Omori K, Kotera J. Overview of PDEs and their regulation. *Circulation research* 2007, **100**(3): 309-327.
13. Middelhaufe S, Garzia L, Ohndorf UM, Kachholz B, Zollo M, Steegborn C. Domain mapping on the human metastasis regulator protein h-Prune reveals a C-terminal dimerization domain. *The Biochemical journal* 2007, **407**(2): 199-205.

14. D'Angelo A, Garzia L, Andre A, Carotenuto P, Aglio V, Guardiola O, *et al.* Prune cAMP phosphodiesterase binds nm23-H1 and promotes cancer metastasis. *Cancer cell* 2004, **5**(2): 137-149.
15. Acin-Perez R, Salazar E, Kamenetsky M, Buck J, Levin LR, Manfredi G. Cyclic AMP produced inside mitochondria regulates oxidative phosphorylation. *Cell metabolism* 2009, **9**(3): 265-276.
16. Millar JK, Pickard BS, Mackie S, James R, Christie S, Buchanan SR, *et al.* DISC1 and PDE4B are interacting genetic factors in schizophrenia that regulate cAMP signaling. *Science* 2005, **310**(5751): 1187-1191.
17. Modis K, Panopoulos P, Coletta C, Papapetropoulos A, Szabo C. Hydrogen sulfide-mediated stimulation of mitochondrial electron transport involves inhibition of the mitochondrial phosphodiesterase 2A, elevation of cAMP and activation of protein kinase A. *Biochem Pharmacol* 2013, **86**(9): 1311-1319.
18. Zhang F, Qi Y, Zhou K, Zhang GF, Linask K, Xu H. The cAMP phosphodiesterase Prune localizes to the mitochondrial matrix and promotes mtDNA replication by stabilizing TFAM. *EMBO reports* 2015, **16**(4): 520-527.
19. Wang Z, Nicolas C, Fischmeister R, Brenner C. Enzymatic assays for probing mitochondrial apoptosis. *Methods Mol Biol* 2015, **1265**: 407-414.
20. Mehel H, Emons J, Vettel C, Wittkopper K, Seppelt D, Dewenter M, *et al.* Phosphodiesterase-2 Is Up-Regulated in Human Failing Hearts and Blunts beta-Adrenergic Responses in Cardiomyocytes. *J Am Coll Cardiol* 2013, **62**(17): 1596-1606.
21. Klarenbeek J, Goedhart J, van Batenburg A, Groenewald D, Jalink K. Fourth-generation epac-based FRET sensors for cAMP feature exceptional brightness, photostability and dynamic range: characterization of dedicated sensors for FLIM, for ratiometry and with high affinity. *PloS one* 2015, **10**(4): e0122513.
22. Belzacq-Casagrande AS, Martel C, Pertuiset C, Borgne-Sanchez A, Jacotot E, Brenner C. Pharmacological screening and enzymatic assays for apoptosis. *Frontiers in bioscience : a journal and virtual library* 2009, **14**: 3550-3562.
23. Francis SH, Blount MA, Corbin JD. Mammalian Cyclic Nucleotide Phosphodiesterases: Molecular Mechanisms and Physiological Functions. *Physiol Rev* 2011, **91**(2): 651-690.
24. Keravis T, Lugnier C. Cyclic nucleotide phosphodiesterase (PDE) isozymes as targets of the intracellular signalling network: benefits of PDE inhibitors in various diseases and perspectives for future therapeutic developments. *British journal of pharmacology* 2012, **165**(5): 1288-1305.
25. Di Benedetto G, Scalzotto E, Mongillo M, Pozzan T. Mitochondrial Ca(2)(+) uptake induces cyclic AMP generation in the matrix and modulates organelle ATP levels. *Cell metabolism* 2013, **17**(6): 965-975.



26. Maurice DH, Ke H, Ahmad F, Wang Y, Chung J, Manganiello VC. Advances in targeting cyclic nucleotide phosphodiesterases. *Nature reviews Drug discovery* 2014, **13**(4): 290-314.
27. Millar JK, Pickard BS, Mackie S, James R, Christie S, Buchanan SR, *et al.* DISC1 and PDE4B are interacting genetic factors in schizophrenia that regulate cAMP signaling. *Science* 2005, **310**(5751): 1187-1191.
28. Asirvatham AL, Galligan SG, Schillace RV, Davey MP, Vasta V, Beavo JA, *et al.* A-kinase anchoring proteins interact with phosphodiesterases in T lymphocyte cell lines. *J Immunol* 2004, **173**(8): 4806-4814.
29. Mongillo M, McSorley T, Evellin S, Sood A, Lissandron V, Terrin A, *et al.* Fluorescence resonance energy transfer-based analysis of cAMP dynamics in live neonatal rat cardiac myocytes reveals distinct functions of compartmentalized phosphodiesterases. *Circulation research* 2004, **95**(1): 67-75.
30. Kilkenny C, Browne W, Cuthill IC, Emerson M, Altman DG. Animal research: reporting in vivo experiments: the ARRIVE guidelines. *British journal of pharmacology* 2010, **160**(7): 1577-1579.
31. Thompson WJ, Appleman MM. Characterization of cyclic nucleotide phosphodiesterases of rat tissues. *The Journal of biological chemistry* 1971, **246**(10): 3145-3150.
32. Saucerman JJ, McCulloch AD. Cardiac beta-adrenergic signaling: from subcellular microdomains to heart failure. *Annals of the New York Academy of Sciences* 2006, **1080**: 348-361.
33. Coletta C, Modis K, Olah G, Brunyanszki A, Herzig DS, Sherwood ER, *et al.* Endothelial dysfunction is a potential contributor to multiple organ failure and mortality in aged mice subjected to septic shock: preclinical studies in a murine model of cecal ligation and puncture. *Crit Care* 2014, **18**(5).
34. Morel E, Marcantoni A, Gastineau M, Birkedal R, Rochais F, Garnier A, *et al.* cAMP-binding protein Epac induces cardiomyocyte hypertrophy. *Circulation research* 2005, **97**(12): 1296-1304.
35. Rochais F, Vandecasteele G, Lefebvre F, Lugnier C, Lum H, Mazet J, *et al.* Negative feedback exerted by cAMP-dependent protein kinase and cAMP phosphodiesterase on subsarcolemmal cAMP signals in intact cardiac myocytes: an in vivo study using adenovirus-mediated expression of CNG channels. *The Journal of biological chemistry* 2004, **279**: 52095-52105.

## Legend to figures

**Figure 1. Expression of different PDE isoforms in hearts and mitochondria.** (A) Expression of PDE 2A, 3A, 4A, 4B and 4D in hearts and isolated mitochondria by western-blot; heart homogenate (H), mitochondria (M). (B) PDE2A expression in mitochondria (M), mitoplast (MP) and post mitoplast (pMP). (C) Transmission electron microscopy analysis of PDE2A in mitochondria.

**Figure 2. cAMP-PDE activity in cardiac mitochondria.** (A, B) cAMP-PDEs activity was measured by radioenzymatic assay and defined as the fraction of total cAMP-PDE activity inhibited 100nM Bay 60-7550 (Bay), 1  $\mu$ M cilostamide(Cil) and Ro 20-1724 (Ro) in heart ventricle (A) and mitochondria (B) (n=3). (C) Mitochondrial cAMP levels measured by ELISA under basal condition or following stimulation of isolated mitochondria with bicarbonate (15 mM), inhibition of PDE2 with Bay, PDE3 with Cil and PDE4 with Ro (n=4). \* $P$ <0.05, \*\* $P$ <0.01, \*\*\* $P$ <0.001.

**Figure 3. Effect of PDEs inhibition on basal or  $\text{HCO}_3^-$  induced mitochondrial cAMP signal in neonatal cardiomyocytes.** Representative kinetics of percentage increase in CFP/YFP recorded in rat neonatal cardiomyocytes infected with 4mt-Epac-S<sup>H187</sup> exposed to 100 nM Bay (A), 1  $\mu$ M Cil (C) and 10 $\mu$ M Ro(E) in basal condition or following stimulation of  $\text{HCO}_3^-$ (B, D, F) (n=8-14).

**Figure 4. PDEs regulate  $\text{Ca}^{2+}$ -induced mitochondrial permeability transition (MPT)** (A) Evaluation of  $\Delta\Psi_m$  loss induced by calcium in mitochondria isolated from mice rats in response to PDE2, PDE3 and PDE4 inhibitions by specific inhibitors Bay, Cil and Ro under basal

condition or upon  $\text{HCO}_3^-$  stimulation. **(B)** Evaluation of mitochondrial swelling induced by calcium in response to PDE2, PDE3 and PDE4 inhibitions by specific inhibitors Bay, Cil and Ro under basal condition or upon  $\text{HCO}_3^-$  stimulation. **(C)** Half-time of  $\Delta\Psi_m$  loss induced by  $10\ \mu\text{M}\ \text{Ca}^{2+}$  calculated from A. **(D)** Half-time of swelling induced by  $10\ \mu\text{M}\ \text{Ca}^{2+}$  calculated from B. PDEs inhibitors have been used at the same concentrations as Figure 3.

**Figure 5. Bioenergetic analysis in isolated heart mitochondria from WT and TG mice.** **(A)** Western blot analysis of PDE2A expression in heart and mitochondria isolated from WT and TG mice.  $40\ \mu\text{g}$  of heart homogenate and mitochondria proteins from WT mice and  $4\ \mu\text{g}$  of heart homogenate and mitochondria proteins from TG mice were analyzed. **(B)** Expression level of PDE2 proteins relative to voltage-dependent anion channel (VDAC) in isolated mitochondria from WT and TG mice. **(C)** Representative graph of coupling assay of isolated mitochondria. Point-to-point oxygen consumption rate (OCR) data are shown with succinate as the substrate followed by addition of ADP, oligomycin, FCCP, and antimycin A. **(D)** Averaged metabolic profile calculated from panel (B).  $**P < 0.01$ ,  $***P < 0.001$  versus WT ( $n=3$ ).

**Figure 6. Effect of PDE2 on mitochondrial membrane potential loss and swelling induced by  $\text{Ca}^{2+}$  in PDE2 TG and WT mice.** **(A, C)** Evaluation of  $\Delta\Psi_m$  loss induced by  $\text{Ca}^{2+}$  in WT and TG cardiac isolated mitochondria in response to sAC stimulation by  $15\ \text{mM}\ \text{HCO}_3^-$  and sAC inhibition by  $25\ \mu\text{M}\ 2\text{HE}$  and PDE2A inhibition by  $100\ \text{nM}\ \text{Bay}$  at basal condition or following  $15\ \text{mM}\ \text{HCO}_3^-$  stimulation. **(B, D)** Evaluation of mitochondrial swelling induced by  $\text{Ca}^{2+}$  in WT and TG cardiac isolated mitochondria in response to sAC stimulation by  $15\ \text{mM}\ \text{HCO}_3^-$  and sAC inhibition by  $25\ \mu\text{M}\ 2\text{HE}$  and PDE2A inhibition by  $100\ \text{nM}\ \text{Bay}$  at basal condition or following  $15\ \text{mM}\ \text{HCO}_3^-$  stimulation. **(E)** Half-time of  $\Delta\Psi_m$  loss induced by  $10$

$\mu\text{M Ca}^{2+}$  calculated from A and C. **(F)** Half-time of swelling induced by  $10 \mu\text{M Ca}^{2+}$  calculated from B and D. \* $P < 0.05$ , \*\* $P < 0.01$ , \*\*\* $P < 0.001$  versus WT (n=4, 9 mice).

**Figure 7. Effect of PDE2 on mitochondrial  $\text{Ca}^{2+}$  accumulation in PDE2 TG and WT mice.**

**(A)** Evaluation of mitochondrial  $\text{Ca}^{2+}$  accumulation in mitochondria isolated from WT and TG mice in response to sAC stimulation by  $15 \text{ mM HCO}_3^-$  and sAC inhibition by  $25 \mu\text{M 2HE}$ . **(B)** Measurement of  $\text{Ca}^{2+}$  accumulation in response to PDE2A inhibition by  $100 \text{ nM Bay}$  at basal condition or following  $15 \text{ mM HCO}_3^-$  stimulation. **(C)** Half-time of  $\text{Ca}^{2+}$  accumulation calculated from A and B. \*\* $P < 0.01$  (n=3, 7 mice).

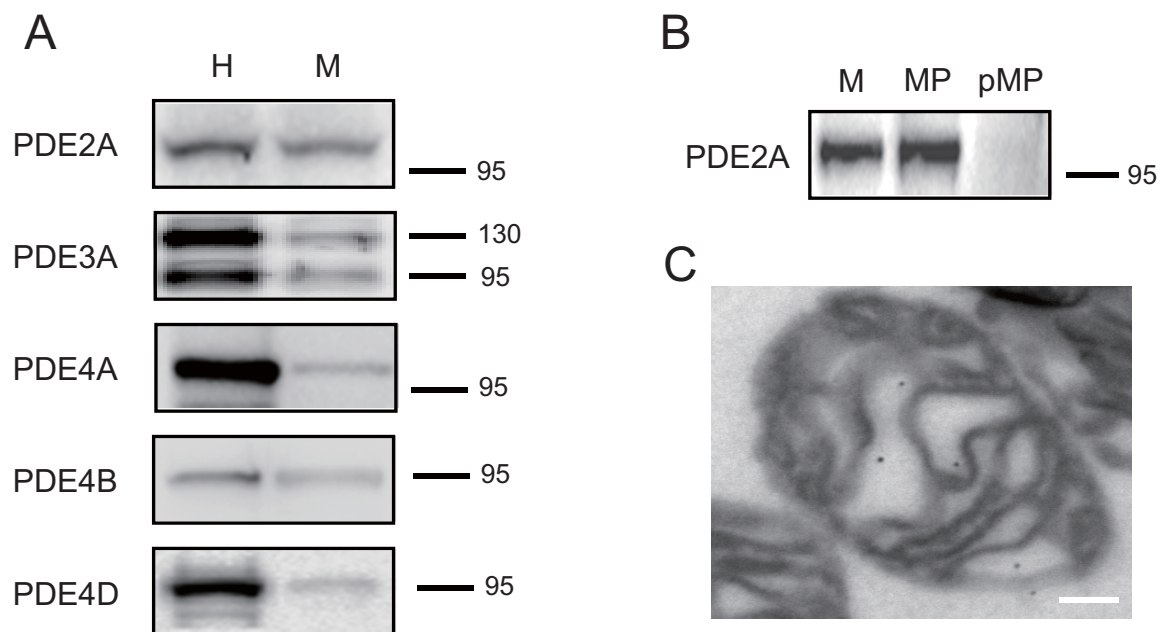


Fig. 1

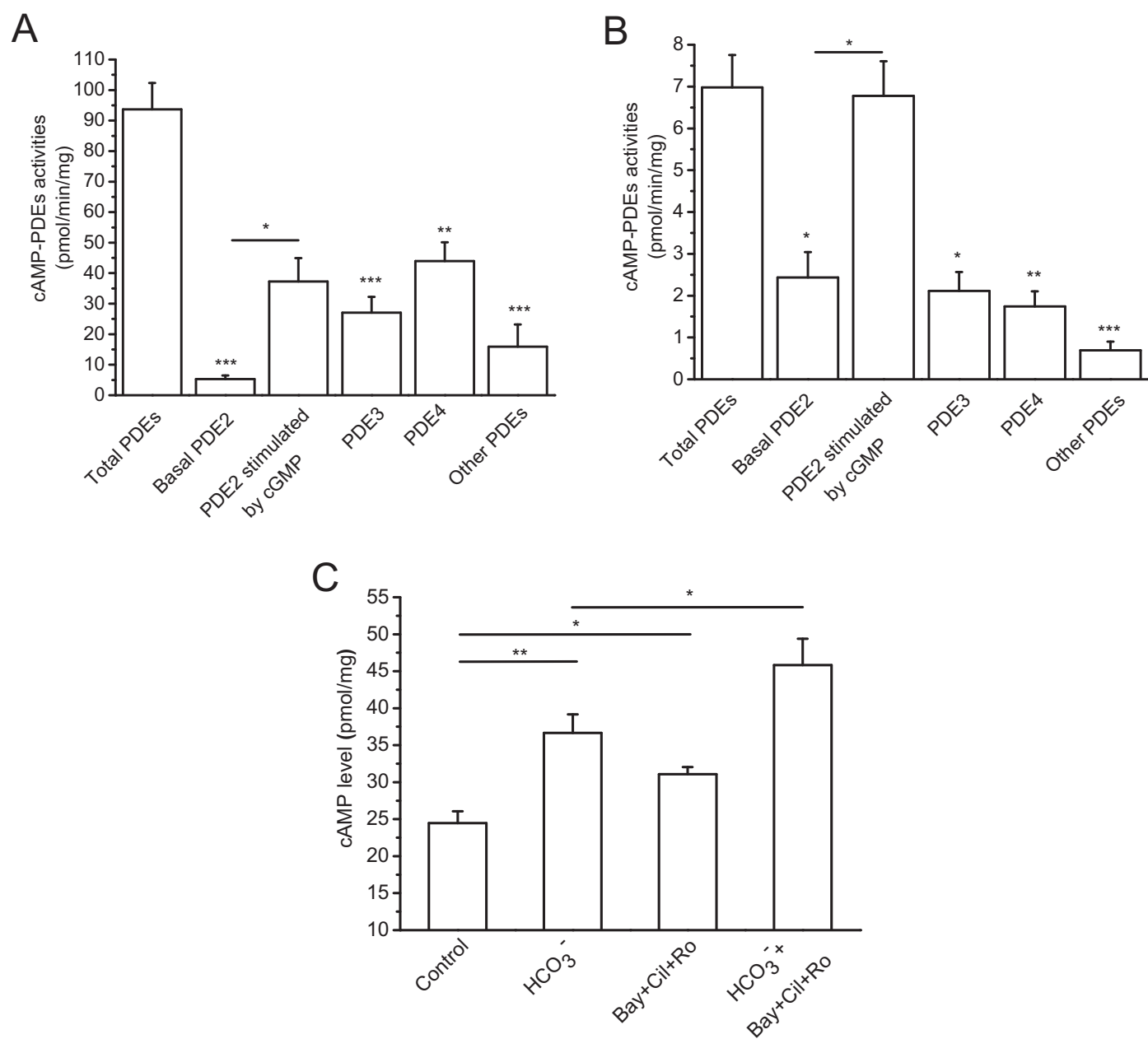


Fig. 2

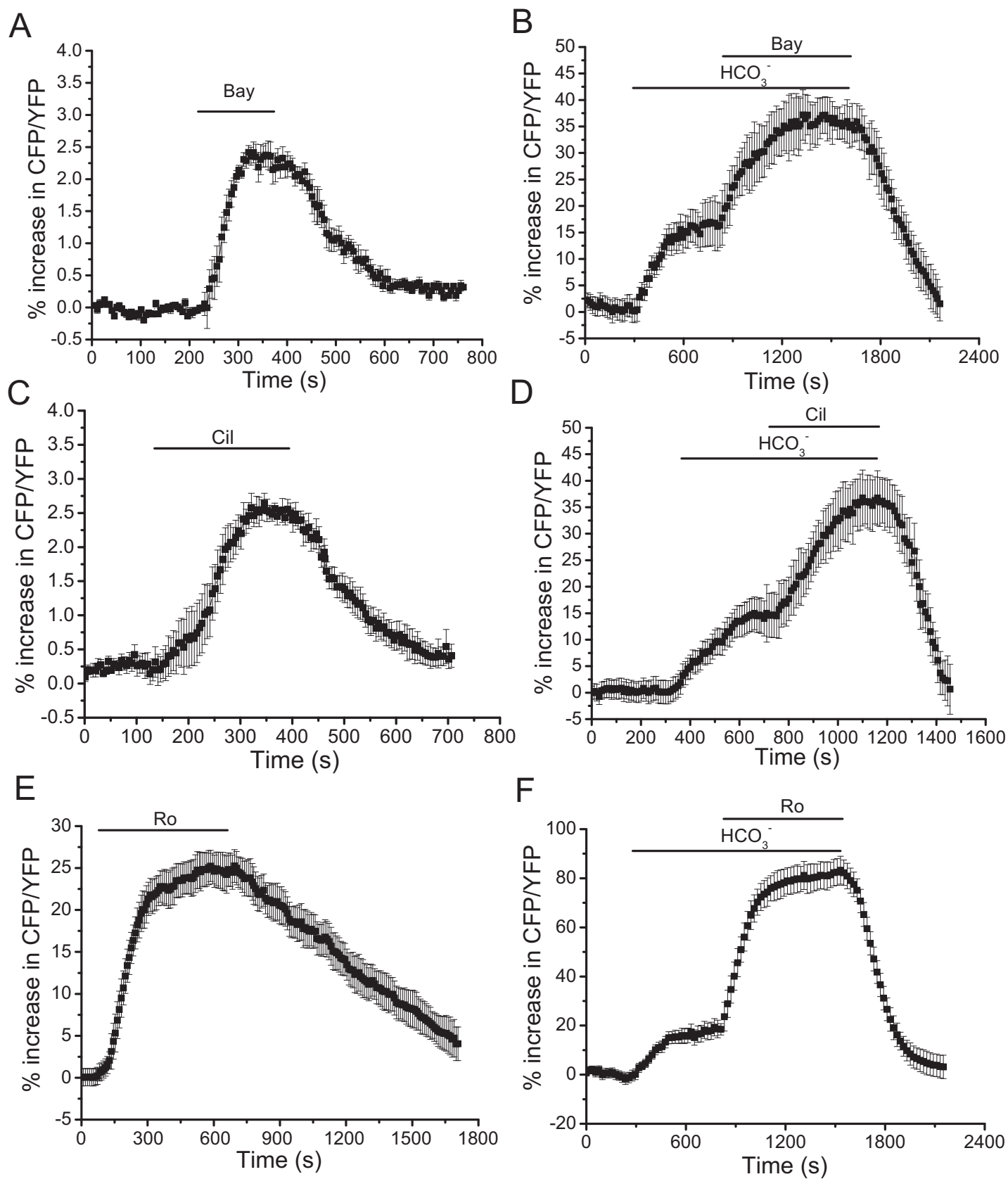


Fig. 3



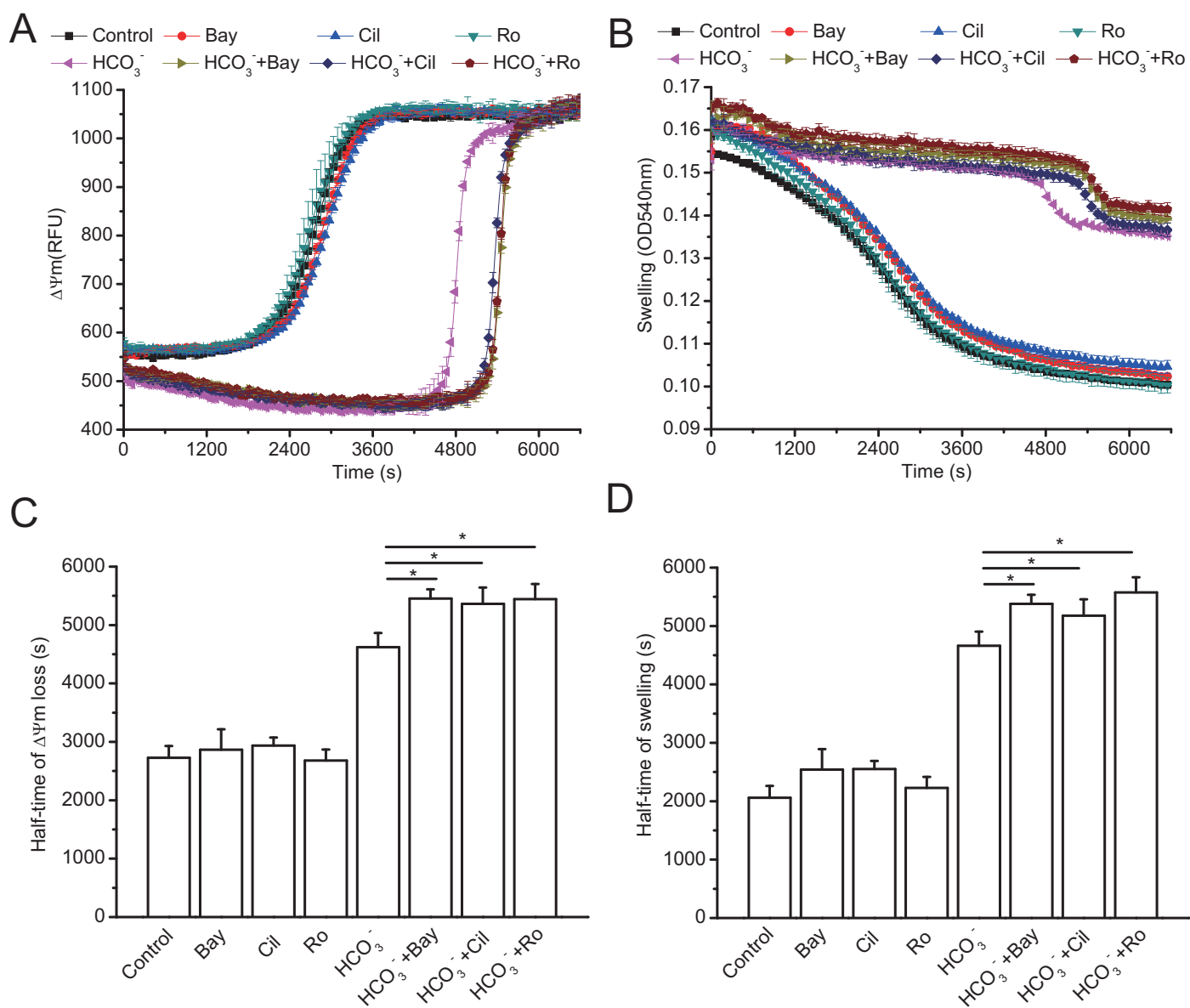


Fig. 4

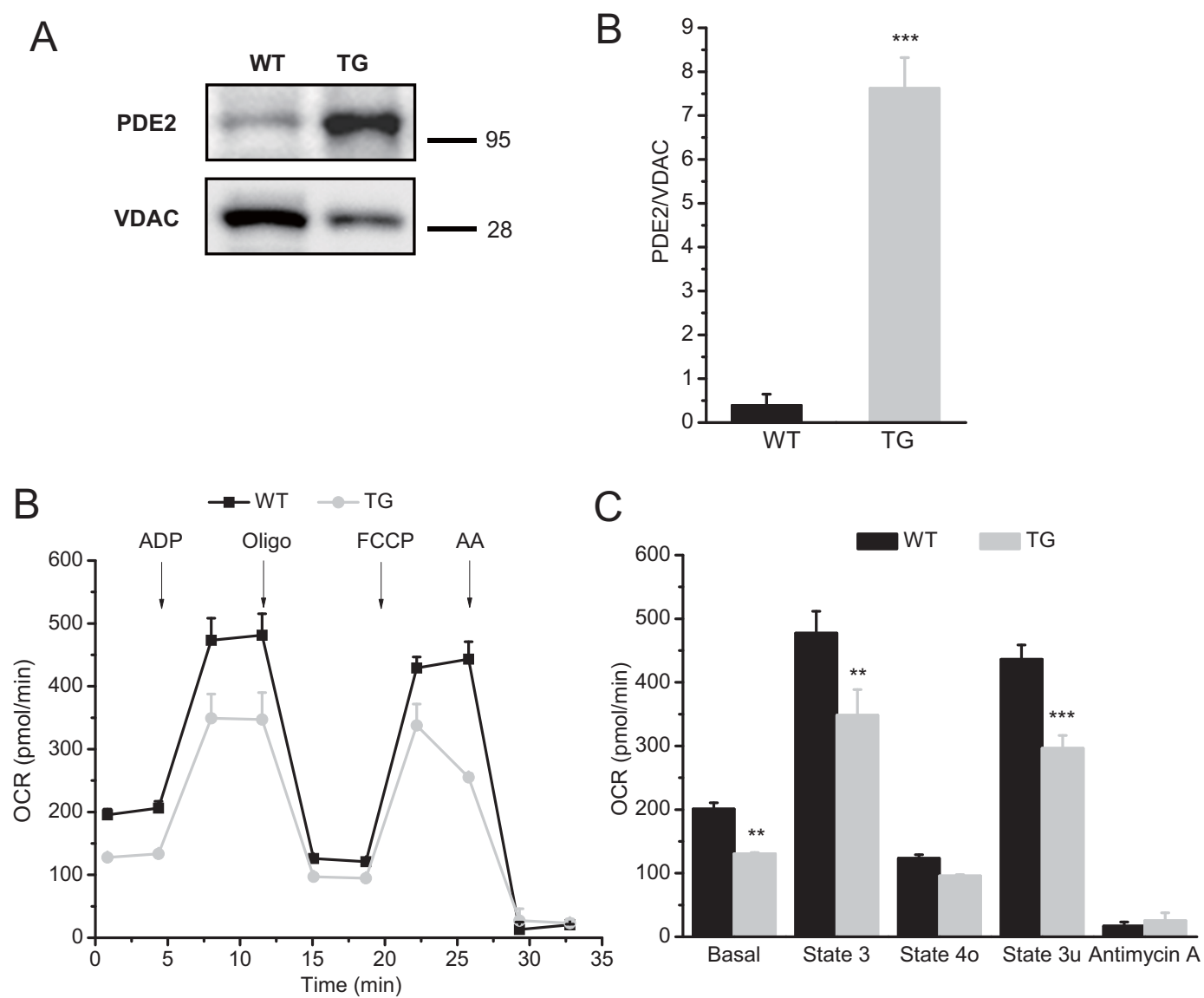


Fig. 5

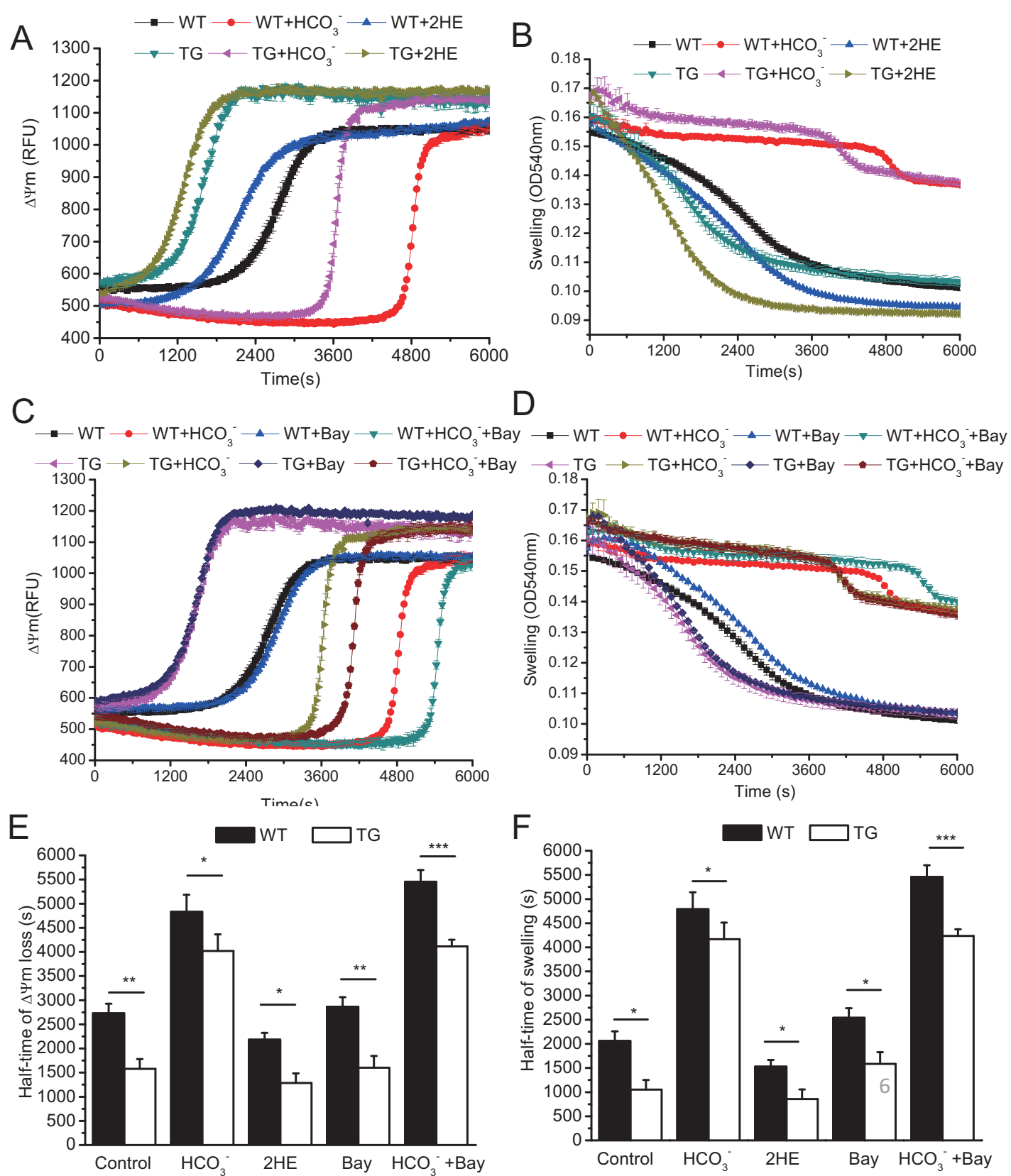


Fig. 6

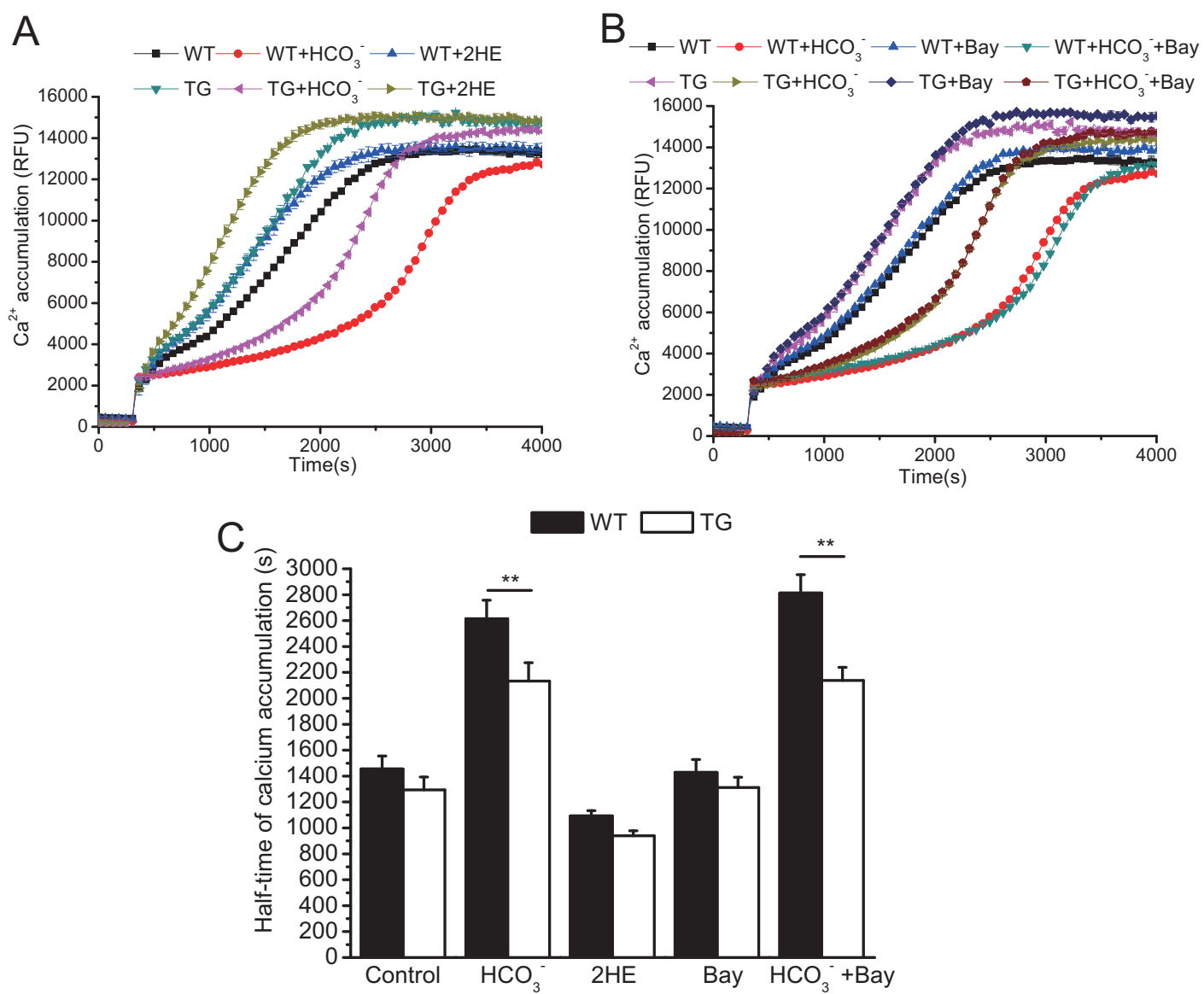


Fig. 7

# **Phosphodiesterases localized in cardiac mitochondria regulate mitochondrial cAMP and membrane potential**

**Wang Z et al**

## **PDEs expression in heart failure model**

To evaluate the expression level of different PDE isoforms in a pathological model, we induced HF in rats by transverse aortic constriction (TAC) during 22 weeks. As shown in Table 1, TAC rats showed a strong cardiac and lung hypertrophy, which are characteristic features of HF. Accordingly, cardiac function was diminished (not shown). Expression level of different PDEs was analyzed in heart ventricle homogenates and mitochondrial fraction by western-blot. As shown in Fig. 6A-B, PDE2A protein expression was not increased in heart homogenate and significantly increased in mitochondria. PDE4D protein expression was both significantly increased in homogenate and in mitochondria. PDE4A and PDE4B were significantly decreased in heart homogenate but did not change in mitochondria.

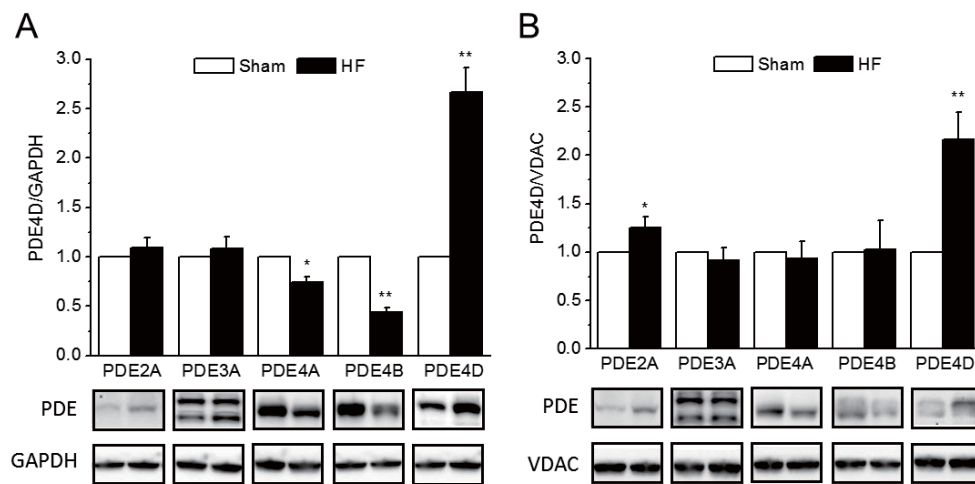


**Figure S1. Expression levels of different PDE isoforms in hearts and mitochondria isolated from Sham and HF rats**

(A) Expression level of different PDE isoforms in Sham (white bars) and heart failure (HF, black bars) heart homogenates (H) normalized by GAPDH. Representative Western blot images are shown on top (Sham on left and HF on right). (B) Expression level of different PDE isoforms relative to VDAC in isolated mitochondria (M) in HF versus Sham. Representative blots are shown on top (Sham on left and HF on right). Data are mean  $\pm$  SEM of 4 Sham and 4 HF rats, detected in four independent immunoblots. \* $P < 0.05$ , \*\* $P < 0.01$  versus Sham.

## 5 Discussion and perspectives

In the present study, we demonstrated that (i) a functional  $\text{HCO}_3^-$ -sAC-cAMP-Epac1 signaling cascade is contained within cardiac mitochondria, and (ii) this cAMP signaling pathway could be blunted by PDEs (PDE2A, PDE3A, PDE4A, PDE4B and PDE4D). We found that overexpression or activation of sAC could protect from regulated cell deaths, apoptosis as well as necrosis induced by  $\text{H}_2\text{O}_2$ , CPT and  $\text{TNF}\alpha$ /actinomycin D in primary cardiomyocytes. Moreover, cAMP produced within mitochondria in response to  $\text{HCO}_3^-$  and  $\text{Ca}^{2+}$  could stimulate oxygen consumption, ATP production and increase of mitochondrial membrane potential. cAMP could also protect the mitochondrial  $\text{Ca}^{2+}$  accumulation via, at least, two effectors, Epac1 and MCU, as a consequence, prevented MPT (Figure 22). We identified PDE2A, PDE3A, PDE4A, PDE4B and PDE4D in rat cardiac mitochondria. We found that these PDE isoforms could regulate mitochondrial cAMP level by radioenzymatic assay in cardiac mitochondrial lysates and by FRET in live neonatal cardiomyocyte. PDE2 represented 35% of total mitochondrial cAMP-PDE activity and its activity was enhanced ~3-fold by 5  $\mu\text{M}$  cGMP. PDE3 and PDE4 activities represented, respectively, 30% and 25% of total in mitochondria isolated from adult rat heart.

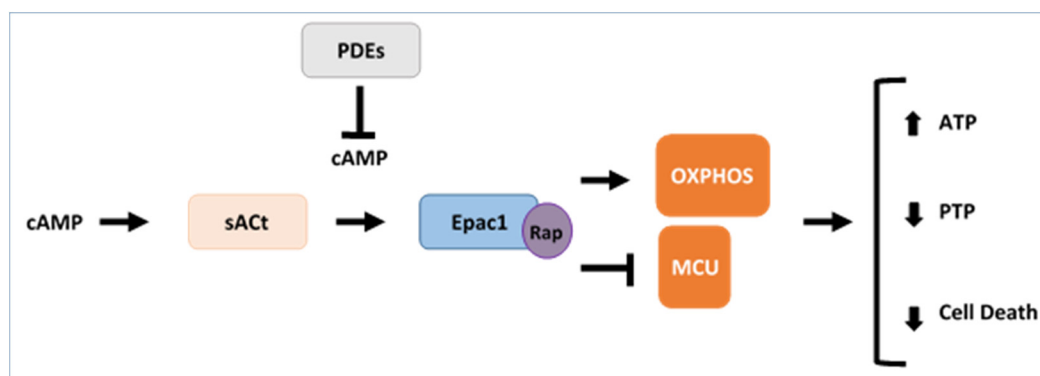


**Figure 22. Physiological roles of cAMP signalosome in cardiac mitochondria.** Epac1 participates to a cAMP signaling pathway into cardiac mitochondria, which can be activated by bicarbonate ( $\text{HCO}_3^-$ ) to decrease calcium ( $\text{Ca}^{2+}$ ) entry via the mitochondrial calcium uniporter (MCU) and increase oxidative phosphorylation (OXPHOS). Consequently, ATP level increases, the permeability transition pore (PTP) closes and cells resist to cell death.



It is known that sAC can be localized in mitochondria to produce cAMP in response to  $\text{HCO}_3^-$  and  $\text{Ca}^{2+}$ <sup>226</sup>. But little was known about its biological functions. We identified endogenous sAC in cardiac mitochondria and showed that it can produce cAMP in response to  $\text{HCO}_3^-$  and  $\text{Ca}^{2+}$  in isolated mitochondria and cardiomyocytes. Moreover, cAMP produced within mitochondria stimulated oxygen consumption, increased the  $\Delta\Psi_m$  and ATP production. Thus, our data are in good agreement with pioneer studies revealing the existence of a mitochondrial cAMP signaling in various cell types<sup>225,226</sup>. Based on our study,  $\text{HCO}_3^-$  was more potent than  $\text{Ca}^{2+}$ , which is in line with the fact that  $\text{HCO}_3^-$  and  $\text{Ca}^{2+}$  stimulatory effects are not redundant:  $\text{HCO}_3^-$  induces the active site closure, whereas  $\text{Ca}^{2+}$  increases ATP affinity<sup>225</sup>. Interestingly, 2HE can totally prevent the effect of  $\text{HCO}_3^-$ , indicating that maybe sAC is the unique source of cAMP in mitochondria and it is independent of pH.

$\text{Ca}^{2+}$  plays a major role in cell death regulation. Mitochondrial  $\text{Ca}^{2+}$  accumulation can trigger the opening of a high-conductance pore in the IM. This phenomenon is associated with drastic changes in mitochondrial morphology and functional activity<sup>38</sup>. We showed that increasing of cAMP by  $\text{HCO}_3^-$  could delay mitochondrial  $\Delta\Psi_m$  loss and swelling induced by  $\text{Ca}^{2+}$  in isolated mitochondria, suggesting that cAMP elevation confers a protection of mitochondria from  $\text{Ca}^{2+}$ -induced MPT. And this was confirmed in neonatal cardiomyocytes by silencing sAC with siRNA. It remains to determine the effect of cAMP on MPT in neonatal cardiomyocytes by overexpressing of sAC with adenovirus. And it will be also interesting to study this regulation in adult cardiomyocytes by silencing or overexpressing sAC.

Using modulation of sAC by genetic and pharmacological manipulations in primary cardiomyocytes, our study demonstrates for the first time that activation of the mitochondrial cAMP pathway exerts a protection of various cell deaths, apoptosis as well as necrosis. In contrast, inhibition of sAC by 2HE significantly increased the cell death. Thus, activation of mitochondrial cAMP pathway may preserve cardiomyocytes from death. In that respect, in a pathological rat model of HF induced by pressure overload, which goes along with strong cardiac hypertrophy, cardiac function alteration,

tissue remodeling, bioenergetics alterations and cardiomyocyte cell death<sup>378,385</sup>.  $\text{Ca}^{2+}$  induced a faster depolarization and  $\text{Ca}^{2+}$  uptake in HF than in sham mitochondria. In line with this,  $\text{Ca}^{2+}$  induced a faster mitochondrial swelling in HF than in sham mitochondria. We found that sAC was down regulated in mitochondria isolated from HF rat. This confirms that MPT is altered in HF, which could make mitochondria more vulnerable to  $\text{Ca}^{2+}$  overload<sup>386</sup>. Interestingly, mitochondria from HF rats still responded to  $\text{HCO}_3^-$  stimulation of mitochondrial cAMP production by sAC, by delaying  $\Delta\Psi_m$  loss,  $\text{Ca}^{2+}$  entry and MPT (i.e. matrix swelling). This opens some possibility to the definition of therapeutic strategies based on the stimulation of this local pathway to limit/prevent cell death in cardiac pathologies.

PKA is reported to localize in the mitochondrial matrix<sup>230-232</sup>, and is proposed to phosphorylate cytochrome c oxidase (COXIV-I) to enhance oxidative phosphorylation<sup>225</sup>. However, it has been also suggested that PKA activation inhibits OXPHOS<sup>235-237</sup>. Recently, Lefkimmatis et al found that the mitochondrial matrix of HEK and HeLa cells contains low or null PKA activity by using mitochondrial targeting FRET sensor<sup>227</sup>. And they also found that the OM is rich in PKA activity<sup>227</sup>. In our study, PKA was not involved in the mitochondrial cAMP effects by testing the effects of two different pharmacological PKA inhibitors, H89 and KT5720, on the induction of MPT by  $\text{Ca}^{2+}$ . Moreover, these inhibitors had no significant effect on  $\Delta\Psi_m$  and swelling, indicating that PKA may not be involved in MPT regulation. Thus, we focused our interest on Epac, because it emerged in the past decade as another important player in cAMP signaling<sup>387</sup>. Although Epac has been shown to be localized inside mitochondria by heterologous expression<sup>388</sup>. To our knowledge there has been no report on a role for this protein in mitochondrial function. Epac2-selective inhibitor ESI05 had no effect, the non-selective inhibitor ESI09 or the Epac1-selective inhibitor CE3F4 antagonized the induction of MPT by  $\text{Ca}^{2+}$ . This indicates that Epac1 but not Epac2 is involved in the regulation of MPT. We observed that inhibition of Epac1 decreased the oxygen consumption. These data thus point to Epac1 as a key effector in mitochondrial cAMP effects. The Epac1 silencing by siRNA indicated that a decreased level of Epac1

in neonatal cardiomyocytes decreased  $\Delta\Psi_m$  and in parallel accelerated the mitochondrial  $\text{Ca}^{2+}$  entry. In the heart, Epac1 was recently shown to be localized and functionally involved also in nuclear signalling, and regulates arrhythmogenic sarcoplasmic reticulum  $\text{Ca}^{2+}$  leak<sup>389</sup>. By  $\text{Ca}^{2+}$  accumulation measurement, we found that MCU is the major effector of Epac1 for the regulation of mitochondrial  $\text{Ca}^{2+}$  movements. Thus, we propose that activation of mitochondrial Epac1 protects the organelle from  $\text{Ca}^{2+}$  overload and from subsequent MPT via MCU modulation. In the future, it remains to determine the molecular composition and organization of the mitochondrial cAMP signalosome. Is Epac1 anchored to the IM? If yes, does it face the intermembrane space or the matrix? Is there one large polyprotein complex or several small complexes, which communicates in response to cAMP levels in the matrix? Are Rap proteins (e.g. Rap1 or 2) the small G proteins that mediate the effect of Epac1 (Figure 23): It is important to see whether other proteins make the link with MCU. Thus, several regulators of MCU, such as MICU1 and 2 could be also involved.

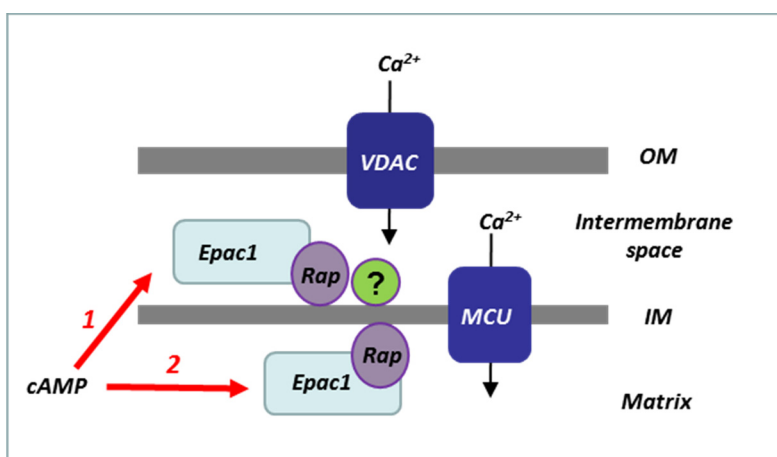


**Figure 23. Scheme of the location of actors of the mitochondrial cAMP pathway and their anchorage at the IM.** First hypothesis (“matrix-intermembrane space hypothesis”): cAMP is produced in the matrix, exported in the intermembrane space, where it can activate Epac1) and its GTPase rap or second hypothesis (“all in matrix”), cAMP is produced in the matrix and Epac1 and Rap are anchored in the inner membrane facing the matrix.

PDEs degrade cAMP and/or cGMP by hydrolysis of phosphodiester bonds. Thereby, they play important role in the regulation of a host of cellular functions involved in signal transduction and synaptic transmission by regulating intracellular levels of these ubiquitous second messengers<sup>262,390</sup>. Different PDE subtypes have been found in

subcellular compartement including nuclear, ER, SR and Golgi<sup>244</sup>. Until now, only PDE4 and PDE2 have been found in mitochondria<sup>374,391,392</sup>. Acin-Perez et al found that mitochondrial PDE2A is located in the matrix and that the unique N terminus of PDE2A isoform 2 specifically leads to mitochondrial localization of this isoform rodent liver and brain. PDE4B was reported to partially colocalize with DISC1 in the mitochondria of SH-SY5Y and LAN5 cells<sup>393</sup>. Asirvatham et al showed that mitochondrial AKAP149 bind to PKA and PDE4A comprising regulatory modules to maintain cAMP homeostasis in the T cell<sup>394</sup>. Here we identified that PDE2A, 3A, 4A, 4B and 4D were localized in mitochondria matrix from rat heart by detecting them in mitoplasts by western blot and in isolated mitochondria by immunolabelling and transmission electron microscopy.

In isolated rat heart mitochondria, we showed that PDE2 represented 35% of total cAMP-PDE activity, followed by PDE3 and PDE4 which represented 30% and 25% of total respectively. In line with our study, Acin-Perez et al showed that PDE2A was present in brain and liver mitochondrial fractions and to be responsible for cAMP-PDE activity<sup>391</sup>. However, in neonatal cardiomyocytes infected with 4mt-Epac-S<sup>H187</sup>, inhibition of PDE2 and 3 caused a very small increase in cAMP but inhibition of PDE4 resulted in 25% increase in basal condition. And upon HCO<sub>3</sub><sup>-</sup> stimulation, inhibition of PDE2 and 3 caused 40% and inhibition of PDE4 reached to 80%. This is not consistent with PDE activity in isolated mitochondria from adult rat heart. But it is similar to PDE3 and PDE4 inhibition in neonatal cardiomyocytes<sup>395</sup>. This revealed a difference in PDE2 activity in isolated mitochondria from adult rat heart and in neonatal cardiomyocytes, which is not observed for PDE3 and PDE4.

We showed that cAMP produced with mitochondria regulates Ca<sup>2+</sup> accumulation and permeability transition. Consistent with this, Acin-Perez reported that inhibition of PDE2 caused an increase in oxygen consumption and ATP production in mouse brain mitochondria. Here, we showed mitochondria isolated from PDE2 TG mice had a lower oxygen consumption rate than WT mice. We also found that upon HCO<sub>3</sub><sup>-</sup> stimulation, inhibition of PDE2, PDE3 and PDE4 delayed  $\Delta\Psi_m$  loss and swelling induced by Ca<sup>2+</sup>.

Moreover, mitochondria isolated from PDE2 TG mice showed a faster  $\Delta\Psi_m$  loss and swelling compared to mitochondria isolated from WT mice. These results indicate that PDEs forms a local a mitochondrial signalling pathway with sAC to regulate mitochondrial  $\text{Ca}^{2+}$  accumulation and permeability transition. Moreover, these results raise important questions regarding the association of PDEs /or with other proteins within soluble partners in the matrix and/or IM proteins. It has been shown that PDE4-small heat-shock protein 20 complex promotes Ser phosphorylation to trigger its cardioprotective actions<sup>396</sup> and PDE4A bind to mitochondrial AKAP149 to maintain cAMP homeostasis in the T cell<sup>397</sup>. Thus it would be interesting to identify the interactome of mitochondrial PDEs to better understand the local signalization.

## 6 References

- 1 Sherratt, H. S. A. Mitochondria - Structure and Function. *Rev Neurol* **147**, 417-430 (1991).
- 2 Forbes, J. M. & Cooper, M. E. Mechanisms of diabetic complications. *Physiological reviews* **93**, 137-188, doi:10.1152/physrev.00045.2011 (2013).
- 3 White, R. L. & Wittenberg, B. A. Mitochondrial NAD(P)H, ADP, oxidative phosphorylation, and contraction in isolated heart cells. *American journal of physiology. Heart and circulatory physiology* **279**, H1849-1857 (2000).
- 4 Gautheron, D. C. Mitochondrial oxidative phosphorylation and respiratory chain: review. *Journal of inherited metabolic disease* **7 Suppl 1**, 57-61 (1984).
- 5 Kholodenko, B. N. Control of mitochondrial oxidative phosphorylation. *Journal of theoretical biology* **107**, 179-188 (1984).
- 6 Nicholls, D. G. Forty years of Mitchell's proton circuit: From little grey books to little grey cells. *Biochimica et biophysica acta* **1777**, 550-556, doi:10.1016/j.bbabi.2008.03.014 (2008).
- 7 Nicholls, D. G. Mitochondrial membrane potential and aging. *Aging cell* **3**, 35-40 (2004).
- 8 Brownlee, M. Biochemistry and molecular cell biology of diabetic complications. *Nature* **414**, 813-820, doi:10.1038/414813a (2001).
- 9 Rizzuto, R., De Stefani, D., Raffaello, A. & Mammucari, C. Mitochondria as sensors and regulators of calcium signalling. *Nat Rev Mol Cell Bio* **13**, 566-578, doi:10.1038/nrm3412 (2012).
- 10 Arnandis, T. *et al.* Calpains mediate epithelial-cell death during mammary gland involution: mitochondria and lysosomal destabilization. *Cell death and differentiation* **19**, 1536-1548, doi:10.1038/cdd.2012.46 (2012).
- 11 Ulivieri, C. Cell death: insights into the ultrastructure of mitochondria. *Tissue & cell* **42**, 339-347, doi:10.1016/j.tice.2010.10.004 (2010).
- 12 Contreras, L., Drago, I., Zampese, E. & Pozzan, T. Mitochondria: the calcium connection. *Biochimica et biophysica acta* **1797**, 607-618, doi:10.1016/j.bbabi.2010.05.005 (2010).
- 13 J, O. U., Pan, S. & Sheu, S. S. Perspectives on: SGP symposium on mitochondrial physiology and medicine: molecular identities of mitochondrial

- Ca<sup>2+</sup> influx mechanism: updated passwords for accessing mitochondrial Ca<sup>2+</sup>-linked health and disease. *The Journal of general physiology* **139**, 435-443, doi:10.1085/jgp.201210795 (2012).
- 14 Baumgartner, H. K. *et al.* Calcium elevation in mitochondria is the main Ca<sup>2+</sup> requirement for mitochondrial permeability transition pore (mPTP) opening. *The Journal of biological chemistry* **284**, 20796-20803, doi:10.1074/jbc.M109.025353 (2009).
  - 15 De Stefani, D., Raffaello, A., Teardo, E., Szabo, I. & Rizzuto, R. A forty-kilodalton protein of the inner membrane is the mitochondrial calcium uniporter. *Nature* **476**, 336-340, doi:10.1038/nature10230 (2011).
  - 16 Santo-Domingo, J. & Demaurex, N. Calcium uptake mechanisms of mitochondria. *Biochimica et biophysica acta* **1797**, 907-912, doi:10.1016/j.bbabbio.2010.01.005 (2010).
  - 17 Luongo, T. S. *et al.* The Mitochondrial Calcium Uniporter Matches Energetic Supply with Cardiac Workload during Stress and Modulates Permeability Transition. *Cell reports* **12**, 23-34, doi:10.1016/j.celrep.2015.06.017 (2015).
  - 18 Bazil, J. N. & Dash, R. K. A minimal model for the mitochondrial rapid mode of Ca<sup>2+</sup> uptake mechanism. *PloS one* **6**, e21324, doi:10.1371/journal.pone.0021324 (2011).
  - 19 Palty, R. *et al.* NCLX is an essential component of mitochondrial Na<sup>+</sup>/Ca<sup>2+</sup> exchange. *Proceedings of the National Academy of Sciences of the United States of America* **107**, 436-441, doi:10.1073/pnas.0908099107 (2010).
  - 20 Halliwell, B. & Gutteridge, J. M. Oxygen free radicals and iron in relation to biology and medicine: some problems and concepts. *Archives of biochemistry and biophysics* **246**, 501-514 (1986).
  - 21 Aruoma, O. I., Grootveld, M. & Bahorun, T. Free radicals in biology and medicine: from inflammation to biotechnology. *BioFactors* **27**, 1-3 (2006).
  - 22 Todd, K., Ghiso, J. & Rostagno, A. Oxidative stress and mitochondria-mediated cell death mechanisms triggered by the familial Danish dementia ADan amyloid. *Neurobiology of disease* **85**, 130-143, doi:10.1016/j.nbd.2015.10.003 (2016).
  - 23 Jaeschke, H., McGill, M. R. & Ramachandran, A. Oxidant stress, mitochondria, and cell death mechanisms in drug-induced liver injury: lessons learned from acetaminophen hepatotoxicity. *Drug metabolism reviews* **44**, 88-106, doi:10.3109/03602532.2011.602688 (2012).



- 24 Bayir, H. & Kagan, V. E. Bench-to-bedside review: Mitochondrial injury, oxidative stress and apoptosis--there is nothing more practical than a good theory. *Critical care* **12**, 206, doi:10.1186/cc6779 (2008).
- 25 Halestrap, A. P., Doran, E., Gillespie, J. P. & O'Toole, A. Mitochondria and cell death. *Biochemical Society transactions* **28**, 170-177 (2000).
- 26 Halestrap, A. P., Gillespie, J. P., O'Toole, A. & Doran, E. Mitochondria and cell death: a pore way to die? *Symposia of the Society for Experimental Biology* **52**, 65-80 (2000).
- 27 Kroemer, G. & Reed, J. C. Mitochondrial control of cell death. *Nat Med* **6**, 513-519, doi:10.1038/74994 (2000).
- 28 Labedzka, K., Grzanka, A. & Izdebska, M. [Mitochondria and cell death]. *Postepy higieny i medycyny doswiadczalnej* **60**, 439-446 (2006).
- 29 Piantadosi, C. A. & Suliman, H. B. Redox regulation of mitochondrial biogenesis. *Free Radical Bio Med* **53**, 2043-2053, doi:10.1016/j.freeradbiomed.2012.09.014 (2012).
- 30 Ohlmeier, S., Hiltunen, J. K. & Bergmann, U. Protein phosphorylation in mitochondria - A study on fermentative and respiratory growth of *Saccharomyces cerevisiae*. *Electrophoresis* **31**, 2869-2881, doi:10.1002/elps.200900759 (2010).
- 31 Anderson, K. A. & Hirschey, M. D. Mitochondrial protein acetylation regulates metabolism. *Lysine-Based Post-Translational Modification of Proteins* **52**, 23-35, doi:10.1042/Bse0520023 (2012).
- 32 Wang, F. *et al.* Phosphorylation and ubiquitination of dynamin-related proteins (AtDRP3A/3B) synergically regulate mitochondrial proliferation during mitosis. *Plant Journal* **72**, 43-56, doi:10.1111/j.1365-313X.2012.05052.x (2012).
- 33 Huang, W. *et al.* Reactive oxygen species burst induced by aluminum stress triggers mitochondria-dependent programmed cell death in peanut root tip cells. *Plant physiology and biochemistry : PPB / Societe francaise de physiologie vegetale* **82**, 76-84, doi:10.1016/j.plaphy.2014.03.037 (2014).
- 34 Perez-Ortiz, J. M., Tranque, P., Burgos, M., Vaquero, C. F. & Llopis, J. Glitazones induce astrogloma cell death by releasing reactive oxygen species from mitochondria: modulation of cytotoxicity by nitric oxide. *Molecular pharmacology* **72**, 407-417, doi:10.1124/mol.106.032458 (2007).

- 35 Orrenius, S. Reactive oxygen species in mitochondria-mediated cell death. *Drug metabolism reviews* **39**, 443-455, doi:10.1080/03602530701468516 (2007).
- 36 Bains, S. K. *et al.* Mitochondria control of cell death induced by anti-HLA-DR antibodies. *Leukemia* **17**, 1357-1365, doi:10.1038/sj.leu.2402976 (2003).
- 37 Jing, L. *et al.* Coenzyme Q10 protects astrocytes from ROS-induced damage through inhibition of mitochondria-mediated cell death pathway. *International journal of biological sciences* **11**, 59-66, doi:10.7150/ijbs.10174 (2015).
- 38 Orrenius, S., Gogvadze, V. & Zhivotovsky, B. Calcium and mitochondria in the regulation of cell death. *Biochemical and biophysical research communications* **460**, 72-81, doi:10.1016/j.bbrc.2015.01.137 (2015).
- 39 Santulli, G., Xie, W. J., Reiken, S. R. & Marks, A. R. Mitochondrial calcium overload is a key determinant in heart failure. *Proceedings of the National Academy of Sciences of the United States of America* **112**, 11389-11394, doi:10.1073/pnas.1513047112 (2015).
- 40 Haworth, R. A. & Hunter, D. R. The Ca<sup>2+</sup>-induced membrane transition in mitochondria. II. Nature of the Ca<sup>2+</sup> trigger site. *Archives of biochemistry and biophysics* **195**, 460-467 (1979).
- 41 Hunter, D. R. & Haworth, R. A. The Ca<sup>2+</sup>-induced membrane transition in mitochondria. I. The protective mechanisms. *Archives of biochemistry and biophysics* **195**, 453-459 (1979).
- 42 Hunter, D. R. & Haworth, R. A. The Ca<sup>2+</sup>-induced membrane transition in mitochondria. III. Transitional Ca<sup>2+</sup> release. *Archives of biochemistry and biophysics* **195**, 468-477 (1979).
- 43 Halestrap, A. P., Clarke, S. J. & Javadov, S. A. Mitochondrial permeability transition pore opening during myocardial reperfusion--a target for cardioprotection. *Cardiovascular research* **61**, 372-385, doi:10.1016/S0008-6363(03)00533-9 (2004).
- 44 Crompton, M., Virji, S. & Ward, J. M. Cyclophilin-D binds strongly to complexes of the voltage-dependent anion channel and the adenine nucleotide translocase to form the permeability transition pore. *European journal of biochemistry / FEBS* **258**, 729-735 (1998).
- 45 Giorgio, V. *et al.* Dimers of mitochondrial ATP synthase form the permeability transition pore. *Proceedings of the National Academy of Sciences of the United States of America* **110**, 5887-5892, doi:10.1073/pnas.1217823110 (2013).

- 46 Kwong, J. Q. & Molkentin, J. D. Physiological and pathological roles of the mitochondrial permeability transition pore in the heart. *Cell metabolism* **21**, 206-214, doi:10.1016/j.cmet.2014.12.001 (2015).
- 47 Leung, A. W., Varanyuwatana, P. & Halestrap, A. P. The mitochondrial phosphate carrier interacts with cyclophilin D and may play a key role in the permeability transition. *The Journal of biological chemistry* **283**, 26312-26323, doi:10.1074/jbc.M805235200 (2008).
- 48 Izzo, V., Bravo-San Pedro, J. M., Sica, V., Kroemer, G. & Galluzzi, L. Mitochondrial Permeability Transition: New Findings and Persisting Uncertainties. *Trends in cell biology*, doi:10.1016/j.tcb.2016.04.006 (2016).
- 49 Kroemer, G., Galluzzi, L. & Brenner, C. Mitochondrial membrane permeabilization in cell death. *Physiological reviews* **87**, 99-163, doi:10.1152/physrev.00013.2006 (2007).
- 50 Tait, S. W. & Green, D. R. Mitochondria and cell death: outer membrane permeabilization and beyond. *Nature reviews. Molecular cell biology* **11**, 621-632, doi:10.1038/nrm2952 (2010).
- 51 Golstein, P. & Kroemer, G. Cell death by necrosis: towards a molecular definition. *Trends in biochemical sciences* **32**, 37-43, doi:10.1016/j.tibs.2006.11.001 (2007).
- 52 Rosca, M. G. & Hoppel, C. L. Mitochondria in heart failure. *Cardiovascular research* **88**, 40-50, doi:10.1093/cvr/cvq240 (2010).
- 53 Murray, A. J., Edwards, L. M. & Clarke, K. Mitochondria and heart failure. *Current opinion in clinical nutrition and metabolic care* **10**, 704-711, doi:10.1097/MCO.0b013e3282f0ecbe (2007).
- 54 Ingwall, J. S. Energy metabolism in heart failure and remodelling. *Cardiovascular research* **81**, 412-419, doi:10.1093/cvr/cvn301 (2009).
- 55 Neubauer, S. The failing heart--an engine out of fuel. *The New England journal of medicine* **356**, 1140-1151, doi:10.1056/NEJMra063052 (2007).
- 56 Beer, M. *et al.* Absolute concentrations of high-energy phosphate metabolites in normal, hypertrophied, and failing human myocardium measured noninvasively with P-31-SLOOP magnetic resonance spectroscopy. *Journal of the American College of Cardiology* **40**, 1267-1274, doi:Pii S0735-1097(02)02160-5

Doi 10.1016/S0735-1097(02)02160-5 (2002).

- 57 Sanbe, A., Tanonaka, K., Kobayasi, R. & Takeo, S. Effects of long-term therapy with ACE inhibitors, captopril, enalapril andtrandolapril, on myocardial energy metabolism in rats with heart failure following myocardial infarction. *Journal of molecular and cellular cardiology* **27**, 2209-2222 (1995).
- 58 Shen, W. *et al.* Progressive loss of myocardial ATP due to a loss of total purines during the development of heart failure in dogs: a compensatory role for the parallel loss of creatine. *Circulation* **100**, 2113-2118 (1999).
- 59 Sabbah, H. N. *et al.* Mitochondrial abnormalities in myocardium of dogs with chronic heart failure. *Journal of molecular and cellular cardiology* **24**, 1333-1347 (1992).
- 60 McCutcheon, L. J. *et al.* Respiratory chain defect of myocardial mitochondria in idiopathic dilated cardiomyopathy of Doberman pinscher dogs. *Canadian journal of physiology and pharmacology* **70**, 1529-1533 (1992).
- 61 Rosca, M. G. *et al.* Altered expression of the adenine nucleotide translocase isoforms and decreased ATP synthase activity in skeletal muscle mitochondria in heart failure. *Journal of molecular and cellular cardiology* **46**, 927-935, doi:10.1016/j.yjmcc.2009.02.009 (2009).
- 62 Wang, W. *et al.* Superoxide flashes in single mitochondria. *Cell* **134**, 279-290, doi:10.1016/j.cell.2008.06.017 (2008).
- 63 Ide, T. *et al.* Mitochondrial electron transport complex I is a potential source of oxygen free radicals in the failing myocardium. *Circulation research* **85**, 357-363 (1999).
- 64 Davidson, S. M. Endothelial mitochondria and heart disease. *Cardiovascular research* **88**, 58-66, doi:10.1093/cvr/cvq195 (2010).
- 65 Ajith, T. A. & Jayakumar, T. G. Mitochondria-targeted agents: Future perspectives of mitochondrial pharmaceuticals in cardiovascular diseases. *World journal of cardiology* **6**, 1091-1099, doi:10.4330/wjc.v6.i10.1091 (2014).
- 66 Ide, T. *et al.* Mitochondrial DNA damage and dysfunction associated with oxidative stress in failing hearts after myocardial infarction. *Circulation research* **88**, 529-535 (2001).
- 67 Tsutsui, H., Kinugawa, S. & Matsushima, S. Oxidative stress and mitochondrial DNA damage in heart failure. *Circulation journal : official journal of the Japanese Circulation Society* **72 Suppl A**, A31-37 (2008).

- 68 Luo, M. & Anderson, M. E. Mechanisms of altered Ca<sup>2+</sup> handling in heart failure. *Circulation research* **113**, 690-708, doi:10.1161/CIRCRESAHA.113.301651 (2013).
- 69 Ott, M., Robertson, J. D., Gogvadze, V., Zhivotovsky, B. & Orrenius, S. Cytochrome c release from mitochondria proceeds by a two-step process. *Proceedings of the National Academy of Sciences of the United States of America* **99**, 1259-1263, doi:10.1073/pnas.241655498 (2002).
- 70 Nakayama, H. *et al.* Ca<sup>2+</sup>- and mitochondrial-dependent cardiomyocyte necrosis as a primary mediator of heart failure. *The Journal of clinical investigation* **117**, 2431-2444, doi:10.1172/JCI31060 (2007).
- 71 Houser, S. R., Piacentino, V., 3rd & Weisser, J. Abnormalities of calcium cycling in the hypertrophied and failing heart. *Journal of molecular and cellular cardiology* **32**, 1595-1607, doi:10.1006/jmcc.2000.1206 (2000).
- 72 Halestrap, A. P. Calcium, mitochondria and reperfusion injury: a pore way to die. *Biochemical Society transactions* **34**, 232-237, doi:10.1042/BST20060232 (2006).
- 73 Territo, P. R., Mootha, V. K., French, S. A. & Balaban, R. S. Ca<sup>2+</sup> activation of heart mitochondrial oxidative phosphorylation: role of the F<sub>0</sub>/F<sub>1</sub>-ATPase. *American journal of physiology. Cell physiology* **278**, C423-435 (2000).
- 74 Gunter, T. E., Buntinas, L., Sparagna, G., Eliseev, R. & Gunter, K. Mitochondrial calcium transport: mechanisms and functions. *Cell calcium* **28**, 285-296, doi:10.1054/ceca.2000.0168 (2000).
- 75 Liu, T. & O'Rourke, B. Enhancing mitochondrial Ca<sup>2+</sup> uptake in myocytes from failing hearts restores energy supply and demand matching. *Circulation research* **103**, 279-288, doi:10.1161/CIRCRESAHA.108.175919 (2008).
- 76 Griffiths, E. J. *et al.* Mitochondrial calcium transporting pathways during hypoxia and reoxygenation in single rat cardiomyocytes. *Cardiovascular research* **39**, 423-433 (1998).
- 77 Murata, M., Akao, M., O'Rourke, B. & Marban, E. Mitochondrial ATP-sensitive potassium channels attenuate matrix Ca<sup>2+</sup> overload during simulated ischemia and reperfusion: possible mechanism of cardioprotection. *Circulation research* **89**, 891-898 (2001).
- 78 Namekata, I., Shimada, H., Kawanishi, T., Tanaka, H. & Shigenobu, K. Reduction by SEA0400 of myocardial ischemia-induced cytoplasmic and

- mitochondrial Ca<sup>2+</sup> overload. *European journal of pharmacology* **543**, 108-115, doi:10.1016/j.ejphar.2006.06.012 (2006).
- 79 Ruiz-Meana, M., Garcia-Dorado, D., Miro-Casas, E., Abellan, A. & Soler-Soler, J. Mitochondrial Ca<sup>2+</sup> uptake during simulated ischemia does not affect permeability transition pore opening upon simulated reperfusion. *Cardiovascular research* **71**, 715-724, doi:10.1016/j.cardiores.2006.06.019 (2006).
  - 80 Garcia-Rivas Gde, J., Carvajal, K., Correa, F. & Zazueta, C. Ru360, a specific mitochondrial calcium uptake inhibitor, improves cardiac post-ischaemic functional recovery in rats in vivo. *British journal of pharmacology* **149**, 829-837, doi:10.1038/sj.bjp.0706932 (2006).
  - 81 Michels, G. *et al.* Regulation of the human cardiac mitochondrial Ca<sup>2+</sup> uptake by 2 different voltage-gated Ca<sup>2+</sup> channels. *Circulation* **119**, 2435-2443, doi:10.1161/CIRCULATIONAHA.108.835389 (2009).
  - 82 Sharov, V. G., Todor, A. V., Imai, M. & Sabbah, H. N. Inhibition of mitochondrial permeability transition pores by cyclosporine A improves cytochrome C oxidase function and increases rate of ATP synthesis in failing cardiomyocytes. *Heart failure reviews* **10**, 305-310, doi:10.1007/s10741-005-7545-1 (2005).
  - 83 Javadov, S., Huang, C., Kirshenbaum, L. & Karmazyn, M. NHE-1 inhibition improves impaired mitochondrial permeability transition and respiratory function during postinfarction remodelling in the rat. *Journal of molecular and cellular cardiology* **38**, 135-143, doi:10.1016/j.yjmcc.2004.10.007 (2005).
  - 84 Sharov, V. G., Todor, A., Khanal, S., Imai, M. & Sabbah, H. N. Cyclosporine A attenuates mitochondrial permeability transition and improves mitochondrial respiratory function in cardiomyocytes isolated from dogs with heart failure. *Journal of molecular and cellular cardiology* **42**, 150-158, doi:10.1016/j.yjmcc.2006.09.013 (2007).
  - 85 Nakayama, H. *et al.* Ca<sup>2+</sup>- and mitochondrial-dependent cardiomyocyte necrosis as a primary mediator of heart failure. *Journal of Clinical Investigation* **117**, 2431-2444, doi:10.1172/JC131060 (2007).
  - 86 Oliveira, P. J. *et al.* Enhanced permeability transition explains the reduced calcium uptake in cardiac mitochondria from streptozotocin-induced diabetic rats. *FEBS letters* **554**, 511-514 (2003).



- 87 Griffiths, E. J. & Halestrap, A. P. Mitochondrial non-specific pores remain closed during cardiac ischaemia, but open upon reperfusion. *The Biochemical journal* **307** ( Pt 1), 93-98 (1995).
- 88 Kerr, P. M., Suleiman, M. S. & Halestrap, A. P. Reversal of permeability transition during recovery of hearts from ischemia and its enhancement by pyruvate. *The American journal of physiology* **276**, H496-502 (1999).
- 89 Javadov, S. A. *et al.* Ischaemic preconditioning inhibits opening of mitochondrial permeability transition pores in the reperfused rat heart. *The Journal of physiology* **549**, 513-524, doi:10.1113/jphysiol.2003.034231 (2003).
- 90 Crompton, M., Barksby, E., Johnson, N. & Capano, M. Mitochondrial intermembrane junctional complexes and their involvement in cell death. *Biochimie* **84**, 143-152 (2002).
- 91 Baines, C. P. *et al.* Loss of cyclophilin D reveals a critical role for mitochondrial permeability transition in cell death. *Nature* **434**, 658-662, doi:10.1038/nature03434 (2005).
- 92 Nakagawa, T. *et al.* Cyclophilin D-dependent mitochondrial permeability transition regulates some necrotic but not apoptotic cell death. *Nature* **434**, 652-658, doi:10.1038/nature03317 (2005).
- 93 Piot, C. *et al.* Effect of cyclosporine on reperfusion injury in acute myocardial infarction. *The New England journal of medicine* **359**, 473-481, doi:10.1056/NEJMoa071142 (2008).
- 94 Griffiths, E. J., Ocampo, C. J., Savage, J. S., Stern, M. D. & Silverman, H. S. Protective effects of low and high doses of cyclosporin A against reoxygenation injury in isolated rat cardiomyocytes are associated with differential effects on mitochondrial calcium levels. *Cell calcium* **27**, 87-95, doi:10.1054/ceca.1999.0094 (2000).
- 95 Cung, T. T. *et al.* Cyclosporine before PCI in Patients with Acute Myocardial Infarction. *New Engl J Med* **373**, 1021-1031, doi:10.1056/Nejmoe1505489 (2015).
- 96 Francis, S. H. & Corbin, J. D. Structure and function of cyclic nucleotide-dependent protein kinases. *Annual review of physiology* **56**, 237-272, doi:10.1146/annurev.ph.56.030194.001321 (1994).
- 97 Buck, J., Sinclair, M. L., Schapal, L., Cann, M. J. & Levin, L. R. Cytosolic adenylyl cyclase defines a unique signaling molecule in mammals. *Proceedings*



- of the National Academy of Sciences of the United States of America **96**, 79-84 (1999).
- 98 Kamenetsky, M. *et al.* Molecular details of cAMP generation in mammalian cells: a tale of two systems. *J Mol Biol* **362**, 623-639, doi:10.1016/j.jmb.2006.07.045 (2006).
  - 99 Hurley, J. H. Structure, mechanism, and regulation of mammalian adenylyl cyclase. *The Journal of biological chemistry* **274**, 7599-7602 (1999).
  - 100 Pavan, B., Biondi, C. & Dalpiaz, A. Adenylyl cyclases as innovative therapeutic goals. *Drug discovery today* **14**, 982-991, doi:10.1016/j.drudis.2009.07.007 (2009).
  - 101 Reimann, E. M., Walsh, D. A. & Krebs, E. G. Purification and properties of rabbit skeletal muscle adenosine 3',5'-monophosphate-dependent protein kinases. *The Journal of biological chemistry* **246**, 1986-1995 (1971).
  - 102 Corbin, J. D., Keely, S. L. & Park, C. R. The distribution and dissociation of cyclic adenosine 3':5'-monophosphate-dependent protein kinases in adipose, cardiac, and other tissues. *The Journal of biological chemistry* **250**, 218-225 (1975).
  - 103 Sandberg, M., Tasken, K., Oyen, O., Hansson, V. & Jahnsen, T. Molecular cloning, cDNA structure and deduced amino acid sequence for a type I regulatory subunit of cAMP-dependent protein kinase from human testis. *Biochemical and biophysical research communications* **149**, 939-945 (1987).
  - 104 Lee, D. C., Carmichael, D. F., Krebs, E. G. & McKnight, G. S. Isolation of a cDNA clone for the type I regulatory subunit of bovine cAMP-dependent protein kinase. *Proceedings of the National Academy of Sciences of the United States of America* **80**, 3608-3612 (1983).
  - 105 Clegg, C. H., Cadd, G. G. & McKnight, G. S. Genetic characterization of a brain-specific form of the type I regulatory subunit of cAMP-dependent protein kinase. *Proceedings of the National Academy of Sciences of the United States of America* **85**, 3703-3707 (1988).
  - 106 Solberg, R., Tasken, K., Keiserud, A. & Jahnsen, T. Molecular cloning, cDNA structure and tissue-specific expression of the human regulatory subunit RI beta of cAMP-dependent protein kinases. *Biochemical and biophysical research communications* **176**, 166-172 (1991).
  - 107 Scott, J. D. *et al.* The molecular cloning of a type II regulatory subunit of the cAMP-dependent protein kinase from rat skeletal muscle and mouse brain.

*Proceedings of the National Academy of Sciences of the United States of America* **84**, 5192-5196 (1987).

- 108 Oyen, O., Myklebust, F., Scott, J. D., Hansson, V. & Jahnsen, T. Human testis cDNA for the regulatory subunit RII alpha of cAMP-dependent protein kinase encodes an alternate amino-terminal region. *FEBS letters* **246**, 57-64 (1989).
- 109 Jahnsen, T. *et al.* Molecular cloning, cDNA structure, and regulation of the regulatory subunit of type II cAMP-dependent protein kinase from rat ovarian granulosa cells. *The Journal of biological chemistry* **261**, 12352-12361 (1986).
- 110 Levy, F. O. *et al.* Molecular cloning, complementary deoxyribonucleic acid structure and predicted full-length amino acid sequence of the hormone-inducible regulatory subunit of 3'-5'-cyclic adenosine monophosphate-dependent protein kinase from human testis. *Molecular endocrinology* **2**, 1364-1373, doi:10.1210/mend-2-12-1364 (1988).
- 111 Uhler, M. D. *et al.* Isolation of cDNA clones coding for the catalytic subunit of mouse cAMP-dependent protein kinase. *Proceedings of the National Academy of Sciences of the United States of America* **83**, 1300-1304 (1986).
- 112 Uhler, M. D., Chrivia, J. C. & McKnight, G. S. Evidence for a second isoform of the catalytic subunit of cAMP-dependent protein kinase. *The Journal of biological chemistry* **261**, 15360-15363 (1986).
- 113 Showers, M. O. & Maurer, R. A. A cloned bovine cDNA encodes an alternate form of the catalytic subunit of cAMP-dependent protein kinase. *The Journal of biological chemistry* **261**, 16288-16291 (1986).
- 114 Beebe, S. J. *et al.* Molecular cloning of a tissue-specific protein kinase (C gamma) from human testis--representing a third isoform for the catalytic subunit of cAMP-dependent protein kinase. *Molecular endocrinology* **4**, 465-475, doi:10.1210/mend-4-3-465 (1990).
- 115 Wilkes, D., Charitakis, K. & Basson, C. T. Inherited disposition to cardiac myxoma development. *Nature reviews. Cancer* **6**, 157-165, doi:10.1038/nrc1798 (2006).
- 116 de Rooij, J. *et al.* Epac is a Rap1 guanine-nucleotide-exchange factor directly activated by cyclic AMP. *Nature* **396**, 474-477 (1998).
- 117 Kawasaki, H. *et al.* A family of cAMP-binding proteins that directly activate Rap1. *Science* **282**, 2275-2279, doi:DOI 10.1126/science.282.5397.2275 (1998).

- 118 Kitayama, H., Sugimoto, Y., Matsuzaki, T., Ikawa, Y. & Noda, M. A Ras-Related Gene with Transformation Suppressor Activity. *Cell* **56**, 77-84, doi:10.1016/0092-8674(89)90985-9 (1989).
- 119 de Rooij, J. *et al.* Mechanism of regulation of the Epac family of cAMP-dependent RapGEFs. *The Journal of biological chemistry* **275**, 20829-20836, doi:10.1074/jbc.M001113200 (2000).
- 120 de Rooij, J. *et al.* Mechanism of regulation of the Epac family of cAMP-dependent RapGEFs. *Journal of Biological Chemistry* **275**, 20829-20836, doi:DOI 10.1074/jbc.M001113200 (2000).
- 121 Rehmann, H. *et al.* Structure of Epac2 in complex with a cyclic AMP analogue and RAP1B. *Nature* **455**, 124-U193, doi:10.1038/nature07187 (2008).
- 122 Rehmann, H., Das, J., Knipscheer, P., Wittinghofer, A. & Bos, J. L. Structure of the cyclic-AMP-responsive exchange factor Epac2 in its auto-inhibited state. *Nature* **439**, 625-628, doi:10.1038/nature04468 (2006).
- 123 Selvaratnam, R., Mazhab-Jafari, M. T., Das, R. & Melacini, G. The Auto-Inhibitory Role of the EPAC Hinge Helix as Mapped by NMR. *PloS one* **7**, doi:ARTN e48707 10.1371/journal.pone.0048707 (2012).
- 124 Selvaratnam, R., Chowdhury, S., VanSchouwen, B. & Melacini, G. Mapping allostery through the covariance analysis of NMR chemical shifts. *Proceedings of the National Academy of Sciences of the United States of America* **108**, 6133-6138, doi:10.1073/pnas.1017311108 (2011).
- 125 Selvaratnam, R. *et al.* The Projection Analysis of NMR Chemical Shifts Reveals Extended EPAC Autoinhibition Determinants. *Biophysical journal* **102**, 630-639, doi:10.1016/j.bpj.2011.12.030 (2012).
- 126 Das, R. *et al.* Dynamically Driven Ligand Selectivity in Cyclic Nucleotide Binding Domains. *Journal of Biological Chemistry* **284**, 23682-23696, doi:10.1074/jbc.M109.011700 (2009).
- 127 Das, R. *et al.* Entropy-driven cAMP-dependent allosteric control of inhibitory interactions in exchange proteins directly activated by cAMP. *Journal of Biological Chemistry* **283**, 19691-19703, doi:10.1074/jbc.M802164200 (2008).
- 128 Boulton, S. *et al.* Tapping the translation potential of cAMP signalling: molecular basis for selectivity in cAMP agonism and antagonism as revealed

- p>by NMR.
- Biochemical Society transactions*
- 42**
- , 302-307, doi:10.1042/Bst20130282 (2014).
- 129 Parnell, E., Palmer, T. M. & Yarwood, S. J. The future of EPAC-targeted therapies: agonism versus antagonism. *Trends Pharmacol Sci* **36**, 203-214, doi:10.1016/j.tips.2015.02.003 (2015).
  - 130 Rangarajan, S. *et al.* Cyclic AMP induces integrin-mediated cell adhesion through Epac and Rap1 upon stimulation of the beta(2)-adrenergic receptor. *Journal of Cell Biology* **160**, 487-493, doi:10.1083/jcb.200209105 (2003).
  - 131 Enserink, J. M. *et al.* The cAMP-Epac-Rap1 pathway regulates cell spreading and cell adhesion to laminin-5 through the alpha3beta1 integrin but not the alpha6beta4 integrin. *The Journal of biological chemistry* **279**, 44889-44896, doi:10.1074/jbc.M404599200 (2004).
  - 132 Cullere, X. *et al.* Regulation of vascular endothelial barrier function by Epac, a cAMP-activated exchange factor for Rap GTPase. *Blood* **105**, 1950-1955, doi:10.1182/blood-2004-05-1987 (2005).
  - 133 Kooistra, M. R. H., Corada, M., Dejana, E. & Bos, J. L. Epac1 regulates integrity of endothelial cell junctions through VE-cadherin. *FEBS letters* **579**, 4966-4972, doi:10.1016/j.febslet.2005.07.080 (2005).
  - 134 Ozaki, N. *et al.* cAMP-GEFII is a direct target of cAMP in regulated exocytosis. *Nature cell biology* **2**, 805-811 (2000).
  - 135 Li, J. *et al.* Cyclic adenosine 5 '-monophosphate-stimulated neurotensin secretion is mediated through Rap1 downstream of both Epac and protein kinase A signaling pathways. *Molecular endocrinology* **21**, 159-171, doi:10.1210/me.2006-0340 (2007).
  - 136 Seino, S. & Shibasaki, T. PKA-dependent and PKA-independent pathways for cAMP-regulated exocytosis. *Physiological reviews* **85**, 1303-1342, doi:10.1152/physrev.00001.2005 (2005).
  - 137 Maillet, M. *et al.* Crosstalk between Rap1 and Rac regulates secretion of sAPP alpha. *Nature cell biology* **5**, 633-U636, doi:10.1038/ncb1007 (2003).
  - 138 Kiermayer, S. *et al.* Epac activation converts cAMP from a proliferative into a differentiation signal in PC12 Cells. *Molecular biology of the cell* **16**, 5639-5648, doi:10.1091/mcb.E05-05-0432 (2005).

- 139 Vitali, E. *et al.* cAMP effects in neuroendocrine tumors: The role of Epac and PKA in cell proliferation and adhesion. *Experimental cell research* **339**, 241-251, doi:10.1016/j.yexcr.2015.11.011 (2015).
- 140 Ulucan, C. *et al.* Developmental changes in gene expression of Epac and its upregulation in myocardial hypertrophy. *Am J Physiol-Heart C* **293**, H1662-H1672, doi:10.1152/ajpheart.00159.2007 (2007).
- 141 Mangmool, S., Hemplueksa, P., Parichatikanond, W. & Chattipakorn, N. Epac is Required for GLP-1R-Mediated Inhibition of Oxidative Stress and Apoptosis in Cardiomyocytes. *Molecular endocrinology* **29**, 583-596, doi:10.1210/me.2014-1346 (2015).
- 142 Grandoch, M., Fleckenstein, D., Schmidt, M. & Weber, A. A. Epac-mediated inhibition of TNF-alpha-induced apoptosis. *N-S Arch Pharmacol* **377**, 16-16 (2008).
- 143 Metrich, M. *et al.* Epac mediates beta-adrenergic receptor-induced cardiomyocyte hypertrophy. *Circulation research* **102**, 959-965, doi:10.1161/Circresaha.107.164947 (2008).
- 144 Morel, E. *et al.* cAMP-binding protein Epac induces cardiomyocyte hypertrophy. *Circulation research* **97**, 1296-1304, doi:10.1161/01.Res.0000194325.31359.86 (2005).
- 145 Courilleau, D. *et al.* Identification of a Tetrahydroquinoline Analog as a Pharmacological Inhibitor of the cAMP-binding Protein Epac. *Journal of Biological Chemistry* **287**, 44192-44202, doi:10.1074/jbc.M112.422956 (2012).
- 146 Tsalkova, T. *et al.* Isoform-specific antagonists of exchange proteins directly activated by cAMP. *Proceedings of the National Academy of Sciences of the United States of America* **109**, 18613-18618, doi:10.1073/pnas.1210209109 (2012).
- 147 Rehmann, H. Epac-Inhibitors: Facts and Artefacts. *Scientific reports* **3**, doi:Artn 3032  
10.1038/Srep03032 (2013).
- 148 Chen, H. J. *et al.* 5-Cyano-6-oxo-1,6-dihydro-pyrimidines as potent antagonists targeting exchange proteins directly activated by cAMP. *Bioorg Med Chem Lett* **22**, 4038-4043, doi:10.1016/j.bmcl.2012.04.082 (2012).

- 149 Herbst, K. J., Coltharp, C., Amzel, L. M. & Zhang, J. Direct Activation of Epac by Sulfonylurea Is Isoform Selective. *Chem Biol* **18**, 243-251, doi:10.1016/j.chembiol.2010.12.007 (2011).
- 150 Almahariq, M. *et al.* Exchange protein directly activated by cAMP modulates regulatory T-cell-mediated immunosuppression. *Biochemical Journal* **465**, 295-303, doi:10.1042/Bj20140952 (2015).
- 151 Brown, L. M., Rogers, K. E., Aroonsakool, N., McCammon, J. A. & Insel, P. A. Allosteric Inhibition of Epac COMPUTATIONAL MODELING AND EXPERIMENTAL VALIDATION TO IDENTIFY ALLOSTERIC SITES AND INHIBITORS. *Journal of Biological Chemistry* **289**, 29148-29157, doi:10.1074/jbc.M114.569319 (2014).
- 152 Brown, L. M., Rogers, K. E., McCammon, J. A. & Insel, P. A. Identification and Validation of Modulators of Exchange Protein Activated by cAMP (Epac) Activity. *Journal of Biological Chemistry* **289**, 8217-8230, doi:10.1074/jbc.M114.548636 (2014).
- 153 Rehmann, H., Schwede, F., Doskeland, S. O., Wittinghofer, A. & Bos, J. L. Ligand-mediated activation of the cAMP-responsive guanine nucleotide exchange factor Epac. *Journal of Biological Chemistry* **278**, 38548-38556, doi:10.1074/jbc.M306292200 (2003).
- 154 Enserink, J. M. *et al.* A novel Epac-specific cAMP analogue demonstrates independent regulation of Rap1 and ERK. *Nature cell biology* **4**, 901-906, doi:10.1038/ncb874 (2002).
- 155 Zhang, C. L. *et al.* The cAMP Sensor Epac2 Is a Direct Target of Antidiabetic Sulfonylurea Drugs. *Science* **325**, 607-610, doi:10.1126/science.1172256 (2009).
- 156 Takahashi, T. *et al.* Antidiabetic Sulfonylureas and cAMP Cooperatively Activate Epac2A. *Sci Signal* **6**, doi:ARTN ra94 10.1126/scisignal.2004581 (2013).
- 157 Rehmann, H. Epac2: a sulfonylurea receptor? *Biochemical Society transactions* **40**, 6-10, doi:10.1042/BST20110640 (2012).
- 158 McPhee, I. *et al.* Cyclic nucleotide signalling: a molecular approach to drug discovery for Alzheimer's disease. *Biochemical Society transactions* **33**, 1330-1332 (2005).



- 159 Biel, M., Schneider, A. & Wahl, C. Cardiac HCN channels: Structure, function, and modulation. *Trends Cardiovas Med* **12**, 206-213, doi:Pii S1050-1738(02)00162-7
- Doi 10.1016/S1050-1738(02)00162-7 (2002).
- 160 Mangoni, M. E. & Nargeot, J. Genesis and regulation of the heart automaticity. *Physiological reviews* **88**, 919-982, doi:10.1152/physrev.00018.2007 (2008).
- 161 Poh, K. K., Wood, M. J. & Cury, R. C. Prominent posterior mitral annular calcification causing embolic stroke and mimicking left atrial fibroma. *European heart journal* **28**, 2216-2216, doi:10.1093/eurheartj/ehm052 (2007).
- 162 Bois, P., Guinamard, R., Chemaly, A. E., Faivre, J. F. & Bescond, J. Molecular regulation and pharmacology of pacemaker channels. *Current pharmaceutical design* **13**, 2338-2349 (2007).
- 163 Kamp, T. J. & Hell, J. W. Regulation of cardiac L-type calcium channels by protein kinase A and protein kinase C. *Circulation research* **87**, 1095-1102 (2000).
- 164 Marx, S. O. *et al.* PKA phosphorylation dissociates FKBP12.6 from the calcium release channel (ryanodine receptor): Defective regulation in failing hearts. *Cell* **101**, 365-376, doi:Doi 10.1016/S0092-8674(00)80847-8 (2000).
- 165 Kiss, E. *et al.* beta-adrenergic regulation of cAMP and protein phosphorylation in phospholamban-knockout mouse hearts. *Am J Physiol-Heart C* **272**, H785-H790 (1997).
- 166 Simmerman, H. K. B. & Jones, L. R. Phospholamban: Protein structure, mechanism of action, and role in cardiac function. *Physiological reviews* **78**, 921-947 (1998).
- 167 Bers, D. M. Calcium cycling and signaling in cardiac myocytes. *Annual review of physiology* **70**, 23-49, doi:10.1146/annurev.physiol.70.113006.100455 (2008).
- 168 Muller, F. U. *et al.* Activation and inactivation of cAMP-response element-mediated gene transcription in cardiac myocytes. *Cardiovascular research* **52**, 95-102 (2001).
- 169 MacLennan, D. H. & Kranias, E. G. Phospholamban: a crucial regulator of cardiac contractility. *Nature reviews. Molecular cell biology* **4**, 566-577, doi:10.1038/nrm1151 (2003).



- 170 Morel, E. *et al.* cAMP-binding protein Epac induces cardiomyocyte hypertrophy. *Circulation research* **97**, 1296-1304, doi:10.1161/01.RES.0000194325.31359.86 (2005).
- 171 Somekawa, S. *et al.* Enhanced functional gap junction neofunction by protein kinase A-dependent and Epac-dependent signals downstream of cAMP in cardiac myocytes. *Circulation research* **97**, 655-662, doi:10.1161/01.RES.0000183880.49270.f9 (2005).
- 172 Metrich, M. *et al.* Epac mediates beta-adrenergic receptor-induced cardiomyocyte hypertrophy. *Circulation research* **102**, 959-965, doi:10.1161/CIRCRESAHA.107.164947 (2008).
- 173 Metrich, M. *et al.* Epac activation induces histone deacetylase nuclear export via a Ras-dependent signalling pathway. *Cellular signalling* **22**, 1459-1468, doi:10.1016/j.cellsig.2010.05.014 (2010).
- 174 Guellich, A., Mehel, H. & Fischmeister, R. Cyclic AMP synthesis and hydrolysis in the normal and failing heart. *Pflügers Archiv : European journal of physiology* **466**, 1163-1175, doi:10.1007/s00424-014-1515-1 (2014).
- 175 Perrino, C., Prasad, S. V. N., Patel, M. & Rockman, H. A. Normalization of beta-adrenergic receptor signaling by targeted inhibition of phosphoinositide-3 kinase rescues cardiac function and survival in murine heart failure. *Circulation* **110**, 290-290 (2004).
- 176 Esposito, G. *et al.* Genetic alterations that inhibit in vivo pressure-overload hypertrophy prevent cardiac dysfunction despite increased wall stress. *Circulation* **105**, 85-92, doi:DOI 10.1161/hc0102.101365 (2002).
- 177 Chen, Y. Q. *et al.* Soluble adenylyl cyclase as an evolutionarily conserved bicarbonate sensor. *Science* **289**, 625-628, doi:DOI 10.1126/science.289.5479.625 (2000).
- 178 Han, H. *et al.* Calcium-sensing soluble adenylyl cyclase mediates TNF signal transduction in human neutrophils. *Journal of Experimental Medicine* **202**, 353-361, doi:10.1084/jem.20050778 (2005).
- 179 Litvin, T. N., Kamenetsky, M., Zarifyan, A., Buck, J. & Levin, L. R. Kinetic properties of "soluble" adenylyl cyclase - Synergism between calcium and bicarbonate. *Journal of Biological Chemistry* **278**, 15922-15926, doi:10.1074/jbc.M212475200 (2003).

- 180 Townsend, P. D. *et al.* Stimulation of Mammalian G-protein-responsive Adenylyl Cyclases by Carbon Dioxide. *Journal of Biological Chemistry* **284**, 784-791, doi:10.1074/jbc.M807239200 (2009).
- 181 Feng, Q. P. *et al.* Two domains are critical for the nuclear localization of soluble adenylyl cyclase. *Biochimie* **88**, 319-328, doi:10.1016/j.biochi.2005.09.003 (2006).
- 182 Geng, W. D. *et al.* Cloning and characterization of the human soluble adenylyl cyclase. *Am J Physiol-Cell Ph* **288**, C1305-C1316, doi:10.1152/ajpcell.00584.2004 (2005).
- 183 Xie, F. & Conti, M. Expression of the soluble adenylyl cyclase during rat spermatogenesis: evidence for cytoplasmic sites of cAMP production in germ cells. *Developmental biology* **265**, 196-206, doi:10.1016/j.ydbio.2003.09.020 (2004).
- 184 Zippin, J. H. *et al.* Compartmentalization of bicarbonate-sensitive adenylyl cyclase in distinct signaling microdomains. *Faseb Journal* **16**, 82-+, doi:10.1096/fj.02-0598fje (2002).
- 185 Hurley, J. D., Gardiner, J. V., Jones, P. M. & Bloom, S. R. Cloning and Molecular Characterization of Complementary Deoxyribonucleic-Acid Corresponding to a Novel Form of Pituitary Adenylate Cyclase-Activating Polypeptide Messenger-Ribonucleic-Acid in the Rat Testis. *Endocrinology* **136**, 550-557, doi:Doi 10.1210/En.136.2.550 (1995).
- 186 Buck, J., Sinclair, M. L., Schapal, L., Cann, M. J. & Levin, L. R. Cytosolic adenylyl cyclase defines a unique signaling molecule in mammals. *Proceedings of the National Academy of Sciences of the United States of America* **96**, 79-84, doi:Doi 10.1073/Pnas.96.1.79 (1999).
- 187 Reed, B. Y. *et al.* Identification and characterization of a gene with base substitutions associated with the absorptive hypercalciuria phenotype and low spinal bone density. *J Clin Endocr Metab* **87**, 1476-1485, doi:Doi 10.1210/Jc.87.4.1476 (2002).
- 188 Sinclair, M. L. *et al.* Specific expression of soluble adenylyl cyclase in male germ cells. *Molecular reproduction and development* **56**, 6-11, doi:Doi 10.1002/(Sici)1098-2795(200005)56:1<6::Aid-Mrd2>3.0.Co;2-M (2000).
- 189 Chen, J., Levin, L. R. & Buck, J. Role of soluble adenylyl cyclase in the heart. *American journal of physiology. Heart and circulatory physiology* **302**, H538-543, doi:10.1152/ajpheart.00701.2011 (2012).

- 190 Jaiswal, B. S. & Conti, M. Identification and functional analysis of splice variants of the germ cell soluble adenylyl cyclase. *Journal of Biological Chemistry* **276**, 31698-31708, doi:DOI 10.1074/jbc.M011698200 (2001).
- 191 Wuttke, M. S., Buck, J. & Levin, L. R. Bicarbonate-regulated soluble adenylyl cyclase. *JOP : Journal of the pancreas* **2**, 154-158 (2001).
- 192 Farrell, J. *et al.* Somatic 'Soluble' Adenylyl Cyclase Isoforms Are Unaffected in Sacy(tm1Lex)/Sacy(tm1Lex) 'Knockout' Mice. *PloS one* **3**, doi:ARTN e3251 10.1371/journal.pone.0003251 (2008).
- 193 Steegborn, C., Litvin, T. N., Levin, L. R., Buck, J. & Wu, H. Bicarbonate activation of adenylyl cyclase via promotion of catalytic active site closure and metal recruitment. *Nature structural & molecular biology* **12**, 32-37, doi:10.1038/nsmb880 (2005).
- 194 Tresguerres, M., Levin, L. R. & Buck, J. Intracellular cAMP signaling by soluble adenylyl cyclase. *Kidney international* **79**, 1277-1288, doi:10.1038/ki.2011.95 (2011).
- 195 Kamenetsky, M. *et al.* Molecular details of cAMP generation in mammalian cells: A tale of two systems. *J Mol Biol* **362**, 623-639, doi:10.1016/j.jmb.2006.07.045 (2006).
- 196 Jaiswal, B. S. & Conti, M. Calcium regulation of the soluble adenylyl cyclase expressed in mammalian spermatozoa. *Proceedings of the National Academy of Sciences of the United States of America* **100**, 10676-10681, doi:10.1073/pnas.1831008100 (2003).
- 197 Zippin, J. H. *et al.* Bicarbonate-responsive "soluble" adenylyl cyclase defines a nuclear cAMP microdomain. *Journal of Cell Biology* **164**, 527-534, doi:10.1083/jcb.200311119 (2004).
- 198 Zippin, J. H., Chadwick, P. A., Levin, L. R., Buck, J. & Magro, C. M. Soluble Adenylyl Cyclase Defines a Nuclear cAMP Microdomain in Keratinocyte Hyperproliferative Skin Diseases. *Journal of Investigative Dermatology* **130**, 1279-1287, doi:10.1038/jid.2009.440 (2010).
- 199 Corredor, R. G. *et al.* Soluble adenylyl cyclase activity is necessary for retinal ganglion cell survival and axon growth. *The Journal of neuroscience : the official journal of the Society for Neuroscience* **32**, 7734-7744, doi:10.1523/JNEUROSCI.5288-11.2012 (2012).

- 200 Ladilov, Y. & Appukuttan, A. Role of soluble adenylyl cyclase in cell death and growth. *Biochimica et biophysica acta* **1842**, 2646-2655, doi:10.1016/j.bbadis.2014.06.034 (2014).
- 201 Wu, K. Y. *et al.* Soluble adenylyl cyclase is required for netrin-1 signaling in nerve growth cones. *Nature neuroscience* **9**, 1257-1264, doi:10.1038/nn1767 (2006).
- 202 Corredor, R. G. *et al.* Soluble Adenylyl Cyclase Activity Is Necessary for Retinal Ganglion Cell Survival and Axon Growth. *Journal of Neuroscience* **32**, 7734-7744, doi:10.1523/Jneurosci.5288-11.2012 (2012).
- 203 Marquez, B. & Suarez, S. S. Soluble adenylyl cyclase is required for activation of sperm but does not have a direct effect on hyperactivation. *Reprod Fert Develop* **20**, 247-252, doi:10.1071/RD07146 (2008).
- 204 Vander Heiden, M. G. & Thompson, C. B. Bcl-2 proteins: regulators of apoptosis or of mitochondrial homeostasis? *Nature cell biology* **1**, E209-E216, doi:Doi 10.1038/70237 (1999).
- 205 Appukuttan, A., Kasseckert, S. A., Kumar, S., Reusch, H. P. & Ladilov, Y. Oxysterol-induced apoptosis of smooth muscle cells is under the control of a soluble adenylyl cyclase. *Cardiovascular research* **99**, 734-742, doi:10.1093/cvr/cvt137 (2013).
- 206 Kumar, S., Kostin, S., Flacke, J. P., Reusch, H. P. & Ladilov, Y. Soluble Adenylyl Cyclase Controls Mitochondria-dependent Apoptosis in Coronary Endothelial Cells. *Journal of Biological Chemistry* **284**, 14760-14768, doi:10.1074/jbc.M900925200 (2009).
- 207 Appukuttan, A. *et al.* Type 10 adenylyl cyclase mediates mitochondrial Bax translocation and apoptosis of adult rat cardiomyocytes under simulated ischaemia/reperfusion. *Cardiovascular research* **93**, 340-349, doi:10.1093/cvr/cvr306 (2012).
- 208 Kumar, S. *et al.* Ischemic acidosis causes apoptosis in coronary endothelial cells through activation of caspase-12. *Cardiovascular research* **73**, 172-180, doi:10.1016/j.cardiores.2006.09.018 (2007).
- 209 Ladilov, Y. *et al.* Mechanism of Ca<sup>2+</sup> overload in endothelial cells exposed to simulated ischemia. *Cardiovascular research* **47**, 394-403, doi:Doi 10.1016/S0008-6363(00)00108-5 (2000).

- 210 Ladilov, Y. V., Balser, C. & Piper, H. M. Protection of rat cardiomyocytes against simulated ischemia and reoxygenation by treatment with protein kinase C activator. *Circulation research* **82**, 451-457 (1998).
- 211 Kim, B. J., Ryu, S. W. & Song, B. J. JNK- and p38 kinase-mediated phosphorylation of Bax leads to its activation and mitochondrial translocation and to apoptosis of human hepatoma HepG2 cells. *Journal of Biological Chemistry* **281**, 21256-21265, doi:10.1074/jbc.M510644200 (2006).
- 212 Technikova-Dobrova, Z. *et al.* Cyclic adenosine monophosphate-dependent phosphorylation of mammalian mitochondrial proteins: Enzyme and substrate characterization and functional role. *Biochemistry* **40**, 13941-13947, doi:10.1021/bi011066p (2001).
- 213 Papa, S., Sardanelli, A. M., Scacco, S. & Technikova-Dobrova, Z. cAMP-dependent protein kinase and phosphoproteins in mammalian mitochondria. An extension of the cAMP-mediated intracellular signal transduction. *FEBS letters* **444**, 245-249, doi:Doi 10.1016/S0014-5793(99)00070-8 (1999).
- 214 Zhang, L. Z. *et al.* Gene expression signatures of cAMP/protein kinase A (PKA)-promoted, mitochondrial-dependent apoptosis - Comparative analysis of wild-type and camp-deathless S49 lymphoma cells. *Journal of Biological Chemistry* **283**, 4304-4313, doi:10.1074/jbc.M708673200 (2008).
- 215 Cieslak, D. & Lazou, A. Regulation of BAD protein by PKA, PKC delta and phosphatases in adult rat cardiac myocytes subjected to oxidative stress. *Mol Cells* **24**, 224-231 (2007).
- 216 Li, Z., Ji, G. C. & Neugebauer, V. Mitochondrial Reactive Oxygen Species Are Activated by mGluR5 through IP3 and Activate ERK and PKA to Increase Excitability of Amygdala Neurons and Pain Behavior. *Journal of Neuroscience* **31**, 1114-1127, doi:10.1523/Jneurosci.5387-10.2011 (2011).
- 217 Nagasaka, S. *et al.* Protein kinase A catalytic subunit alters cardiac mitochondrial redox state and membrane potential via the formation of reactive oxygen species. *Circulation Journal* **71**, 429-436, doi:Doi 10.1253/Circj.71.429 (2007).
- 218 Jang, E. R. & Lee, C. S. 7-Ketocholesterol induces apoptosis in differentiated PC12 cells via reactive oxygen species-dependent activation of NF-kappa B and Akt pathways. *Neurochemistry international* **58**, 52-59, doi:10.1016/j.neuint.2010.10.012 (2011).

- 219 Lizard, G. *et al.* Glutathione is implied in the control of 7-ketocholesterol-induced apoptosis, which is associated with radical oxygen species production. *Faseb Journal* **12**, 1651-1663 (1998).
- 220 Maulik, N., Yoshida, T. & Das, D. K. Oxidative stress developed during the reperfusion of ischemic myocardium induces apoptosis. *Free Radical Bio Med* **24**, 869-875, doi:Doi 10.1016/S0891-5849(97)00388-2 (1998).
- 221 Acin-Perez, R. *et al.* Modulation of mitochondrial protein phosphorylation by soluble adenylyl cyclase ameliorates cytochrome oxidase defects. *EMBO molecular medicine* **1**, 392-406, doi:10.1002/emmm.200900046 (2009).
- 222 Acin-Perez, R. *et al.* Cyclic AMP Produced inside Mitochondria Regulates Oxidative Phosphorylation. *Cell metabolism* **9**, 265-276, doi:10.1016/j.cmet.2009.01.012 (2009).
- 223 Zippin, J. H. *et al.* Compartmentalization of bicarbonate-sensitive adenylyl cyclase in distinct signaling microdomains. *FASEB journal : official publication of the Federation of American Societies for Experimental Biology* **17**, 82-84, doi:10.1096/fj.02-0598fje (2003).
- 224 DiPilato, L. M., Cheng, X. & Zhang, J. Fluorescent indicators of cAMP and Epac activation reveal differential dynamics of cAMP signaling within discrete subcellular compartments. *Proceedings of the National Academy of Sciences of the United States of America* **101**, 16513-16518, doi:10.1073/pnas.0405973101 (2004).
- 225 Acin-Perez, R. *et al.* Cyclic AMP produced inside mitochondria regulates oxidative phosphorylation. *Cell Metab* **9**, 265-276, doi:10.1016/j.cmet.2009.01.012 (2009).
- 226 Di Benedetto, G., Scalzotto, E., Mongillo, M. & Pozzan, T. Mitochondrial Ca(2)(+) uptake induces cyclic AMP generation in the matrix and modulates organelle ATP levels. *Cell Metab* **17**, 965-975, doi:10.1016/j.cmet.2013.05.003 (2013).
- 227 Lefkimmiatis, K., Leronni, D. & Hofer, A. M. The inner and outer compartments of mitochondria are sites of distinct cAMP/PKA signaling dynamics. *The Journal of cell biology* **202**, 453-462, doi:10.1083/jcb.201303159 (2013).
- 228 Acin-Perez, R. *et al.* Modulation of mitochondrial protein phosphorylation by soluble adenylyl cyclase ameliorates cytochrome oxidase defects. *EMBO molecular medicine* **1**, 392-406, doi:10.1002/emmm.200900046 (2009).



- 229 Ponsioen, B. *et al.* Detecting cAMP-induced Epac activation by fluorescence resonance energy transfer: Epac as a novel cAMP indicator. *EMBO reports* **5**, 1176-1180, doi:10.1038/sj.embor.7400290 (2004).
- 230 Sardanelli, A. M. *et al.* Topology of the mitochondrial cAMP-dependent protein kinase and its substrates. *FEBS letters* **396**, 276-278, doi:Doi 10.1016/0014-5793(96)01112-X (1996).
- 231 Schwoch, G., Trinczek, B. & Bode, C. Localization of Catalytic and Regulatory Subunits of Cyclic Amp-Dependent Protein-Kinases in Mitochondria from Various Rat-Tissues. *Biochemical Journal* **270**, 181-188 (1990).
- 232 Technikovadobrova, Z., Sardanelli, A. M. & Papa, S. Phosphorylation of Mitochondrial Proteins in Bovine Heart - Characterization of Kinases and Substrates. *FEBS letters* **322**, 51-55, doi:Doi 10.1016/0014-5793(93)81109-D (1993).
- 233 Valsecchi, F., Ramos-Espiritu, L. S., Buck, J., Levin, L. R. & Manfredi, G. cAMP and Mitochondria. *Physiology* **28**, 199-209, doi:10.1152/physiol.00004.2013 (2013).
- 234 Technikovadobrova, Z., Sardanelli, A. M., Stanca, M. R. & Papa, S. Camp-Dependent Protein-Phosphorylation in Mitochondria of Bovine Heart. *FEBS letters* **350**, 187-191, doi:Doi 10.1016/0014-5793(94)00760-8 (1994).
- 235 Bender, E. & Kadenbach, B. The allosteric ATP-inhibition of cytochrome c oxidase activity is reversibly switched on by cAMP-dependent phosphorylation. *FEBS letters* **466**, 130-134, doi:Doi 10.1016/S0014-5793(99)01773-1 (2000).
- 236 Robin, M. A., Prabu, S. K., Raza, H., Anandatheerthavarada, H. K. & Avadhani, N. G. Phosphorylation enhances mitochondrial targeting of GSTA4-4 through increased affinity for binding to cytoplasmic Hsp70. *Journal of Biological Chemistry* **278**, 18960-18970, doi:10.1074/jbc.M301807200 (2003).
- 237 Helling, S. *et al.* Phosphorylation and kinetics of mammalian cytochrome c oxidase. *Mol Cell Proteomics* **7**, 1714-1724, doi:10.1074/mcp.M800137-MCP200 (2008).
- 238 Prabu, S. K. *et al.* Protein kinase A-mediated phosphorylation modulates cytochrome c oxidase function and augments hypoxia and myocardial ischemia-related injury. *Journal of Biological Chemistry* **281**, 2061-2070, doi:10.1074/jbc.M507741200 (2006).
- 239 Means, C. K. *et al.* An entirely specific type I A-kinase anchoring protein that can sequester two molecules of protein kinase A at mitochondria. *Proceedings*



- of the National Academy of Sciences of the United States of America **108**, E1227-E1235, doi:10.1073/pnas.1107182108 (2011).
- 240 Qiao, J. B., Mei, F. C., Popov, V. L., Vergara, L. A. & Cheng, X. D. Cell cycle-dependent subcellular localization of exchange factor directly activated by cAMP. *Journal of Biological Chemistry* **277**, 26581-26586, doi:10.1074/jbc.M203571200 (2002).
  - 241 Kim, S., Mizoguchi, A., Kikuchi, A. & Takai, Y. Tissue and Subcellular Distributions of the Smg-21/Rap1/Krev-1 Proteins Which Are Partly Distinct from Those of C-Ras P21s. *Molecular and cellular biology* **10**, 2645-2652 (1990).
  - 242 Thomson, M. What are guanosine triphosphate-binding proteins doing in mitochondria? *Bba-Mol Cell Res* **1403**, 211-218, doi:Doi 10.1016/S0167-4889(98)00069-X (1998).
  - 243 Azevedo, M. F. *et al.* Clinical and molecular genetics of the phosphodiesterases (PDEs). *Endocrine reviews* **35**, 195-233, doi:10.1210/er.2013-1053 (2014).
  - 244 Maurice, D. H. *et al.* Advances in targeting cyclic nucleotide phosphodiesterases. *Nature reviews. Drug discovery* **13**, 290-314, doi:10.1038/nrd4228 (2014).
  - 245 Lefievre, L., de Lamirande, E. & Gagnon, C. Presence of cyclic nucleotide phosphodiesterases PDE1A, existing as a stable complex with calmodulin, and PDE3A in human spermatozoa. *Biology of reproduction* **67**, 423-430 (2002).
  - 246 Fidock, M., Miller, M. & Lanfear, J. Isolation and differential tissue distribution of two human cDNAs encoding PDE1 splice variants. *Cellular signalling* **14**, 53-60 (2002).
  - 247 Polli, J. W. & Kincaid, R. L. Molecular-Cloning of DNA Encoding a Calmodulin-Dependent Phosphodiesterase Enriched in Striatum. *Proceedings of the National Academy of Sciences of the United States of America* **89**, 11079-11083, doi:DOI 10.1073/pnas.89.22.11079 (1992).
  - 248 Loughney, K. *et al.* Isolation and characterization of cDNAs corresponding to two human calcium, calmodulin-regulated, 3',5'-cyclic nucleotide phosphodiesterases. *The Journal of biological chemistry* **271**, 796-806 (1996).
  - 249 Vandeput, F. *et al.* Cyclic nucleotide phosphodiesterase PDE1C1 in human cardiac myocytes. *The Journal of biological chemistry* **282**, 32749-32757, doi:10.1074/jbc.M703173200 (2007).

- 250 Yan, C. *et al.* Molecular cloning and characterization of a calmodulin-dependent phosphodiesterase enriched in olfactory sensory neurons. *Proceedings of the National Academy of Sciences of the United States of America* **92**, 9677-9681 (1995).
- 251 Yan, C., Zhao, A. Z., Bentley, J. K. & Beavo, J. A. The calmodulin-dependent phosphodiesterase gene PDE1C encodes several functionally different splice variants in a tissue-specific manner. *The Journal of biological chemistry* **271**, 25699-25706 (1996).
- 252 Yanaka, N., Kurosawa, Y., Minami, K., Kawai, E. & Omori, K. cGMP-phosphodiesterase activity is up-regulated in response to pressure overload of rat ventricles. *Bioscience, biotechnology, and biochemistry* **67**, 973-979, doi:10.1271/bbb.67.973 (2003).
- 253 Miller, C. L. *et al.* Cyclic nucleotide phosphodiesterase 1A: a key regulator of cardiac fibroblast activation and extracellular matrix remodeling in the heart. *Basic research in cardiology* **106**, 1023-1039, doi:10.1007/s00395-011-0228-2 (2011).
- 254 Reed, T. M., Repaske, D. R., Snyder, G. L., Greengard, P. & Vorhees, C. V. Phosphodiesterase 1B knock-out mice exhibit exaggerated locomotor hyperactivity and DARPP-32 phosphorylation in response to dopamine agonists and display impaired spatial learning. *The Journal of neuroscience : the official journal of the Society for Neuroscience* **22**, 5188-5197 (2002).
- 255 Cai, Y. *et al.* Cyclic nucleotide phosphodiesterase 1 regulates lysosome-dependent type I collagen protein degradation in vascular smooth muscle cells. *Arteriosclerosis, thrombosis, and vascular biology* **31**, 616-623, doi:10.1161/ATVBAHA.110.212621 (2011).
- 256 Schermuly, R. T. *et al.* Phosphodiesterase 1 upregulation in pulmonary arterial hypertension: target for reverse-remodeling therapy. *Circulation* **115**, 2331-2339, doi:10.1161/CIRCULATIONAHA.106.676809 (2007).
- 257 Snyder, P. B., Esselstyn, J. M., Loughney, K., Wolda, S. L. & Florio, V. A. The role of cyclic nucleotide phosphodiesterases in the regulation of adipocyte lipolysis. *Journal of lipid research* **46**, 494-503, doi:10.1194/jlr.M400362-JLR200 (2005).
- 258 Sonnenburg, W. K., Mullaney, P. J. & Beavo, J. A. Molecular cloning of a cyclic GMP-stimulated cyclic nucleotide phosphodiesterase cDNA. Identification and distribution of isozyme variants. *The Journal of biological chemistry* **266**, 17655-17661 (1991).

- 259 Yang, Q. *et al.* A novel cyclic GMP stimulated phosphodiesterase from rat brain. *Biochemical and biophysical research communications* **205**, 1850-1858, doi:10.1006/bbrc.1994.2886 (1994).
- 260 Rosman, G. J. *et al.* Isolation and characterization of human cDNAs encoding a cGMP-stimulated 3',5'-cyclic nucleotide phosphodiesterase. *Gene* **191**, 89-95 (1997).
- 261 Martinez, S. E. *et al.* The two GAF domains in phosphodiesterase 2A have distinct roles in dimerization and in cGMP binding. *Proceedings of the National Academy of Sciences of the United States of America* **99**, 13260-13265, doi:10.1073/pnas.192374899 (2002).
- 262 Bender, A. T. & Beavo, J. A. Cyclic nucleotide phosphodiesterases: Molecular regulation to clinical use. *Pharmacological reviews* **58**, 488-520, doi:10.1124/pr.58.3.5 (2006).
- 263 Lugnier, C. Cyclic nucleotide phosphodiesterase (PDE) superfamily: A new target for the development of specific therapeutic agents. *Pharmacol Therapeut* **109**, 366-398, doi:10.1016/j.pharmthera.2005.07.003 (2006).
- 264 Richter, W. *et al.* Signaling from beta(1)- and beta(2)-adrenergic receptors is defined by differential interactions with PDE4. *Embo Journal* **27**, 384-393, doi:10.1038/sj.emboj.7601968 (2008).
- 265 Richter, W., Mika, D., Blanchard, E., Day, P. & Conti, M. beta(1)-adrenergic receptor antagonists signal via PDE4 translocation. *EMBO reports* **14**, 276-283, doi:10.1038/embor.2013.4 (2013).
- 266 Conti, M., Hsieh, M., Zamah, A. M. & Oh, J. S. Novel signaling mechanisms in the ovary during oocyte maturation and ovulation. *Molecular and cellular endocrinology* **356**, 65-73, doi:10.1016/j.mce.2011.11.002 (2012).
- 267 Rivet-Bastide, M. *et al.* cGMP-stimulated cyclic nucleotide phosphodiesterase regulates the basal calcium current in human atrial myocytes. *The Journal of clinical investigation* **99**, 2710-2718, doi:10.1172/JCI119460 (1997).
- 268 Sadhu, K., Hensley, K., Florio, V. A. & Wolda, S. L. Differential expression of the cyclic GMP-stimulated phosphodiesterase PDE2A in human venous and capillary endothelial cells. *The journal of histochemistry and cytochemistry : official journal of the Histochemistry Society* **47**, 895-906 (1999).
- 269 Hartzell, H. C. & Fischmeister, R. Opposite effects of cyclic GMP and cyclic AMP on Ca<sup>2+</sup> current in single heart cells. *Nature* **323**, 273-275, doi:10.1038/323273a0 (1986).

- 270 Hartzell, H. C. & Simmons, M. A. Comparison of effects of acetylcholine on calcium and potassium currents in frog atrium and ventricle. *The Journal of physiology* **389**, 411-422 (1987).
- 271 Dittrich, M. *et al.* Local response of L-type Ca<sup>2+</sup> current to nitric oxide in frog ventricular myocytes. *J Physiol-London* **534**, 109-121, doi:DOI 10.1111/j.1469-7793.2001.00109.x (2001).
- 272 Vandecasteele, G., Verde, I., Rucker-Martin, C., Donzeau-Gouge, P. & Fischmeister, R. Cyclic GMP regulation of the L-type Ca<sup>2+</sup> channel current in human atrial myocytes. *J Physiol-London* **533**, 329-340, doi:DOI 10.1111/j.1469-7793.2001.0329a.x (2001).
- 273 Mongillo, M. *et al.* Compartmentalized phosphodiesterase-2 activity blunts beta-adrenergic cardiac inotropy via an NO/cGMP-dependent pathway. *Circulation research* **98**, 226-234, doi:10.1161/01.Res.0000200178.34179.93 (2006).
- 274 Stangherlin, A. *et al.* cGMP Signals Modulate cAMP Levels in a Compartment-Specific Manner to Regulate Catecholamine-Dependent Signaling in Cardiac Myocytes. *Circulation research* **108**, 929-U110, doi:10.1161/Circresaha.110.230698 (2011).
- 275 Podzuweit, T., Nennstiel, P. & Muller, A. Isozyme-Selective Inhibition of Cgmp-Stimulated Cyclic-Nucleotide Phosphodiesterases by Erythro-9-(2-Hydroxy-3-Nonyl) Adenine. *Cellular signalling* **7**, 733-738, doi:Doi 10.1016/0898-6568(95)00042-N (1995).
- 276 Keravis, T. & Lugnier, C. Cyclic Nucleotide Phosphodiesterases (PDE) and Peptide Motifs. *Current pharmaceutical design* **16**, 1114-1125 (2010).
- 277 Schaeffer, H. J. & Schwender, C. F. Enzyme inhibitors. 26. Bridging hydrophobic and hydrophilic regions on adenosine deaminase with some 9-(2-hydroxy-3-alkyl)adenines. *Journal of medicinal chemistry* **17**, 6-8 (1974).
- 278 Boess, F. G. *et al.* Inhibition of phosphodiesterase 2 increases neuronal cGMP, synaptic plasticity and memory performance. *Neuropharmacology* **47**, 1081-1092, doi:10.1016/j.neuropharm.2004.07.040 (2004).
- 279 Seybold, J. *et al.* Tumor necrosis factor-alpha-dependent expression of phosphodiesterase 2: role in endothelial hyperpermeability. *Blood* **105**, 3569-3576, doi:10.1182/blood-2004-07-2729 (2005).

- 280 Chambers, R. J. *et al.* A new chemical tool for exploring the physiological function of the PDE2 isozyme. *Bioorg Med Chem Lett* **16**, 307-310, doi:10.1016/j.bmcl.2005.10.005 (2006).
- 281 Wechsler, J. *et al.* Isoforms of cyclic nucleotide phosphodiesterase PDE3A in cardiac myocytes. *The Journal of biological chemistry* **277**, 38072-38078, doi:10.1074/jbc.M203647200 (2002).
- 282 Omori, K. & Kotera, J. Overview of PDEs and their regulation. *Circulation research* **100**, 309-327, doi:10.1161/01.Res.0000256354.95791.F1 (2007).
- 283 Dunkerley, H. A. *et al.* Reduced phosphodiesterase 3 activity and phosphodiesterase 3A level in synthetic vascular smooth muscle cells: Implications for use of phosphodiesterase 3 inhibitors in cardiovascular tissues. *Molecular pharmacology* **61**, 1033-1040, doi:DOI 10.1124/mol.61.5.1033 (2002).
- 284 Beca, S., Aschars-Sobbi, R., Panama, B. K. & Backx, P. H. Regulation of murine cardiac function by phosphodiesterases type 3 and 4. *Curr Opin Pharmacol* **11**, 714-719, doi:10.1016/j.coph.2011.10.017 (2011).
- 285 Begum, N., Hockman, S. & Manganiello, V. C. Phosphodiesterase 3A (PDE3A) Deletion Suppresses Proliferation of Cultured Murine Vascular Smooth Muscle Cells (VSMCs) via Inhibition of Mitogen-activated Protein Kinase (MAPK) Signaling and Alterations in Critical Cell Cycle Regulatory Proteins. *Journal of Biological Chemistry* **286**, 26238-26249, doi:10.1074/jbc.M110.214155 (2011).
- 286 Sun, B. *et al.* Role of phosphodiesterase type 3A and 3B in regulating platelet and cardiac function using subtype-selective knockout mice. *Cellular signalling* **19**, 1765-1771, doi:10.1016/j.cellsig.2007.03.012 (2007).
- 287 Dunkerley, H. A. *et al.* Reduced phosphodiesterase 3 activity and phosphodiesterase 3A level in synthetic vascular smooth muscle cells: implications for use of phosphodiesterase 3 inhibitors in cardiovascular tissues. *Molecular pharmacology* **61**, 1033-1040 (2002).
- 288 Begum, N., Hockman, S. & Manganiello, V. C. Phosphodiesterase 3A (PDE3A) deletion suppresses proliferation of cultured murine vascular smooth muscle cells (VSMCs) via inhibition of mitogen-activated protein kinase (MAPK) signaling and alterations in critical cell cycle regulatory proteins. *The Journal of biological chemistry* **286**, 26238-26249, doi:10.1074/jbc.M110.214155 (2011).

- 289 Choi, Y. H. *et al.* Alterations in regulation of energy homeostasis in cyclic nucleotide phosphodiesterase 3B-null mice. *Journal of Clinical Investigation* **116**, 3240-3251, doi:10.1172/JCI24867 (2006).
- 290 Zmuda-Trzebiatowska, E., Oknianska, A., Manganiello, V. & Degerman, E. Role of PDE3B in insulin-induced glucose uptake, GLUT-4 translocation and lipogenesis in primary rat adipocytes. *Cellular signalling* **18**, 382-390, doi:10.1016/j.cellsig.2005.05.007 (2006).
- 291 Hidaka, H. *et al.* Selective inhibitor of platelet cyclic adenosine monophosphate phosphodiesterase, cilostamide, inhibits platelet aggregation. *The Journal of pharmacology and experimental therapeutics* **211**, 26-30 (1979).
- 292 Houslay, M. D., Baillie, G. S. & Maurice, D. H. cAMP-Specific phosphodiesterase-4 enzymes in the cardiovascular system: a molecular toolbox for generating compartmentalized cAMP signaling. *Circulation research* **100**, 950-966, doi:10.1161/01.RES.0000261934.56938.38 (2007).
- 293 Conti, M. *et al.* Cyclic AMP-specific PDE4 phosphodiesterases as critical components of cyclic AMP signaling. *Journal of Biological Chemistry* **278**, 5493-5496, doi:10.1074/jbc.R200029200 (2003).
- 294 Bolger, G. *et al.* A Family of Human Phosphodiesterases Homologous to the Dunce Learning and Memory Gene-Product of *Drosophila-Melanogaster* Are Potential Targets for Antidepressant Drugs. *Molecular and cellular biology* **13**, 6558-6571 (1993).
- 295 Beard, M. B. *et al.* UCR1 and UCR2 domains unique to the cAMP-specific phosphodiesterase family form a discrete module via electrostatic interactions. *Journal of Biological Chemistry* **275**, 10349-10358, doi:DOI 10.1074/jbc.275.14.10349 (2000).
- 296 Rena, G. *et al.* Molecular cloning, genomic positioning, promoter identification, and characterization of the novel cyclic AMP-specific phosphodiesterase PDE4A10. *Molecular pharmacology* **59**, 996-1011 (2001).
- 297 Wallace, D. A. *et al.* Identification and characterization of PDE4A11, a novel, widely expressed long isoform encoded by the human PDE4A cAMP phosphodiesterase gene. *Molecular pharmacology* **67**, 1920-1934, doi:10.1124/mol.104.009423 (2005).
- 298 Smith, P. G. *et al.* The phosphodiesterase PDE4B limits cAMP-associated PI3K/AKT-dependent apoptosis in diffuse large B-cell lymphoma. *Blood* **105**, 308-316, doi:10.1182/blood-2004-01-0240 (2005).



- 299 Wang, P., Wu, P., Ohleth, K. M., Egan, R. W. & Billah, M. M. Phosphodiesterase 4B2 is the predominant phosphodiesterase species and undergoes differential regulation of gene expression in human monocytes and neutrophils. *Molecular pharmacology* **56**, 170-174 (1999).
- 300 Engels, P., Sullivan, M., Muller, T. & Lubbert, H. Molecular cloning and functional expression in yeast of a human cAMP-specific phosphodiesterase subtype (PDE IV-C). *FEBS letters* **358**, 305-310 (1995).
- 301 Houslay, M. D. & Adams, D. R. PDE4 cAMP phosphodiesterases: modular enzymes that orchestrate signalling cross-talk, desensitization and compartmentalization. *Biochemical Journal* **370**, 1-18, doi:Doi 10.1042/Bj20021698 (2003).
- 302 Jin, S. L. C. & Conti, M. Induction of the cyclic nucleotide phosphodiesterase PDE4B is essential for LPS-activated TNF-alpha responses. *Proceedings of the National Academy of Sciences of the United States of America* **99**, 7628-7633, doi:10.1073/pnas.122041599 (2002).
- 303 Jin, S. L. C., Lan, L., Zoudilova, M. & Conti, M. Specific role of phosphodiesterase 4B in lipopolysaccharide-induced signaling in mouse macrophages. *Journal of immunology* **175**, 1523-1531 (2005).
- 304 Lehnart, S. E. *et al.* Phosphodiesterase 4D deficiency in the ryanodine-receptor complex promotes heart failure and arrhythmias. *Cell* **123**, 25-35, doi:10.1016/j.cell.2005.07.030 (2005).
- 305 Coquil, J. F., Franks, D. J., Wells, J. N., Dupuis, M. & Hamet, P. Characteristics of a new binding protein distinct from the kinase for guanosine 3':5'-monophosphate in rat platelets. *Biochimica et biophysica acta* **631**, 148-165 (1980).
- 306 Francis, S. H., Lincoln, T. M. & Corbin, J. D. Characterization of a novel cGMP binding protein from rat lung. *The Journal of biological chemistry* **255**, 620-626 (1980).
- 307 Hamet, P. & Coquil, J. F. Cyclic GMP binding and cyclic GMP phosphodiesterase in rat platelets. *Journal of cyclic nucleotide research* **4**, 281-290 (1978).
- 308 Turko, I. V., Francis, S. H. & Corbin, J. D. Binding of cGMP to both allosteric sites of cGMP-binding cGMP-specific phosphodiesterase (PDE5) is required for its phosphorylation. *Biochemical Journal* **329**, 505-510 (1998).



- 309 Zoraghi, R., Bessay, E. P., Corbin, J. D. & Francis, S. H. Structural and functional features in human PDE5A1 regulatory domain that provide for allosteric cGMP binding, dimerization, and regulation. *Journal of Biological Chemistry* **280**, 12051-12063, doi:10.1074/jbc.M413611200 (2005).
- 310 Kotera, J. *et al.* Genomic origin and transcriptional regulation of two variants of cGMP-binding cGMP-specific phosphodiesterases. *European Journal of Biochemistry* **262**, 866-872, doi:DOI 10.1046/j.1432-1327.1999.00450.x (1999).
- 311 Lin, C. S., Lau, A., Tu, R. & Lue, T. F. Expression of three isoforms of cGMP-binding cGMP-specific phosphodiesterase (PDE5) in human penile cavernosum. *Biochemical and biophysical research communications* **268**, 628-635, doi:10.1006/bbrc.2000.2187 (2000).
- 312 Loughney, K. *et al.* Isolation and characterization of cDNAs encoding PDE5A, a human cGMP-binding, cGMP-specific 3',5'-cyclic nucleotide phosphodiesterase. *Gene* **216**, 139-147, doi:Doi 10.1016/S0378-1119(98)00303-5 (1998).
- 313 Corbin, J. D. Mechanisms of action of PDE5 inhibition in erectile dysfunction. *International journal of impotence research* **16**, S4-S7, doi:10.1038/sj.ijir.3901205 (2004).
- 314 Francis, S. H., Morris, G. Z. & Corbin, J. D. Molecular mechanisms that could contribute to prolonged effectiveness of PDE5 inhibitors to improve erectile function. *International journal of impotence research* **20**, 333-342, doi:10.1038/ijir.2008.4 (2008).
- 315 Rosen, R. C. & Kostis, J. B. Overview of phosphodiesterase 5 inhibition in erectile dysfunction. *American Journal of Cardiology* **92**, 9M-18M, doi:10.1016/S0002-9149(03)00824-5 (2003).
- 316 Dunkem, T. R. & Hatzelmann, A. The effect of Sildenafil on human platelet secretory function is controlled by a complex interplay between phosphodiesterases 2, 3 and 5. *Cellular signalling* **17**, 331-339, doi:10.1016/j.cellsig.2004.07.007 (2005).
- 317 Ito, M. *et al.* Characterization of the isoenzymes of cyclic nucleotide phosphodiesterase in human platelets and the effects of E4021. *Cellular signalling* **8**, 575-581, doi:Doi 10.1016/S0898-6568(96)00112-X (1996).
- 318 Prickaerts, J. *et al.* Phosphodiesterase type 5 inhibition improves early memory consolidation of object information. *Neurochemistry international* **45**, 915-928, doi:10.1016/j.neuint.2004.03.022 (2004).

- 319 Kass, D. A., Champion, H. C. & Beavo, J. A. Phosphodiesterase type 5 - Expanding roles in cardiovascular regulation. *Circulation research* **101**, 1084-1095, doi:10.1161/Circresaha.107.162511 (2007).
- 320 Kukreja, R. C. *et al.* Cardioprotection with phosphodiesterase-5 inhibition - a novel preconditioning strategy. *Journal of molecular and cellular cardiology* **36**, 165-173, doi:10.1016/j.yjmcc.2003.11.001 (2004).
- 321 Kumar, P., Francis, G. S. & Tang, W. H. W. Phosphodiesterase 5 inhibition in heart failure: mechanisms and clinical implications. *Nature Reviews Cardiology* **6**, 349-355, doi:10.1038/nrcardio.2009.32 (2009).
- 322 Takimoto, E. *et al.* Chronic inhibition of cyclic GMP phosphodiesterase 5A prevents and reverses cardiac hypertrophy. *Nat Med* **11**, 214-222, doi:10.1038/nm1175 (2005).
- 323 Lugnier, C., Schoeffter, P., Lebec, A., Strouthou, E. & Stoclet, J. C. Selective-Inhibition of Cyclic-Nucleotide Phosphodiesterases of Human, Bovine and Rat Aorta. *Biochemical pharmacology* **35**, 1743-1751, doi:Doi 10.1016/0006-2952(86)90333-3 (1986).
- 324 Dugan, A. *et al.* The discovery of tadalafil: A novel and highly selective PDE5 inhibitor. 1: 5,6,11,11a-tetrahydro-1H-imidazo[1',5':1,6]pyrido[3,4-b]indole-1,3(2H)-dione analogues. *Journal of medicinal chemistry* **46**, 4525-4532, doi:10.1021/jm030056e (2003).
- 325 Tcheudji, J. F. K. *et al.* Molecular organization of bovine rod cGMP-phosphodiesterase 6. *J Mol Biol* **310**, 781-791, doi:DOI 10.1006/jmbi.2001.4813 (2001).
- 326 Ridge, K. D., Abdulaev, N. G., Sousa, M. & Palczewski, K. Phototransduction: crystal clear. *Trends in biochemical sciences* **28**, 479-487, doi:10.1016/S0968-0004(03)00172-5 (2003).
- 327 Morin, F., Lugnier, C., Kameni, J. & Voisin, P. Expression and role of phosphodiesterase 6 in the chicken pineal gland. *Journal of neurochemistry* **78**, 88-99 (2001).
- 328 Pugh, E. N. Transfected cyclic nucleotide-gated channels as biosensors. *Journal of General Physiology* **116**, 143-145, doi:DOI 10.1085/jgp.116.2.143 (2000).
- 329 Michaeli, T. *et al.* Isolation and characterization of a previously undetected human cAMP phosphodiesterase by complementation of cAMP phosphodiesterase-deficient *Saccharomyces cerevisiae*. *The Journal of biological chemistry* **268**, 12925-12932 (1993).

- 330 Han, P., Zhu, X. & Michaeli, T. Alternative splicing of the high affinity cAMP-specific phosphodiesterase (PDE7A) mRNA in human skeletal muscle and heart. *The Journal of biological chemistry* **272**, 16152-16157 (1997).
- 331 Sasaki, T., Kotera, J., Yuasa, K. & Omori, K. Identification of human PDE7B, a cAMP-specific phosphodiesterase. *Biochemical and biophysical research communications* **271**, 575-583, doi:10.1006/bbrc.2000.2661 (2000).
- 332 Smith, S. J. *et al.* Ubiquitous expression of phosphodiesterase 7A in human proinflammatory and immune cells. *American journal of physiology. Lung cellular and molecular physiology* **284**, L279-289, doi:10.1152/ajplung.00170.2002 (2003).
- 333 Li, L., Yee, C. & Beavo, J. A. CD3- and CD28-dependent induction of PDE7 required for T cell activation. *Science* **283**, 848-851 (1999).
- 334 Zhang, L. Z. *et al.* Cyclic nucleotide phosphodiesterase 7B mRNA: an unfavorable characteristic in chronic lymphocytic leukemia. *International Journal of Cancer* **129**, 1162-1169, doi:10.1002/ijc.25785 (2011).
- 335 Banerjee, A. *et al.* Imidazopyridazinones as novel PDE7 inhibitors: SAR and in vivo studies in Parkinson's disease model. *Bioorg Med Chem Lett* **22**, 6286-6291, doi:10.1016/j.bmcl.2012.07.077 (2012).
- 336 Kadoshima-Yamaoka, K. *et al.* ASB16165, a novel inhibitor for phosphodiesterase 7A (PDE7A), suppresses IL-12-induced IFN-gamma production by mouse activated T lymphocytes. *Immunol Lett* **122**, 193-197, doi:10.1016/j.imlet.2009.01.004 (2009).
- 337 Zhang, L. Z. *et al.* Cyclic nucleotide phosphodiesterase profiling reveals increased expression of phosphodiesterase 7B in chronic lymphocytic leukemia. *Proceedings of the National Academy of Sciences of the United States of America* **105**, 19532-19537, doi:10.1073/pnas.0806152105 (2008).
- 338 Gamanuma, M. *et al.* Comparison of enzymatic characterization and gene organization of cyclic nucleotide phosphodiesterase 8 family in humans. *Cellular signalling* **15**, 565-574 (2003).
- 339 Soderling, S. H., Bayuga, S. J. & Beavo, J. A. Cloning and characterization of a cAMP-specific cyclic nucleotide phosphodiesterase. *Proceedings of the National Academy of Sciences of the United States of America* **95**, 8991-8996 (1998).

- 340 Wang, P., Wu, P., Egan, R. W. & Billah, M. M. Human phosphodiesterase 8A splice variants: cloning, gene organization, and tissue distribution. *Gene* **280**, 183-194, doi:DOI 10.1016/S0378-1119(01)00783-1 (2001).
- 341 Dunlap, J. C., Loros, J. J., Liu, Y. & Crosthwaite, S. K. Eukaryotic circadian systems: cycles in common. *Genes Cells* **4**, 1-10, doi:DOI 10.1046/j.1365-2443.1999.00239.x (1999).
- 342 Galperin, M. Y., Nikolskaya, A. N. & Koonin, E. V. Novel domains of the prokaryotic two-component signal transduction systems. *FEMS microbiology letters* **203**, 11-21, doi:DOI 10.1111/j.1574-6968.2001.tb10814.x (2001).
- 343 Fisher, D. A., Smith, J. F., Pillar, J. S., St Denis, S. H. & Cheng, J. B. Isolation and characterization of PDE8A, a novel human cAMP-specific phosphodiesterase. *Biochemical and biophysical research communications* **246**, 570-577, doi:DOI 10.1006/bbrc.1998.8684 (1998).
- 344 Hayashi, M. *et al.* Molecular cloning and characterization of human PDE8B, a novel thyroid-specific isozyme of 3',5'-cyclic nucleotide phosphodiesterase. *Biochemical and biophysical research communications* **250**, 751-756, doi:DOI 10.1006/bbrc.1998.9379 (1998).
- 345 Dong, H. L., Osmanova, V., Epstein, P. M. & Brocke, S. Phosphodiesterase 8 (PDE8) regulates chemotaxis of activated lymphocytes. *Biochemical and biophysical research communications* **345**, 713-719, doi:10.1016/j.bbrc.2006.04.143 (2006).
- 346 Vang, A. G. *et al.* PDE8 Regulates Rapid Tef Cell Adhesion and Proliferation Independent of ICER. *PloS one* **5**, doi:ARTN e12011 10.1371/journal.pone.0012011 (2010).
- 347 Patrucco, E., Albergine, M. S., Santana, L. F. & Beavo, J. A. Phosphodiesterase 8A (PDE8A) regulates excitation-contraction coupling in ventricular myocytes. *Journal of molecular and cellular cardiology* **49**, 330-333, doi:10.1016/j.yjmcc.2010.03.016 (2010).
- 348 Tsai, L. C. L., Shimizu-Albergine, M. & Beavo, J. A. The High-Affinity cAMP-Specific Phosphodiesterase 8B Controls Steroidogenesis in the Mouse Adrenal Gland. *Molecular pharmacology* **79**, 639-648, doi:10.1124/mol.110.069104 (2011).
- 349 Rentero, C., Monfort, A. & Puigdomenech, P. Identification and distribution of different mRNA variants produced by differential splicing in the human

- phosphodiesterase 9A gene. *Biochemical and biophysical research communications* **301**, 686-692 (2003).
- 350 Wang, P., Wu, P., Egan, R. W. & Billah, M. M. Identification and characterization of a new human type 9 cGMP-specific phosphodiesterase splice variant (PDE9A5). Differential tissue distribution and subcellular localization of PDE9A variants. *Gene* **314**, 15-27 (2003).
  - 351 Schmidt, C. J. Phosphodiesterase Inhibitors as Potential Cognition Enhancing Agents. *Curr Top Med Chem* **10**, 222-230 (2010).
  - 352 Guipponi, M. *et al.* Identification and characterization of a novel cyclic nucleotide phosphodiesterase gene (PDE9A) that maps to 21q22.3: alternative splicing of mRNA transcripts, genomic structure and sequence. *Hum Genet* **103**, 386-392, doi:DOI 10.1007/s004390050838 (1998).
  - 353 Hutson, P. H. *et al.* The selective phosphodiesterase 9 (PDE9) inhibitor PF-04447943 (6-[(3S,4S)-4-methyl-1-(pyrimidin-2-ylmethyl)pyrrolidin-3-yl]-1-(tetrahydro-2H-pyran-4-yl)-1,5-dihydro-4H-pyrazolo[3,4-d]pyrimidin-4-one) enhances synaptic plasticity and cognitive function in rodents. *Neuropharmacology* **61**, 665-676, doi:10.1016/j.neuropharm.2011.05.009 (2011).
  - 354 Fujishige, K. *et al.* Cloning and characterization of a novel human phosphodiesterase that hydrolyzes both cAMP and cGMP (PDE10A). *Journal of Biological Chemistry* **274**, 18438-18445, doi:DOI 10.1074/jbc.274.26.18438 (1999).
  - 355 Loughney, K. *et al.* Isolation and characterization of PDE10A, a novel human 3', 5'-cyclic nucleotide phosphodiesterase. *Gene* **234**, 109-117 (1999).
  - 356 Fujishige, K., Kotera, J. & Omori, K. Striatum- and testis-specific phosphodiesterase PDE10A isolation and characterization of a rat PDE10A. *European journal of biochemistry / FEBS* **266**, 1118-1127 (1999).
  - 357 Seeger, T. F. *et al.* Immunohistochemical localization of PDE10A in the rat brain. *Brain research* **985**, 113-126 (2003).
  - 358 Hebb, A. L. O., Robertson, H. A. & Denovan-Wright, E. M. Striatal phosphodiesterase mRNA and protein levels are reduced in Huntington's disease transgenic mice prior to the onset of motor symptoms. *Neuroscience* **123**, 967-981, doi:10.1016/j.neuroscience.2003.11.009 (2004).
  - 359 Hu, H., McCaw, E. A., Hebb, A. L., Gomez, G. T. & Denovan-Wright, E. M. Mutant huntingtin affects the rate of transcription of striatum-specific isoforms

- of phosphodiesterase 10A. *The European journal of neuroscience* **20**, 3351-3363, doi:10.1111/j.1460-9568.2004.03796.x (2004).
- 360 Kleiman, R. J. *et al.* Chronic Suppression of Phosphodiesterase 10A Alters Striatal Expression of Genes Responsible for Neurotransmitter Synthesis, Neurotransmission, and Signaling Pathways Implicated in Huntington's Disease. *Journal of Pharmacology and Experimental Therapeutics* **336**, 64-76, doi:10.1124/jpet.110.173294 (2011).
  - 361 Siuciak, J. A. *et al.* Genetic deletion of the striatum-enriched phosphodiesterase PDE10A: Evidence for altered striatal function. *Neuropharmacology* **51**, 374-385, doi:10.1016/j.neuropharm.2006.01.012 (2006).
  - 362 Siuciak, J. A. *et al.* Inhibition of the striatum-enriched phosphodiesterase PDEIOA: A novel approach to the treatment of psychosis. *Neuropharmacology* **51**, 386-396, doi:10.1016/j.neuropharm.2006.04.013 (2006).
  - 363 Schmidt, C. J. *et al.* Preclinical characterization of selective phosphodiesterase 10A inhibitors: a new therapeutic approach to the treatment of schizophrenia. *The Journal of pharmacology and experimental therapeutics* **325**, 681-690, doi:10.1124/jpet.107.132910 (2008).
  - 364 Rodefer, J. S., Murphy, E. R. & Baxter, M. G. PDE10A inhibition reverses subchronic PCP-induced deficits in attentional set-shifting in rats. *European Journal of Neuroscience* **21**, 1070-1076, doi:10.1111/j.1460-9568.2005.03937.x (2005).
  - 365 Fawcett, L. *et al.* Molecular cloning and characterization of a distinct human phosphodiesterase gene family: PDE11A. *Proceedings of the National Academy of Sciences of the United States of America* **97**, 3702-3707, doi:DOI 10.1073/pnas.050585197 (2000).
  - 366 Hetman, J. M. *et al.* Cloning and characterization of two splice variants of human phosphodiesterase 11A. *Proceedings of the National Academy of Sciences of the United States of America* **97**, 12891-12895, doi:DOI 10.1073/pnas.200355397 (2000).
  - 367 Yuasa, K. *et al.* Isolation and characterization of two novel phosphodiesterase PDE11A variants showing unique structure and tissue-specific expression. *Journal of Biological Chemistry* **275**, 31469-31479, doi:DOI 10.1074/jbc.M003041200 (2000).
  - 368 Yuasa, K., Ohgaru, T., Asahina, M. & Omori, K. Identification of rat cyclic nucleotide phosphodiesterase 11A (PDE11A): comparison of rat and human



- PDE11A splicing variants. *European journal of biochemistry / FEBS* **268**, 4440-4448 (2001).
- 369 Yuasa, K., Kanoh, Y., Okumura, K. & Omori, K. Genomic organization of the human phosphodiesterase PDE11A gene. Evolutionary relatedness with other PDEs containing GAF domains. *European journal of biochemistry / FEBS* **268**, 168-178 (2001).
  - 370 Loughney, K., Taylor, J. & Florio, V. A. 3',5'-cyclic nucleotide phosphodiesterase 11A: localization in human tissues. *International journal of impotence research* **17**, 320-325, doi:10.1038/sj.ijir.3901317 (2005).
  - 371 D'Andrea, M. R. *et al.* Expression of PDE11A in normal and malignant human tissues. *The journal of histochemistry and cytochemistry : official journal of the Histochemistry Society* **53**, 895-903, doi:10.1369/jhc.5A6625.2005 (2005).
  - 372 Wayman, C. *et al.* Phosphodiesterase 11 (PDE11) regulation of spermatozoa physiology. *International journal of impotence research* **17**, 216-223, doi:10.1038/sj.ijir.3901307 (2005).
  - 373 Keravis, T. & Lugnier, C. Cyclic nucleotide phosphodiesterase (PDE) isozymes as targets of the intracellular signalling network: benefits of PDE inhibitors in various diseases and perspectives for future therapeutic developments. *British journal of pharmacology* **165**, 1288-1305, doi:10.1111/j.1476-5381.2011.01729.x (2012).
  - 374 Millar, J. K. *et al.* DISC1 and PDE4B are interacting genetic factors in schizophrenia that regulate cAMP signaling. *Science* **310**, 1187-1191, doi:10.1126/science.1112915 (2005).
  - 375 Acin-Perez, R. *et al.* A Phosphodiesterase 2A Isoform Localized to Mitochondria Regulates Respiration. *Journal of Biological Chemistry* **286**, 30423-30432, doi:10.1074/jbc.M111.266379 (2011).
  - 376 Zhang, F. *et al.* The cAMP phosphodiesterase Prune localizes to the mitochondrial matrix and promotes mtDNA replication by stabilizing TFAM. *EMBO reports* **16**, 520-527 (2015).
  - 377 Joubert, F. *et al.* Local energetic regulation of sarcoplasmic and myosin ATPase is differently impaired in rats with heart failure. *The Journal of physiology* **586**, 5181-5192 (2008).
  - 378 Joubert, F. *et al.* Local energetic regulation of sarcoplasmic and myosin ATPase is differently impaired in rats with heart failure. *J Physiol-London* **586**, 5181-5192, doi:10.1113/jphysiol.2008.157677 (2008).



- 379 Hubert, F. *et al.* Alteration of vascular reactivity in heart failure: role of phosphodiesterases 3 and 4. *British journal of pharmacology* **171**, 5361-5375, doi:10.1111/bph.12853 (2014).
- 380 Klarenbeek, J., Goedhart, J., van Batenburg, A., Groenewald, D. & Jalink, K. Fourth-generation epac-based FRET sensors for cAMP feature exceptional brightness, photostability and dynamic range: characterization of dedicated sensors for FLIM, for ratiometry and with high affinity. *PloS one* **10**, e0122513 (2015).
- 381 Chao, T. C. *et al.* In vivo growth suppression of CT-26 mouse colorectal cancer cells by adenovirus-expressed small hairpin RNA specifically targeting thymosin beta-4 mRNA. *Cancer Gene Ther* **21**, 389-396, doi:10.1038/cgt.2014.43 (2014).
- 382 Wang, Z., Nicolas, C., Fischmeister, R. & Brenner, C. Enzymatic assays for probing mitochondrial apoptosis. *Methods in molecular biology* **1265**, 407-414, doi:10.1007/978-1-4939-2288-8\_30 (2015).
- 383 Taussig, R. & Gilman, A. G. Mammalian Membrane-Bound Adenylyl Cyclases. *Journal of Biological Chemistry* **270**, 1-4 (1995).
- 384 Coletta, C. *et al.* Endothelial dysfunction is a potential contributor to multiple organ failure and mortality in aged mice subjected to septic shock: preclinical studies in a murine model of cecal ligation and puncture. *Critical care* **18**, doi:Artn 511  
10.1186/S13054-014-0511-3 (2014).
- 385 Marcil, M. *et al.* Compensated volume overload increases the vulnerability of heart mitochondria without affecting their functions in the absence of stress. *Journal of molecular and cellular cardiology* **41**, 998-1009, doi:10.1016/j.yjmcc.2006.08.117 (2006).
- 386 Marcil, M. *et al.* Compensated volume overload increases the vulnerability of heart mitochondria without affecting their functions in the absence of stress. *Journal of molecular and cellular cardiology* **41**, 998-1009, doi:10.1016/j.yjmcc.2006.08.117 (2006).
- 387 Metrich, M. *et al.* Role of the cAMP-binding protein Epac in cardiovascular physiology and pathophysiology. *Pflugers Archiv : European journal of physiology* **459**, 535-546, doi:10.1007/s00424-009-0747-y (2010).
- 388 Qiao, J., Mei, F. C., Popov, V. L., Vergara, L. A. & Cheng, X. Cell cycle-dependent subcellular localization of exchange factor directly activated by

- cAMP. *The Journal of biological chemistry* **277**, 26581-26586, doi:10.1074/jbc.M203571200 (2002).
- 389 Pereira, L. *et al.* Novel Epac fluorescent ligand reveals distinct Epac1 vs. Epac2 distribution and function in cardiomyocytes. *Proceedings of the National Academy of Sciences of the United States of America* **112**, 3991-3996, doi:10.1073/pnas.1416163112 (2015).
- 390 Sharma, S., Kumar, K., Deshmukh, R. & Sharma, P. L. Phosphodiesterases: Regulators of cyclic nucleotide signals and novel molecular target for movement disorders. *European journal of pharmacology* **714**, 486-497, doi:10.1016/j.ejphar.2013.06.038 (2013).
- 391 Acin-Perez, R. *et al.* A phosphodiesterase 2A isoform localized to mitochondria regulates respiration. *The Journal of biological chemistry* **286**, 30423-30432, doi:10.1074/jbc.M111.266379 (2011).
- 392 Modis, K., Panopoulos, P., Coletta, C., Papapetropoulos, A. & Szabo, C. Hydrogen sulfide-mediated stimulation of mitochondrial electron transport involves inhibition of the mitochondrial phosphodiesterase 2A, elevation of cAMP and activation of protein kinase A. *Biochem Pharmacol* **86**, 1311-1319, doi:10.1016/j.bcp.2013.08.064 (2013).
- 393 Millar, J. K. *et al.* DISC1 and PDE4B are interacting genetic factors in schizophrenia that regulate cAMP signaling. *Science* **310**, 1187-1191, doi:10.1126/science.1112915 (2005).
- 394 Asirvatham, A. L. *et al.* A-kinase anchoring proteins interact with phosphodiesterases in T lymphocyte cell lines. *J Immunol* **173**, 4806-4814 (2004).
- 395 Mongillo, M. *et al.* Fluorescence resonance energy transfer-based analysis of cAMP dynamics in live neonatal rat cardiac myocytes reveals distinct functions of compartmentalized phosphodiesterases. *Circulation research* **95**, 67-75, doi:10.1161/01.Res.0000134629.84732.11 (2004).
- 396 Martin, T. P., Currie, S. & Baillie, G. S. The cardioprotective role of small heat-shock protein 20. *Biochemical Society transactions* **42**, 270-273, doi:10.1042/BST20130272 (2014).
- 397 Asirvatham, A. L. *et al.* A-kinase anchoring proteins interact with phosphodiesterases in T lymphocyte cell lines. *Journal of immunology* **173**, 4806-4814 (2004).

## **7 Annexes**

**Article 1: Enzymatic assays for probing mitochondrial apoptosis**

**Article 2: VDAC phosphorylation, a lipid sensor influencing the cell fate**

**Article 3: The protein disulfide isomerases PDIA4 and PDIA6 mediate resistance to cisplatin-induced cell death in lung adenocarcinoma**

## **Enzymatic assays for probing mitochondrial apoptosis**

**Zhenyu Wang<sup>1,2</sup>, Claire Nicolas<sup>1,2</sup>, Rodolphe Fischmeister<sup>1,2</sup> and  
Catherine Brenner<sup>1,2</sup>**

<sup>1</sup>: INSERM UMR-S 769, LabEx LERMIT, Châtenay-Malabry, France; <sup>2</sup>: Université de Paris-Sud,  
Faculté de Pharmacie, Châtenay-Malabry, France

Correspondence to: Dr. Catherine Brenner, INSERM UMR-S 769, Université de  
Paris-Sud, LabEx LERMIT, 5 rue Baptiste Clément,  
Châtenay-Malabry, France;  
E-mail: [catherine.brenner-jan@u-psud.fr](mailto:catherine.brenner-jan@u-psud.fr)

## Summary

Isolated mitochondria are an invaluable analytical tool to probe mitochondrial function and evaluate apoptosis induction via the so-called mitochondrial pathway. Irrespective of their tissue origin (e.g. heart, liver, muscle, brain), these organelles participate actively to cell and life decision by producing energy for cell metabolism, but also by undergoing a lethal and irreversible mitochondrial membrane permeabilization (MMP) in stress and pathological conditions. MMP consequences consist, at least in part, in loss of mitochondrial transmembrane potential ( $\Delta\Psi_m$ ), matrix swelling, arrest of respiration and ATP production, and cytochrome *c* release from the intermembrane space to the cytosol. These parameters can be evaluated *in vitro* via several miniaturized assays, which have tremendous applications in the field of pharmacology, toxicology, diagnosis as well as drug discovery.

**Key words:** apoptosis, cytochrome *c*, fluorescence, heart, inner transmembrane potential, mitochondria.

## 1 Introduction

During mitochondrial apoptosis, mitochondrial membrane permeabilization (MMP) has been previously defined as an irreversible process that leads to the cell death (1-3). Thus, MMP influences functional and morphological features of mitochondria depending on the nature, the intensity and the duration of the pro-apoptotic signal. Main stimuli of MMP are ions such as calcium ( $\text{Ca}^{2+}$ ), reactive oxygen species (ROS) (e.g. anion superoxide, hydrogen peroxide), proteins (e.g. BAX, BID) and lipids and target the inner membrane, the outer membrane or both. Then, MMP results in loss of transmembrane potential ( $\Delta\Psi_m$ ), matrix swelling, arrest of respiration and ATP production, ROS and cytochrome *c* release from the intermembrane space to the cytosol (4-6). In some tissues such as the heart, abnormal mitochondrial fusion and fission can accompany mitochondrial apoptosis, but its contribution as cause *vs* a consequence remains to be defined. Some of MMP parameters can be easily measured *in vitro* via several miniaturized assays to gain insights into pro-apoptotic mitochondrial alterations.

Here, we described the methods for (1) the isolation of fresh mitochondria from rat heart by a procedure adapted to the myofibrillar structure of the tissue, (2) the subsequent quantification of  $\Delta\Psi_m$  by a fluorescent probe Rhodamine 123 (7) and the colloidosmotic matrix swelling by spectrophotometry (8), (3) the oxygen consumption by the phosphorescent probe Mito-ID® (9), and (4) the release of intermembrane space proteins, such as cytochrome *c* by western-blot (10). These assays are demonstrated to be useful analytical tools as well as high throughput screening tools implemented on technological platforms. Hence, they could have broad applications in the field of pharmacology, toxicology, and diagnosis as well as drug discovery.

## 2 Materials

All chemicals need to be of the highest purity available. All the reagents are from Sigma unless indicated otherwise. Ultrapure water is systematically used.

## 2.1 Isolation buffers

1. Buffer H: weigh 102.8g sucrose, 1.146g 2-[[1,3-dihydroxy-2-(hydroxymethyl)propan-2-yl]amino]ethanesulfonic acid (TES), 76mg ethylene glycol tetraacetic acid (EGTA). Add water to a volume of 900mL. Mix and adjust pH to 7.2 with potassium hydroxide (KOH), add water to a volume of 1 L. Mix and aliquot into 50mL tubes and store at -20°C.
2. Buffer H<sup>+</sup> Bovine serum albumin (BSA): weigh 102.8g sucrose, 1.146g TES, 76mg EGTA, 1g BSA. Add water to a volume of 950mL. Mix and adjust pH to 7.2 with KOH. Complete to 1L with water. Aliquot into 50mL and store at -20°C.

## 2.2 Mitochondria membrane potential and swelling

1. Buffer S: weigh 68.46g sucrose, 2.09g 3-(N-morpholino)propanesulfonic acid (MOPS), 3.8mg EGTA, 82μL Phosphoric acid (H<sub>3</sub>PO<sub>4</sub>). Add water to a volume of 950mL. Mix and adjust pH to 7.4 with KOH. Complete to 1 L with water. Aliquot into 50mL tubes and store at -20°C.
2. Succinate stock solution: weigh 1.35g succinate; adjust the volume to 10mL with water to get a concentration of 500mM. Aliquot and store at -20°C.
3. Rotenone stock solution: dissolve 6.99mg of rotenone in 10mL of absolute ethanol to a concentration of 2mM. Aliquot and store at -20°C. (see **Note 1**)
4. Rhodamine 123 stock solution: weigh 3.81mg rhodamine 123 (Invitrogen), make up to 10mL with absolute ethanol to get a concentration of 1mM. Store at -20°C. (see **Note 2**)

## 2.3 Oxygen consumption

1. Measurement buffer: 250mM sucrose, 15mM Potassium chloride (KCl), 1mM EGTA, 5mM Magnesium chloride (MgCl<sub>2</sub>), 30mM Potassium phosphate dibasic (K<sub>2</sub>HPO<sub>4</sub>), pH 7.4
2. Reconstitute Mito-ID® Extracellular O<sub>2</sub> Sensor kit (Enzo Life Sciences, Inc.) in 1mL of nuclease-free water or media to obtain a 1μM stock solution. Mix gently. Aliquot into 100μL in tubes and store at -20°C. (see **Note 3**)



3. Succinate stock solution: use the same as for membrane potential and swelling measurement.
4. Glutamate stock solution: weigh 0.94g glutamate, add water to 10mL to a concentration of 500mM. Aliquot and store at -20°C.
5. Malate stock solution: weigh 0.45g malate, add water to 10mL to obtain a concentration of 500mM. Aliquot and store at -20°C.
6. ADP stock solution: weigh 0.7g ADP, make up to 10mL with water to a concentration of 165mM. Aliquot and store at -20°C.

## **2.4 SDS Polyacrylamide Gel**

1. Loading buffer (5×): Tris 300mM, Glycerol 50%, sodium dodecylsulfate (SDS) 12.5%, dithiothreitol (DTT) 50mM, BromoPhenol Blue 0.05%, pH 6.8.
2. 4-15% precast gel (BioRad Mini- PROTEAN TGX)
3. Migration buffer (10×): weigh 30g Tris Base, 144g Glycine, 10g SDS. Add water to a volume of 950mL. Mix and adjust pH to 8.3. Complete to 1 L with water.
4. DTT (10×): weigh 1.54g DTT, make up to 10mL with water. Aliquot and store at -20°C.

## **2. 5 Immunoblot**

1. Membrane (Trans-Blot Turbo Transfer Pack Bio-Rad)
2. Trans-blot Turbo transfer system (Bio-Rad)
3. Phosphate buffered saline (PBS)-Tween (10×): weigh 624mg Sodium dihydrogen phosphate monohydrate ( $\text{NaH}_2\text{PO}_4$ ) 2.98g  $\text{Na}_2\text{HPO}_4$  - Sodium phosphate dibasic ( $\text{Na}_2\text{HPO}_4$ ), 204.5g Sodium chloride ( $\text{NaCl}$ ), 12.5mL Tween 20, make up to 2.5L with water.
4. Antibody anti-cytochrome *c* (BD Pharmingen)
5. Ultra-sensitive enhanced chemiluminescent (ECL) substrate, e.g. Supersignal West Femto Maximum Sensitivity Substrate (Thermo Scientific)
6. Gel imaging system, e.g. Chemidoc (BioRad)

### **3. Methods**

#### **3.1 Rat heart isolated mitochondria**

1. Kill the rat after injection of pentobarbital and excise the heart rapidly and place it in cold buffer H. (see **Note 4**)
2. Rinse the heart free of blood by using ice-cold buffer H.
3. Cut the heart into pieces in 10mL of Buffer H with a scalpel blade and transfer them into a 50mL falcon tube.
4. Grind the heart with the Polytron 2-3 times rapidly. (see **Note 5**)
5. Use the Potter to homogenize the mix.
6. Transfer the homogenate to a 15mL Falcon tube and add 5mL of Buffer H with BSA to fill the tube to 15mL.
7. Centrifuge at 500 g for 10 min at 4°C. (see **Note 6**)
8. Collect the supernatant by eliminating the maximum of lipids and discard the pellet. (see **Note 7**) Centrifuge at 3,000 g for 10 min at 4°C, 2 times (see **Note 8**).
9. Discard the supernatant and gently resuspend the pellet containing mitochondria in 200 $\mu$ L Buffer H without BSA. (see **Note 9**)
10. Determine protein concentration in an aliquot by the BCA method following manufacturer's instruction using bovine serum albumin as standard. Keep the mitochondria on ice until use. (see **Note 10**)

#### **3.2 Mitochondrial transmembrane potential ( $\Delta\Psi_m$ ) and swelling**

1. Prepare buffer S with final concentration of 5mM succinate and 2 $\mu$ M rotenone.
2. Prepare compounds (calcium as control of pro-apoptotic inducer or compound to be tested) in 4 $\times$  concentrations with buffer S. (see **Note 11**)
3. Add 50 $\mu$ L of compounds or buffer S (control) per well of microtiter plate 96 wells black with transparent and flat bottom.
4. Add 50 $\mu$ L of buffer S per well.
5. Dilute freshly isolated cardiac mitochondria at 0.25  $\mu$ g/ $\mu$ L with buffer S and add rhodamine 123 to obtain a final concentration of 1 $\mu$ M. Add 100 $\mu$ L of mitochondria in each well. (see **Note 12**)

6. Shake the plate for 5s and then start to measure for 60min with 2 parameters at room temperature. For membrane potential, measure the fluorescence at  $\lambda_{\text{ex}} = 485\text{nm}$  and  $\lambda_{\text{em}} = 535\text{nm}$ . For swelling, measure absorbance at 540nm.

### 3.3 Oxygen consumption

1. Warm up a microtiter plate 96 wells black flat bottom to 30°C.
2. For compound testing, prepare compounds at 10 $\times$  and add 20 $\mu\text{L}$  in the well. (see **Note 8**)
3. Dilute the respiratory substrate (glutamate/malate for complex I or succinate for complex II) with measurement buffer and add 20 $\mu\text{L}$  of this solution to obtain concentrations of 5mM (succinate) or 12.5/12.5 mM (glutamate/malate).
4. Dilute mitochondria suspension to 0.5 $\mu\text{g}/\mu\text{L}$  with measurement buffer and add 100 $\mu\text{L}$  to each well. (see **Note13**)
5. Dilute ADP with measurement buffer and add 20 $\mu\text{L}$  to obtain a final concentration of 1.65mM.
6. Add 30 $\mu\text{L}$  of measurement buffer to each well.
7. Add 10 $\mu\text{L}$  Mito-ID® Extracellular O<sub>2</sub> Sensor probe in each well. (see **Note 14**)
8. Using a syringe dispenser, quickly add 100 $\mu\text{L}$  of oil to each well. (see **Note 15**)
9. Insert the plate into a fluorescence plate reader pre-warmed to 30°C. Measure the probe signal for 30-60 min using excitation and emission wavelengths of 380nm and 650nm respectively. (see **Note 16**)

### 3.4 Cytochrome *c* release

1. Use the same reaction system as membrane potential to increase the volume by 75 times. The final volume is 15mL (see **Note 12**). Incubate mitochondria with the compounds or buffer (control) for 30min.
2. Centrifuge at 9,000 *g* for 15min at 4°C.
3. Collect supernatant in acetone-compatible tube.
4. Add four times the sample volume of cold acetone to the tube. (see **Note 17**)
5. Vortex the tube and incubate overnight at -20°C.

6. Centrifuge at 15,000 *g* for 15 min at 4°C.
7. Decant and properly collect of the supernatant. (see **Note 18**)
8. Allow the acetone to evaporate from the uncapped tube at room temperature for 30 min.
9. Add 20μL of water and vortex thoroughly to dissolve protein pellet.
10. Take the same volume to measure cytochrome *c* by SDS-PAGE and immunoblot.

### **3.5 SDS-PAGE and western blot**

1. Add 14μL of cytochrome *c* samples, 4μL of loading buffer (5×), 2μL of DTT (10×) into an eppendorf tube, mix and heat for 5min at 95°C.
2. Load the samples in the precast gel.
3. Migrate for 15min at 300V.
4. Place the membrane and bottom stack on the cassette base, place the gel on top of membrane, roll the assembled sandwich to expel trapped air bubbles. Close and lock the cassette lid. Transfer for 3min at 2.5V.
5. Block the membrane with 5% of milk in PBS-Tween.
6. Incubate membrane with diluted anti-cytochrome *c* primary antibody in 5% w/v milk PBS-Tween at 4°C with gentle shaking, overnight.
7. Wash the membrane with PBS-Tween for 6×5min.
8. Incubate the membrane with Horseradish Peroxidase-Conjugated secondary antibody for 1h at room temperature.
9. Wash the membrane with PBS-Tween for 6×5min.
10. Incubate the membrane with an ultra-sensitive enhanced chemiluminescent substrate for 5min.
11. Take images with a gel imaging system.

### **3.5 Statistical analysis**

Data can be analyzed using Student's *t*-test and two-way ANOVA for comparisons of mean values to the different treatments tested. Results are presented as the mean ±

standard deviation (SD) of replicates experiments. Significance: \*:  $p < 0.05$ , \*\*:  $p < 0.01$ ; \*\*\*:  $p < 0.001$ . Significance is not shown in the figures for clarity reasons.

## Notes

Note 1: Rotenone in organic solvents decomposes and is oxidized upon exposure to light and air. It is imperative to protect the stock solution from direct light by using an aluminium foil. Rotenone is highly toxic: avoid skin contact and inhalation.

Note 2: Rhodamine 123 is light sensitive, so keep it in aluminium foil and avoid exposure to light for long time.

Note 3: Protect the stock solution from direct light by using an aluminium foil. Avoid repeated freeze-thaw cycles.

Note 4: All the steps must be performed on ice.

Note 5: Pre-cool the glassware and homogenizer with pestle in an ice-bath 5 min before starting the procedure. Homogenization as well as the following steps must be carried out on ice to minimize the activation of proteases and phospholipases.

Note 6: Turn on the centrifuge and preset it 4°C.

Note 7: White layer on the top of the tube.

Note 8: Avoid the formation of bubbles during the resuspension process. At the last time, use buffer H without BSA.

Note 9: Do not dilute the mitochondria with buffer as mitochondria retain their functionality for a longer time when kept concentrated, minimizing exposure to oxygen.

Note 10: Mitochondria are ready to be used in experiments; use the preparation within 1–3 h for better functional responses.

Note 11: If the compound is not soluble in water, it can be dissolved in DMSO or other solvent and then diluted with buffer S. It is better to use less concentration of organic solvent. And it is important to use the same concentration of organic solvent in the control well.

Note 12: In order to use less time, it is better to use multi-channel pipette to do this step.

Note13: If the rate of oxygen consumption is too fast, we can dilute the mitochondria to 0.25µg/µL.

Note 14: shake the plate for 10s.

Note 15: Pre-warm mineral oil to 30°C on a water bath.

Note 16: Adjust the gain for an optimal reading of a positive control, and use the same parameters for a series of experiment.

Note 17: Pre-cold (-20°C) acetone, a volume four times that of the protein samples to be precipitated.

Note 18: Be careful to not dislodge the protein pellet.

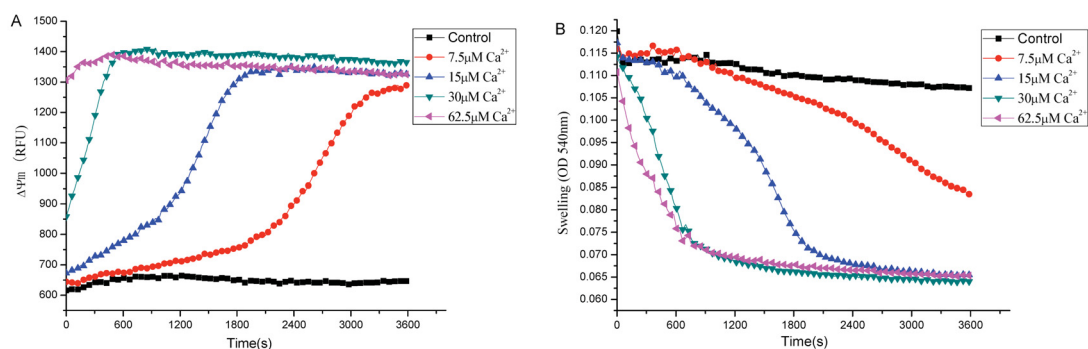


Fig.1. Co-evaluation of  $\text{Ca}^{2+}$  effect on the mitochondrial inner transmembrane membrane potential ( $\Delta\Psi_m$ ) and matrix volume of cardiac mitochondria in microtiter plates. (A). Loss of  $\Delta\Psi_m$  was simultaneously measured in real time following addition of increasing  $\text{Ca}^{2+}$  concentrations or without  $\text{Ca}^{2+}$  (Control) by fluorescence. (B). Mitochondrial swelling induced by different concentrations of  $\text{Ca}^{2+}$  was concomitantly monitored by absorbance.

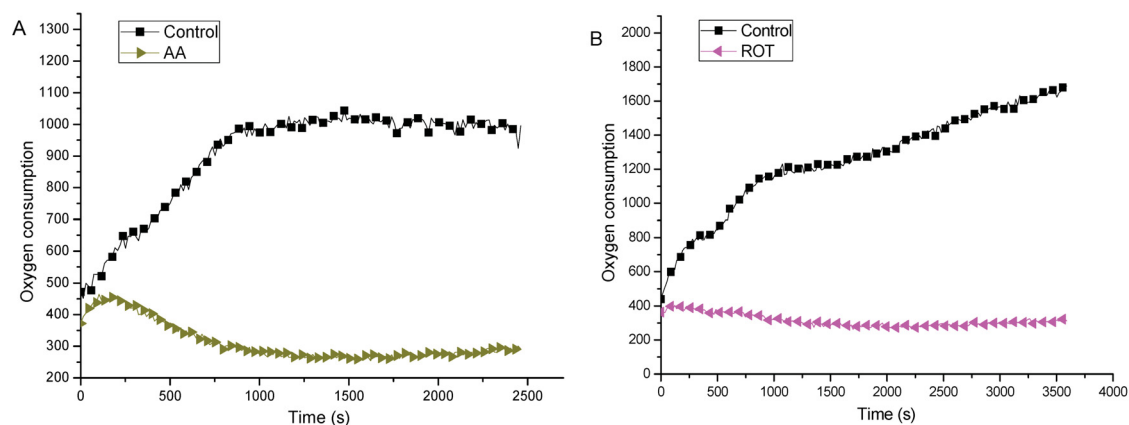


Fig.2. Assessment of ADP-stimulated mitochondrial respiration with Mito-ID® Extracellular  $\text{O}_2$  Sensor Kit. A: Oxygen consumption is driven by succinate (Control) and is inhibited by antimycin A (AA). B: Oxygen consumption is driven by glutamate/malate (Control) and treated with blocker rotenone (ROT).





Fig.3 Immunoblot of cytochrome *c* release from cardiac mitochondria treated with 10 $\mu$ M Ca<sup>2+</sup> or not (Control). The same volume of sample has been separated and electro-transferred according to (11) and immunorevealed using chemiluminescence.

## Reference

1. Martinou JC. Apoptosis - Key to the mitochondrial gate. *Nature* 1999;399:411-412.
2. Brenner C, Kroemer G. Apoptosis. Mitochondria--the death signal integrators. *Science* 2000;289:1150-1151.
3. Kroemer G, Galluzzi L, Brenner C. Mitochondrial membrane permeabilization in cell death. *Physiol Rev* 2007 87:99-163.
4. Zamzami N, Marchetti P, Castedo M, Decaudin D, Macho A, Hirsch T, Susin SA, et al. Sequential reduction of mitochondrial transmembrane potential and generation of reactive oxygen species in early programmed cell death. *J. Exp. Med.* 1995;182:367-377.
5. Gogvadze V, Robertson JD, Zhivotovsky B, Orrenius S. Cytochrome c release occurs via  $\text{Ca}^{2+}$ -dependent and  $\text{Ca}^{2+}$ -independent mechanisms that are regulated by Bax. *J Biol Chem* 1996;276:19066-19071.
6. Liu X, Kim CN, Yang J, Jemmerson R, Wang X. Induction of apoptic program in cell-free extracts: requirement for dATP and cytochrome C. *Cell* 1996;86:147-157.
7. Crompton M, McGuinness O, Nazareth W. The involvement of cyclosporin A binding proteins in regulating and uncoupling mitochondrial energy transduction. *Biochim Biophys Acta* 1992;1101:214-217.
8. Belzacq-Casagrande A, Martel C, Pertuiset C, Borgne-Sanchez A, Jacotot E, Brenner C. Pharmacological screening and enzymatic assays for apoptosis. *Front Biosci.* 2009;14:3550-3562.
9. Porceddu M, Buron N, Roussel C, Labbe G, Fromenty B, Borgne-Sanchez A. Prediction of Liver Injury Induced by Chemicals in Human with a Multiparametric Assay on Isolated Mouse Liver Mitochondria. *Toxicol Sci* 2012.
10. Martel C, Allouche M, Esposti DD, Fanelli E, Boursier C, Henry C, Chopineau J, et al. GSK3-mediated VDAC phosphorylation controls outer mitochondrial membrane permeability during lipid accumulation. *Hepatology* 2013.
11. Laemmli UK. Cleavage of structural proteins during the assembly of the head of bacteriophage T4. *Nature* 1970;227:680-685.



## Review

## VDAC phosphorylation, a lipid sensor influencing the cell fate

Cécile Martel<sup>a,b</sup>, Zhenyu Wang<sup>c,d,e</sup>, Catherine Brenner<sup>c,d,e,\*</sup><sup>a</sup> Research Centre, Montreal Heart Institute, Montreal, Quebec, Canada<sup>b</sup> Department of Pharmacology, Université de Montréal, Montreal, Quebec, Canada<sup>c</sup> INSERM UMR-S 769, LabEx LERMIT, Châtenay-Malabry, France<sup>d</sup> IFR141-IPSTI, CIBLOT Platform, Châtenay-Malabry, France<sup>e</sup> Université de Paris-Sud, Faculté de Pharmacie, Châtenay-Malabry, France

## ARTICLE INFO

Available online 1 August 2014

## Keywords:

Apoptosis

Post-translational modification

Mitochondria

Cell death

Lipid

## ABSTRACT

The voltage-dependent anion channel (VDAC) or porin is a major membrane protein integrated into the mitochondrial outer membrane in eukaryotes. It is encoded as three isoforms (VDAC1 to 3), which play differential roles in metabolism and cell death. As a channel, VDAC mediates metabolites, ions and water movements through the outer membrane in physiological conditions, but it can also participate to mitochondrial membrane permeabilization, an apoptotic checkpoint in stress and pathological conditions. Indeed, due to its subcellular location, VDAC interacts with many molecules as diverse as NAD<sup>+</sup>, lipids and cytosolic proteins such as hexokinase, tubulin, GSK3, Bax and Bcl-2 family members and mitochondrial proteins, such as the adenine nucleotide translocase (ANT). All these interactions can influence VDAC role in cell fate determination. In the recent past, major efforts focused on VDAC1 channel function and regulation by calcium and reactive oxygen species, and comparatively, fewer studies have been undertaken on VDAC2 and 3 and their pathophysiological involvement. Here, we review recent insights into the role of VDAC isoforms in cell death, and its regulation by phosphorylation or protein–lipid interactions and discuss the putative consequences of this post-translational modification on cell fate, notably in the context of lipid accumulation. This might have important implications for the understanding of basic mechanisms of mitochondrial lipid sensing and might contribute to define a novel therapeutic target for future investigation.

© 2014 Elsevier B.V. and Mitochondria Research Society. All rights reserved.

## Contents

1. Introduction	69
2. VDAC in cell fate decisions	70
3. VDAC, its post-translational modifications and their implication	71
4. VDAC–lipid interactions	71
5. VDAC phosphorylation in lipid-induced liver pathology	73
6. Open question and perspectives	74
Acknowledgments	74
References	74

**Abbreviations:** ACSL, long-chain acyl-CoA synthetase; ANT, adenine nucleotide translocase; BN-PAGE, blue-native polyacrylamide gel electrophoresis; Ca<sup>2+</sup>, calcium; CL, cardiolipin; CPT1a, carnitine palmitoyltransferase 1a; CypD, cyclophilin D; DOG, diacylglycerol; DOPE, dioleoylphosphatidylethanolamine; FA, fatty acid; H<sub>2</sub>O<sub>2</sub>, hydrogen peroxide; KO, knock-out; IM, inner membrane; LPC, lysophosphatidylcholine; LPE, lysophosphatidylethanolamine; O<sub>2</sub><sup>•−</sup>, superoxide anion; OM, outer membrane; PC, phosphatidylcholine; PG, phosphatidylglycerol; PTP, permeability transition pore; TNF-α, tumor necrosis factor alpha; VDAC, voltage-dependent anion channel.

\* Corresponding author at: INSERM UMR-S 769, Faculté de Pharmacie, Université Paris-Sud, 5 Rue J.-B. Clément, 92290 Châtenay-Malabry, France.

E-mail address: [catherine.brenner-jan@u-psud.fr](mailto:catherine.brenner-jan@u-psud.fr) (C. Brenner).

## 1. Introduction

The existence of channels in the mitochondrial outer membrane (OM) has been evidenced concomitantly by electrophysiology and electron microscopy in the 1970s (for review: Colombini and Mannella, 2012). These channels were named voltage-dependent anion channel (VDAC) or porin by analogy with bacterial porins and constitute a family of β barrel-membrane proteins encoded by three genes generating three protein isoforms, i.e. VDAC1, 2, and 3 in mammals (Colombini and Mannella, 2012; Shinohara et al., 2000). VDAC is responsible of

the OM permeability, in contrast to the inner membrane (IM) whose permeability is more strictly limited and mediated by specific mitochondrial proteins such as the mitochondrial carriers. VDAC is an anion channel with multiple conductances depending on voltage and able to switch to cationic selectivity in a closed state. Systematic in vitro manipulation of membrane composition suggested that the lipid composition of the OM, enriched in cholesterol, is highly favorable to VDAC activity. Of note, VDAC has also been found in the plasma membrane and caveolae of various cell types and tissues (for review: Shoshan-Barmatz et al., 2009) and harboring NADH ferricyanide reductase activity (Baker et al., 2004; Belzacq-Casagrande et al., 2009; Martel et al., 2013), but this is still considered as controversial and requires further studies (Gonzalez-Gronow et al., 2013; Low et al., 2012).

Since its discovery, VDAC has been shown to play a major role in cellular energetic metabolism due to its capacity to allow the exchange of molecules (exclusion limit  $\approx$  5–6 kDa) between the cytosol and the mitochondrial intermembrane space (for review: Maldonado and Lemasters, 2012). Thus, VDAC controls the so-called OM leakiness to essential molecules such as calcium ( $\text{Ca}^{2+}$ ), metabolites, water, NADH, ADP as well as ATP. More recently, VDAC has been proposed to participate to the permeability transition pore (PTP) and/or to mitochondrial apoptosis (Granville and Gottlieb, 2003; Lemasters and Holmuhamedov, 2006; Shimizu et al., 1999; Shoshan-Barmatz and Ben-Hail, 2012; Shoshan-Barmatz and Golan, 2012; Shoshan-Barmatz et al., 2010) creating a strong interest in the scientific community. However, these novel roles are still debated, notably because of the generation of knockout mice for individual VDAC isoforms, which have unanticipated and relatively silent phenotypes (Krauskopf et al., 2006) (for a comprehensive review on genetic models: Raghavan et al., 2012).

To date, major efforts have focused on the investigation of VDAC1 and led to its crystallization and 3D structure elucidation by three groups following three different approaches (Bayrhuber et al., 2008; Hiller et al., 2008; Ujwal et al., 2008). This is due to its abundance in most tissues and organisms in comparison to other isoforms, provided that their relative quantification had been made rigorously (e.g. plants, fungi, *Neurospora crassa*, mouse/rat liver) (Messina et al., 2012; Yamamoto et al., 2006). This led to our general conception of this family as mitochondrial gatekeepers (for recent review: Colombini and Mannella, 2012). However, some recent work emerged on the post-translational modifications of various VDAC isoforms (Huang et al., 2013; Kerner et al., 2012; Martel et al., 2013; Maurya and Mahalakshmi, 2013; Reddy, 2013), suggesting diverse roles as well as diverse modes of regulation. Thus, VDAC1, but not VDAC2 or 3, selectively transfers apoptotic  $\text{Ca}^{2+}$  signals from the endoplasmic reticulum to mitochondria (De Stefani et al., 2011). Therefore, in this review, some concepts will be re-evaluated in light of recent findings and a novel concept of a mitochondrial lipid sensor via VDAC influencing the cell fate will be proposed, which might have many implications for further studies. When known, we indicated the VDAC isoform and when unknown or when all isoforms are concerned, we mentioned VDAC without any distinction.

## 2. VDAC in cell fate decisions

Besides a pro-survival role as a channel for metabolites (for review: Colombini and Mannella, 2012 and below), it is admitted that VDAC can also be involved in cell death. However, molecular mechanisms by which VDAC influences cell death execution are not totally understood yet (McCommis and Baines, 2012; Shoshan-Barmatz et al., 2008, 2010). Importantly, these mechanisms might be different for each isoform and depend on the VDAC isoform ratio. This is notably supported by genetic studies in mice and embryonic stem cells (Messina et al., 2012; Raghavan et al., 2012). Thus, the knock-out (KO) of all VDAC isoforms as well as the KO of VDAC2 are lethal and therefore cannot be exploited for further mechanistic studies (Cheng et al., 2003). In contrast, VDAC1  $-/-$  or VDAC3  $-/-$  mice are viable and clearly

exhibit some defects in mitochondrial ultrastructure and a reduction in respiratory activity (Anflous et al., 2001; Sampson et al., 2001; Weeber et al., 2002; Wu et al., 1999) irrespective of underlying unclear molecular mechanisms (Messina et al., 2012; Raghavan et al., 2012).

VDAC1 channel was implicated in cell death induction for its ability to interact with BAX and form larger channels than BAX alone or VDAC1 alone (Shimizu et al., 2000). BAX belongs to the BCL-2 protein family, which is composed of several anti- or pro-apoptotic members and regulates cell death either independently or in association with the PTP. BAX plays a role in apoptosis and mitochondrial function regulation via multiple protein–protein interactions with BCL-2, BAK, BID or other members of the family (Antonsson et al., 1997; Roucou et al., 2002; Vela et al., 2013), and also mitochondrial proteins such as proteins from the import machinery and from the fusion/fission family (Landes and Martinou, 2011). BAX and BCL-2 participate to numerous other cell functions (e.g. oncogenesis, autophagy, DNA repair), but this is beyond the scope of the review. Briefly, detailed molecular mechanisms of VDAC1 and BAX/BCL2 cooperation are complex and depend largely on the pathophysiological cell model or the organ studied. Thus, if BAX is mainly a cytosolic protein, a pool of Bax can be loosely attached to the outer membrane in physiological conditions. Apoptosis induction triggers BAX translocation to the OM and the oligomerization of mitochondrial BAX, with the exposure of specific amino acids resulting in a new lethal conformation (Antonsson et al., 2000). In some models, the formation of BAX–VDAC large channels, participates more or less directly in the massive and rapid release of cytochrome *c* into the cytosol, impairing mitochondrial respiration, favoring reactive oxygen species production, stimulating mitochondrial fission and activating the apoptosome and a caspase-dependent cascade of event leading to cell death. This pathway is blocked by the anti-apoptotic BCL-2 in a stoichiometric relationship, plausibly by conformation-dependent protein–protein interactions involving the BH4 domain of Bcl-2 (Shimizu et al., 2000) and by hexokinase II (Pastorino et al., 2002; Shoshan-Barmatz et al., 2010). This signaling pathway was evidenced by subcellular and molecular experiments with recombinant proteins, electrophysiological measurements of channels in black lipid membranes and proteoliposomes. Moreover, mutagenesis helped to identify important residues or domains of BAX/BCL-2 that are important for its own channel activity (e.g. alpha 5 and alpha 6 helices) and its capacity to dimerize (i.e. BH3 domain) and to interact with VDAC. It has also been evidenced by electrophysiology that Bid might also form channels with VDAC1 rather than Bax (Rostovtseva et al., 2004). Experiments with shRNA, designed to decrease VDAC1 expression level and VDAC1 overexpression experiments confirmed the implication of VDAC1 in apoptosis in various cells types (Shoshan-Barmatz et al., 2008; Zaid et al., 2005). However, VDAC-deficient mice failed to confirm an essential role of VDAC in cell death (Baines et al., 2007). As a result, VDAC1 KO and VDAC3 KO mice and fibroblasts isolated from double KO mice and down-regulated for VDAC2 (i.e. cells mimicking triple knock-out cells) did not recapitulate previous cellular studies regarding cell death execution (Baines et al., 2007). This led the authors to claim that VDAC are dispensable for mitochondrial-dependent cell death but this is so counterintuitive for several (independent) researchers that more investigations are still awaited to clarify the debate (Brenner and Moulin, 2012; Galluzzi and Kroemer, 2007; Messina et al., 2012).

Otherwise, some researchers proposed that VDAC1 might participate to the dynamic polyprotein complex PTP, whose prolonged opening triggers a bioenergetic catastrophe and is lethal in many models. Initially, electrophysiologists described PTP opening as a sudden change in mitochondrial membrane permeability that can be prevented by a cyclic peptide named cyclosporine A (Szabo and Zoratti, 1993). In accordance with a polyprotein structure, PTP might be composed by VDAC1 in the OM, cyclophilin D (CypD) in the matrix and the ANT or ADP/ATP carrier in the IM (for review: Halestrap and Brenner, 2003). By

definition, PTP allows the passage of molecules of 1.5 kDa such as metabolites, ions and water, its activity being tightly regulated by several factors such as the voltage (i.e. the membrane potential), pH, intramitochondrial calcium concentration, lipids and redox state. Indeed, an association of VDAC1–ANT–CypD was based on biochemical studies, combining purification of native proteins under mild detergent conditions to preserve protein–protein and protein–lipid contacts and reconstitution in biomembranes (Beutner et al., 1996; Marzo et al., 1998; Woodfield et al., 1998). But, as previously said, genetic invalidation of some VDAC isoforms failed to confirm its essential role in PTP (Baines et al., 2007). Therefore, it is tempting to hypothesize that several different protein homo- or hetero-oligomers can participate in the so-called PTP and that VDAC could constitute one unit that mimics in some circumstances the PTP.

As shown by crystallographic structure determination, VDAC1 is a 19β barrel-protein, the intramembranous barrels being connected by hydrophilic stretches of amino acids accessible to the intermembrane space or the cytosol. Therefore, oxidative stress and notably, pro-oxidant radicals such as superoxide anion ( $O_2^{\bullet-}$ ) and hydrogen peroxide ( $H_2O_2$ ) preferentially modify exposed residues such as reactive thiols and trigger the mitochondrial apoptosis pathway (Le Bras et al., 2005; Orrenius, 2007; Ott et al., 2007). Thus, Madesh and Hajnoczky found that  $O_2^{\bullet-}$  but not  $H_2O_2$  stimulates OM permeabilization and massive cytochrome c release through VDAC1 oxidation in hepatocytes (Madesh and Hajnoczky, 2001). This VDAC1 specific mechanism was independent of BCL-2 family members and IM permeabilization and leads to caspase activation and apoptosis execution.

Although VDAC1 appeared to be a pro-apoptotic protein through oligomerization induced by many stimuli (e.g. staurosporine, curcumin,  $As_2O_3$ , etoposide, cisplatin, selenite, tumor necrosis factor alpha (TNF-α),  $H_2O_2$ , and UV irradiation) (Keinan et al., 2010), the role of VDAC2 seemed to be anti-apoptotic via the sequestration of BAK (Cheng et al., 2003; Lazarou et al., 2010; Ma et al., 2013). In VDAC2  $-/-$  MEF cells, BAK rearranges into homo-oligomers and forms oligomeric pores and the cells are more susceptible to apoptotic death (Cheng et al., 2003; Lazarou et al., 2010). In thymocytes, VDAC2–BAK complex functions as a rheostat to control cell survival (Ren et al., 2009). Conversely, overexpression of VDAC2 blocks BAK activation and inhibits the cell death pathway (Cheng et al., 2003). In addition, in contrast to VDAC1 and 3, VDAC2 does not interact with BCL-X<sub>L</sub> to facilitate calcium matrix accumulation, a mechanism described to facilitate mitochondrial membrane permeabilization and participate to cell death signaling (Huang et al., 2013). Moreover, tubulin inhibits VDAC1 and VDAC2 but not VDAC3 which is more involved in metabolite transport (Maldonado and Lemasters, 2012).

In summary, despite the growing body of evidence and the variety of models investigated, a direct role of VDAC in cell death is still discussed and it is plausible that VDAC participates to several molecular and cellular mechanisms, themselves dependent on the metabolic context, such as lipid accumulation as discussed below.

### 3. VDAC, its post-translational modifications and their implication

As a nuclear encoded protein imported into mitochondria, VDAC has been shown to be co-translationally or post-translationally modified (Table 1). VDAC modification refers mainly to acetylation, phosphorylation and S-nitrosylation. Recently, it has been reported that VDAC can be modified by O-linked β-N-acetyl glucosamine (O-GlcNAc), but its role and how it affects VDAC activity is not yet known (Johnsen et al., 2013). Interestingly, most of these modifications can be modulated by the pathophysiological context and, notably be controlled by at least metabolic stress, aging, cancer and cardiovascular diseases (Fig. 1). Thus, BCL-X<sub>L</sub> levels can affect cell survival through an effect on acetyl-CoA cell content and Nα-acetylation (Yi et al., 2011). These modifications may also affect VDAC protein activity, its stability toward proteasome degradation (Yuan et al., 2008) and organelle accumulation as well as its interaction with other proteins, such as hexokinase and tubulin. For example, in rat liver mitochondria, VDAC1, but not VDAC2 or 3, can be irreversibly acetylated at its N-terminus following methionine cleavage co-translationally despite detection of uncleaved N-terminal peptide by the mass spectrometry (Distler et al., 2007). The functional consequence of this modification is ignored, but deserves further study for a better knowledge of VDAC biosynthesis.

In all species studied, i.e. from mammals to plants, VDAC has been found to be phosphorylated (Tables 2 and 3). Of note, all phosphorylation events were not determined by mass spectrometry analysis (i.e. the gold standard). When conducted following 1D electrophoresis separation of mitochondrial proteins and transfer to a membrane, this approach leads to the possibility of a false positive result and unfortunately, cannot determine the site of phosphorylation or the proportion of VDAC monomer that is truly phosphorylated.

Briefly, phosphorylation on serine, threonine as well as tyrosine by a diversity of kinases (e.g. GSK3β, PKA, PKC, CaM-II, p38) has been described under stimulation and/or various physiopathological conditions (Tables 2 and 3, Fig. 1) (Martel et al., 2013; Pastorino et al., 2005; Sun et al., 2008). This suggests the existence of microdomains within mitochondria membrane containing preferentially certain VDAC isoforms and certain kinases forming large polyprotein complexes, such as PKA (Lefkimmatis et al., 2013). This is supported by studies designed to investigate the oligomerization of VDAC in blue-native gels (BN-PAGE) or cross-linking and 1D-electrophoresis (SDS-PAGE) revealing the existence of VDAC into several mitochondrial polyprotein complexes (see below, Faustin et al., 2011; Keinan et al., 2010; Martel et al., 2013).

### 4. VDAC–lipid interactions

It has been shown that lipids can play an important role in protein function and structure, especially in the case of membrane proteins (for review: Marsh, 2008; McIntosh and Simon, 2006; Smith, 2012; Vitrac et al., 2011). Such effects of lipids have been described for proteins involved in mitochondrial pathway of apoptosis, especially the members of the BCL-2 family. Indeed, lipid composition of liposomes affects

**Table 1**

Post-translational modifications of human VDAC isoforms. Data of phosphorylation, acetylation, NAD binding and S-nitrosylation are from the Nexprot database ([www.nextprot.org](http://www.nextprot.org)). Residues in italics have not been experimentally evidenced and are proposed by similarity or in silico prediction. ND, not detected.

Isoform	Phosphorylation	Acetylation	NAD binding sites	S-Nitrosylation	References
VDAC1 (2–283)	Ser13, Tyr67, Thr107	Ala2, Lys6, Lys20, <i>Lys109, Lys252, Lys 266</i>	242–244 260–264	ND	Bienvenut et al. (2012); Gauci et al. (2009); Kayser et al. (1989); Olsen et al. (2006); Sol et al. (2012); Thinnis et al. (1989); and Van Damme et al. (2012)
VDAC2 (2–294)	Ser115 Thr118	Ala2, Lys31, <i>Lys120</i>	253–255 271–275	Cys47	Choudhary et al. (2009); Gauci et al. (2009); Lam et al. (2010); and Sol et al. (2012)
VDAC3 (2–283)	Thr4, Ser241	Cys2, Lys20, Lys90	242–244 260–264	ND	Choudhary et al. (2009); Gauci et al. (2009); Lam et al. (2010); Oppermann et al. (2012); and Sol et al. (2012)



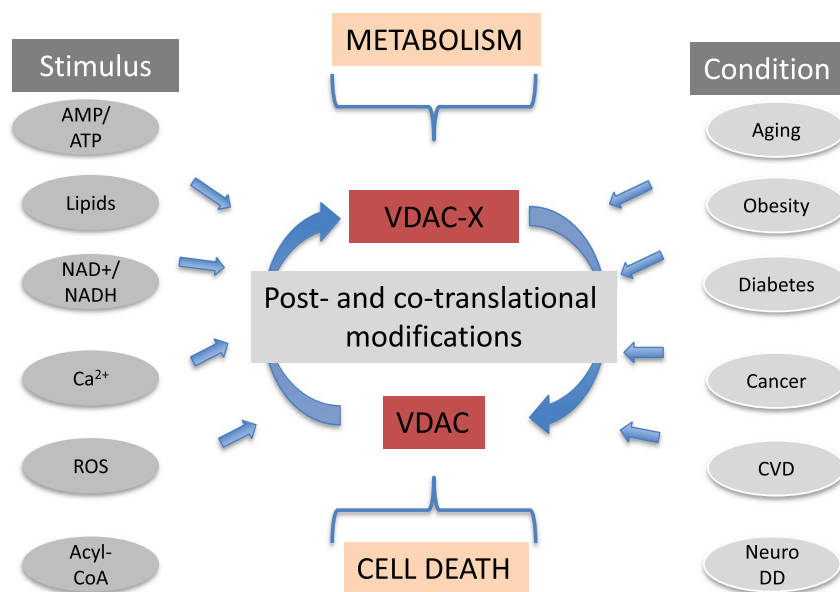


**Fig. 1.** Stimuli and/or pathophysiological conditions influencing VDAC post- and translational modification. From literature and our own work, we hypothesize that phosphorylation might modulate the role of VDAC metabolism versus cell death. ROS, reactive oxygen species, NeuroDD, neurodegenerative diseases, and CVD, cardiovascular diseases.

permeability and cytochrome c release from BAX-proteoliposomes (Basanez et al., 2002), irrespective of changes in the incorporation of BAX into the liposomes. Lipids that possess a positive intrinsic curvature, such as lysophosphatidylcholine (LPC) or lysophosphatidylethanolamine (LPE) enhanced the permeability of BAX-incorporated liposomes, whereas dioleoylphosphatidylethanolamine (DOPE) and diacylglycerol (DOG), which exacerbate a negative curvature showed an inhibition of such permeability. Interestingly, cardiolipin (CL), which is mostly found in mitochondrial membranes (van Meer et al., 2008), promotes the binding of a cleaved BID to lipid membranes and is necessary to BID-induced permeability of BAX-liposomes (Kuwana et al., 2002; Lutter et al., 2000). This cleaved BID also displays lipid transfer activity (Esposti et al., 2001) and is capable of inducing a negative curvature, which could destabilize lipid membranes (Epand et al., 2002).

As a membrane channel, VDAC is obviously susceptible to be influenced by membrane lipids. Impact of membrane lipid composition on

VDAC channels behavior has been studied for the first time in 2006 by evaluating the gating properties of VDAC after reconstitution in a planar lipid bilayer of various compositions (Rostovtseva et al., 2006). Non-lamellar lipids such as PE and CL generated an asymmetrical gating of VDAC channels, favoring the channel closure at negative voltages, without modification of its orientation into lipid bilayers. Interestingly, VDAC insertion was more efficient in PE membranes than in phosphatidylcholine (PC) containing membranes.

A close relationship between VDAC and cholesterol molecules has been suggested since the 90s. In 1988, Jancsik and colleagues suggested that in rat liver mitochondria, VDAC release from OM requires disruption of cholesterol molecules (Jancsik et al., 1988). Furthermore, addition of sterol is needed to maintain its channel-forming ability (Popp et al., 1995) and purification of VDAC through binding on hydroxyapatite/celite columns revealed the presence of cholesterol molecules together with VDAC fractions (De Pinto et al., 1989). Lately, two studies

**Table 2**  
VDAC phosphorylation evidenced by mass spectrometry and mutagenesis. This table lists all the phosphorylation sites found experimentally in VDAC isoforms by mass spectrometry analysis and demonstrated by mutagenesis irrespective of the origin species or tissue. ND, not determined.

Isoform	Site	Species & tissues	Protein kinases	Effect of phosphorylation	Reference
VDAC1	Ser12	Rat liver mitochondria	CaM-II/GSK3β	ND	Distler et al. (2007)
	Ser136	Rat liver mitochondria	PKC	ND	Distler et al. (2007)
	Ser193	HK2	Nek1/PKC	Prevention of cell death	Chen et al. (2009)
	Ser12	HMEC	GSK3/CaM-II/CKI	Sensitization to apoptosis via inhibition of phosphorylated VDAC1 degradation	Kerner et al. (2012); and Yuan et al. (2008)
	Ser103		CKI	ND	Kerner et al. (2012); Lee et al. (2007); and Munton et al. (2007)
	Ser117	Mouse brain, Mouse liver mitochondria	CKI/p38MAPK	ND	Kerner et al. (2012); and Olsen et al. (2006)
	Ser101	HeLa	GSK3/cdc2/CaM-II	ND	
	Ser102		PKC/cdc2/GSK3β	ND	
	Ser104		CKI/p38MAPK/GSK3β	ND	
	Thr107	HeLa	PKC/GSK3 β/CaM-II	ND	Kerner et al. (2012); and Olsen et al. (2006)
VDAC2	Tyr80	Mouse brain	SRC/EGFR	ND	Ballif et al. (2008); and Kerner et al. (2012)
	Tyr208		EGFR/SRC/INSR	ND	
	Tyr237	Rat liver mitochondria	INSR	ND	Distler et al. (2007)
	Ser115	HeLa	CKI/CDK5/GSK3β	ND	Kerner et al. (2012); and Olsen et al. (2006)
	Thr118	HeLa	PKC/CKI/GSK3β	ND	Kerner et al. (2012); and Olsen et al. (2006)
VDAC3	Ser241	Rat liver mitochondria	CKI/PKA	ND	Distler et al. (2007)
	Thr33	Rat liver mitochondria	PKC	ND	Distler et al. (2007)
	Tyr49	Mouse brain	CKII/GSK3β/CaM-II	ND	Ballif et al. (2008); and Kerner et al. (2012)

**Table 3**

VDAC phosphorylation evidenced by electrophoresis followed by coloration or immunodetection. Numerous studies report VDAC phosphorylation by immunodetection with anti-phospho-serine, -tyrosine and -threonine. When conducted following 1D electrophoresis separation of mitochondrial proteins and transfer to a membrane, this approach led to the possibility of false positive result and cannot determine the site of phosphorylation nor the proportion of VDAC monomer that is truly phosphorylated. ND, not determined.

Isoform	Site	Species & tissues	Protein kinases	Effect of phosphorylation	Reference
VDAC1	Thr	Mice tg2576	GSK3 $\beta$	Facilitation of the leakage of mitochondrial proapoptotic molecules	Cuadrado-Tejedor et al. (2011)
VDAC1	ND	Mouse heart mitochondria	PKC $\epsilon$	Decrease of single channel current and opening probability	Baines et al. (2003)
VDAC1	Thr51	HeLa	GSK3 $\beta$	Disruption of the binding of HK-II to VDAC	Pastorino et al. (2005)
VDAC1	Tyr	Rabbit heart	p38 MAP kinase	Regulation of cell survival in myocardial ischemia and reperfusion	Schwartz et al. (2007)
VDAC	ND	Mouse liver mitochondria	GSK3 $\beta$ /PKA	Regulation of its interaction with Tubulin	Sheldon et al. (2011)
VDAC	ND	Rat mitochondria	Akt/GSK3 $\beta$	Alteration of mitochondrial function under energy deficient conditions	Das et al. (2008)
VDAC	Thr	Mouse liver	GSK3 $\beta$	Control of outer mitochondrial membrane permeability during lipid accumulation	Martel et al. (2013)
VDAC	Thr 51	Tubular epithelial cells, mouse kidneys/livers	GSK3 $\beta$	Prevention of PTP, attenuation of tubular cell death	Wang et al. (2013)
VDAC	ND	Rice	CKII/PKC	ND	Al Bitar et al. (2003)
VDAC	Ser	Neonatal rat cardiomyocytes	GSK3 $\beta$	Prevention of PTP opening	Javadov et al. (2009)
VDAC	ND	Rat liver mitochondria	PKA	Closure of the channel	Bera and Ghosh (2001)
VDAC	Tyr	SN56 & HT22 neurons	PKA/Src-kinase	Closure of the channel	Herrera et al. (2011)
VDAC	Tyr	Guinea pig brain	ND	Adaptation to stress situations	Liberatori et al. (2004)
VDAC	ND	HEK293	PKC $\epsilon$	Regulation of binding to HKII and the opening of the PTP	Sun et al. (2008)
VDAC	Tyr	Mouse sperm	ND	Regulation of channel activity or interaction with other sperm proteins	Arcelay et al. (2008)
VDAC	ND	Rat brain mitochondria	PKA	Control of cytochrome c leakage	Banerjee and Ghosh (2006)

from the same group identified VDAC as part of polyprotein complexes binding cholesterol and participating in hormone-induced mitochondrial cholesterol transport and steroidogenesis in Leydig cells (Liu et al., 2006; Rone et al., 2012). VDAC interacts with TSPO, PAP7, cAMP dependent protein kinase-regulatory subunit I or PKAR1 $\alpha$ , and StAR to form the so-called “transducesome” (Rone et al., 2009), which upon hormone stimulation favors cholesterol transfer to the OM. In addition, together with TSPO, CYP11A1, ATAD3A, and OPA1, VDAC takes part in cholesterol transport to the IM. Besides, VDAC has been identified as the main cholesterol-binding protein from the intermembrane contact sites of rat liver mitochondria (Campbell and Chan, 2007). Of note, the analysis of putative promoter sequences of human VDAC1 and murine VDAC1/2 revealed the presence of a sterol repressor element, which regulates the synthesis of proteins that are involved in cholesterol trafficking (Messina et al., 2000; Sampson et al., 1997). Furthermore, disruption of VDAC-hexokinase binding in cancer cells resulted in a decrease of cholesterol content in the OM and increased sensitivity to mitochondrial matrix swelling, suggesting that VDAC influences cholesterol distribution in the OM and may impact on oxidative phosphorylation and apoptosis sensitivity in cancer cells (Campbell and Chan, 2008). Very recently, it has been proposed that a glycine motif GxxxG in the N-terminal part of the protein, localized in positions 20–24, could be responsible for cholesterol binding (Thinnes and Burckhardt, 2012). It appears that VDAC is not only involved in cholesterol transport across the OM, but could also be part of a complex allowing the transport of fatty acids through the OM in rat liver mitochondria (Lee et al., 2011). The authors postulated that VDAC could act as an anchor linking the long-chain acyl-CoA synthetase (ACSL) from the outer surface of the OM and the carnitine palmitoyltransferase 1a (CPT1a), which would be facing the intermembrane space. In the proposed model, upon activation by ACSL, acyl-CoAs are then transferred across the OM by VDAC to the intermembrane space where they can be converted by CPT1a into acylcarnitines. The role of VDAC in the transport through the OM of metabolites such as ADP, NADH, has been well established. It is only recently that these studies suggested that VDAC is also implicated in lipid metabolism pathways, in particular, fatty acids and cholesterol transport.

In addition to modifications of intrinsic VDAC channel gating properties, interaction with lipids may impact VDAC association with its various protein partners. As an example, the close relationship between

VDAC and tubulin has been widely studied since the first evidence of a physical interaction (Carre et al., 2002) (for review: Rostovtseva and Bezrukov, 2012). Briefly, addition of tubulin during recording of currents from single channels incorporated in planar lipid membranes increased the voltage sensitivity of the channel and promoted a closed state of VDAC at low transmembrane potentials (Rostovtseva et al., 2008) preventing the entry of ATP in the mitochondria via VDAC (Gurnev et al., 2011) and ultimately altering mitochondrial metabolism (Maldonado and Lemasters, 2012). Then, this inhibition has been demonstrated to be strongly dependent on lipid composition and charge of the membrane. It appeared that the conductance of VDAC upon tubulin inhibition was not affected by variations in lipid composition (using DOPC and DOPE) (Rostovtseva et al., 2012). The frequency of tubulin induced-VDAC closure but not the duration of the closed state, however, was sensitive to such changes. Thus, DOPE membranes increased substantially the frequency of channel blockage in comparison with POPC membranes. Next, it has been suggested that membrane charge could modulate the conductance of the tubulin-blocked state of the channel: its conductance would be decreased by positive and increased by the negative charge of the lipids (Gurnev et al., 2012).

VDAC oligomerization has been associated with increased mitochondrial membrane permeabilization and apoptosis (for review: Shoshan-Barmatz et al., 2013). Interestingly, modifications of mitochondrial membrane lipid composition during apoptosis, i.e. increased phosphatidylglycerol (PG) and decreased CL (Matsko et al., 2001; Ostrander et al., 2001), have been described to favor VDAC oligomers (Betaneli et al., 2012).

In summary, structural lipids from mitochondrial OM have a strong impact on VDAC function, as well as its ability to interact with other proteins. Nonetheless, little is known about how VDAC could be influenced by non-structural lipids.

## 5. VDAC phosphorylation in lipid-induced liver pathology

Fatty acids (FAs), especially palmitate, are recognized to be able to induce mitochondrial membrane permeabilization in various cell types (Koshkin et al., 2008; Paumen et al., 1997; Rogers et al., 2014; Sparagna et al., 2000). This induction can either be direct (de Pablo et al., 1999; Furuno et al., 2001; Oyanagi et al., 2011; Wieckowski and Wojtczak, 1998) mostly by activation of PTP or mediated by



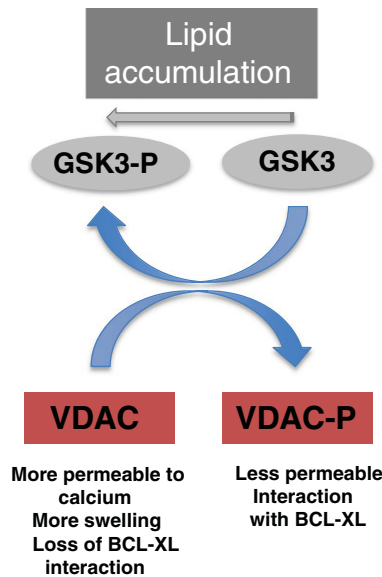


**Fig. 2.** VDAC phosphorylation by glycogen synthase kinase 3 (GSK-3) and cell fate decision. In high fat conditions, VDAC is dephosphorylated and its permeability to calcium increased. This enhances the sensitivity of mitochondria to calcium-induced swelling via disruption of VDAC–BCL-X<sub>L</sub> binding.

endoplasmic reticulum stress signaling (for review: Fu et al., 2012; Gentile et al., 2011). It has even been proposed that palmitate can cooperate with Ca<sup>2+</sup> to induce leaking from mitochondrial membranes by lipid pore formation possibly due to a loss of membrane integrity (Agafonov et al., 2003, 2007; Belosludtsev et al., 2009). Surprisingly, none of these studies investigated the involvement of VDAC in such FA-induced mitochondrial membrane permeabilization.

We showed that in cultured immortalized hepatocytes, FA incubation for 24 h increased the mitochondrial sensitivity to Ca<sup>2+</sup>-induced loss of membrane potential and reduced VDAC phosphorylation (Martel et al., 2013). These alterations were also observed in mitochondria isolated from genetically obese or high fat diet fed mice liver. Notably, VDAC phosphorylation level is correlated with steatosis severity in patients, suggesting that VDAC's lack of phosphorylation may represent a hallmark of chronic lipid exposure during steatosis in mammals. In accordance with other studies (Cuadrado-Tejedor et al., 2011; Pastorino et al., 2005; Sheldon et al., 2011; Wang et al., 2013), our pharmacological and genetic manipulation pointed to GSK3 as the kinase responsible for this phosphorylation, as its activity was diminished by lipid accumulation within the hepatocytes. Furthermore, this also amplifies VDAC enzymatic activity and modulates the ionic channel permeability of VDAC in response to Ca<sup>2+</sup>, which may influence mitochondrial OM permeability and mitochondrial metabolism (Bathori et al., 2006; Tan and Colombini, 2007).

Lipid-induced lack of phosphorylation not only disturbed VDAC intrinsic gating properties, but also resulted in a change of its interactome. Indeed, in normal mouse liver mitochondria, phosphorylated VDAC is part of a complex containing at least GSK3 and the anti-apoptotic Bcl-X<sub>L</sub>. Despite separately known interactions between these two proteins and VDAC (Arbel et al., 2012; Cuadrado-Tejedor et al., 2011; Huang et al., 2013; Malia and Wagner, 2007; Pastorino et al., 2005; Sheldon et al., 2011; Vander Heiden et al., 2001; Wang et al., 2013), they are described for the first time as physically interacting altogether. In fact, this complex is likely to participate in the preservation of the mitochondrial OM integrity, as its disruption after lipid induction is associated with an increased sensitivity to membrane permeabilization. As summarized in Fig. 2, VDAC phosphorylation could be considered as a sensor of lipotoxicity controlling the balance between survival adaptive response and stress signals leading to hepatocyte cell death.

## 6. Open question and perspectives

After 40 years of functional and structural study, VDAC appeared to be at the crossroad between metabolism and cell death. However, VDAC can still be viewed as a friend or a foe depending on the isoform considered (McCommis and Baines, 2012). Many aspects of VDAC isoform regulation remain to be learned and we anticipate that the technological advances of -omic studies will help to better understand the pathophysiological relevance of the various VDAC post-translational modifications in the future. Notably, more information on VDAC2 isoform and VDAC acetylation is needed. This might have important implication for the targeting of mitochondria in pathologies, which exhibit a mitochondrial dysfunction such as cancer and cardiovascular diseases (Fulda et al., 2010; Krasnov et al., 2013; Rosano, 2011). The recent finding that VDAC can behave as a lipid sensor (Martel et al., 2013) also opens new avenues for novel therapeutic strategies for pathologies in which a lipid storage deregulation has been described such as steatosis, diabetes as well as metabolic syndrome.

## Acknowledgments

We apologize to the colleagues that were not cited in the article despite their contribution to the field. The authors are supported by LabEx LERMIT and ANR (ANR-13-ISV1-0001-01). CM is funded by the Fonds de recherche du Québec – Santé, Canada. ZW receives a fellowship from the Government of China.

## References

- Agafonov, A., Gritsenko, E., Belosludtsev, K., Kovalev, A., Gateau-Roesch, O., Saris, N.E., Mironova, G.D., 2003. A permeability transition in liposomes induced by the formation of Ca<sup>2+</sup>/palmitic acid complexes. *Biochim. Biophys. Acta* 1609, 153–160.
- Agafonov, A.V., Gritsenko, E.N., Shlyapnikova, E.A., Kharakoz, D.P., Belosludtseva, N.V., Lezhnev, E.I., Saris, N.E., Mironova, G.D., 2007. Ca<sup>2+</sup>-induced phase separation in the membrane of palmitate-containing liposomes and its possible relation to membrane permeabilization. *J. Membr. Biol.* 215, 57–68.
- Al Bitar, F., Roosen, N., Smeyers, M., Vauterin, M., Van Bostel, J., Jacobs, M., Homble, F., 2003. Sequence analysis, transcriptional and posttranscriptional regulation of the rice VDAC family. *Biochim. Biophys. Acta* 1625, 43–51.
- Anflous, K., Armstrong, D.D., Craigen, W.J., 2001. Altered mitochondrial sensitivity for ADP and maintenance of creatine-stimulated respiration in oxidative striated muscles from VDAC1-deficient mice. *J. Biol. Chem.* 276, 1954–1960.
- Antonsson, B., Conti, F., Ciavatta, A., Montessuit, S., Lewis, S., Martinou, I., Bernasconi, L., Bernard, A., Mermod, J.J., Mazzei, G., Maundrell, K., Gambale, F., Sadoul, R., Martinou, J.C., 1997. Inhibition of Bax channel-forming activity by Bcl-2. *Science* 277, 370–372.
- Antonsson, B., Montessuit, S., Lauper, S., Eskes, R., Martinou, J.C., 2000. Bax oligomerization is required for channel-forming activity in liposomes and to trigger cytochrome c release from mitochondria. *Biochem. J.* 345 (Pt 2), 271–278.
- Arbel, N., Ben-Hail, D., Shoshan-Barmatz, V., 2012. Mediation of the antiapoptotic activity of Bcl-X<sub>L</sub> protein upon interaction with VDAC1 protein. *J. Biol. Chem.* 287, 23152–23161.
- Arcelay, E., Salicioni, A.M., Wertheimer, E., Visconti, P.E., 2008. Identification of proteins undergoing tyrosine phosphorylation during mouse sperm capacitation. *Int. J. Dev. Biol.* 52, 463–472.
- Baines, C.P., Song, C.X., Zheng, Y.T., Wang, G.W., Zhang, J., Wang, O.L., Guo, Y., Bolli, R., Cardwell, E.M., Ping, P., 2003. Protein kinase Cε interacts with and inhibits the permeability transition pore in cardiac mitochondria. *Circ. Res.* 92, 873–880.
- Baines, C.P., Kaiser, R.A., Sheiko, T., Craigen, W.J., Molkenin, J.D., 2007. Voltage-dependent anion channels are dispensable for mitochondrial-dependent cell death. *Nat. Cell Biol.* 9, 550–555.
- Baker, M.A., Ly, J.D., Lawen, A., 2004. Characterization of VDAC1 as a plasma membrane NADH-oxidoreductase. *Biofactors* 21, 215–221.
- Ballif, B.A., Carey, G.R., Sunyaev, S.R., Gygi, S.P., 2008. Large-scale identification and evolution indexing of tyrosine phosphorylation sites from murine brain. *J. Proteome Res.* 7, 311–318.
- Banerjee, J., Ghosh, S., 2006. Phosphorylation of rat brain mitochondrial voltage-dependent anion as a potential tool to control leakage of cytochrome c. *J. Neurochem.* 98, 670–676.
- Basanez, G., Sharpe, J.C., Galanis, J., Brandt, T.B., Hardwick, J.M., Zimmerberg, J., 2002. Bax-type apoptotic proteins porate pure lipid bilayers through a mechanism sensitive to intrinsic monolayer curvature. *J. Biol. Chem.* 277, 49360–49365.
- Bathori, G., Csordas, G., Garcia-Perez, C., Davies, E., Hajnoczky, G., 2006. Ca<sup>2+</sup>-dependent control of the permeability properties of the mitochondrial outer membrane and voltage-dependent anion-selective channel (VDAC). *J. Biol. Chem.* 281, 17347–17358.
- Bayrhuber, M., Meins, T., Habeck, M., Becker, S., Giller, K., Villinger, S., Vornheim, C., Griesinger, C., Zweckstetter, M., Zeth, K., 2008. Structure of the human voltage-dependent anion channel. *Proc. Natl. Acad. Sci. U. S. A.* 105, 15370–15375.

- Belosludtsev, K.N., Saris, N.E., Belosludtseva, N.V., Trudovishnikov, A.S., Lukyanova, L.D., Mironova, G.D., 2009. Physiological aspects of the mitochondrial cyclosporin A-insensitive palmitate/Ca<sup>2+</sup>-induced pore: tissue specificity, age profile and dependence on the animal's adaptation to hypoxia. *J. Bioenerg. Biomembr.* 41, 395–401.
- Belzacq-Casagrande, A.S., Martel, C., Pertuiset, C., Borgne-Sanchez, A., Jacotot, E., Brenner, C., 2009. Pharmacological screening and enzymatic assays for apoptosis. *Front. Biosci. (Landmark Ed.)* 14, 3550–3562.
- Bera, A.K., Ghosh, S., 2001. Dual mode of gating of voltage-dependent anion channel as revealed by phosphorylation. *J. Struct. Biol.* 135, 67–72.
- Betaneli, V., Petrov, E.P., Schwille, P., 2012. The role of lipids in VDAC oligomerization. *Biophys. J.* 102, 523–531.
- Beutner, G., Ruck, A., Riede, B., Welte, W., Brdiczka, D., 1996. Complexes between kinases, mitochondrial porin and adenylate translocator in rat brain resemble the permeability transition pore. *FEBS Lett.* 396, 189–195.
- Bienvener, W.V., Sumpton, D., Martinez, A., Lilla, S., Espagne, C., Meinel, T., Giglione, C., 2012. Comparative large scale characterization of plant versus mammal proteins reveals similar and idiosyncratic N-alpha-acetylation features. *Mol. Cell. Proteomics* 11 (M111 015131).
- Brenner, C., Moulin, M., 2012. Physiological roles of the permeability transition pore. *Circ. Res.* 111, 1237–1247.
- Campbell, A.M., Chan, S.H., 2007. The voltage dependent anion channel affects mitochondrial cholesterol distribution and function. *Arch. Biochem. Biophys.* 466, 203–210.
- Campbell, A.M., Chan, S.H., 2008. Mitochondrial membrane cholesterol, the voltage dependent anion channel (VDAC), and the Warburg effect. *J. Bioenerg. Biomembr.* 40, 193–197.
- Carre, M., Andre, N., Carles, G., Borghi, H., Brichese, L., Briand, C., Braguer, D., 2002. Tubulin is an inherent component of mitochondrial membranes that interacts with the voltage-dependent anion channel. *J. Biol. Chem.* 277, 33664–33669.
- Chen, Y., Craigen, W.J., Riley, D.J., 2009. Nek1 regulates cell death and mitochondrial membrane permeability through phosphorylation of VDAC1. *Cell Cycle* 8, 257–267.
- Cheng, E.H., Sheiko, T.V., Fisher, J.K., Craigen, W.J., Korsmeyer, S.J., 2003. VDAC2 inhibits BAK activation and mitochondrial apoptosis. *Science* 301, 513–517.
- Choudhary, C., Kumar, C., Gnad, F., Nielsen, M.L., Rehman, M., Walther, T.C., Olsen, J.V., Mann, M., 2009. Lysine acetylation targets protein complexes and co-regulates major cellular functions. *Science* 325, 834–840.
- Colombini, M., Mannela, C.A., 2012. VDAC, the early days. *Biochim. Biophys. Acta* 1818, 1438–1443.
- Cuadrado-Tejedor, M., Vilarino, M., Cabodevilla, F., Del Rio, J., Frechilla, D., Perez-Mediavilla, A., 2011. Enhanced expression of the voltage-dependent anion channel 1 (VDAC1) in Alzheimer's disease transgenic mice: an insight into the pathogenic effects of amyloid-beta. *J. Alzheimers Dis.* 23, 195–206.
- Das, S., Wong, R., Rajapakse, N., Murphy, E., Steenbergen, C., 2008. Glycogen synthase kinase 3 inhibition slows mitochondrial adenine nucleotide transport and regulates voltage-dependent anion channel phosphorylation. *Circ. Res.* 103, 983–991.
- de Pablo, M.A., Susin, S.A., Jacotot, E., Larochette, N., Costantini, P., Ravagnan, L., Zamzami, N., Kroemer, G., 1999. Palmitate induces apoptosis via a direct effect on mitochondria. *Apoptosis* 4, 81–87.
- De Pinto, V., Benz, R., Palmieri, F., 1989. Interaction of non-classical detergents with the mitochondrial porin. A new purification procedure and characterization of the pore-forming unit. *Eur. J. Biochem.* 183, 179–187.
- De Stefani, D., Raffaello, A., Teardo, E., Szabo, I., Rizzuto, R., 2011. A forty-kilodalton protein of the inner membrane is the mitochondrial calcium uniporter. *Nature* 476, 336–340.
- Distler, A.M., Kerner, J., Hoppel, C.L., 2007. Post-translational modifications of rat liver mitochondrial outer membrane proteins identified by mass spectrometry. *Biochim. Biophys. Acta* 1774, 628–636.
- Epand, R.F., Martinou, J.C., Fornallaz-Mulhauser, M., Hughes, D.W., Epand, R.M., 2002. The apoptotic protein tBid promotes leakage by altering membrane curvature. *J. Biol. Chem.* 277, 32632–32639.
- Esposito, M.D., Erler, J.T., Hickman, J.A., Dive, C., 2001. Bid, a widely expressed proapoptotic protein of the Bcl-2 family, displays lipid transfer activity. *Mol. Cell. Biol.* 21, 7268–7276.
- Faustin, B., Rossignol, R., Deniaud, A., Rocher, C., Claverol, S., Malgat, M., Brenner, C., Letellier, T., 2011. The respiratory-dependent assembly of ANT1 differentially regulates Bax and Ca<sup>2+</sup> mediated cytochrome c release. *Front. Biosci. (Elite Ed.)* 3, 395–409.
- Fu, S., Watkins, S.M., Hotamisligil, G.S., 2012. The role of endoplasmic reticulum in hepatic lipid homeostasis and stress signaling. *Cell Metab.* 15, 623–634.
- Fulda, S., Galluzzi, L., Kroemer, G., 2010. Targeting mitochondria for cancer therapy. *Nat. Rev. Drug Discov.* 9, 447–464.
- Furuno, T., Kanno, T., Arita, K., Asami, M., Utsumi, T., Doi, Y., Inoue, M., Utsumi, K., 2001. Roles of long chain fatty acids and carnitine in mitochondrial membrane permeability transition. *Biochem. Pharmacol.* 62, 1037–1046.
- Galluzzi, L., Kroemer, G., 2007. Mitochondrial apoptosis without VDAC. *Nat. Cell Biol.* 9, 487–489.
- Gauci, S., Helbig, A.O., Slijper, M., Krijgsvelde, J., Heck, A.J., Mohammed, S., 2009. Lys-N and trypsin cover complementary parts of the phosphoproteome in a refined SCX-based approach. *Anal. Chem.* 81, 4493–4501.
- Gentile, C.L., Frye, M.A., Pagliassotti, M.J., 2011. Fatty acids and the endoplasmic reticulum in nonalcoholic fatty liver disease. *Biofactors* 37, 8–16.
- Gonzalez-Gronow, M., Ray, R., Wang, F., Pizzo, S.V., 2013. The voltage-dependent anion channel (VDAC) binds tissue-type plasminogen activator and promotes activation of plasminogen on the cell surface. *J. Biol. Chem.* 288, 498–509.
- Granville, D.J., Gottlieb, R.A., 2003. The mitochondrial voltage-dependent anion channel (VDAC) as a therapeutic target for initiating cell death. *Curr. Med. Chem.* 10, 1527–1533.
- Guarne, P.A., Rostovtseva, T.K., Bezrukov, S.M., 2011. Tubulin-blocked state of VDAC studied by polymer and ATP partitioning. *FEBS Lett.* 585, 2363–2366.
- Guarne, P.A., Queralt-Martin, M., Aguilera, V.M., Rostovtseva, T.K., Bezrukov, S.M., 2012. Probing tubulin-blocked state of VDAC by varying membrane surface charge. *Biophys. J.* 102, 2070–2076.
- Halestrap, A.P., Brenner, C., 2003. The adenine nucleotide translocase: a central component of the mitochondrial permeability transition pore and key player in cell death. *Curr. Med. Chem.* 10, 1507–1525.
- Herrera, J.L., Fernandez, C., Diaz, M., Cury, D., Marin, R., 2011. Estradiol and tamoxifen differentially regulate a plasmalemmal voltage-dependent anion channel involved in amyloid-beta induced neurotoxicity. *Steroids* 76, 840–844.
- Hiller, S., Garces, R.G., Malia, T.J., Orekhov, V.Y., Colombini, M., Wagner, G., 2008. Solution structure of the integral human membrane protein VDAC-1 in detergent micelles. *Science* 321, 1206–1210.
- Huang, H., Hu, X., Eno, C.O., Zhao, G., Li, C., White, C., 2013. An interaction between Bcl-X<sub>L</sub> and the voltage-dependent anion channel (VDAC) promotes mitochondrial Ca<sup>2+</sup> uptake. *J. Biol. Chem.* 288, 19870–19881.
- Jancsik, V., Linden, M., Dorbani, L., Rendón, A., Nelson, B.D., 1988. Studies on the relationship between the inner and outer membranes of rat liver mitochondria as determined by subfractionation with digitonin. *Arch. Biochem. Biophys.* 264, 295–301.
- Javadov, S., Rajapurohitam, V., Kilic, A., Zeidan, A., Choi, A., Karmazyn, M., 2009. Anti-hypertrophic effect of NHE-1 inhibition involves GSK-3beta-dependent attenuation of mitochondrial dysfunction. *J. Mol. Cell. Cardiol.* 46, 998–1007.
- Johnsen, V.L., Belke, D.D., Hughey, C.C., Hittel, D.S., Hepple, R.T., Koch, L.G., Britton, S.L., Shearer, J., 2013. Enhanced cardiac protein glycosylation (O-GlcNAc) of selected mitochondrial proteins in rats artificially selected for low running capacity. *Physiol. Genomics* 45, 17–25.
- Kayser, H., Kratzin, H.D., Thinner, F.P., Gotz, H., Schmidt, W.E., Eckart, K., Hilschmann, N., 1989. Identification of human porins. II. Characterization and primary structure of a 31-kDa porin from human B lymphocytes (porin 31HL). *Biol. Chem. Hoppe Seyler* 370, 1265–1278.
- Keinan, N., Tyomkin, D., Shoshan-Barmatz, V., 2010. Oligomerization of the mitochondrial protein voltage-dependent anion channel is coupled to the induction of apoptosis. *Mol. Cell. Biol.* 30, 5698–5709.
- Kerner, J., Lee, K., Tandler, B., Hoppel, C.L., 2012. VDAC proteomics: post-translation modifications. *Biochim. Biophys. Acta* 1818, 1520–1525.
- Koshkin, V., Dai, F.F., Robson-Doucette, C.A., Chan, C.B., Wheeler, M.B., 2008. Limited mitochondrial permeabilization is an early manifestation of palmitate-induced lipotoxicity in pancreatic beta-cells. *J. Biol. Chem.* 283, 7936–7948.
- Krasnov, G.S., Dmitriev, A.A., Lakunina, V.A., Kirpiy, A.A., Kudryavtseva, A.V., 2013. Targeting VDAC-bound hexokinase II: a promising approach for concomitant anti-cancer therapy. *Expert Opin. Ther. Targets* 17, 1221–1233.
- Krauskopf, A., Eriksson, O., Craigen, W.J., Forte, M.A., Bernardi, P., 2006. Properties of the permeability transition in VDAC1(−/−) mitochondria. *Biochim. Biophys. Acta* 1757, 590–595.
- Kuwana, T., Mackey, M.R., Perkins, G., Ellisman, M.H., Latterich, M., Schneider, R., Green, D.R., Newmeyer, D.D., 2002. Bid, Bax, and lipids cooperate to form supramolecular openings in the outer mitochondrial membrane. *Cell* 111, 331–342.
- Lam, Y.W., Yuan, Y., Isaac, J., Babu, C.V., Meller, J., Ho, S.M., 2010. Comprehensive identification and modified-site mapping of S-nitrosylated targets in prostate epithelial cells. *PLoS One* 5, e9075.
- Landes, T., Martinou, J.C., 2011. Mitochondrial outer membrane permeabilization during apoptosis: the role of mitochondrial fission. *Biochim. Biophys. Acta* 1813, 540–545.
- Lazarou, M., Stojanovski, D., Frazier, A.E., Kotevski, A., Dewson, G., Craigen, W.J., Kluck, R.M., Vaux, D.L., Ryan, M.T., 2010. Inhibition of Bak activation by VDAC2 is dependent on the Bak transmembrane anchor. *J. Biol. Chem.* 285, 36876–36883.
- Le Bras, M., Clement, M.V., Pervaiz, S., Brenner, C., 2005. Reactive oxygen species and the mitochondrial signaling pathway of cell death. *Histol. Histopathol.* 20, 205–219.
- Lee, J., Xu, Y., Chen, Y., Sprung, R., Kim, S.C., Xie, S., Zhao, Y., 2007. Mitochondrial phosphoproteome revealed by an improved IMAC method and MS/MS/MS. *Mol. Cell. Proteomics* 6, 669–676.
- Lee, K., Kerner, J., Hoppel, C.L., 2011. Mitochondrial carnitine palmitoyltransferase 1a (CPT1a) is part of an outer membrane fatty acid transfer complex. *J. Biol. Chem.* 286, 25655–25662.
- Lefkimiatis, K., Leronni, D., Hofer, A.M., 2013. The inner and outer compartments of mitochondria are sites of distinct cAMP/PKA signaling dynamics. *J. Cell Biol.* 202, 453–462.
- Lemasters, J.J., Holmuhamedov, E., 2006. Voltage-dependent anion channel (VDAC) as mitochondrial governor—thinking outside the box. *Biochim. Biophys. Acta* 1762, 181–190.
- Liberatori, S., Canas, B., Tani, C., Bini, L., Buonocore, G., Godovac-Zimmermann, J., Mishra, O. P., Delivoria-Papadopoulos, M., Bracci, R., Pallini, V., 2004. Proteomic approach to the identification of voltage-dependent anion channel protein isoforms in guinea pig brain synaptosomes. *Proteomics* 4, 1335–1340.
- Liu, J., Rone, M.B., Papadopoulos, V., 2006. Protein-protein interactions mediate mitochondrial cholesterol transport and steroid biosynthesis. *J. Biol. Chem.* 281, 38879–38893.
- Low, H., Crane, F.L., Morre, D.J., 2012. Putting together a plasma membrane NADH oxidase: a tale of three laboratories. *Int. J. Biochem. Cell Biol.* 44, 1834–1838.
- Lutter, M., Fang, M., Luo, X., Nishijima, M., Xie, X., Wang, X., 2000. Cardiolipin provides specificity for targeting of tBid to mitochondria. *Nat. Cell Biol.* 2, 754–761.
- Ma, S., Hockings, C., Anwari, K., Kratina, T., Fennell, S., Lazarou, M., Ryan, M.T., Kluck, R.M., Dewson, G., 2013. Assembly of the Bak apoptotic pore: a critical role for the Bak protein alpha6 helix in the multimerization of homodimers during apoptosis. *J. Biol. Chem.* 288, 26027–26038.

- Madesh, M., Hajnoczky, G., 2001. VDAC-dependent permeabilization of the outer mitochondrial membrane by superoxide induces rapid and massive cytochrome c release. *J. Cell Biol.* 155, 1003–1015.
- Maldonado, E.N., Lemasters, J.J., 2012. Warburg revisited: regulation of mitochondrial metabolism by voltage-dependent anion channels in cancer cells. *J. Pharmacol. Exp. Ther.* 342, 637–641.
- Malia, T.J., Wagner, G., 2007. NMR structural investigation of the mitochondrial outer membrane protein VDAC and its interaction with antiapoptotic Bcl-X<sub>L</sub>. *Biochemistry* 46, 514–525.
- Marsh, D., 2008. Protein modulation of lipids, and vice-versa, in membranes. *Biochim. Biophys. Acta* 1778, 1545–1575.
- Martel, C., Allouche, M., Esposti, D.D., Fanelli, E., Boursier, C., Henry, C., Chopineau, J., Calamita, G., Kroemer, G., Lemoine, A., Brenner, C., 2013. Glycogen synthase kinase 3-mediated voltage-dependent anion channel phosphorylation controls outer mitochondrial membrane permeability during lipid accumulation. *Hepatology* 57, 93–102.
- Marzo, I., Brenner, C., Zamzami, N., Susin, S.A., Beutner, G., Brdiczka, D., Remy, R., Xie, Z.H., Reed, J.C., Kroemer, G., 1998. The permeability transition pore complex: a target for apoptosis regulation by caspases and bcl-2-related proteins. *J. Exp. Med.* 187, 1261–1271.
- Matsko, C.M., Hunter, O.C., Rabinowich, H., Lotze, M.T., Amoscato, A.A., 2001. Mitochondrial lipid alterations during Fas- and radiation-induced apoptosis. *Biochem. Biophys. Res. Commun.* 287, 1112–1120.
- Maurya, S.R., Mahalakshmi, R., 2013. Modulation of human mitochondrial voltage-dependent anion channel 2 (hVDAC-2) structural stability by cysteine-assisted barrel-lipid interactions. *J. Biol. Chem.* 288, 25584–25592.
- McCommiss, K.S., Baines, C.P., 2012. The role of VDAC in cell death: friend or foe? *Biochim. Biophys. Acta* 1818, 1444–1450.
- McIntosh, T.J., Simon, S.A., 2006. Roles of bilayer material properties in function and distribution of membrane proteins. *Annu. Rev. Biophys. Biomol. Struct.* 35, 177–198.
- Messina, A., Guarino, F., Oliva, M., van den Heuvel, L.P., Smeitink, J., De Pinto, V., 2000. Characterization of the human porin isoform 1 (hVDAC1) gene by amplification on the whole human genome: A tool for porin deficiency analysis. *Biochem. Biophys. Res. Commun.* 270, 787–792.
- Messina, A., Reina, S., Guarino, F., De Pinto, V., 2012. VDAC isoforms in mammals. *Biochim. Biophys. Acta* 1818, 1466–1476.
- Munton, R.P., Tweedie-Cullen, R., Livingstone-Zatchej, M., Weinandy, F., Waidelich, M., Longo, D., Gehrig, P., Potthast, F., Rutishauser, D., Gerrits, B., Panse, C., Schlapbach, R., Mansuy, I.M., 2007. Qualitative and quantitative analyses of protein phosphorylation in naive and stimulated mouse synaptosomal preparations. *Mol. Cell. Proteomics* 6, 283–293.
- Olsen, J.V., Blagoev, B., Gnäd, F., Macek, B., Kumar, C., Mortensen, P., Mann, M., 2006. Global, in vivo, and site-specific phosphorylation dynamics in signaling networks. *Cell* 127, 635–648.
- Oppermann, F.S., Grundner-Culemann, K., Kumar, C., Gruss, O.J., Jallepalli, P.V., Daub, H., 2012. Combination of chemical genetics and phosphoproteomics for kinase signaling analysis enables confident identification of cellular downstream targets. *Mol. Cell. Proteomics* 11 (O111), 012351.
- Orrenius, S., 2007. Reactive oxygen species in mitochondria-mediated cell death. *Drug Metab. Rev.* 39, 443–455.
- Ostrand, D.B., Sparagna, G.C., Amoscato, A.A., McMillin, J.B., Dowhan, W., 2001. Decreased cardiolipin synthesis corresponds with cytochrome c release in palmitate-induced cardiomyocyte apoptosis. *J. Biol. Chem.* 276, 38061–38067.
- Ott, M., Gogvadze, V., Orrenius, S., Zhivotovskiy, B., 2007. Mitochondria, oxidative stress and cell death. *Apoptosis* 12, 913–922.
- Oyanagi, E., Yano, H., Uchida, M., Utsumi, K., Sasaki, J., 2011. Protective action of L-carnitine on cardiac mitochondrial function and structure against fatty acid stress. *Biochem. Biophys. Res. Commun.* 412, 61–67.
- Pastorino, J.G., Shulga, N., Hoek, J.B., 2002. Mitochondrial binding of hexokinase II inhibits Bax-induced cytochrome c release and apoptosis. *J. Biol. Chem.* 277, 7610–7618.
- Pastorino, J.G., Hoek, J.B., Shulga, N., 2005. Activation of glycogen synthase kinase 3 $\beta$  disrupts the binding of hexokinase II to mitochondria by phosphorylating voltage-dependent anion channel and potentiates chemotherapy-induced cytotoxicity. *Cancer Res.* 65, 10545–10554.
- Paumen, M.B., Ishida, Y., Muramatsu, M., Yamamoto, M., Honjo, T., 1997. Inhibition of carnitine palmitoyltransferase I augments sphingolipid synthesis and palmitate-induced apoptosis. *J. Biol. Chem.* 272, 3324–3329.
- Popp, B., Schmid, A., Benz, R., 1995. Role of sterols in the functional reconstitution of water-soluble mitochondrial porins from different organisms. *Biochemistry* 34, 3352–3361.
- Raghavan, A., Sheiko, T., Graham, B.H., Craigen, W.J., 2012. Voltage-dependant anion channels: novel insights into isoform function through genetic models. *Biochim. Biophys. Acta* 1818, 1477–1485.
- Reddy, P.H., 2013. Amyloid beta-induced glycogen synthase kinase 3 $\beta$  phosphorylated VDAC1 in Alzheimer's disease: implications for synaptic dysfunction and neuronal damage. *Biochim. Biophys. Acta* 1832, 1913–1921.
- Ren, D., Kim, H., Tu, H.C., Westergaard, T.D., Fisher, J.K., Rubens, J.A., Korsmeyer, S.J., Hsieh, J.J., Cheng, E.H., 2009. The VDAC2–BAK rheostat controls thymocyte survival. *Sci. Signal.* 2, ra48.
- Rogers, C., Davis, B., Neuffer, P.D., Murphy, M.P., Anderson, E.J., Robidoux, J., 2014. A transient increase in lipid peroxidation primes preadipocytes for delayed mitochondrial inner membrane permeabilization and ATP depletion during prolonged exposure to fatty acids. *Free Radic. Biol. Med.* 67, 330–341.
- Rone, M.B., Fan, J., Papadopoulos, V., 2009. Cholesterol transport in steroid biosynthesis: role of protein–protein interactions and implications in disease states. *Biochim. Biophys. Acta* 1791, 646–658.
- Rone, M.B., Midzak, A.S., Issop, L., Rammouz, G., Jagannathan, S., Fan, J., Ye, X., Blonder, J., Veenstra, T., Papadopoulos, V., 2012. Identification of a dynamic mitochondrial protein complex driving cholesterol import, trafficking, and metabolism to steroid hormones. *Mol. Endocrinol.* 26, 1868–1882.
- Rosano, C., 2011. Molecular model of hexokinase binding to the outer mitochondrial membrane porin (VDAC1): implication for the design of new cancer therapies. *Mitochondrion* 11, 513–519.
- Rostovtseva, T.K., Bezrukov, S.M., 2012. VDAC inhibition by tubulin and its physiological implications. *Biochim. Biophys. Acta* 1818, 1526–1535.
- Rostovtseva, T.K., Antonsson, B., Suzuki, M., Youle, R.J., Colombini, M., Bezrukov, S.M., 2004. Bid, but not Bax, regulates VDAC channels. *J. Biol. Chem.* 279, 13575–13583.
- Rostovtseva, T.K., Kazemi, N., Weinrich, M., Bezrukov, S.M., 2006. Voltage gating of VDAC is regulated by nonlamellar lipids of mitochondrial membranes. *J. Biol. Chem.* 281, 37496–37506.
- Rostovtseva, T.K., Sheldon, K.L., Hassanzadeh, E., Monge, C., Saks, V., Bezrukov, S.M., Sackett, D.L., 2008. Tubulin binding blocks mitochondrial voltage-dependent anion channel and regulates respiration. *Proc. Natl. Acad. Sci. U. S. A.* 105, 18746–18751.
- Rostovtseva, T.K., Gurnev, P.A., Chen, M.Y., Bezrukov, S.M., 2012. Membrane lipid composition regulates tubulin interaction with mitochondrial voltage-dependent anion channel. *J. Biol. Chem.* 287, 29589–29598.
- Roucous, X., Montessuit, S., Antonsson, B., Martinou, J.C., 2002. Bax oligomerization in mitochondrial membranes requires tBid (caspase-8-cleaved Bid) and a mitochondrial protein. *Biochem. J.* 368, 915–921.
- Sampson, M.J., Lovell, R.S., Craigen, W.J., 1997. The murine voltage-dependent anion channel gene family. Conserved structure and function. *J. Biol. Chem.* 272, 18966–18973.
- Sampson, M.J., Decker, W.K., Beaudet, A.L., Ruitenbeek, W., Armstrong, D., Hicks, M.J., Craigen, W.J., 2001. Immobile sperm and infertility in mice lacking mitochondrial voltage-dependent anion channel type 3. *J. Biol. Chem.* 276, 39206–39212.
- Schwartz, H., Carter, J.M., Abdurehman, M., Russ, M., Buerke, U., Schlitt, A., Muller-Werdan, U., Prondzinsky, R., Werdan, K., Buerke, M., 2007. Myocardial ischemia/reperfusion causes VDAC phosphorylation which is reduced by cardioprotection with a p38 MAP kinase inhibitor. *Proteomics* 7, 4579–4588.
- Sheldon, K.L., Maldonado, E.N., Lemasters, J.J., Rostovtseva, T.K., Bezrukov, S.M., 2011. Phosphorylation of voltage-dependent anion channel by serine/threonine kinases governs its interaction with tubulin. *PLoS One* 6, e25539.
- Shimizu, S., Narita, M., Tsujimoto, Y., 1999. Bcl-2 family proteins regulate the release of apoptogenic cytochrome c by the mitochondrial channel VDAC. *Nature* 399, 483–487.
- Shimizu, S., Ide, T., Yanagida, T., Tsujimoto, Y., 2000. Electrophysiological study of a novel large pore formed by Bax and the voltage-dependent anion channel that is permeable to cytochrome c. *J. Biol. Chem.* 275, 12321–12325.
- Shinohara, Y., Ishida, T., Hino, M., Yamazaki, N., Baba, Y., Terada, H., 2000. Characterization of porin isoforms expressed in tumor cells. *Eur. J. Biochem.* 267, 6067–6073.
- Shoshan-Barmatz, V., Ben-Hail, D., 2012. VDAC, a multi-functional mitochondrial protein as a pharmacological target. *Mitochondrion* 12, 24–34.
- Shoshan-Barmatz, V., Golan, M., 2012. Mitochondrial VDAC1: function in cell life and death and a target for cancer therapy. *Curr. Med. Chem.* 19, 714–735.
- Shoshan-Barmatz, V., Keinan, N., Zaid, H., 2008. Uncovering the role of VDAC in the regulation of cell life and death. *J. Bioenerg. Biomembr.* 40, 183–191.
- Shoshan-Barmatz, V., Zakar, M., Rosenthal, K., Abu-Hamad, S., 2009. Key regions of VDAC1 functioning in apoptosis induction and regulation by hexokinase. *Biochim. Biophys. Acta* 1787, 421–430.
- Shoshan-Barmatz, V., De Pinto, V., Zweckstetter, M., Raviv, Z., Keinan, N., Arbel, N., 2010. VDAC, a multi-functional mitochondrial protein regulating cell life and death. *Mol. Aspects Med.* 31, 227–285.
- Shoshan-Barmatz, V., Mizrahi, D., Keinan, N., 2013. Oligomerization of the mitochondrial protein VDAC1: from structure to function and cancer therapy. *Prog. Mol. Biol. Transl. Sci.* 117, 303–334.
- Smith, A.W., 2012. Lipid–protein interactions in biological membranes: a dynamic perspective. *Biochim. Biophys. Acta* 1818, 172–177.
- Sol, E.M., Wagner, S.A., Weinert, B.T., Kumar, A., Kim, H.S., Deng, C.X., Choudhary, C., 2012. Proteomic investigations of lysine acetylation identify diverse substrates of mitochondrial deacetylase sirt3. *PLoS One* 7, e50545.
- Sparagna, G.C., Hickson-Bick, D.L., Buja, L.M., McMillin, J.B., 2000. A metabolic role for mitochondria in palmitate-induced cardiac myocyte apoptosis. *Am. J. Physiol. Heart Circ. Physiol.* 279, H2124–H2132.
- Sun, L., Shukair, S., Naik, T.J., Moazed, F., Ardehali, H., 2008. Glucose phosphorylation and mitochondrial binding are required for the protective effects of hexokinases I and II. *Mol. Cell. Biol.* 28, 1007–1017.
- Szabo, I., Zoratti, M., 1993. The mitochondrial permeability transition pore may comprise VDAC molecules. I. Binary structure and voltage dependence of the pore. *FEBS Lett.* 330, 201–205.
- Tan, W., Colombini, M., 2007. VDAC closure increases calcium ion flux. *Biochim. Biophys. Acta* 1768, 2510–2515.
- Thinness, F.P., Burckhardt, G., 2012. On a fully closed state of native human type-1 VDAC enriched in Nonidet P40. *Mol. Genet. Metab.* 107, 632–633.
- Thinness, F.P., Gotz, H., Kayser, H., Benz, R., Schmidt, W.E., Kratzin, H.D., Hilschmann, N., 1989. Identification of human porins. I. Purification of a porin from human B-lymphocytes (porin 31HL) and the topochemical proof of its expression on the plasmalemma of the progenitor cell. *Biol. Chem. Hoppe Seyler* 370, 1253–1264.
- Ujwal, R., Cascio, D., Colletier, J.P., Faham, S., Zhang, J., Toro, L., Ping, P., Abramson, J., 2008. The crystal structure of mouse VDAC1 at 2.3 Å resolution reveals mechanistic insights into metabolite gating. *Proc. Natl. Acad. Sci. U. S. A.* 105, 17742–17747.
- Van Damme, P., Lasa, M., Polevoda, B., Gazquez, C., Elsegui-Artola, A., Kim, D.S., De Juan-Pardo, E., Demeyer, K., Hole, K., Larrea, E., Timmerman, E., Prieto, J., Arnesen, T., Sherman, F., Gevaert, K., Aldabe, R., 2012. N-terminal acetylome



- analyses and functional insights of the N-terminal acetyltransferase NatB. *Proc. Natl. Acad. Sci. U. S. A.* 109, 12449–12454.
- van Meer, G., Voelker, D.R., Feigenson, G.W., 2008. Membrane lipids: where they are and how they behave. *Nat. Rev. Mol. Cell Biol.* 9, 112–124.
- Vander Heiden, M.G., Li, X.X., Gottlieb, E., Hill, R.B., Thompson, C.B., Colombini, M., 2001. Bcl-X<sub>L</sub> promotes the open configuration of the voltage-dependent anion channel and metabolite passage through the outer mitochondrial membrane. *J. Biol. Chem.* 276, 19414–19419.
- Vela, L., Gonzalo, O., Naval, J., Marzo, I., 2013. Direct interaction of Bax and Bak proteins with Bcl-2 homology domain 3 (BH3)-only proteins in living cells revealed by fluorescence complementation. *J. Biol. Chem.* 288, 4935–4946.
- Vitrac, H., Bogdanov, M., Heacock, P., Dowhan, W., 2011. Lipids and topological rules of membrane protein assembly: balance between long and short range lipid–protein interactions. *J. Biol. Chem.* 286, 15182–15194.
- Wang, Z., Ge, Y., Bao, H., Dworkin, L., Peng, A., Gong, R., 2013. Redox-sensitive glycogen synthase kinase 3 $\beta$ -directed control of mitochondrial permeability transition: rheostatic regulation of acute kidney injury. *Free Radic. Biol. Med.* 65, 849–858.
- Weeber, E.J., Levy, M., Sampson, M.J., Anflous, K., Armstrong, D.L., Brown, S.E., Sweatt, J.D., Craigen, W.J., 2002. The role of mitochondrial porins and the permeability transition pore in learning and synaptic plasticity. *J. Biol. Chem.* 277, 18891–18897.
- Wieckowski, M.R., Wojtczak, L., 1998. Fatty acid-induced uncoupling of oxidative phosphorylation is partly due to opening of the mitochondrial permeability transition pore. *FEBS Lett.* 423, 339–342.
- Woodfield, K., Ruck, A., Brdiczka, D., Halestrap, A.P., 1998. Direct demonstration of a specific interaction between cyclophilin-D and the adenine nucleotide translocase confirms their role in the mitochondrial permeability transition. *Biochem. J.* 336 (Pt 2), 287–290.
- Wu, S., Sampson, M.J., Decker, W.K., Craigen, W.J., 1999. Each mammalian mitochondrial outer membrane porin protein is dispensable: effects on cellular respiration. *Biochim. Biophys. Acta* 1452, 68–78.
- Yamamoto, T., Yamada, A., Watanabe, M., Yoshimura, Y., Yamazaki, N., Yamauchi, T., Kataoka, M., Nagata, T., Terada, H., Shinohara, Y., 2006. VDAC1, having a shorter N-terminus than VDAC2 but showing the same migration in an SDS-polyacrylamide gel, is the predominant form expressed in mitochondria of various tissues. *J. Proteome Res.* 5, 3336–3344.
- Yi, C.H., Pan, H., Seebacher, J., Jang, I.H., Hyberts, S.G., Heffron, G.J., Vander Heiden, M.G., Yang, R., Li, F., Locasale, J.W., Sharfi, H., Zhai, B., Rodriguez-Mias, R., Luithardt, H., Cantley, L.C., Daley, G.Q., Asara, J.M., Gygi, S.P., Wagner, G., Liu, C.F., Yuan, J., 2011. Metabolic regulation of protein N-alpha-acetylation by Bcl-X<sub>L</sub> promotes cell survival. *Cell* 146, 607–620.
- Yuan, S., Fu, Y., Wang, X., Shi, H., Huang, Y., Song, X., Li, L., Song, N., Luo, Y., 2008. Voltage-dependent anion channel 1 is involved in endostatin-induced endothelial cell apoptosis. *FASEB J.* 22, 2809–2820.
- Zaid, H., Abu-Hamad, S., Israelson, A., Nathan, I., Shoshan-Barmatz, V., 2005. The voltage-dependent anion channel-1 modulates apoptotic cell death. *Cell Death Differ.* 12, 751–760.

# The protein disulfide isomerases PDIA4 and PDIA6 mediate resistance to cisplatin-induced cell death in lung adenocarcinoma

G Tufo<sup>1,2</sup>, AWE Jones<sup>3</sup>, Z Wang<sup>1,2</sup>, J Hamelin<sup>4</sup>, N Tajeddine<sup>5</sup>, DD Esposti<sup>4</sup>, C Martel<sup>1,2,6</sup>, C Boursier<sup>7</sup>, C Gallerne<sup>1,2</sup>, C Migdal<sup>2,8</sup>, C Lemaire<sup>1,9</sup>, G Szabadkai<sup>3,10</sup>, A Lemoine<sup>4</sup>, G Kroemer<sup>5,11,12,13,14</sup> and C Brenner<sup>\*,1,2</sup>

Intrinsic and acquired chemoresistance are frequent causes of cancer eradication failure. Thus, long-term cis-diaminedichloroplatine(II) (CDDP) or cisplatin treatment is known to promote tumor cell resistance to apoptosis induction via multiple mechanisms involving gene expression modulation of oncogenes, tumor suppressors and blockade of pro-apoptotic mitochondrial membrane permeabilization. Here, we demonstrate that CDDP-resistant non-small lung cancer cells undergo profound remodeling of their endoplasmic reticulum (ER) proteome (> 80 proteins identified by proteomics) and exhibit a dramatic overexpression of two protein disulfide isomerases, PDIA4 and PDIA6, without any alteration in ER-cytosol  $\text{Ca}^{2+}$  fluxes. Using pharmacological and genetic inhibition, we show that inactivation of both proteins directly stimulates CDDP-induced cell death by different cellular signaling pathways. PDIA4 inactivation restores a classical mitochondrial apoptosis pathway, while knockdown of PDIA6 favors a non-canonical cell death pathway sharing some necroptosis features. Overexpression of both proteins has also been found in lung adenocarcinoma patients, suggesting a clinical importance of these proteins in chemoresistance.

*Cell Death and Differentiation* (2014) 21, 685–695; doi:10.1038/cdd.2013.193; published online 24 January 2014

One of the major aims of chemotherapy is to induce apoptosis to eradicate cancer cells, but cancer cells are intrinsically resistant or acquire chemoresistance to apoptosis that may lead to treatment failure.<sup>1,2</sup> Thus, many chemotherapeutic agents such as the DNA-damaging agent cisplatin (cis-diaminedichloroplatine(II) (CDDP)) initiate a mitochondrial cell death pathway involving Bcl-2 family members, p53, mitochondrial membrane permeabilization (MMP), cytochrome *c* release and caspase activation in tumor cells.<sup>3–5</sup> Following several years of treatment, CDDP-treated tumors, such as lung, ovarian, testicular and head and neck carcinomas, develop resistance to CDDP-induced apoptosis. Although causes of chemoresistance can be multiple, adaptation to endoplasmic reticulum (ER) stress, as a result of chronic and mild unfolded protein response (UPR), might be a key driver of malignancy and resistance to therapy.<sup>6–9</sup>

The UPR is activated when misfolded proteins accumulate in the ER as a result of exogenous and/or endogenous stress signals.<sup>8</sup> Although ER stress responses represent homeostatic mechanisms allowing cells to survive, prolonged or

excessive activation of the UPR can result in cell death by inducing primarily mitochondrial apoptosis.<sup>10,11</sup> UPR is regulated by the balance between expression levels and post-translational modification status of ER sensor proteins, including ER to nucleus signaling 1 (IRE1), protein kinase RNA-like endoplasmic reticulum kinase (PERK) and activating transcription factor 6 (ATF6). It is frequently accompanied by an altered calcium homeostasis and autophagy.<sup>8</sup> Moreover, 78 kDa glucose-regulated protein (GRP78) overexpression has been associated with enhanced tumor growth and resistance to chemotherapy.<sup>12,13</sup> However, how the UPR switches between the pro-survival and pro-apoptotic signaling pathways<sup>14,15</sup> and therefore how it might contribute to cancer cell resistance is still unknown.

Here we addressed the hypothesis that CDDP resistance of non-small lung cancer (NSLC) relies on specific adaptation mechanisms involving ER resident proteins such as protein disulfide isomerase (PDI) without any alteration of  $\text{Ca}^{2+}$  fluxes between ER and mitochondria. A set of CDDP-resistant NSLC A549 cell lines<sup>16</sup> and lung cancer patients biopsies

<sup>1</sup>INSERM UMR-S 769, LabEx LERMIT, Châtenay-Malabry, France; <sup>2</sup>Faculté de Pharmacie, Université de Paris-Sud, Châtenay-Malabry, France; <sup>3</sup>Department of Cell and Developmental Biology, University College London, London, UK; <sup>4</sup>APHP Hôpital P. Brousse, Biochimie et oncogénétique, INSERM U1004, Villejuif, France; <sup>5</sup>INSERM U848, Institut Gustave Roussy, Université Paris-Sud 11, PR1, 39 rue Camille Desmoulins, Villejuif, France; <sup>6</sup>Montreal Heart Institute, Centre de Recherche, Montreal, Quebec, Canada; <sup>7</sup>IFR 141-IPSIT, Châtenay-Malabry, France; <sup>8</sup>INSERM U 996, Châtenay-Malabry, France; <sup>9</sup>Department of Biology, University of Versailles–St Quentin, Versailles, France; <sup>10</sup>Department of Biomedical Sciences, University of Padua, Padua, Italy; <sup>11</sup>Université Paris Descartes/Paris V, Sorbonne Paris Cité, Paris, France; <sup>12</sup>Metabolomics Platform, Institut Gustave Roussy, Villejuif, France; <sup>13</sup>Equipe 11 labellisée par la Ligue contre le Cancer, Centre de Recherche des Cordeliers, Paris, France and <sup>14</sup>Pôle de Biologie, Hôpital Européen Georges Pompidou, AP-HP, 75015 Paris, France

\*Corresponding author: C Brenner, INSERM UMR-S 769, Université de Paris-Sud, LabEx LERMIT, 5 rue Baptiste Clément, Châtenay Malabry 92290, France. Tel: +33 6 6099 3277; Fax: +33 1 4683 5475; E-mail: catherine.brenner-jan@u-psud.fr

**Keywords:** apoptosis; chemotherapy; necroptosis

**Abbreviations:** ATF6, activating transcription factor 6; CDDP, cis-diaminedichloroplatine(II); DTT, dithiothreitol; IRE1, ER to nucleus signaling 1; MMP, mitochondrial membrane permeabilization; MS, mass spectrometry; NSLC, non-small lung cancer; PDI, protein disulfide isomerase; PERK, protein kinase RNA-like endoplasmic reticulum kinase; GRP78, 78 kDa glucose-regulated protein;  $\Delta\Psi_m$ , transmembrane inner potential

Received 23.5.13; revised 14.11.13; accepted 02.12.13; Edited by P Mehlen; published online 24.1.14

were investigated to identify novel anti-apoptotic proteins responsible for CDDP resistance. Accordingly, pharmacological inhibition and genetic manipulation of PDIA4 and PDIA6 restored cell death induction in CDDP-resistant clones, revealing for the first time their role in cancer cell adaptation and chemoresistance.

## Results

**Chronic adaptation of lung carcinoma cells to CDDP involves the alteration of the UPR pathway in the ER.** A549 lung adenocarcinoma cells (wild type, WT) were cultured in the presence of low doses of CDDP (5  $\mu$ M), until the appearance of resistant cells able to survive and maintain their resistance phenotype in the absence of the selection pressure and three clones, named A549 R1, R2 and R3, were isolated.<sup>16</sup> Using a clonogenic assay, the proliferation capacity of these clones was evaluated following culture of a similar number of cells of the resistant clones for 48 h before

plating. Resistant cells appeared to grow faster than WT cells with a significant difference between each clone and WT ( $P < 0.01$ ; Figures 1a and b).

Two essential parameters of apoptosis were measured according to international criteria,<sup>17</sup> collapse of mitochondrial transmembrane potential ( $\Delta\Psi_m$ ) and hypodiploidy (SubG1 peak) by flow cytometry. As expected,<sup>16,18</sup> WT cells showed dose-dependent loss of  $\Delta\Psi_m$  with 25 and 50  $\mu$ M CDDP at 24 h, indicating that CDDP treatment induces the mitochondrial pathway of apoptosis (Figure 1c). CDDP-induced loss of  $\Delta\Psi_m$  was significantly prevented in all resistant clones, although to various extent. In addition, a large fraction of WT cells appeared as a SubG1 population at 48 h following CDDP treatment, confirming the apoptosis induction by CDDP, but no significant enhancement of this event was found in resistant clones (Figure 1d). As CDDP has no direct effect on highly purified isolated mitochondria (not shown), data from the first set of experiments indicated that resistance to CDDP-induced apoptosis of R1, R2 and R3 clones involves a mechanism upstream of MMP.

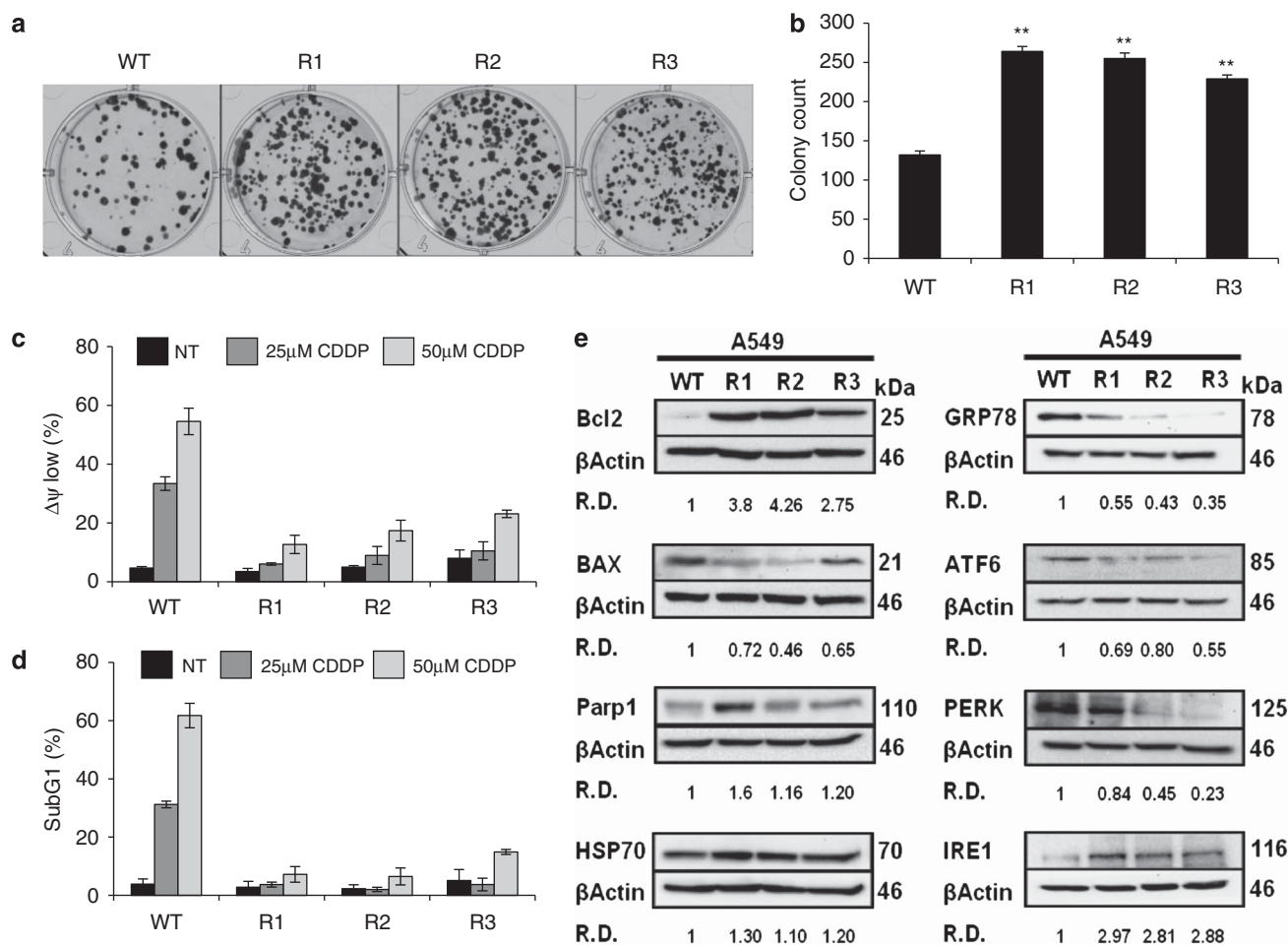


**Figure 1** CDDP-resistance lung cell model. (a) A549 wild-type cells (WT) and resistant R1 to R3 clones from 4-day precultures were plated and incubated for 14 days. (b) Colony count shows that R1 grows faster than R2, R3 and WT cells. Data points are mean  $\pm$  S.E.M. from three experiments performed in triplicate ( $n = 3$ , mean  $\pm$  S.E.M.). (c and d) WT and resistant clones were incubated with 0 (NT), 25 and 50  $\mu$ M CDDP. (c) The level of the  $\Delta\Psi_m$  was measured with the TMRM fluorescent probe by flow cytometry at 24 h ( $n = 6$ , mean  $\pm$  S.D.). (d) DNA content was measured with propidium iodide at 48 h ( $n = 6$ , mean  $\pm$  S.D.). (e) Western blotting analysis of apoptotic proteins, chaperones and ER stress markers in A549 WT and R1 to R3 clones. Thirty micrograms of cellular proteins have been immunoblotted by antibodies against BCL-2, BAX, PARP1, PERK, IRE1, ATF6 and GRP78. Western blots are representative of three independent experiments

Next, we characterized expression levels of several apoptosis-related proteins by immunoblotting (Figure 1e). Indeed, we observed increased Bcl-2, Hsp70 and PARP1 expression in parallel with a decreased Bax expression in the CDDP-resistant clones. This result is in line with a previously described balance between anti- and pro-apoptotic proteins directly regulating MMP and chemoresistance.<sup>15,19–22</sup>

However, these observations did not unravel the pathways upstream of MMP, which can be involved in the development of CDDP resistance. It has been previously established that ER homeostasis can be a common extra-nuclear target of CDDP.<sup>23</sup> Moreover, our previous work established a role of the UPR and consequent ER stress as one of the most potent endogenous inducers of MMP and cell death.<sup>11</sup> This led us to hypothesize that alteration of the UPR might be involved in the resistance to CDDP-induced cell death. Thus, we evaluated the expression of three UPR sensors, ATF6, IRE1 and PERK, and their major partner, GRP78.<sup>8</sup> Confirming our hypothesis, all these proximal UPR factors were differentially regulated in the CDDP-resistant clones as compared with WT. ATF6 and PERK expression was downregulated, whereas the IRE1 expression increased (Figure 1e). Surprisingly, we also observed a dramatic reduction in the expression of GRP78 in all the resistant clones (Figure 1e). These results suggested that adaptation to ER stress, as shown by the differential modulation of ER proteins levels, might be a central process to the chronically acquired chemoresistance but that there is no canonical ER stress *per se*.

**Altered ER  $\text{Ca}^{2+}$  homeostasis is not required for resistance to CDDP.**  $\text{Ca}^{2+}$  release from the ER and subsequent mitochondrial  $\text{Ca}^{2+}$  overload and MMP have

been shown to have a crucial role in ER stress-induced cancer cell death.<sup>11,24</sup> Thus we investigated whether development of CDDP resistance was associated with alterations of ER  $\text{Ca}^{2+}$  homeostasis and  $\text{Ca}^{2+}$ -mediated MMP. First, we expressed ERD1, a FRET-based ER-targeted recombinant  $\text{Ca}^{2+}$  probe<sup>25</sup> in WT and R1 cells (i.e., the clone showing the highest level of resistance) and measured steady-state  $\text{Ca}^{2+}$  levels under control conditions and following 24 h treatment with CDDP (75  $\mu\text{M}$ ), using an acceptor bleaching method previously established in our laboratory.<sup>26</sup> We did not find any significant differences between the steady ER  $\text{Ca}^{2+}$  concentrations ( $[\text{Ca}^{2+}]_{\text{ER}}$ ) in the WT and R1 cells (Figure 2a). Moreover, we observed no ER  $\text{Ca}^{2+}$  depletion following CDDP treatment. Thapsigargin, an inhibitor of ER  $\text{Ca}^{2+}$  accumulation,<sup>27</sup> induced a large drop in the FRET signal, validating the experimental method (Figure 2a). In line with these results, no increase in cytosolic  $[\text{Ca}^{2+}]$  ( $[\text{Ca}^{2+}]_{\text{c}}$ ) was found following CDDP treatment, as measured in WT cells loaded with the fluorescence  $\text{Ca}^{2+}$ -sensitive dye Fura-2 (Figure 2b). Finally, in order to assess the contribution of cellular  $\text{Ca}^{2+}$  signaling to CDDP-induced cell death, we applied extracellular (EGTA, Figure 2c) and intracellular (BAPTA-AM, Figure 2d)  $\text{Ca}^{2+}$  chelators, and an inhibitor of  $\text{Ca}^{2+}$  release from the ER (2-APB, Figure 2e) and quantified cell death in WT cells following 24 h treatment with CDDP. Neither EGTA nor 2-APB had any effect on the efficiency of CDDP to induce cell death, while BAPTA-AM pretreatment led to a significant but small protection ( $52.3 \pm 1.57\%$  cell death in control WT cells *versus*  $41.4 \pm 2.62\%$  in the presence of BAPTA-AM, 10  $\mu\text{M}$ , Figure 2d). In conclusion, neither  $\text{Ca}^{2+}$  influx nor  $\text{Ca}^{2+}$  release from the ER contributed significantly to

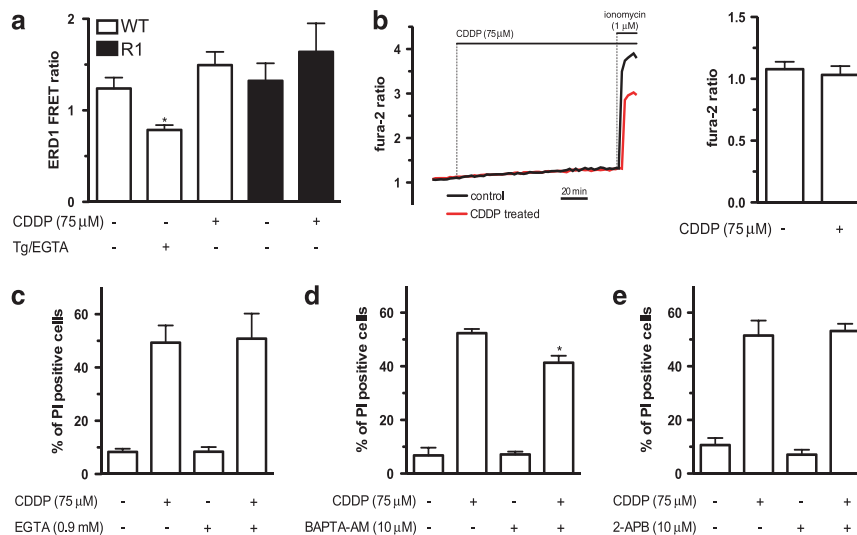


**Figure 2**  $\text{Ca}^{2+}$  signaling is not implied in CDDP-induced cell death. (a) Steady state  $[\text{Ca}^{2+}]_{\text{ER}}$  was measured by ERD1 probe FRET efficiency in WT and R1 A549 cells left either untreated or after 24 h treatment with CDDP (75  $\mu\text{M}$ ), as described in the Materials and Methods section (see also Supplementary Figure S1). As positive control, WT cells were treated with thapsigargin in the absence of extracellular  $\text{Ca}^{2+}$  and the presence of 100  $\mu\text{M}$  EGTA. Results shown are the mean  $\pm$  S.E.M. of at least three different cell preparations (\* $P < 0.05$ ). (b) Timelapse imaging of  $[\text{Ca}^{2+}]_{\text{c}}$  for 180 min following CDDP treatment. Representative traces are shown on the left panel. CDDP was applied as indicated, and fura-2 loading was tested by the addition of 1  $\mu\text{M}$  ionomycin. On the right panel, mean  $\pm$  S.E.M. of background-corrected 340 nm/380 nm Fura-2 ratios are shown from at least three different cell populations following 60 min of CDDP treatment. (c–e). The effect of extracellular (EGTA, c), intracellular (BAPTA-AM, d)  $\text{Ca}^{2+}$  chelation and inhibition of  $\text{Ca}^{2+}$  release from the ER (2-APB, e) on CDDP-induced cell death. The chelators and inhibitor were applied in the culture medium at the indicated concentrations either to control cells or to cells treated with CDDP (75  $\mu\text{M}$ , 24 h), and cell death was measured by determination of the ratio of PI-positive cells, as described in the Materials and Methods section. Results shown are the mean  $\pm$  S.E.M. of at least three different cell preparations (\* $P < 0.05$ )



CDDP-mediated cell death, implying that alterations in ER  $\text{Ca}^{2+}$  homeostasis cannot explain the CDDP resistance of resistant cells. The slight inhibition of CDDP-induced cell death in BAPTA-AM-treated cells might reflect inhibition of calpains, which have been previously shown to marginally contribute to caspase activation following CDDP treatment of A549 cells.<sup>16</sup>

**Proteomics identifies ER adaptations mediating CDDP resistance.** In order to identify novel ER-resident pathways contributing to CDDP resistance, we used an unbiased approach consisting of the comparison of the ER proteomes from WT and R1 cells. Proteins of an ER-enriched fraction, obtained by differential centrifugation, were separated by 2D denaturing electrophoresis. At least three replicate gels per cell type were silver-stained for quantitative analysis of the ER proteome. Among 492 ER proteins found in R1 and WT (not shown), 80 were overexpressed 2–10-fold in R1 compared with WT (Supplementary Figure S2). Forty spots were further analyzed by nanoLC/MS/MS, and 23 were identified by their MASCOT score and SwissProt accession number (Supplementary Table S1). Among this set, we identified a group of genuine ER proteins related to protein-folding functions, which belong to the PDI family. PDIA4 levels were increased 11.2-fold while PDIA6 was upregulated 7.75-fold in ER as measured by densitometry of 2D electrophoresis gels (Figure 3a). Moreover, these proteins were found to be overexpressed in total cell lysates of all CDDP-resistant clones by immunoblotting of 1D gels, except for PDIA4 whose expression remained unchanged in R3 cells (Figure 3b). These results suggested an importance of these proteins in the development of ER-mediated adaptation to CDDP-induced cellular stress. Therefore, we further explored their regulation and role.

PDI proteins are soluble  $\text{Ca}^{2+}$ -binding chaperones containing thioredoxin-like domains,<sup>28</sup> but little information is available on physiological PDIA4 and PDIA6 activity. Therefore, we determined whether changes in PDIA4 and PDIA6 protein levels lead to a change in cellular PDI enzymatic activity. Using an *in vitro* assay of insulin disulfide bonds reduction, we identified an enhancement of PDI activity in all resistant clones compared with WT cells (Figure 3c). Total PDI activity was increased in R1, R2 and R3 cells by 39, 37 and 42% of the WT, respectively. Next, we treated the resistant cells with bacitracin, a pan inhibitor of PDIs, and observed an increase in the CDDP-induced loss of  $\Delta\Psi_m$ , restoring almost completely CDDP sensitivity for the highest dose of PDI inhibitor (Figure 3d).<sup>29</sup> These results indicate that pharmacological PDI inhibition rescues MMP induction by CDDP and suggests that PDIs might have a direct role in CDDP resistance.

**Genetic downregulation of some PDI isoforms reverses CDDP resistance.** Twenty-one genes are known to encode PDI family members. With the aim of identifying PDI isoform(s) responsible for CDDP resistance, we transfected pools of siRNAs to selectively and individually inhibit the expression of various PDI isoforms. Four isoforms have been selected because of their previously characterized role in survival to ER stress (PDIA1),<sup>30</sup> in  $\text{Ca}^{2+}$  exchange (PDIA3)<sup>31</sup> and their overexpression in the present study (PDIA4 and PDIA6). Thus, siRNAs against these four isoforms allowed efficient knockdown in A549-resistant clones with limited off-target effects in 48 h (Supplementary Figure S3). We compared the impact of the depletion of PDIA1, PDIA3, PDIA4 or PDIA6 on cell viability (Figure 4a). Knockdown of PDIA4 and PDIA6 increased the CDDP-induced cell death. In contrast, depletion of PDIA1 and PDIA3 had no effect on cell viability (Figure 4a). These

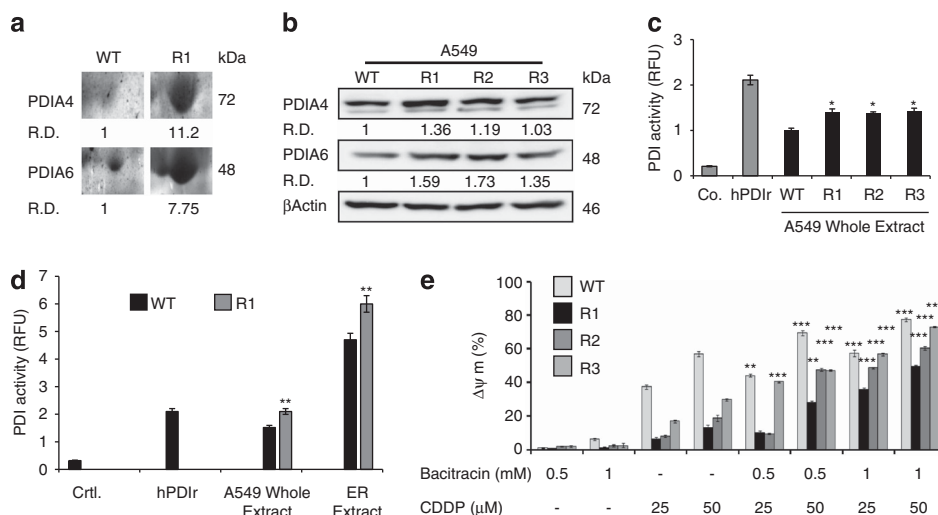


**Figure 3** PDIA4 and PDIA6 identification in resistant cells. (a) Semi-quantitative analysis of PDIA4 and PDIA6 amounts in WT and R1 cells. Proteins have been separated by 2D gel electrophoresis, gel has been stained by Blue Coomassie and the intensity of each spot has been determined by densitometry. RD, relative density. (b) Comparison of PDIA4 and PDIA6 expression in WT and R1, R2 and R3 by immunoblotting.  $\beta$ -actin is used as a loading control to quantify proteins. (c) PDI activity was quantified by measuring the PDI-catalyzed reduction of insulin in the presence of DTT in 60  $\mu\text{g}$  of whole extract from A549WT and A549R1 to R3. Co., buffer without PDI and hPDIr 16  $\mu\text{g}$  of purified human recombinant PDI ( $n=3$ , means  $\pm$  S.E.M.). (d) Similarly, PDI activity was evaluated in ER fraction of WT and R1 cells and compared to controls ( $n=3$ , means  $\pm$  S.E.M.). (e) Stimulation of CDDP-induced  $\Delta\Psi_m$  loss by 0.5 or 1 mM Bacitracin in 48 h of treatments ( $n=6$ , means  $\pm$  S.E.M.)

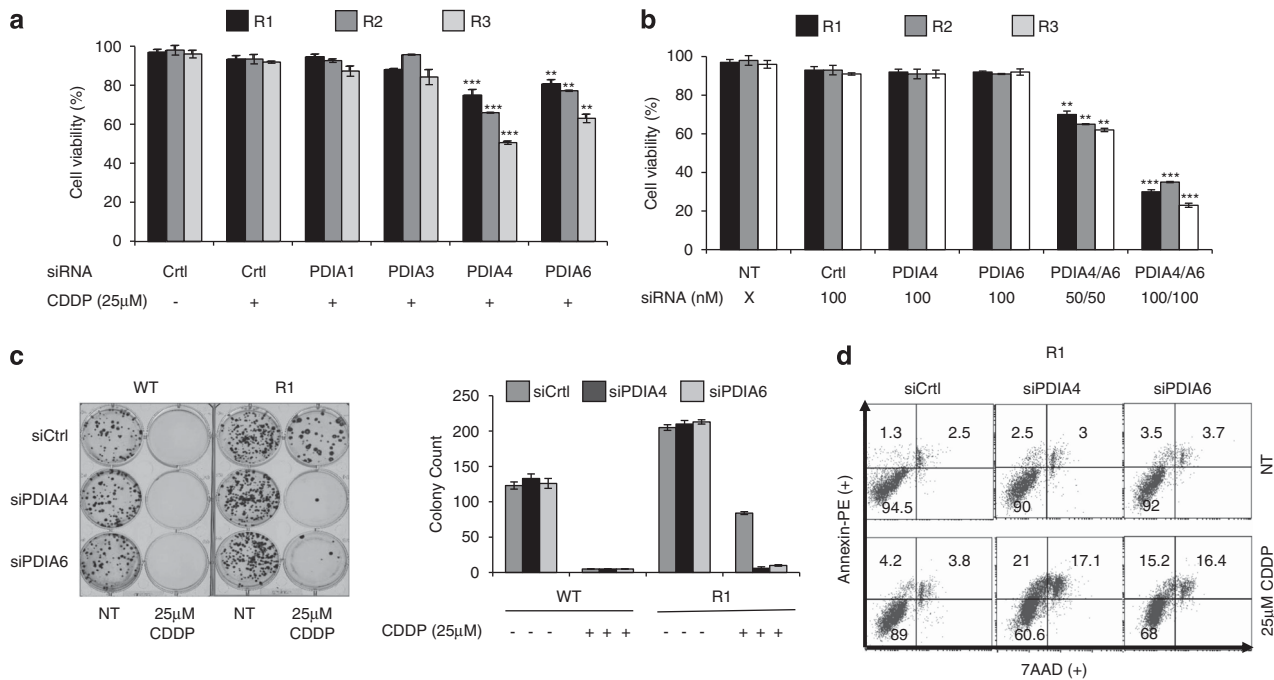


**Figure 4** Short-term and long-term effects of PDI knockdown on CDDP treatments. (a) siRNA silencing of PDIs in R1 to R3 cells. Resistant cells were transfected for 48 h with siRNA Ctrl, PDIA1, PDIA3, PDIA4 and PDIA6, and cell viability was evaluated after CDDP treatment for 48 h by WST-1 assay ( $n=3$ , mean  $\pm$  S.E.M.). Non-targeting siRNA, Ctrl. (b) Co-silencing of PDIA4 and PDIA6 in R1 to R3 cells ( $n=3$ , mean  $\pm$  S.E.M.). (c) Clonogenic assay of WT and R1 from 4-day precultures in the presence of siRNA Ctrl, PDIA4 and PDIA6 for 48 h, and 25  $\mu$ M CDDP were plated in drug-free medium in six-well plates, incubated for 14 days and colony count was determined. (d) Flow cytometry analysis of R1 cells treated by siRNAs and CDDP, as above, labeled with 7-AAD and Annexin V. Percentage of cells are indicated in parts of the panels ( $n=6$ )

results point to a potential direct role of PDIA4 and PDIA6 isoforms in CDDP resistance but exclude a role for PDIA1 and PDIA3. Co-targeting of both proteins was lethal without CDDP treatment, indicating that the presence of at least one of the isoforms is essential for normal cell physiology and that they might have overlapping functions (Figure 4b).

Next, we performed a clonogenic assay to examine the impact of PDI levels on the sensitivity of the clones to CDDP (Figure 4c). Addition of 25  $\mu$ M CDDP abolished the clonogenic potential of WT cells but only reduced the number of R1 colonies by  $>2$ -fold, in line with previous results. After knockdown of PDIA4 or PDIA6 in R1 cells, CDDP became more efficient and a rather limited number of colonies ( $\leq 8 \pm 1$ ) was observed, indicating restoration of CDDP-induced cell death. Similar results were obtained for R2 and R3 (not shown).

Using AnnexinV-PE/7AAD labeling procedure, we showed an increase in early and late apoptosis in the three clones after transfection of individual PDIA4 or PDIA6 siRNAs and CDDP treatment.

**Differential cell death pathways induced by PDIA4 and PDIA6 knockdowns.** Further characterization of cellular mechanisms revealed similarities as well as differences in PDIA4 and PDIA6 knockdown-mediated cell deaths. Thus, whereas loss of transmembrane inner potential ( $\Delta\Psi_m$ ; Figure 5a, Supplementary Figures S4A and B) and hypodiploidy (Figure 5b) were found in all clones after siRNA PDIA4/CDDP treatment, these events occurred only in R1 following siRNA PDIA6 and CDDP treatment. We then

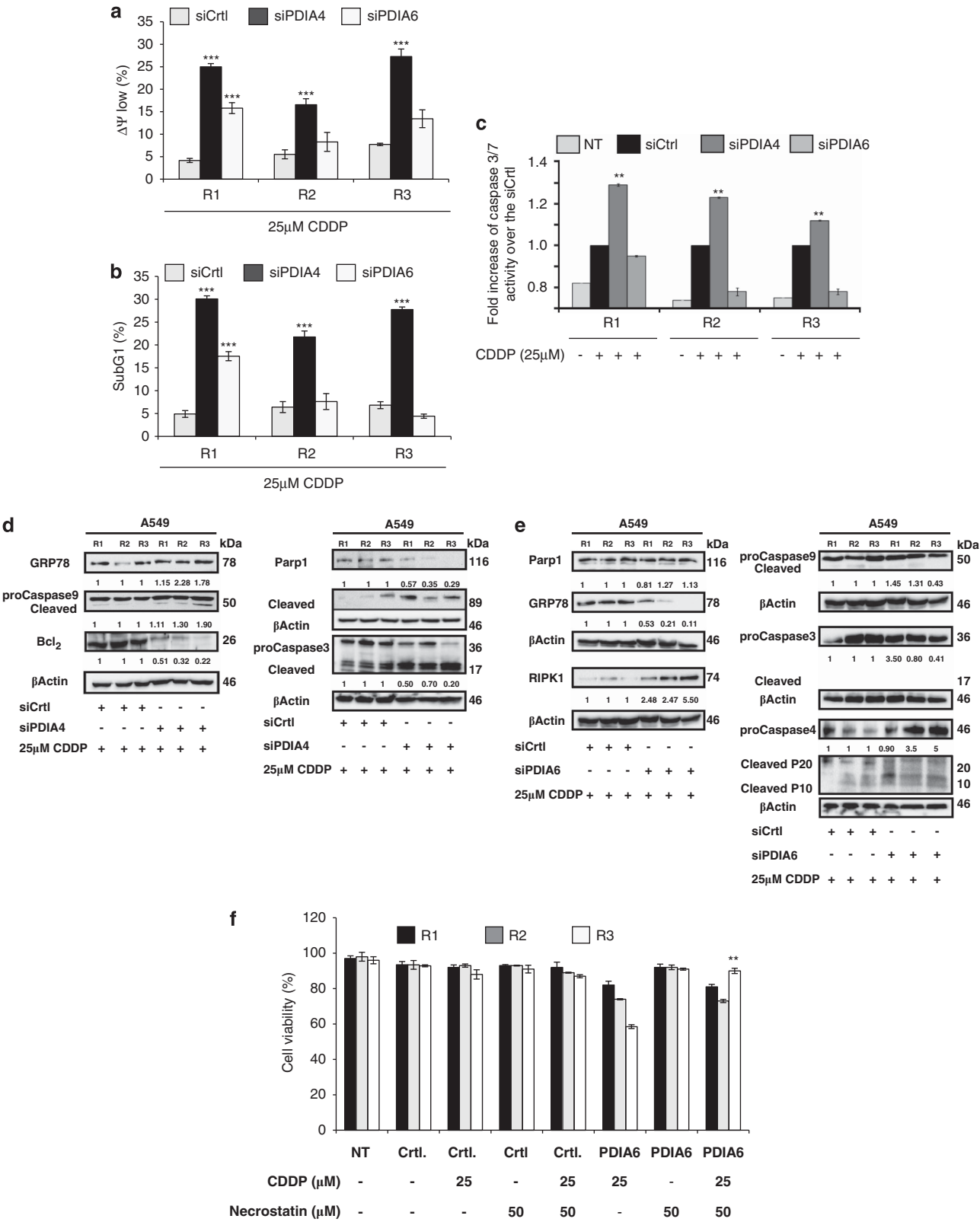
examined the post-mitochondrial caspase activation and found caspases 3/7 activation after siRNA PDIA4 and CDDP treatment and for all resistant clones (Figure 5c, Supplementary Figure S4C and D). However, caspases 3/7 were not activated in any clone by PDIA6 knockdown and CDDP treatment. This result indicates that cell death elicited by siRNA PDIA6/CDDP treatment cannot involve these effector caspases. In contrast, we observed the upregulation of caspase-4, a known inflammation and ER stress-related caspase<sup>32,33</sup> in resistant clones following siRNA PDIA6 and CDDP.

When evaluated by western blotting, PDIA4-dependent cell death pathway recapitulated events that characterize the canonical mitochondrial apoptosis pathway, namely Bcl-2 downregulation, and the cleavage of caspase-3, caspase-9 and PARP1 (Figures 5d and e). In addition, GRP78 expression was slightly enhanced. In contrast, following the treatment siRNA PDIA6/CDDP, no cleavage of the aforementioned proteins was observed, while a marked decrease of GRP78 and an increase in RIPK1 expression was observed (Figure 5e). This is intriguing because RIP1 is a kinase involved in regulated necrosis<sup>34</sup> and, accordingly, 50  $\mu$ M necrostatin 1 blocked the cell death induced in R3 ( $P<0.01$ ) but not in R2 and R1 (Figure 5f). Moreover, the amount of caspase-4 was upregulated in R2 ( $3.5\times$ ) and in R3 ( $5\times$ ), along with only a minor increase in the cleaved fragment p10 in R1 cells (Figure 5e).

Pharmacological inhibition of caspases with z-VAD-fmk, a pan-caspase inhibitor, during siPDIA6/CDDP treatment showed that caspases are essential for the cell death process (Figure 6). As caspase-3, -7 and -9 cannot be

involved in the lethal pathway (see above), we investigated the role of caspase 4. Here, our results were heterogeneous for the three resistant clones. Z-LEVD-fmk, a specific

caspase-4 inhibitor, did not prevent the death after the combined depletion of PDIA6 and CDDP treatment in R1 and R2 clones (Figure 6). In contrast, caspase-4 inhibition



significantly inhibited cell death in R3 cells, indicating a specific role of this caspase in this clone. In summary, in contrast to PDIA4 knockdown, which leads to the induction of the mitochondrial cell death pathway, the combination of PDIA6 downregulation and CDDP stimulates cell death through a non-canonical signaling pathway. This shows that that despite apparent similar resistance to CDDP and the major role of the PDI isoforms, the resistance of these clones can affect multiple cell death pathways.

**Reversal of CDDP resistance in ovarian carcinoma cell line A2780R.** To extend our findings concerning the role of PDIA4 and PDIA6 in CDDP resistance, we evaluated the impact of PDIA isoform depletion on A2780R cells, which represent a CDDP-resistant form of an ovarian carcinoma cell line (Supplementary Figure S5A). Signs of CDDP-triggered early and late apoptosis were clearly enhanced by PDI depletion with a stronger impact of PDIA6 than PDIA4 downregulation (76.4 and 44.8%, respectively) (Supplementary Figure S5B). Moreover, an increase of  $\Delta\Psi_m$  loss and hypoploidy was found following PDI depletion (Supplementary Figures S5C and D), suggesting that PDIA was repressing the mitochondrial apoptotic pathway in A2780R cells.

**PDI overexpression in lung adenocarcinoma patients.** Finally, the pathophysiological relevance of our study was

addressed by immunochemistry in cell lines and lung adenocarcinoma patient biopsies (Supplementary Table S2). In WT and resistant cell lines and patients, we detected a PDIA4-specific cytoplasmic staining pattern compatible with its ER location (Figure 7). PDIA4 was overexpressed in tumoral tissue of CDDP-treated cancer patients (10/10 patients) or CDDP-untreated patients with no mutated EGFR (18/18 patients) but was not detectable in non-tumorous tissue (Figure 7). Unexpectedly, PDIA6 was detected in the nucleus of some patients' tumor cells, especially in metastatic tumors or those harboring a mutation in EGFR exon 19 or 21 (18/38 lung adenocarcinomas, Supplementary Table S2). Interestingly, 3-fold more untreated CDDP tumors exhibited a nuclear location of PDIA6 than formerly treated and resistant tumors to CDDP. In resistant tumors, PDIA6 was mostly expressed at the cytoplasm of tumoral cells. Moreover, PDIA6 was not detected in the nucleus of normal cells, suggesting tumor-associated nuclear translocation of the protein that could be related to the microenvironment of the tumor.

Discussion

Chronic treatment of cancer cells with low doses of CDDP prevent apoptosis execution and confer an enhanced survival capacity.<sup>5,16,22,35</sup> Here, we found that this resistance phenotype correlate with gene expression regulation of several

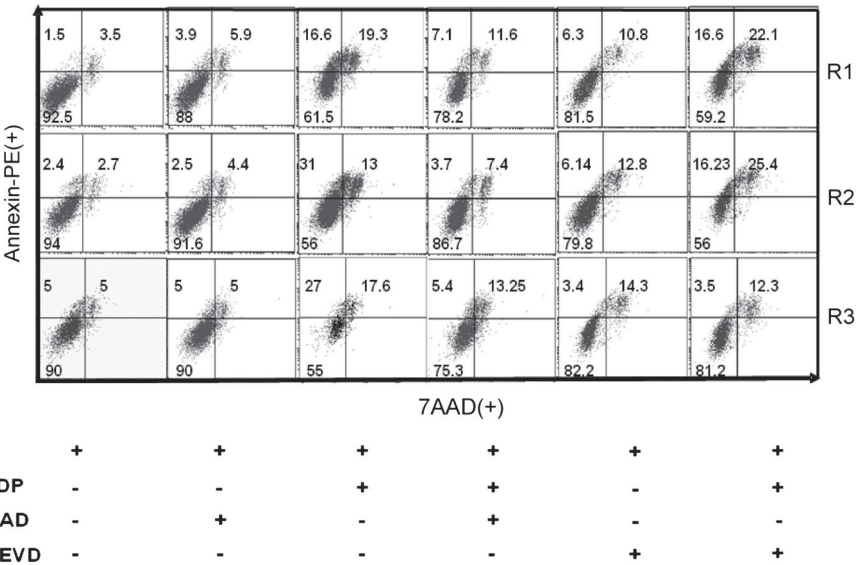


**Figure 6** Caspase role in cell death elicited by PDIA4 and PDIA6 knockdown and CDDP. R1, R2 and R3 cells were treated only with siRNA PDIA6 for 48 h followed by 2 h of 50  $\mu$ M caspase inhibitor Z-VAD or Z-LEVD and/or 48 h of 25  $\mu$ M CDDP treatment. Cells were labeled with 7-AAD and Annexin V to detect early and late apoptosis ( $n = 6$ )

**Figure 5** Characterization of cell death elicited by PDIA4 and PDIA6 knockdown and CDDP in resistant cells. (a) Cells transfected with control siRNA (SiCtrl), siRNA targeting PDIA4 (siPDIA4) or siRNA targeting PDIA6 (siPDIA6) for 48 h followed by 48 h of 25  $\mu$ M CDDP were stained with the fluorescent dye TMRM to visualize mitochondrial  $\Delta\Psi_m$ , (b). with propidium iodide (PI) to visualize DNA content after treatment and analyzed by flow cytometry ( $n = 6$ , mean  $\pm$  S.D.), and (c). analyzed for caspases 3/7 activity. (d) Western blotting analysis of R1, R2 and R3 cells after 48 h of siRNA PDIA4 or control followed by 48 h of 25  $\mu$ M CDDP treatment. Bcl-2, caspases 9 and 3 cleavage, GRP78 expression and PARP1 cleavage were analyzed.  $\beta$ -actin is used as a loading control ( $n = 3$ ). (e) Western blotting analysis of R1, R2 and R3 cells after 48 h of siRNA PDIA4 or control followed by 48 h of 25  $\mu$ M CDDP treatment. Caspase 9, 4 and 3 cleavage, GRP78 expression, PARP1 and RIPK1 expression were analyzed.  $\beta$ -actin is used as a loading control ( $n = 3$ ). (f) Cellular protection by necrostatin of loss of cell viability induced by siRNA PDIA6 and 25  $\mu$ M CDDP ( $n = 3$ )



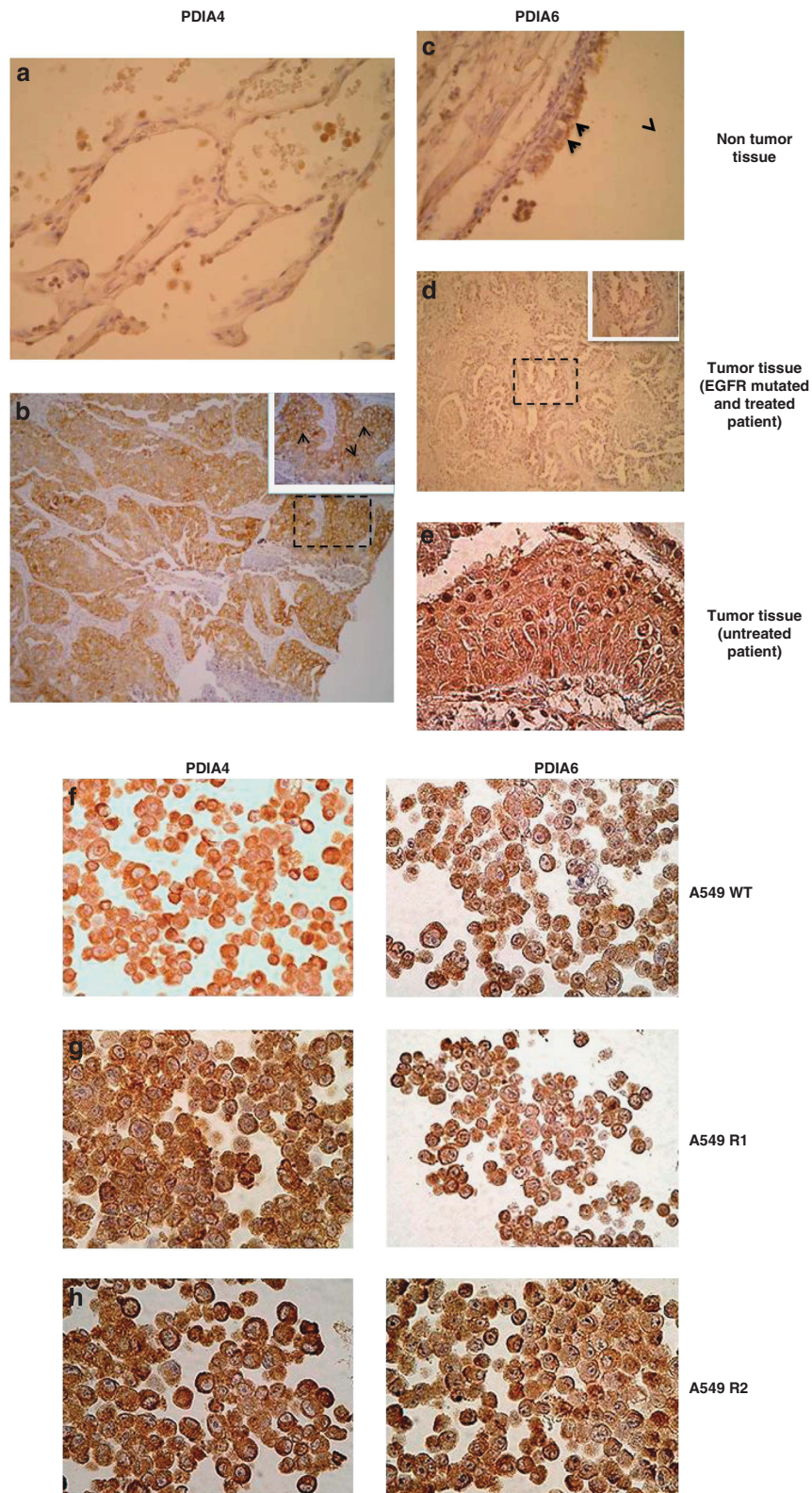


**Figure 7** Immunostaining of patient biopsies and NSLC cell lines. (a) Non-tumor tissue presents substantial negative staining. In this figure, pneumocytes (a) are negative for PDIA4 staining, while a positive staining is seen in macrophages (M) (× 400). (b) Almost all tumor cells show a PDIA4-positive immunostaining (× 100). The staining is cytoplasmic with in some cases a membrane reinforcement (× 400). (c) Non-tumor tissue presents substantial negative staining for PDIA6, with few bronchial cells showing a positive nuclear staining (× 400). (d and e) Some tumor cells show a PDIA6-positive immunostaining. However, the immunostaining is heterogeneous and varies in different tumor sectors (× 100), and it is nuclear (× 400). (f–h) A549 cell lines WT, R1 and R2 show a positive cytoplasmic immunostaining for PDIA4 and PDIA6

classical oncogenes and tumor suppressors (e.g., Bax, Bcl-2, PARP1, HSP70) in a panel of resistant NSLC cells. Interestingly, we found a set of overexpressed ER stress proteins, including IRE1, PDIA4 and PDIA6 and downregulated proteins such as GRP78, PERK and ATF6, supporting that ER proteome remodeling, UPR response and PDI proteins might have an original role in cancer cell resistance to apoptosis. Our results demonstrate for the first time that overexpression of two ER proteins, PDIA4 and PDIA6, has a role in acquired resistance to CDDP-induced apoptosis via mechanisms that operate at a pre-mitochondrial level. Despite belonging to the large PDI family, both proteins appear to mediate non-redundant mechanisms of cell death inhibition and to be overexpressed in patient tumor cells. The significance of our findings lies in the clinical importance of chemoresistance for cancer progression and treatment efficacy.

The PDI family is composed of at least 20 proteins involved in the folding and maturation of ER proteins via disulfide formation and cyclic oxidation/reduction.<sup>28</sup> Little information is available on the specific role, abundance and regulation of each isoform, but they are described as Ca<sup>2+</sup>-binding proteins. As a result, it was tempting to hypothesize that their overexpression might lead to a blockade of Ca<sup>2+</sup> in the ER and that a defect in Ca<sup>2+</sup> fluxes between ER and mitochondria could prevent MMP induction upon CDDP treatment. However, based on ERD1 FRET measurement, no alteration in Ca<sup>2+</sup> storage and release by the ER was observed, excluding a link between Ca<sup>2+</sup> and CDDP resistance, at least in our cellular model of CDDP resistance.

Evidence for an essential role of PDIA4 and PDIA6 is based on the findings that pharmacological inactivation with bacitracin and genetic silencing with siRNA of these specific isoforms restores the sensitivity to CDDP-induced cell death. This was shown for four NSLC cell lines and one ovarian cancer cell line, establishing the relevance of the observation for various cancer types. Recently, a PDI inhibitor, PACMA 31, has been reported to suppress tumor growth in a mouse xenograft model of human OVCAR-8 ovarian cancer.<sup>36</sup> Our results suggest that such a strategy could also be used to reverse CDDP-induced cell death resistance.

Surprisingly, a CDDP-protective function was not observed for other PDIs than PDIA4 and PDIA6. Moreover, mechanisms of PDIA4- and PDIA6-mediated cytoprotection were distinct, notably regarding the role of caspases,  $\Delta\Psi_m$  dissipation and DNA fragmentation. Although PDIA4 knockdown triggered the classical mitochondrial pathway of apoptosis ( $\Delta\Psi_m$  loss, proteolytic maturation/activation of caspases 3, 7 and 9, phosphatidylserine exposure and plasma membrane permeabilization and DNA fragmentation), PDIA6 knockdown induced a different mode of cell death with PS exposure and plasma membrane permeabilization, caspase-4 activation and RIPK1 overexpression but no  $\Delta\Psi_m$  dissipation, caspase-9 cleavage or DNA fragmentation in at least in two out of three clones. This indicates that the specific cytoprotective role of these proteins is not redundant.

Despite a large number of studies linking the UPR to alterations in drug sensitivity and malignancy,<sup>9,10</sup> profound mechanistic insights into these roles have not been established so far. The induction of GRP78 has been commonly used as an indicator for UPR, and the regulation of its

expression in resistant cells and its reversal following PDIA4 and PDIA6 depletion suggests that GRP78 may be an important factor in CDDP resistance. Thus, further studies are required that might reveal a major role of GRP78 in chronic chemoresistance. Of note, we also found that the three clones are cross-resistant to other chemotherapeutics such as oxaliplatin and carboplatin and that PDIA4 knockdown restored death induction with the same profile than CDDP (Supplementary Figure S6). Only oxaliplatin was not reversed by PDIA6 extinction in R3 cells.

Importantly, PDIA4 and PDIA6 expression in samples from lung adenocarcinoma patients correlated with their clinical status. We analyzed lung biopsies from patients at diagnosis of non-small cell lung adenocarcinoma or after treatment by CDDP; PDIA4 was found with a cytoplasmic location compatible with the expected ER location in tumor cells from all patients and cell lines. In contrast, PDIA6 can also be detected in the cytoplasm and in the nucleus in some tumor cells in most of the patients. Unusual locations of PDI proteins have been previously proposed to be related either to their redox function or to their ability to bind DNA and nuclear matrix and to activate transcription factors<sup>37,38</sup> or participated to DNA repair. PDI has recently been found in glial cytoplasmic inclusions of patients with multiple system atrophy,<sup>39</sup> Alzheimer's disease<sup>40</sup> and amyotrophic lateral sclerosis.<sup>41</sup> It is also known that intracellular redistribution of PDIs or modification of its redox activity can be controlled by N-nitrosylation in conditions of nitrosative stress.<sup>42–44</sup> Therefore, it is tempting to speculate that in patient biopsies PDIA6 might redistribute intracellularly as a consequence of yet-to-be elucidated post-translational modifications. The cytosolic location of PDIA6 in CDDP-treated tumors could suggest their role in the DNA damage signaling cascade and provide a novel promising target for chemotherapeutic intervention.<sup>45</sup>

In summary, we demonstrated overexpression of PDIA4 and PDIA6 in CDDP-resistant NSLC cells and in biopsies from lung adenocarcinoma patients. *In vitro*, PDIA4- or PDIA6-targeting siRNAs reversed the CDDP-resistant phenotype and established an unexpected anti-apoptotic role of these proteins. We anticipate that this study may prepare the theoretical grounds to define novel chemotherapeutic strategies based on PDI inhibitors.

## Materials and Methods

**Reagents.** Where not indicated, reagents were from Sigma (Saint-Quentin Fallavier, France). Caspase inhibitors Z-VAD-fmk and Z-LEVD-fmk are from BioVision (Lyon, France).

**Cell lines.** Human A549 and A2780 WT and resistant cells were kindly provided by Professor G Kroemer (Inserm U981, Institut Gustave Roussy, Villejuif, France) and Dr. M Gutmann (Cytomics Pharmaceuticals, Orsay, France). A549 cells were grown in DMEM supplemented with 10% fetal bovine serum, antibiotics and 10% glutamine at 37 °C in a humidified atmosphere with 5% CO<sub>2</sub>. A2780 cells were maintained in RPMI with 10% fetal bovine serum, antibiotics and 10% glutamine. A549-resistant clones R1, R2 and R3 were obtained as described.<sup>16</sup> A2780-resistant cells were maintained with 1  $\mu$ M CDDP once a week to maintain resistance.

**siRNA transfection to knockdown PDI isoforms.** On-Targetplus SMART pool siRNA, a mixture of four siRNA provided as a single reagent were purchased from Dharmacon Research (Illkirch, France). The transfections were



performed according to Martel *et al.*<sup>46</sup> At day 0, A549 and A2780 cells were plated overnight at  $5 \times 10^5$  cells in 96-well plates for cell viability and for caspase activity quantification at  $3 \times 10^4$  in 24-well plates for cytometry analysis. At day 1, the cells were transfected with 100 nM PDI isoforms siRNA oligonucleotides or non-target control oligonucleotides using Dharmafect transfection reagent 2 for 48 h. After siRNA treatment, cells were treated or not with 25  $\mu$ M CDDP.

**Subcellular fractionation.** Cells were harvested at 70% confluency in 175 cm<sup>3</sup> flasks, trypsinized and washed in PBS. Cells were incubated with 5 ml of buffer (250 mM saccharose, 10 mM Tris pH 7.6, 10 mM KCL, 0.15 mM MgCL<sub>2</sub> and 0.4 mM PMSF) for 30 min on ice. Then, cells were broken in Dounce homogenizer (Dominique Dutscher, Brumath, France) (100 hits). Homogenates were centrifuged at  $1000 \times g$  for 10 min to pellet nucleus, cell debris and intact cells. The supernatants were collected and centrifuged twice at 10 000 (mitochondria fraction) and  $20000 \times g$  (mitochondria and membranes debris fraction) for 15 min at 4 °C to pellet mitochondria. Again, the supernatants were centrifuged at  $100000 \times g$  at 4 °C to pellet ER. Finally, cytosolic proteins were precipitated with acetone. ER was solubilized overnight in proteomic buffer (7 M urea, 2 M thio-urea, 20 mM dithiothreitol (DTT), 1% Triton X-100, ampholytes 3–10; Bio-Rad, Marnes la Coquette, France) and centrifuged for 45 min at  $100000 \times g$  at 4 °C.

**Proteomic sample preparation.** ER proteins (125  $\mu$ g) were diluted in proteomic buffer supplemented with bromophenol blue in a final volume of 150  $\mu$ l and loaded overnight on a 17 cm Ready IPG strip 2D electrophoresis pH3-10 (Bio-Rad) for rehydration in a passive mode. The rehydrated strip with protein was placed in Protean IEF cell (Bio-Rad), and proteins were separated following iso-focalization. Strips were equilibrated 10 min in 5 ml of buffer containing 50 mM Tris-HCl, pH 8.8, 6 M urea, 2% SDS, 30% glycerol and 1% DTT. A second equilibration with bromophenol blue was performed in 5 ml of the same buffer with 1.5% iodoacetamide substituted for DTT during 10 min. Strips were transferred onto a 12%-SDS-polyacrylamide gel and overlay with 0.5% agarose in Laemmli buffer. Second-dimension denaturing electrophoresis was driven at 200 V, and gels were stained with silver nitrate in small Dodeca stainer (Bio-Rad). Gels were scanned with GS800 Calibrated densitometer (Bio-Rad), and candidate spots are analyzed with PDQuest software (Bio-Rad).

**Mass spectrometry analysis.** Spots of interest were in-gel digested with sequence-grade trypsin (Promega, Madison WI, USA) and analyzed by tandem mass spectrometry (MS) as previously described.<sup>46</sup> The peptide mass profiles obtained were analyzed using MASCOT MS/MS Ion Search (<http://www.matrixscience.com>) with the following parameters: Swiss-Prot 57.7 database, Homo sapiens taxonomy, one missed cleavage by trypsin, fixed carbamidomethylation of cysteine and variable oxidation of methionine, monoisotopic peptide masses, peptide tolerance of 100 p.p.m. and MS/MS tolerance of 0.5 Da. Validated proteins had at least one peptide matched and a minimum Mascot score of 32 (significance threshold  $P < 0.05$ ).

**Western blotting analysis.** Cells (300 000) were collected and lysed with RIPA buffer. An equal amount of proteins (30  $\mu$ g) was separated by SDS-PAGE and immunoblotted with the following antibodies: ATF6 (Abcam, Thermo Fischer, Illkirch, France); Bax, (BD Biosciences, Heidelberg, Germany); Bcl-2, (Santa Cruz, Saint Quentin, France); Caspase 9, (Abcam); GRP78 (Cell Signaling, Paris, France); HSP70 (Santa Cruz); IRE1 (Abcam); PARP1 (Santa Cruz); PDIA1 (Assay Design Ann Arbor, MI, USA); PDIA3 (Abcam); PDIA4 (Abcam and Santa Cruz); PDIA6 (Santa Cruz and Abcam); PERK (Abcam); and RIPK1 (BioVision).

**Cell viability analysis.** The number of surviving cells was determined by the WST-1 assay (Roche, Boulogne-Billancourt, France).

**Cell death analysis.** A549 and A2780 WT and resistant cells were analyzed for cell death as previously described.<sup>47</sup> Briefly, tetramethylrhodamine methyl ester (TMRM, Invitrogen, Saint Aubin, France) was used to measure the mitochondrial transmembrane potential ( $\Delta\Psi$ m) at 24 h, propidium iodide for cell cycle and subG1 (hypoploidy) at 48 h by flow cytometry (FACSCalibur flow cytometer, BD Biosciences). Finally, early and late apoptosis were analyzed using Annexin-PE/7AAD (BD Pharmingen, San Jose, CA, USA). The caspases 3/7 activities were measured with the Apo-ONE Homogeneous Caspase-3/7 Assay (Promega, San Jose, CA, USA).

**PDI activity assay.** ProteoStat PDI assay kit was used following the manufacturer's instruction (Enzo Life, Villeurbanne, France) by using insulin as substrate to evaluate PDI activity in A549 whole extracts and ER fraction.

**Clonogenic assay.** Cells were harvested, washed with PBS and plated for 2–3 weeks at 37 °C. Then, colonies were stained with 0.25% of crystal violet and counted using GS800 calibrated densitometer (Bio-Rad) and PDQuest software (Bio-Rad).

**[Ca<sup>2+</sup>] measurements in the ER and cytoplasm.** For steady state [Ca<sup>2+</sup>] ER measurements, the ERD1 FRET-based recombinant Ca<sup>2+</sup> probe was used, as previously described.<sup>26</sup> Briefly, cells were plated on 22 mm glass coverslips and, 48 h following transfection, were treated or not with 75  $\mu$ M CDDP for 24 h. Measurements were carried out on a Zeiss LSM510 META confocal system (Marly le Roy, France). The probe was excited by a 405-nm laser diode, emission spectra were acquired from 420–600 nm and the YFP and CFP signals were obtained by un-mixing the spectrum based on previously registered spectra of separate CFP and YFP proteins, as well as the autofluorescence of non-transfected cells. FRET efficiency, which is the function of the ER luminal [Ca<sup>2+</sup>] was quantified using the acceptor bleaching method.<sup>48</sup> Briefly, after five acquisitions YFP was bleached (at both 488 and 514 nm excitation wavelengths, typically by about 80–90%), followed by acquisition of further five image spectra. Reduction of the YFP signal leads to an increase in the CFP signal, which was normalized to the decrease of YFP intensity during bleaching. The normalized increase of CFP intensity is presented as FRET efficiency (Supplementary Figure S1).

For cytosolic [Ca<sup>2+</sup>] measurements, A549-WT and R1 cells were seeded in 24-well plates. Cells were loaded with 1  $\mu$ M Fura-2-AM (Invitrogen) at 37 °C for 20 min. Cells were imaged on Olympus IX71 inverted epifluorescence microscope (Olympus, Hamburg, Germany) fitted with a computer-controlled motorized heated stage (37 °C, Applied Scientific Instrumentation, Eugene, OR, USA), with a  $\times 40$  fluorite objective lens (NA 0.6). Images were collected using a Hamamatsu C10600-10B CCD camera (Hamamatsu Corporation, Massy, France), and recorded and analyzed using the Simple PCI 6.6.0.0 software (Hamamatsu Corporation). Excitation illumination was provided by light from a metal halide arc lamp passing through a computer-controlled filter wheel (Prior Scientific, Rockland, MD, USA), using a Fura-2 filter set (71 000, Chroma Technologies, Bellows Falls, VT, USA). Following 10 min of image acquisition to determine baseline Fura-2 fluorescence, 75  $\mu$ M CDDP was added directly to the appropriate samples, and data were acquired for a further 60 min. Data were acquired at the same time point for each test condition from cells in adjacent wells of the tissue culture plate loaded simultaneously with Fura-2-AM. Statistical significance was assessed through comparison of the background-corrected 340 nm: 380 nm Fura-2 fluorescence ratio of the final 10 frames of the image series using a paired Student's *t*-test.

**Immunohistology.** Forty-two patient lung biopsies from Hospital P Brousse, Villejuif, France and cells from WT and R1 cell lines were analyzed. Immunohistology was performed on 4- $\mu$ m paraffin-embedded formalin-fixed biopsies or cell pellet sections using anti-PDIA4 (Abcam 82587) and PDIA6 (Abcam 89668) antibodies. Antigen retrieval was obtained by heat at 97 °C in a citrate buffer at pH 6. The revelation system was based on a one-step biotin-free immunoperoxidase stain (Envision, DAKO, Glostrup, Denmark) using 3,3'-diamino-benzidine chromogene (DAKO, Glostrup, Denmark) substrate followed by Hemalun counterstaining. Negative controls for each slide were processed concurrently with probed samples by omitting primary antibody.

**Statistical analysis.** Data were analyzed using Student's *t*-test for all pair-wise comparisons of growth rates, and mean responses to the different treatments were tested. Results are presented as the mean  $\pm$  S.D. of three replicate experiments. Significance: \* $P < 0.05$ ; \*\* $P < 0.01$ ; \*\*\* $P < 0.001$ .

## Conflict of Interest

The authors declare no conflict of interest.

**Acknowledgements.** We thank Dr. F Poirier for her technical assistance and Dr. L Galluzzi for the generous gift of resistant cell lines. We are supported by the European Commission (ArtForce); European Research Council, Agence National de la Recherche (ANR); Ligue contre le Cancer (Equipe labellisée); Fondation pour



la Recherche Médicale (FRM); Institut National du Cancer (INCa); LabEx LERMIT; LabEx Immuno-Oncologie; Fondation de France; Fondation Bettencourt-Schueller; AXA Chair for Longevity Research; and Cancéropôle Ile-de-France and Paris Alliance of Cancer Research Institutes (PACRI). GS is supported by Parkinson's UK, Wellcome Trust, Italian Association of Cancer Research (AIRC) and Telethon Italy. ZW receives a fellowship from the China Government.

- Kroemer G, Galluzzi L, Brenner C. Mitochondrial membrane permeabilization in cell death. *Physiol Rev* 2007; **87**: 99–163.
- Hanahan D, Weinberg RA. The hallmarks of cancer. *Cell* 2000; **100**: 57–70.
- Rebillard A, Tekpli X, Meurette O, Sergent O, LeMoigne-Muller G, Vernhet L et al. Cisplatin-induced apoptosis involves membrane fluidification via inhibition of NHE1 in human colon cancer cells. *Cancer Res* 2007; **67**: 7865–7874.
- Galluzzi L, Senovilla L, Vitale I, Michels J, Martins I, Kepp O et al. Molecular mechanisms of cisplatin resistance. *Oncogene* 2012; **31**: 1869–1883.
- Köberle B, Tomicic M, Usanova S, Kaina B. Cisplatin resistance: preclinical findings and clinical implications. *Biochim Biophys Acta* 2010; **1806**: 172–182.
- Ma Y, Hendershot LM. The role of the unfolded protein response in tumour development: friend or foe? *Nat Rev* 2004; **4**: 966–977.
- Zhang K, Kaufman RJ. Signaling the unfolded protein response from the endoplasmic reticulum. *J Biol Chem* 2004; **279**: 25935–25938.
- Ron D, Walter P. Signal integration in the endoplasmic reticulum unfolded protein response. *Nat Rev Mol Cell Biol* 2007; **8**: 519–529.
- Hersey P, Zhang XD. Adaptation to ER stress as a driver of malignancy and resistance to therapy in human melanoma. *Pigment Cell Melanoma Res* 2008; **21**: 358–367.
- Kim I, Xu W, Reed J. Cell death and endoplasmic reticulum stress: disease relevance and therapeutic opportunities. *Nat Rev Drug Discov* 2008; **7**: 1013–1030.
- Deniaud A, Sharaf el dein O, Maillier E, Poncet D, Kroemer G, Lemaire C et al. Endoplasmic reticulum stress induces calcium-dependent permeability transition, mitochondrial outer membrane permeabilization and apoptosis. *Oncogene* 2008; **27**: 285–299.
- Lee AS. GRP78 induction in cancer: therapeutic and prognostic implications. *Cancer Res* 2007; **67**: 3496–3499.
- Han W, Xie J, Li L, Liu Z, Hu X. Necrostatin-1 reverts shikonin-induced necroptosis to apoptosis. *Apoptosis* 2009; **14**: 674–686.
- Kim Y, Haidl G, Schaefer M, Egner U, Herr J. Compartmentalization of a unique ADP/ATP carrier protein SFEC (Sperm Flagellar Energy Carrier, AAC4) with glycolytic enzymes in the fibrous sheath of the human sperm flagellar principal piece. *Dev Biol* 2007; **302**: 463–476.
- Rutkowski DT, Arnold SM, Miller CN, Wu J, Li J, Gunnison KM et al. Adaptation to ER stress is mediated by differential stabilities of pro-survival and pro-apoptotic mRNAs and proteins. *PLoS Biol* 2006; **4**: e374.
- Yao Z, Jones A, Fassone E, Sweeney M, Lebedzinska M, Suski JM et al. PGC-1 $\beta$  mediates adaptive chemoresistance associated with mitochondrial DNA mutations. *Oncogene* 2013; **32**: 2592–2600.
- Galluzzi L, Vitale I, Abrams JM, Alnemri ES, Baehrecke EH, Blagosklonny MV et al. Molecular definitions of cell death subroutines: recommendations of the Nomenclature Committee on Cell Death 2012. *Cell Death Differ* 2012; **19**: 107–120.
- Tajeddine N, Galluzzi L, Kepp O, Hangen E, Morselli E, Senovilla L et al. Hierarchical involvement of Bak, VDAC1 and Bax in cisplatin-induced cell death. *Oncogene* 2008; **27**: 4221–4232.
- Belfi CA, Chatterjee S, Gosky DM, Berger SJ, Berger NA. Increased sensitivity of human colon cancer cells to DNA cross-linking agents after GRP78 up-regulation. *Biochem Biophys Res Commun* 1999; **257**: 361–368.
- Konopleva M, Zhao S, Hu W, Jiang S, Snell V, Weidner D et al. The anti-apoptotic genes Bcl-X(L) and Bcl-2 are over-expressed and contribute to chemoresistance of non-proliferating leukaemic CD34+ cells. *Br J Haematol* 2002; **118**: 521–534.
- Ravagnan L, Gurbuxani S, Susin SA, Maise C, Daugas E, Zamzami N et al. Heat-shock protein 70 antagonizes apoptosis-inducing factor. *Nat Cell Biol* 2001; **3**: 839–843.
- Michels J, Vitale I, Senovilla L, Enot D, Garcia P, Lissa D et al. Synergistic interaction between cisplatin and PARP inhibitors in non-small cell lung cancer. *Cell Cycle* 2013; **12**: 877–883.
- Mandic A, Hansson J, Linder S, Shoshan MC. Cisplatin induces endoplasmic reticulum stress and nucleus-independent apoptotic signaling. *J Biol Chem* 2003; **278**: 9100–9106.
- Chami M, Oulès B, Szabadkai G, Tacine R, Rizzuto R, Paterlini-Bréchet P. Role of SERCA1 truncated isoform in the proapoptotic calcium transfer from ER to mitochondria during ER stress. *Mol Cell* 2008; **32**: 641–651.
- Palmer AE, Jin C, Reed JC, Tsien RY. Bcl-2-mediated alterations in endoplasmic reticulum Ca<sup>2+</sup> analyzed with an improved genetically encoded fluorescent sensor. *Proc Natl Acad Sci USA* 2004; **101**: 17404–17409.
- Vicencio J, Ortiz C, Criollo A, Jones A, Kepp O, Galluzzi L et al. The inositol 1,4,5-trisphosphate receptor regulates autophagy through its interaction with Beclin 1. *Cell Death Differ* 2009; **16**: 1006–1017.
- Inesi G, Sagara Y. Thapsigargin, a high affinity and global inhibitor of intracellular Ca<sup>2+</sup> transport ATPases. *Arch Biochem Biophys* 1992; **298**: 313–317.
- Schwaller M, Wilkinson B, Gilbert HF. Reduction-reoxidation cycles contribute to catalysis of disulfide isomerization by protein-disulfide isomerase. *J Biol Chem* 2003; **278**: 7154–7159.
- Roth RA. Bacitracin: an inhibitor of the insulin degrading activity of glutathione-insulin transhydrogenase. *Biochem Biophys Res Commun* 1981; **98**: 431–438.
- Lovat P, Corazzari M, Armstrong J, Martin S, Pagliarini V, Hill D et al. Increasing melanoma cell death using inhibitors of protein disulfide isomerases to abrogate survival responses to endoplasmic reticulum stress. *Cancer Res* 2008; **68**: 5363–5369.
- Elgaard L, Frickel EM. Calnexin, calreticulin, and ERp57: teammates in glycoprotein folding. *Cell Biochem Biophys* 2003; **39**: 223–247.
- Bian ZM, Elner SG, Elner VM. Dual involvement of caspase-4 in inflammatory and ER stress-induced apoptotic responses in human retinal pigment epithelial cells. *Invest Ophthalmol Vis Sci* 2009; **50**: 6006–6014.
- Hitomi J, Katayama T, Eguchi Y, Kudo T, Taniguchi M, Koyama Y et al. Involvement of caspase-4 in endoplasmic reticulum stress-induced apoptosis and Abeta-induced cell death. *J Cell Biol* 2004; **165**: 347–356.
- Vandenabeele P, Declercq W, Van Herreweghe F, Vanden Berghe T. The role of the kinases RIP1 and RIP3 in TNF-induced necrosis. *Sci Signal* 2010; **3**: re4.
- Michels J, Vitale I, Galluzzi L, Adam J, Olausen K, Kepp O et al. Cisplatin resistance associated with PARP hyperactivation. *Cancer Res* 2013; **73**: 2271–2280.
- Xu S, Butkevich A, Yamada R, Zhou Y, Debnath B, Duncan R et al. Discovery of an orally active small-molecule irreversible inhibitor of protein disulfide isomerase for ovarian cancer treatment. *Proc Natl Acad Sci USA* 2012; **109**: 16348–16353.
- Turano C, Coppari S, Altieri F, Ferraro A. Proteins of the PDI family: unpredicted non-ER locations and functions. *J Cell Physiol* 2002; **193**: 154–163.
- VanderWaal R, Spitz D, Griffith C, Higashikubo R, Roti Roti J. Evidence that protein disulfide isomerase (PDI) is involved in DNA–nuclear matrix anchoring. *J Cell Biochem* 2002; **85**: 689–702.
- Honjo Y, Ito H, Horibe T, Takahashi R, Kawakami K. Protein disulfide isomerase immunopositive glial cytoplasmic inclusions in patients with multiple system atrophy. *Int J Neurosci* 2011; **121**: 543–550.
- Honjo Y, Ito H, Horibe T, Takahashi R, Kawakami K. Protein disulfide isomerase-immunopositive inclusions in patients with Alzheimer disease. *Brain Res* 2010; **1349**: 90–96.
- Walker A, Farg M, Bye C, McLean C, Horne M, Atkin J. Protein disulfide isomerase protects against protein aggregation and is S-nitrosylated in amyotrophic lateral sclerosis. *Brain Res* 2010; **133**: 105–116.
- Uys J, Xiong Y, Townsend D. Nitrosative stress-induced S-glutathionylation of protein disulfide isomerase. *Methods Enzymol* 2011; **490**: 321–332.
- Bernardoni P, Fazi B, Costanzi A, Nardacci R, Montagna C, Filomeni G et al. Reticulon1-C modulates protein disulfide isomerase function. *Cell Death Dis* 2013; **4**: e581.
- Nakamura T, Lipton S. Redox modulation by S-nitrosylation contributes to protein misfolding, mitochondrial dynamics, and neuronal synaptic damage in neurodegenerative diseases. *Cell Death Differ* 2011; **18**: 1478–1486.
- Krynetskaia N, Phadke M, Adhav S, Krynetskiy E. Chromatin-associated proteins HMGB1/2 and PDIA3 trigger cellular response to chemotherapy-induced DNA damage. *Mol Cancer Ther* 2009; **4**: 864–872.
- Martel C, Allouche M, Esposti DD, Fanelli E, Boursier C, Henry C et al. GSK3-mediated VDAC phosphorylation controls outer mitochondrial membrane permeability during lipid accumulation. *Hepatology* 2013; **57**: 93–102.
- Le Bras M, Borgne-Sanchez A, Touat Z, Sharaf el dein O, Deniaud A, Maillier E et al. Chemosensitization by knock-down of adenine nucleotide translocase-2. *Cancer Res* 2006; **66**: 9143–9152.
- Gu Y, Di W, Kellsell D, Zicha D. Quantitative fluorescence resonance energy transfer (FRET) measurement with acceptor photobleaching and spectral unmixing. *J Microsc* 2004; **215**: 162–173.

Supplementary Information accompanies this paper on Cell Death and Differentiation website (<http://www.nature.com/cdd>)

**Titre :** Rôle de l'adénylate cyclase soluble, de phosphodiesterases et d'Epac dans la fonction mitochondriale cardiaque et la mort cellulaire

**Mots clés :** AMPc, adénylate cyclase, Epac, phosphodiesterases, transition de perméabilité mitochondriale, mort cellulaire

**Résumé :** L'AMPc est un messenger important de la régulation neurohormonale du cœur. En activant ses effecteurs, l'AMPc régule de nombreuses fonctions cellulaires telles que l'expression de gènes, le couplage excitation-contraction et le métabolisme cellulaire. Chez les mammifères, l'AMPc est produit par une famille d'adénylate cyclases au sein de plusieurs compartiments subcellulaires solubles ou membranaires. L'existence et le rôle de la signalisation des nucléotides cycliques dans les mitochondries ont été postulés, mais n'ont pas encore été démontrés. De plus, son implication dans la régulation de la mort cellulaire est encore inconnue. Dans cette thèse, nous avons démontré l'expression locale de plusieurs acteurs de la signalisation de l'AMPc dans les mitochondries cardiaques, à savoir une forme tronquée soluble AC (sACt) et la protéine d'échange directement activées par AMPc 1 (Epac1). Nous avons montré un rôle protecteur pour sACt contre la mort cellulaire, l'apoptose, ainsi que la nécrose de cardiomyocytes primaires. Lors de la stimulation par du bicarbonate ( $\text{HCO}_3^-$ ) et du  $\text{Ca}^{2+}$ , la sACt produit de l'AMPc, qui à son tour stimule la

consommation d'oxygène, une augmentation du potentiel mitochondrial de membrane ( $\Delta\Psi_m$ ) et la production d'ATP. L'AMPc est limitant pour l'entrée matricielle de  $\text{Ca}^{2+}$  via l'uniport calcique mitochondrial (MCU) et, en conséquence, prévient la transition de perméabilité mitochondriale (MPT). En outre, dans les mitochondries isolées de cœurs de rats défaillants, la stimulation de la voie de l'AMPc par le  $\text{HCO}_3^-$  prévient la sensibilisation des mitochondries au  $\text{Ca}^{2+}$ . Nous avons également constaté que les familles de phosphodiesterases (PDE), PDE2, 3 et 4, sont exprimées dans les mitochondries cardiaques régulant le taux d'AMPc. Ainsi, ces protéines forment une voie de signalisation locale dans la matrice régulant la fonction mitochondriale cardiaque. Finalement, notre étude a permis d'identifier un lien entre l'AMPc mitochondrial, le métabolisme, certaines PDEs et la mort cellulaire dans le cœur, qui est indépendant de la signalisation AMPc cytosolique. Ceci pourrait constituer un nouveau mécanisme cardioprotecteur via la préservation de la fonction mitochondriale dans un contexte physiopathologique.



**Title :** Role of mitochondrial soluble adenylyl cyclase, phosphodiesterases and Epac in cardiac mitochondrial function and cell death

**Keywords :** cAMP, adenylyl cyclase , Epac, phosphodiesterases, mitochondrial permeability transition, cell death

**Abstract :** cAMP is an important messenger in neurohormonal regulation of the heart. By activating its effectors, cAMP regulates many cellular functions such as gene expression, excitation-contraction coupling and cellular metabolism. In mammals, cAMP is produced by a family of adenylyl cyclase with various subcellular locations and membrane anchorage. The existence and role of cyclic nucleotide signaling in mitochondria has been postulated, but has not yet been demonstrated. Moreover, its implication in the regulation of cell death is still unknown. In this thesis, we demonstrated the local expression of several actors of cAMP signaling within cardiac mitochondria, namely a truncated form of soluble AC (sACt) and the exchange protein directly activated by cAMP 1 (Epac1) and showed a protective role for sACt against cell death, apoptosis as well as necrosis, in primary cardiomyocytes. Upon stimulation with bicarbonate ( $\text{HCO}_3^-$ ) and  $\text{Ca}^{2+}$ , sACt produces cAMP, which in turn stimulates oxygen consumption, increased the

mitochondrial membrane potential ( $\Delta\Psi_m$ ) and ATP production. cAMP is rate-limiting for matrix  $\text{Ca}^{2+}$  entry via the mitochondrial calcium uniporter (MCU) and, as a consequence, prevented mitochondrial permeability transition (MPT). In addition, in mitochondria isolated from failing rat hearts, stimulation of the mitochondrial cAMP pathway by  $\text{HCO}_3^-$  rescued the sensitization of mitochondria to  $\text{Ca}^{2+}$ -induced MPT. We also found that PDE2, 3 and 4 families are located in cardiac mitochondria. They form a local signaling pathway with soluble AC in the matrix, which regulates cardiac mitochondrial functions. Thus, our study identifies a link between mitochondrial cAMP, mitochondrial metabolism, some PDEs and cell death in the heart, which is independent of cytosolic cAMP signaling. This might constitute a novel cardioprotective mechanism through mitochondrial function preservation in pathophysiological conditions.

